THESIS

TRANSLATING BIOMASS GASIFIER RESEARCH TO A MARKET READY STOVE

Submitted by

James William Tillotson

Department of Mechanical Engineering

In partial fulfillment of the requirements

For the Degree of Master of Science

Colorado State University

Fort Collins, Colorado

Spring 2019

Master's Committee:

Advisor: Anthony Marchese

Maggie Clark
Shantanu Jathar

ABSTRACT

TRANSLATING BIOMASS GASIFIER RESEARCH TO A MARKET READY STOVE

Burning solid biomass fuels produces hundreds of emission constituents in the gas, liquid, and solid phase. Many of those products of combustion act as carcinogens, mutagens, teratogens, redox agents , neurotoxins, and allergens to those who are exposed. Some of the most dangerous emissions are carbon monoxide (CO) and particulate matter (PM). Both CO and PM are present in high concentrations in solid fuel combustion exhaust, and are linked to a wide range of health conditions. Those most at risk from exposure to CO and PM are children. Young children under the age of five face a significant threat of contracting lower respiratory tract infections and other comorbidities resulting from exposure to combustion emissions in the home. Exposure is widespread, with approximately 2.8 billion people (36%) worldwide using solid fuels to heat their homes and cook food. The international community has addressed this global health concern through the establishment of a system for systematically evaluating cookstoves against tiered emissions targets with the intention of reducing the cooking related emissions, thereby reducing the human health effects of cooking with solid fuels. Meeting the most stringent ISO-IWA tier 4 guideline requires a 96% reduction in PM emissions over the lowest tier (tier 0) and a 50% reduction in CO emissions over tier 0. Over the last decade significant, research has been conducted to establish what stove designs and combustion strategies can produce the required emissions reduction to have a measureable impact on human health. Among the designs that show promise are top-lit updraft semi-gasifier (TLUD) stoves.

The intent of this research is to evaluate which factors most affect the performance of TLUD stoves with respect to the ISO-IWA tiered rating system and then translate those findings from the laboratory prototypes to a production intent prototype, which can be used for field trials and market evaluation. To achieve this goal three different prototypes and associated experiments are investigated.

First, a laboratory prototype that can be quickly reconfigured and has systems allowing discrete and precise control of a broad number of variables is used to evaluate which variables are most significant to stove emissions performance. This prototype is used to evaluate the effect that seventeen stove geometries, four secondary to primary air flow ratios, four primary airflow rates, five secondary air temperatures, and eight different fuels including four different moisture contents and biomass forms and species. For all of the test cases, the effect of user behavior on the performance of the stove is also evaluated using a three-part test designed to capture the most common modes of operation thought likely for TLUD stoves. The results indicate that when the modular TLUD is operating correctly, tier 4 CO and PM emissions are achievable. A number of test cases achieve tier 4 CO emissions including nearly all the phase 1 cold start test cases; the lowest measured CO emissions being $1.6 \pm 0.5 \frac{g}{MJ_d}$. Some test cases achieve tier 4 PM emissions; the lowest measured PM emissions being $18 \pm 1 \frac{mg}{MJ_d}$. All phase 2 tests where fresh fuel was added to a hot fuel bed could not achieve tier 4 performance, and all low quality fuels also failed to achieve tier 4 emissions. The most significant factors in emissions are user behavior and fuel type. Even in the best case configuration, when the stove is used improperly, and fresh fuel is added to the top of the hot fuel bed, the stove emits significantly greater emissions. Additionally, if a lower quality fuel such as corncobs are used, the emissions are increased significantly.

Once the factors and geometries which result in a well-performing stove are known, those factors must be translated to a standalone cookstove. The Laboratory TLUD stove requires a significant number of external systems to operate, and the objective of the P1 prototype was to explore what would be necessary to create a standalone stove with similar performance to the Modular Laboratory TLUD. The P1 prototype aided in the development of the electronic control package and establish component requirements for the P2 prototype.

The P2 prototype represents a production intent design that reproduces the emissions and performance results seen in the best case Modular Laboratory TLUD experiments. The P2 prototype is also intended to help solve issues with translating information across platforms. During the initial evaluation of the P2 prototype, it was discovered that heating caused the secondary inlet air to become less dense requiring additional secondary air inlet area to be added to the chamber design to compensate for the lower density. It is also established that producing low power outputs with the baseline stove chamber is difficult. A modified chamber with a smaller diameter in the bottom portion of the stove is designed and implemented to ensure adequate turndown and low power emissions. With the P2 design established, two different test procedures using two different initial fuel masses, five different stove geometries, and one alternative fuel is evaluated. All the test cases meet the tier 4 CO emissions requirements for both high power, low power, and indoor emissions criteria. Some individual tests achieve tier 4 high power PM emissions though no test case achieves a statistically average tier 4 result. All high power PM test cases produce tier 3 or better. Almost all low power and indoor PM emissions measurements exceed the tier 4 guideline. In addition to the emissions results, high power efficiency and specific fuel consumption are evaluated for the P2 prototype. Most tests produced tier 2 efficiency for high power operation and tier 3 specific fuel consumption for low power simmer operation. Significant improvement is required to reach tier 4 efficiency using this stove design.

The conclusion of this study is that ISO-IWA tier 4 emissions may be achievable in a laboratory setting using a field ready TLUD semi-gasifier stove. However, additional refinement is needed to reach that objective with confidence using this stove design. The same low emissions results may not be achievable in the field unless the user has been trained, and the highest quality fuels are available to the user. Fuel type, user education, and stove design all have a symbiotic role to play when designing and implementing cookstove programs with the objective of reducing emissions and minimizing adverse human health effects.

ACKNOWLEDGMENTS

This work has been an extraordinary opportunity for me to grow both personally and professionally while allowing me to contribute to the critical task of improving human health and bringing sustainable and efficacious energy solutions to the developing world. For this great privilege, I owe my sincere thanks to many people. I could never have completed this work without the significant support I received during my research.

Firstly, I would like to thank the U.S. Department of Energy for funding this research. I would also like to acknowledge my advisor and committee for their guidance, expertise, and input throughout the course of this work. Jessica Tryner has spearheaded this research, and her extraordinary work in the field of gasification and its application to advanced Cookstoves are second to none. I would also like to acknowledge Dr. Morgan DeFoort, his input during our weekly meetings guided many unique experiment. Dr. Marc Baumgardner was also a critically important member of this research team. The modeling and experimental work Dr. Baumgardner completed was vital to our understanding of the results. Additionally, Marc's support, advice, and encouragement during the first months of fatherhood were indeed a blessing. I would also like to honor Jeffrey Mohr. Without Jeff's enthusiastic, swift, and skillful effort, much of the work we have accomplished would still be in the contemplative stage. It is also important to thank Darryl Beemer, Evan Hoffmann, and Jason Golly for their aid in designing and manufacturing prototypes. I would also like to acknowledge Mr. John Mizia and my fellow stovies for their input, friendship and faithfulness throughout my many years as a student employee of the stoves laboratory at the Powerhouse and more recently as a master student. I have learned so much about life and research from you, and I will never forget the many lessons you have played a pivotal role in teaching me.

Lastly and most importantly I must acknowledge the role my faith and my family has played. My personal motivation for this work is primarily theological in nature. The "what" portion of this work is defined by engineering, and social need, but the "why" that asks what motivates me to undertake such a time consuming endeavor is answered through the lens of a Biblical worldview. It is my desire to be faithful to the Word of God in its command to work hard for the Lord (Colossians 3:23-24), and to honor my colleagues by producing the highest quality work that I am capable of. Completing this work without my incredible wife Cadie would have been exceedingly difficult. She faithfully listens to my endless ideas and selflessly sets aside her desires to support my endeavors. She spent many nights alone with infant children while I worked to research and then write this thesis, an extraordinary sacrifice for which I will be eternally grateful. Finally, I must also thank my daughters Abigail and Hailey for their generous contributions of drool and giggles, and encouragement to finish my "T-sas". More than anyone, they helped me to see the most important personal conclusion of this work, which is that no matter how long it takes, and how difficult it seems, when you have daughters and a wife as extraordanary, intelegent, kind, selfless, and beautiful as I have, anything is possible!

TABLE OF CONTENTS

LIST OF FIGURES

LIST OF EQUATIONS

1. REVIEW OF THE LITERATURE

Indoor Air Quality and Human Health

In an ideal case, the byproducts of burning hydrocarbon-based fuel are carbon dioxide and water[1]. Unfortunately, this ideal applies only in rare cases. More typically, exhaust products include other components, which are the result of incomplete combustion and non-combustion reactions; this is especially true of solid, inhomogeneous, anisotropic fuels such as biomass. Biomass is defined as wood, charcoal, vegetation, agricultural residue, and dung[2]. Smoke, produced by the burning, contains many thousands of hazardous constituents in the gas, liquid and solid phase. Harmful compounds present in wood smoke may include carbon monoxide (CO), many hundreds of saturated, unsaturated, polycyclic aromatic, monoaromatic hydrocarbons, and oxygenated organics such as quinones, phenols, organic alcohols, aldehydes, chlorinated organics, free radicals, and particulate matter, which act as carcinogenic, mutagenic, teratogenic, redox active, neurotoxic, as well as allergenic agents [3].

Perhaps the most dangerous constituent present in large quantities in wood smoke takes the form of a small solid or liquid phase particle. These particles, more frequently referred to as particulate matter or (PM), are especially hazardous when they are sized such that they can reach the alveolar region of the lung which is a primary site of toxicity [4,5].

The depth of PM penetration and location of deposition in the human respiratory tract varies widely by size and respiration rate[4]. Figure 1, adapted from Aerosol Technology by W.C. Hinds, displays the approximate location of 50% penetration for particles in the inhalable, thoracic and respirable fraction.

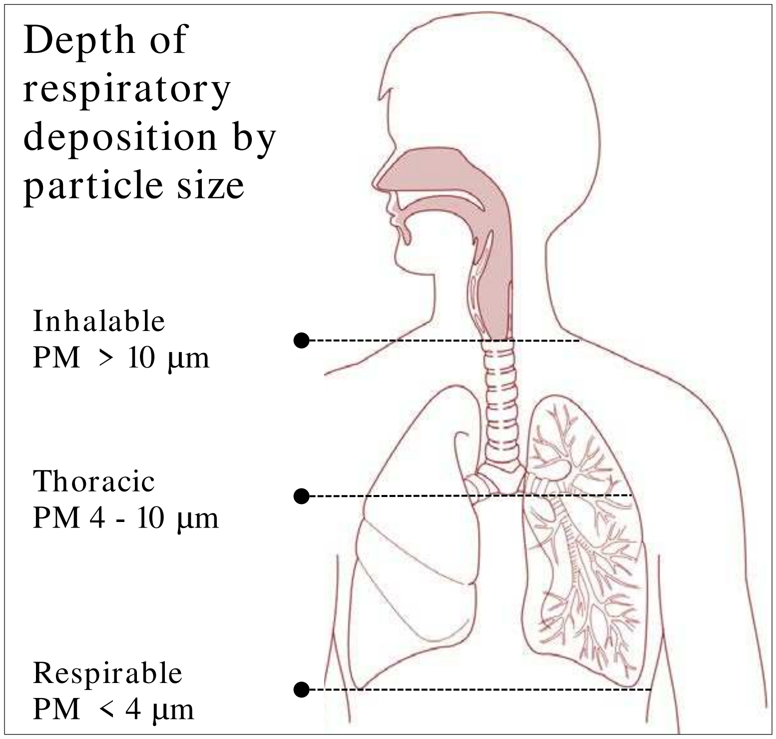

Figure 1 – The depth of penetration for at least 50% of particles in the Inhalable (>10 μm), Thoracic (4 μm - 10 μm) and Respirable (< 4 μm) fractions. Adapted from table 11.5 in Hinds 1999.

For large particles (> 10 μm) such as pollen, dust particles, and water droplets typically do not penetrate further than the throat or sinuses and is known as the inhalable fraction[4]. Approximately 50% of particles with diameters smaller than 10 μm but greater than 4 μm will enter the upper respiratory system and constitute the thoracic fraction[4]. The particles smaller than 4 μm are known as the respirable fraction and are thought to make up the most harmful size of particles which are capable of penetration to the alveolar region where they may deposit and be absorbed into the bloodstream and tissues of the deep lung[4–6].

A myriad of detrimental health impacts and acceleration of a number of comorbid conditions are linked to exposure to fine (particles with median aerodynamic dyameters less than 2.5 μm) and ultra-fine (particle distributions with median diameter less than 100 nm) combustion particles[7,8]. There is a link between indoor air pollution exposure resulting from biomass cooking and low birth weight, chronic obstructive pulmonary disease (COPD), Chronic bronchitis, hut lung which is a variation of pneumoconiosis, cardiovascular disease, cataracts, lung cancer, and a more casual link to the acceleration of HIV and tuberculosis[3,9–15].

The dominating mechanism of morbidity and mortality of PM exposure among children is the Acute Respiratory Infection (ARI). Biomass combustion is tied to acute respiratory infections in Kenya[16], Zimbabwe[17], and rural Guatemala[18]. Figure 2 plots the relative risk factor (RRF) for the development of lower respiratory infection in children under the age of 5 with respect to the nominal household concentration of $PM_{2.5}$ to which they are exposed. The red and red dashed line represents the median RRF and the third order polynomial trend line respectively. The median RRF is bounded on either side by a 95% confidence interval indicated by the black dashed lines. The principal conclusion drawn from Figure 2 is that the risk of ARI is nonlinear third order polynomial. Therefore, a significant reduction in the household concentration of PM is required to lower the risk of ARI in children[19,20].

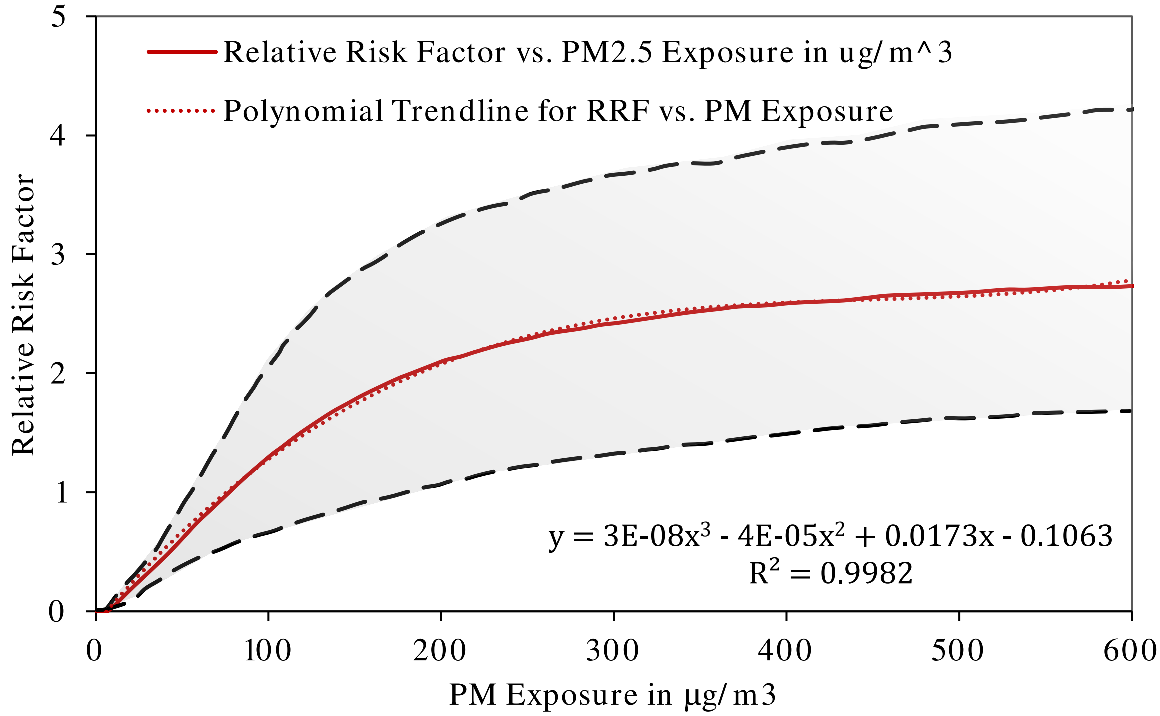

Figure 2 – Relative Risk Factor for the development of lower respiratory infection in children vs. average $PM_{2.5}$ exposure. This figure is modified from data compiled by the WHO from secondhand smoke, and indoor and outdoor air pollution research.[19]

An enormous human health crisis is unfolding, and the fate of approximately 2.8 billion of the world's most impoverished people rest upon its resolution[2]. Worldwide, approximately 41% of the population use solid fuel as the primary household energy source, meaning that these families meet their household cooking and heating needs through burning wood, charcoal, undergrowth, crop refuse, manure, and other fuels.

Figure 3 indicates the global distribution of solid fuels. Over the last three decades, the total number of people using biomass to cook and heat their homes has remained constant although the usage by percentage of the population has fallen by 21% from 62% in 1980 to 41% in 2010[2]. The populations with the highest biomass use are Africa (77%), Southeast Asia (61%), and the Western Pacific (46%) [2].

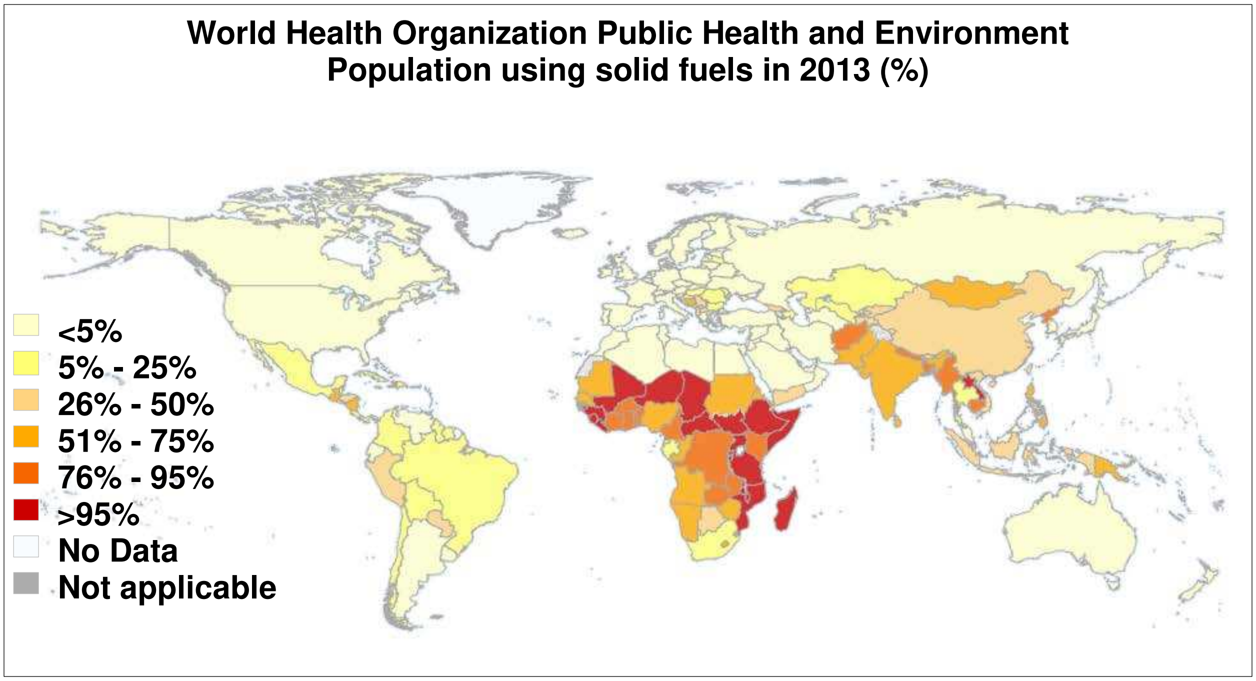

Figure 3 – The global distribution of solid fuel use. Values are in % of the total population within the bounds of each border using solid fuels for energy needs on a daily basis. This plot is produced using data from the World Health Organization map production: Public Health and Geographic Information System.

The energy distribution in developing countries like those in the regions of Africa Southeast Asia and the Western Pacific are dire with 59% of residents cooking with solid fuel; 42% with wood, 8% on coal, 3% on charcoal and dung respectively. Only 41% of developing regions have access to modern energy sources like gas (33%) and electricity (4%) [21]. The rural areas of the least developed countries have biomass penetration as high as 98%[21]. Using solid biomass for cooking and heating results in household air pollution (HAP) comprised of particulate and gaseous emissions, which are one of the most critical environmental health risk factors globally. Exposure to HAP results in a significant global burden of morbidity and mortality.

HAP is responsible for 2.89 million deaths annually [22,23]. Chronic exposure to respirable combustion particles is a dominant risk factor in the global burden of disease. Globally, household air pollution (HAP) is the third largest source of morbidity and mortality, and in many developing regions such as sub-Saharan Africa, HAP is the second leading contributor to the burden of disease behind tobacco smoke exposure and high blood pressure [24]. In Southeast Asia, HAP is the single most significant contributor to the local burden of disease[24].

More than 50% of premature deaths among children under the age of five are the result of the respiration of particulate matter, which can result in lower respiratory infection[10,25]. Figure 4 is a map of the distribution of deaths per 100,000 children globally which are attributed to chronic exposure to HAP.

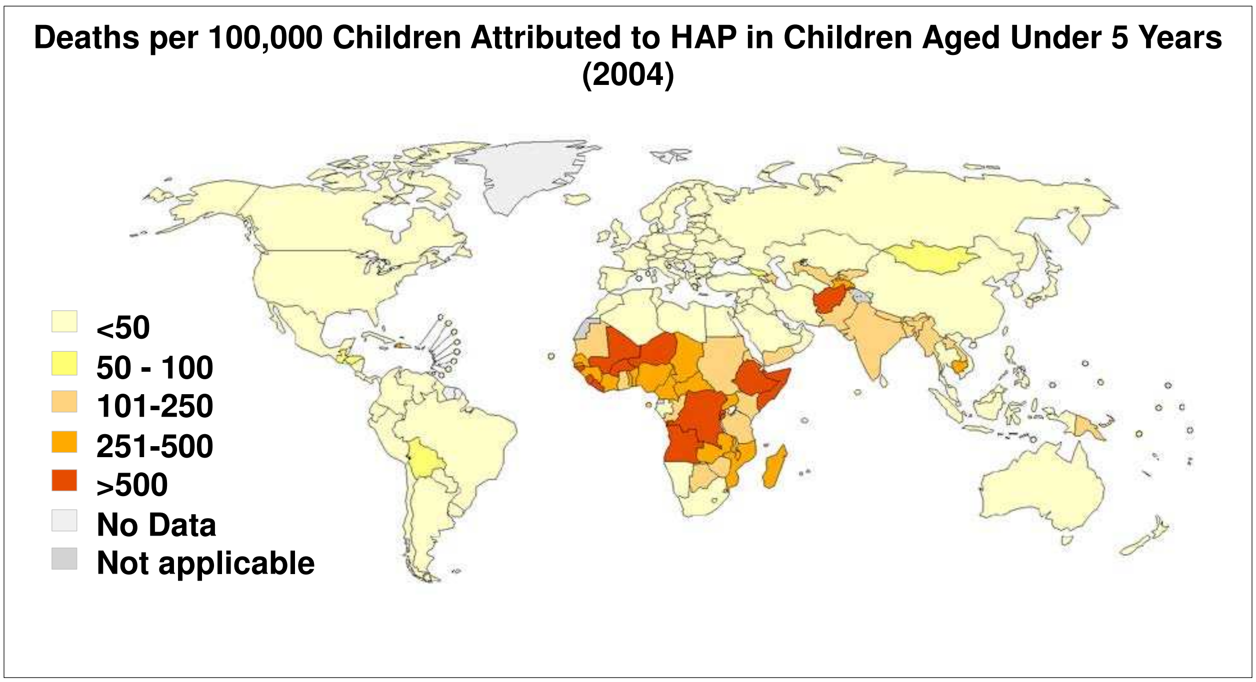

Figure 4 – Deaths Attributed to household air pollution (HAP) in children aged under 5 years old in 2004. This plot is produced using data from the World Health Organization map production: Public Health and Geographic Information System

Observationally, the map in Figure 4 is almost identical in the location and intensity of the regions using biomass for cooking seen in Figure 3, illustrating the link between the use of solid fuels for heating and cooking, and the associated health impacts which result from exposure to the HAP produced by the combustion of solid fuels in the home. The result of these findings is that biomass emissions in the home represent one of the most substantial environmental health risks in the world[24,26].

Biomass fires may also represent a significant source of anthropogenic emissions of greenhouse gases (though some of the carbon based greenhouse gas emissions is recycled), volatile organic compounds, and PM in developing countries[27,28]. These emissions are harmful to the local and global environment. Local deforestation caused in part by harvesting wood for cooking fuel can destabilize the environment via erosion of topsoil, reducing soil fertility and inducing landslides. These changes in the local environment result in dangerous living conditions and reduced soil fertility, which can be a forcing factor in increasing poverty in a region. The widespread use of biomass for cooking and heating has a significant impact on the local environment of the users as well as a global impact. At the local scale, the effects of biomass use have a lasting negative impact on the health, safety, and quality of life for residents of a region.

Haiti is an excellent case study of the local effects of deforestation on the health, wealth, and well-being of the native population. Approximately 88.4% of Haitians use wood biomass for household energy needs[29]. While there is a complex network of conditions, which result in poor forest resource management in Haiti, one of the primary contributing factors, is the illegal harvesting of wood for use as cooking fuel [30]. As a result of poor resource management, there is only 3.2% coverage, compared to 28.4% on the Dominican Republic side of the island as measured in 2000 [31]. The deforestation is well illustrated by the NASA satellite image in Figure 5. The imaged is colorized for vegetation, and the border between the two island nations can be seen based on the vegetation alone. On the left side of the image, Haiti is mostly devoid of vegetation, while on the right the Dominican Republic is covered in verdant forests. The border between the two countries is located at the discontinuity between the two environments.

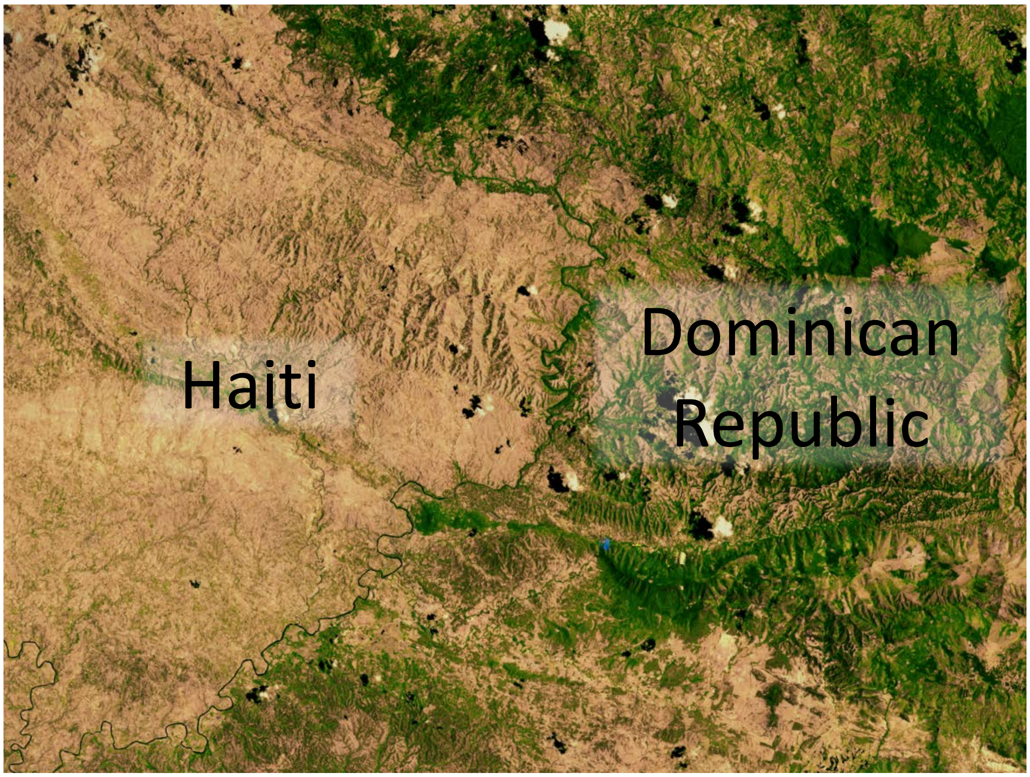

Figure 5 - Satellite imagery of the border between Haiti and the Dominican Republic demonstrating the impact that poor forest management combined with high biomass fuel use has on local vegetation. NASA/Goddard Space Flight Center Scientific Visualization Studio.

In response to the detrimental consequences of using open fires for cooking and heating, a large and growing body of research attempts to quantify the effects of biomass use. Moreover, research institutes and privately held companies work to engineer cooking solutions, which are efficacious, scalable, and economical. Currently, approximately 828 million biomass users cook on improved stoves which is roughly 27% of the total population using biomass for cooking[21], while the remainder cook on primitive stoves often approximated as three-stone fires. This work is no exception and intends to help inform the design of the next generation of biomass cooking systems.

Cookstove Evaluation Methodology

In response to the global scale of the human health and environmental effect of biomass cookstove use, a systematic method for performance evaluation is required. The first step toward an International Organization for Standardization (ISO) standard, in the form of an International Workshop Agreement (IWA), establishes standardized evaluation parameters for cookstoves. IWA 11:2012 resulting from workshops in which more than 90 participants from 22 countries establishes guidelines for cookstove emissions performance evaluation. Among the results of this IWA was a tiered rating system, modeled after those used for industrial engines [32,33], for assessing the emissions performance of a cookstove. The IWA 11:2012 is an evaluation framework that can be applied to other performance testing protocol[34]. Of particular interest to this work are the tiers for gaseous and particulate emissions for both low power simmer and high power maximum stove output operation as well as the efficiency and fuel consumption. The tier 0 performance cutoff is based on stove performance of a three-stone fire and represents the worst performance. Tier 4 represents the aspirational performance thought to be necessary to affect the global human health and emissions concerns related to biomass cooking. The ISO-IWA guidelines for high power CO and PM emissions, low power CO and PM emissions, indoor CO and PM emissions, high power thermal efficiency and low power specific fuel consumption are shown in Table 1 . Low and high power emissions are normalized by the energy delivered to the cooking vessel; indoor emissions are measured as a rate of emission[34]. Thermal efficiency is the fraction of the thermal energy released from the fuel during the cooking task used in heating the contents of the pot[34]. Low power specific fuel consumption is a measure of energy delivered to the pot per unit time normalized against the total volume of the contents of the pot[34].

Table 1 : ISO-IWA Tier System for Cookstove Emissions and Efficiency Evaluation[34]

Tier	**High Power CO (g/MJ$_d$)**	**Low Power CO (g/min/L)**
Tier 0	> 16	> 0.20
Tier 1	≤ 16	≤ 0.20
Tier 2	≤ 11	≤ 0.13
Tier 3	≤ 09	≤ 0.10
Tier 4	≤ 08	≤ 0.09
Tier	**High Power PM (mg/MJ$_d$)**	**Low Power PM (mg/MJ$_d$)**
Tier 0	> 979	> 8
Tier 1	≤ 979	≤ 8
Tier 2	≤ 386	≤ 4
Tier 3	≤ 169	≤ 2
Tier 4	≤ 041	≤ 1
Tier	**Indoor CO Emissions (g/min)**	**Indoor PM Emissions (mg/min)**
Tier 0	> 0.97	≤ 40
Tier 1	≤ 0.97	≤ 40
Tier 2	≤ 0.62	≤ 17
Tier 3	≤ 0.49	≤ 08
Tier 4	≤ 0.42	≤ 02
Tier	**High Power Thermal Efficiency (%)**	**Low Power Specific Consumption (MJ/min/L)**
Tier 0	> 15	≤ 0.050
Tier 1	≤ 15	≤ 0.050
Tier 2	≤ 25	≤ 0.039
Tier 3	≤ 35	≤ 0.028
Tier 4	≤ 45	≤ 0.017

Gasification and TLUD semi-gasifier stove operation

Biomass, a category of materials which stem from plants, is a remarkably diverse and complex fuel. Biomass includes land and water-based vegetation, such as wood, charcoal, agricultural residue, algae, and dung, all in multiple form factors[35,36]. The structure of biomass fuels are mainly inhomogeneous, anisotropic, composite structures comprised of natural polymers; primarily cellulose, hemicellulose, and lignin; inorganics; and water [35–37]. Cellulose comprises between 40% and 50% of woody biomass, with hemicellulose making up 20% to 40% of the composition, and the remainder being lignin, water, and inorganics[35]. The composite structure of the biomass, as well as the fractions of cellulose, hemicellulose, lignin, inorganics, and moisture content influence the products of pyrolysis and combustion.

Three steps comprise the process of solid fuel combustion, heating and drying, devolatilization also known as pyrolysis, and oxidation. A solid organic biomass fuel begins the process of gasification by drying as the temperature rises to 120℃, and the moisture content of the fuel is reduced to zero as the water vaporizes[38]. Heating will continue until the fuel reaches approximately 350℃. From 350℃ to 500℃, the solid fuel undergoes pyrolysis, the process thermally decomposing the solid fuel structure, the result of heating a solid fuel in an oxygen-poor environment. Pyrolysis generates three types of products, volatiles, tars, and char. Volatiles are light hydrocarbons naphthalene anthracene, fluorine, benzopyrene and PAH's in the gas and liquid phase[39]. Tar consists of large molecules in the gas or liquid phase. Char is a solid product comprised primarily of carbon and non-volatiles. The volatile products resulting from the pyrolysis can be oxidized releasing combustion products and heat. Char oxidizes when oxygen is present at the surface of the char where it can react with the carbon and release combustion products and heat. Under typical conditions, the oxidation of char occurs following the release of all volatiles and tars in the previous pyrolysis step. The outward velocity of the volatile products during the pyrolysis phase prevents oxygen from diffusing to the surface of the char.

When a piece of biomass is burning in the open air, all of these processes are happening as a continuum. The drying and pyrolysis produce the gas, which rises to meet with the oxygen-rich air surrounding the biomass. When the ratio of the fuel gas and the air reaches a stoichiometric condition, the flame front forms, the fuel gas converts to exhaust, and heat is released. This flame type is known as a diffusion flame and is the most common and well-understood flame type. There is another flame type significant to this work, known as the inverse diffusion flame. Figure 6 is an illustration of a diffusion flame on the left and the similar inverse diffusion flame on the right. The inverse diffusion flame is similar to the diffusion flame in that the oxidizer and fuel both diffuse toward the stoichiometric flame front. In the case of the inverse diffusion flame, the ambient environment is fuel rich, and the flow of oxidizer is introduced to the fuel rich atmosphere.

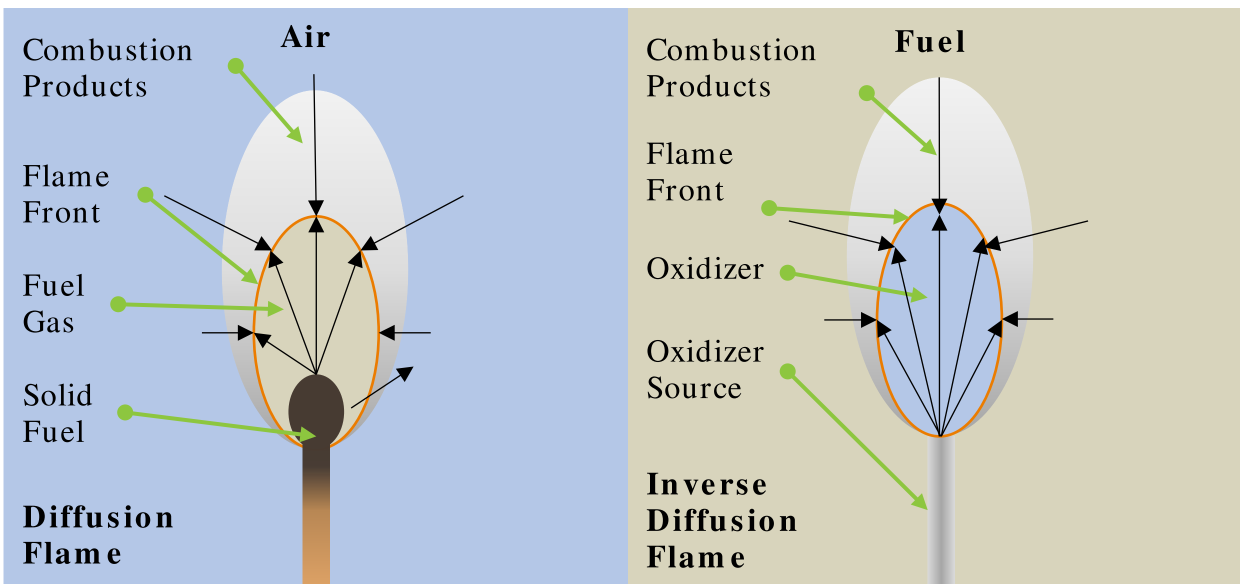

Figure 6 – Illustration of a diffusion flame and inverse diffusion flame.

It can be challenging to control the individual steps in the combustion process when they occur as a continuum. It can be useful to separate the individual steps of solid fuel combustion in order to maintain more control over the system. Figure 7 is an illustration of the combustion process for a top-lit updraft semi-gasifier stove (TLUD) under two discrete operating modes.

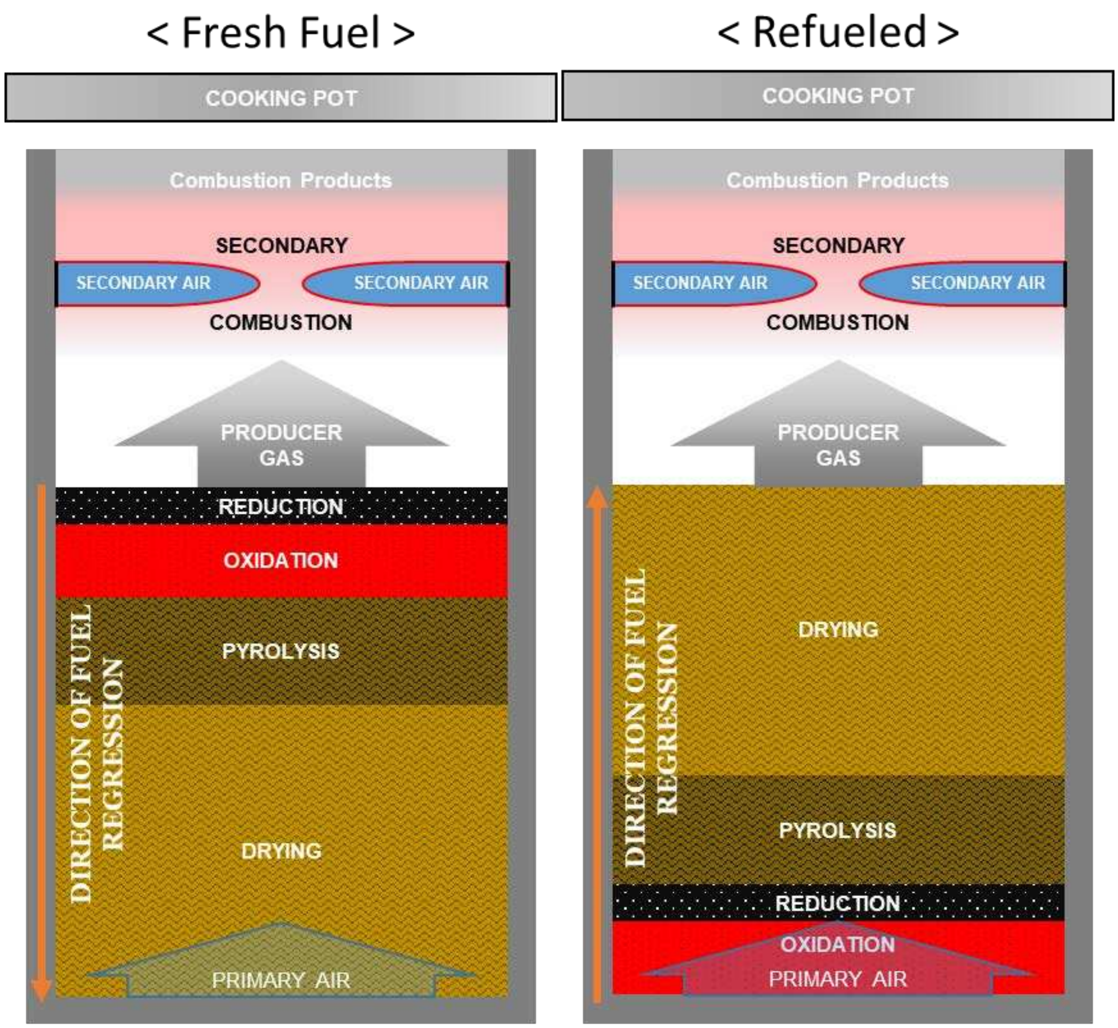

Figure 7 – The illustration on the left is a TLUD operating on a fresh fuel batch. The illustration on the right side is a TLUD operating with a batch of fuel added to the remaining char from a previous fueling.

A TLUD is a gasifier, which separates the process of pyrolysis from the combustion reaction. A small fraction, typically around 25%, of the total air required to reduce the fuel is injected in the first or primary stage of the stove in the fuel bed, which supplies a reaction generating heat sufficient to gasify the fuel without allowing the majority of the volatile gas to oxidize as previously discussed. The result is a plume of volatile pyrolysis gas typically abundant in CO and H_2 rising from the fuel bed.

The pyrolysis gas rising from the fuel bed forms an atmosphere in the secondary combustion stage that is fuel rich. Then oxidizer is introduced as a jet of air injected at the secondary combustion stage. This forms an inverse diffusion flame wherein the oxidizer must pass through the flame front into a fuel rich environment rather than the fuel. The inverse diffusion flame may have implications for emissions production, especially aerosols, as the combustion products from an inverse diffusion flame must pass through a hot fuel rich region outside the flame prior to release into the atmosphere, resulting in conditions more favorable to the formation of fine, superfine and Nano-particles. The combustion products rise from the stove, transfer heat to the cooking surface, and disperse into the local environment. The illustration on the left side of Figure 7 demonstrates the combustion processes associated with a freshly fueled TLUD gasifier stove. In this case, primary air is introduced at the bottom of the fuel bed. Heat release and transfer from the combustion processes occurring above the drying fuel bed dry the fuel bed. As the temperature of the fuel bed increases, the fuel begins to pyrolyze and release volatiles. The oxidation layer is the location in which the primary air reacts with the pyrolyzed fuel and combusting char to generate heat, which in part drives the gasification reaction. Finally, producer gas escapes the fuel bed and reacts with the secondary combustion air to complete the oxidation and further release heat which is then in part transferred to the cooking vessel, in part drives further pyrolysis in the fuel bed, and in part lost in inefficiencies.

Current State of the Art in Improved Biomass Stoves

There are a number of top-lit up-draft semi-gasifier improved cookstoves currently on the market. Independent testing in accordance with Water Boil Test (WBT) protocol was conducted on a number of these stoves, and the results of those tests have been published to the Global Alliance for Clean Cookstoves (GACC) Clean Cooking Catalogue. Several notable stoves include the African Clean Energy Ace 1, Elegance Company Ltd. Elegance 2015, Philips HD4012, Mimi Moto Holding B.V. Mimi Moto. There are a number of significant similarities between these stoves. Each stove is single-family fan-forced top-lit up-draft semi-gasifier cookstove currently or formerly produced for market. While not comprehensive, the list gives a sample of the currently available state of the art improved biomass stoves and their capabilities. The performance specifications for each of the stoves are shown in Table 2.

*Table 2 –IWA and performance specifications for several state-of-the-art TLUD gasifier stoves as published in the Global Alliance for Clean Cookstoves Clean Cooking Catalogue *data averaged from more than one set of tests*

	ACE 1	Elegance 2015	HD4012*	Mimi Moto
Number of Replicate Tests	3	3	6	3
High Power CO (g/MJ_d)	0.82	2.3	1.8465	0.154
High Power PM(mg/MJ_d)	101.1	16.0	104.8	13.94
High Power Thermal Efficiency (%)	41.5	35.44	38.9	46.8
High Power Indoor CO (g/min)	0.023	0.374	0.144	0.014
High Power Indoor PM (mg/min	7.91	6.0	6.898	1.29
Low power CO (g/MJ_d)	0.019	0.087	0.0195	0.00
Low Power PM(mg/MJ_d)	0.84	1.6	0.6065	0.11
Low Power Specific Consumption (MJ/min/L)	0.027	0.043	0.0255	0.014
Low Power Indoor CO (g/min)	0.075	-	-	0.013
Low Power Indoor PM (mg/min	3.33	-	-	0.48
Listed Power Output (kw)	5	-	-	-
Cost (USD)	80-250	17-27	89	40-65

Cells in green represent results exceeding tier 4; blue represents results exceeding tier 3

All of the listed stoves meet or exceed the ISO-IWA Tier 3 interim international guidelines for emissions and performance, and in many cases, each stove can exceed the Tier 4 guidelines as well. Based on the GACC data the Mimi Moto has the best overall WBT emissions and performance, the remaining three have similar performance with various advantages and disadvantages. High power PM emissions and high power thermal efficiency are the most challenging Tier 4 emissions thresholds while the Tier 4 high and low power CO emissions thresholds were easily exceeded by all stoves.

While all stoves listed are excellent improvements over the baseline three stone fire under laboratory testing conditions, other research has shown that gasifiers emissions are highly variable on stove design and a wide range of operating conditions[25,40–43].

A large number of variables may affect the emissions and performances of a TLUD semi-gasifier including fuel type[40,44,45] and size[46], fuel moisture content[46,47], user behavior[41,48–50], stove geometry[41,45], air flow to the primary and secondary combustion stages both the ratio and volume[41,44,51] and temperature of the secondary air flow.

In light of the far-reaching effect of cookstove emissions and the need for efficacious engineering solutions to improve the emissions of cookstoves, the research questions for this body of work are as follows: what parameters affect the emissions and performance of gasifier stoves, and if identified, can those design parameters be integrated into a stove that is usable for real-world cooking tasks? The following research will attempt to provide evidence for what, if any, effects stove geometry, combustion conditions, operational parameters, and fuel type have on stove emissions and performance. Additionally, this research will undertake the translation of those findings from a laboratory prototype to a design, which is near production ready, and usable for cooking tasks by an end user.

This work relies on a systematic experimental approach beginning with an easily modifiable laboratory prototype designated prototype 0 (P0), which allows quick evaluation of a large number of variables. The design variables that lead to the most significant improvements in emissions and performance will be used to design a prototype designated P1 to explore the translation from the laboratory prototype to the stand-alone stove. Finally, the combined knowledge of the first two prototypes will be applied to the design of a near production ready prototype designated P2.

2. P0 LABORATORY MODULAR TLUD COOKSTOVE

To examine the research questions and create a body of data to inform TLUD semi-gasifier stoves design, the P0 Modular Laboratory TLUD Semi-Gasifier Testbed hereafter referred to as the Modular Testbed was designed by Dr. Jessica Tryner at Colorado State University[1]. The Modular Testbed is an experimental gasifier stove designed to allow the rapid reconfiguration of the stove's principal geometry and operating parameters to explore the design space and identify tools to optimize TLUD gasifier cookstove design. The Philips HD4012 TLUD semi-gasifier stove, a common benchmark in TLUD gasifier stove research, influences the geometry of the Modular Testbed[40,42,43].

The Modular Testbed consists of three primary sub-assemblies, the primary air inlet stage, the combustion chamber and the secondary air inlet stage, which are illustrated, in the cross-section of the Modular Testbed in Figure 8. The primary air inlet stage is a stainless steel plenum with four injection holes, permitting the primary air to the bottom of the fuel bed. The combustion chamber assembly is a section of 4-inch diameter schedule 10 stainless pipe outfitted K-type thermocouple array and a fuel-gas sample-port. An alternate version of this section with the K-type thermocouple array and, in lieu of a sampling port, six 2-mm air injection ports for early secondary air injection prior to the secondary stage. Finally, the secondary air injection stage consists of a plenum made of two concentric steel cylinders the inner of which can be interchanged. The inner ring

[1] Additional discussion of the P0 prototype, and the testing done at CSU for this study can be found in the works of Dr. Jessica Tryner. Combustion Phenomena in Biomass Gasifier Cookstoves[60], The Effects of Air Flow Rates, Secondary Air Inlet Geometry, Fuel Type, and Operating Mode on the Performance of Gasifier Cookstoves[61], and Effects of operational mode on particle size and number emissions from a biomass gasifier cookstove[62].

has the secondary air stage holes drilled in it, and eleven different rings have been produced with varying secondary air injection hole sizes and angles.

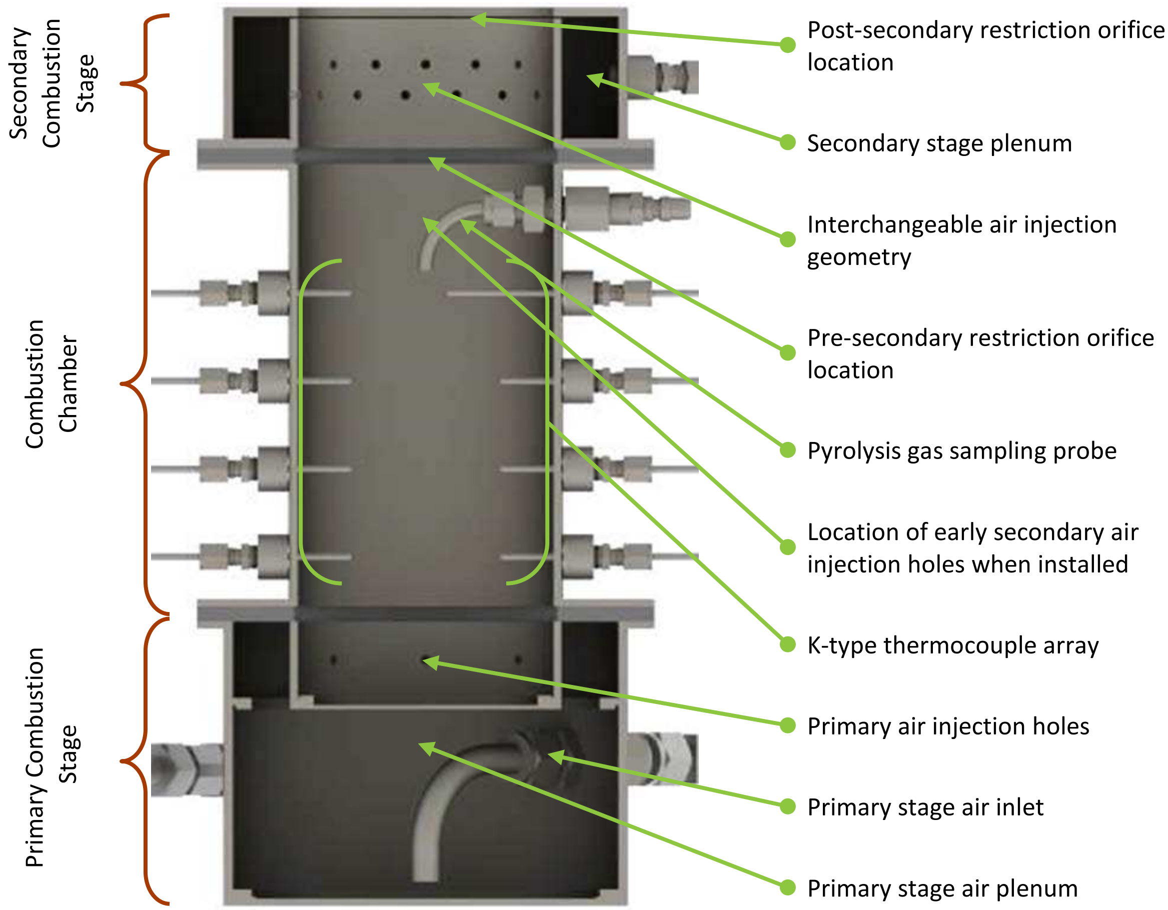

Figure 8 – P0 Modular Laboratory TLUD Cookstove cross-section with component callouts. Labels on the left side of the figure show the three subassemblies of the P0 Modular Laboratory TLUD prototype. Labels on the right side indicate the components of each subassembly. CAD rendering by Dr. Jessica Tryner.

Other design parameters include an insulated chimney 100mm in height and 108-mm in diameter placed directly after the secondary combustion stage, orifice plates for creating a restriction of prior to the secondary combustion stage or after the secondary combustion stage an insulating jacket for the stove is increasing the thermal resistance of the stove body.

All stove components are manufactured from schedule 40 304 stainless steel pipe, 10-gauge 304 stainless steel plate, or 16 gauge 304 stainless steel sheet. All fasteners and hardware are made from 304 stainless steel, and high-temperature aluminum based anti-seize is used on all screw type fasteners during installation to prevent galling and seizing. Sealing surfaces mated together with high-temperature resistant graphite gaskets.

The design space of this TLUD semi-gasifier cookstove includes a number of geometric, operating condition, and fuel variables. The secondary combustion stage geometry varied by inserting a variety of secondary air injection rings, which can change the velocity, swirl, and downward angle of the individual air jets in the second stage. A modified combustion chamber allowed approximately 10% of the secondary air to be injected prior to the secondary combustion stage to induce mixing in the fuel gas prior to reaching the secondary combustion stage.

Operating variables include the temperature and flow rate of the secondary combustion stage air, the flow rate of the primary stage combustion air. PID controlled in-line air heaters provide control of the secondary air injection temperature. The interchangeable secondary air inlet geometry allows the jet velocity, swirl angle, and downward angle of the secondary air injection to be varied. Independently adjustable pot support allows the pot gap between the top surface of the stove and the bottom surface of the pot to be varied, and prevents mass loss due to evaporation during the test from influencing the real-time stove mass measurements. Orifice plates restricted the diameter of the exit of the fuel bed to the secondary air injectors and the top of the stove after secondary air injection from 4 inches to 2.5 inches.

In addition to the stove design and operational parameters different fuel types, bulk densities, and moisture contents are evaluated. The baseline fuel is chipped Douglas Fir (*Pseudotsuga menziesii*) processed in a wood chipper (CJ601E, Snow Joe® + Sun Joe®, Carlstadt NJ. USA). Other fuels include Eucalyptus chips, Lodgepole pine (Pinus contorta) pellets (super premium wood pellet fuel, Rocky Mountain Pellet Company Inc., Confluence Energy, Kremmling CO. USA) and Corncobs (Zea Mays) gathered locally in three bulk densities. Bulk density is measured by placing the fuel a steel cylinder of known volume and of the same diameter as the Modular Testbed using the same handling techniques used when operating the stove. The mass of the fuel added to the cylinder is then measured to acquire the bulk density of the fuel type. Fuel moisture content is measured in accordance with ASTM 871-82(2013), volatile content is measured in accordance with ASTM E872 – 82(2013), and ash content is measured in accordance with D1534 – 93.

20 Channels of temperature data are acquired from Omega type K thermocouples using PicoTech thermocouple loggers (TC-08, Pico Technology, Cambridgeshire, UK) at 1Hz in the PicoLog Recorder software.

Real-time mass data of the stove is collected using a digital balance (MS32001L, Mettler Toledo, Columbus, OH, USA) and LabX® balance data acquisition software.

Emissions are collected by conducting the tests inside a custom fume hood. The fume hood is 1.2m deep by 1.2m wide and 4.3m tall. The hood is designed to have a minimal effect on the stove test. The flow rate through the hood is 0.1 m^3/s, drawn through HEPA filters at the base of the hood to minimize the influence of ambient particulate matter on the test results. Flow through the hood is provided by a roots-type positive displacement pump (Sutorbilt Legend 4LP, Gardner Denver, Inc., Quincy, IL, USA) located downstream of the hood. The hood exhaust line is 0.127 m in diameter. Gaseous and particulate samples are taken from a horizontal section of the exhaust before passing up and out of the building.

Gaseous Carbon Dioxide (CO_2) and Carbon Monoxide (CO) emissions are measured at a sampling rate of 1 Hz using nondispersive infrared (NDIR) emissions analyzers (ULTRAMAT 6, Siemens AG, Munich, Germany). The sample passes from the sampling probe in the hood exhaust, through a heated sample line to prevent condensation, to the analyzers.

Particulate matter (PM) are sampled isokinetically from the exhaust, passed through a PM2.5 cyclone (URG-2000-30EHS, URG Corporation, Chapel Hill, NC,USA), removing any particles larger than 2.5 um. It is not likely that particles larger than 2.5 um originate from the stove, and in addition, the particles thought to be most deteremental to human health are in this size range and smaller. The sample is deposited on a 47-mm TFE coated fiberglass filter (PallFlex Fiberfilm, Pall Corporation, Port Washington, NY, USA). Samples were drawn through the system via a vacuum which was powered by two parallel vacuum diagram pumps (DOA-P707-FB, Gast Manufacturing, inc., Penton Harbor, MI, USA) and controlled via a mass flow controller (MCPH-50SLPM-D-30PSIA, Alicat Scientific, Inc., Tucson, AZ, USA) to maintain constant and correct flow rates through the probe and cyclone. Before and after sampling the filter mass is measured in triplicate gravimetrically with a resolution of 1 µg with a mass balance (MX5, Mettler-Toledo Inc., Columbus, OH, USA).

Emissions Measurements

Filters are left in an equilibrium container that contains PM filtration inlet and exhaust ports, allowing the filters to reach hygroscopic equilibrium with the ambient environment of the measurements laboratory. Prior to weighing the filters the bench top, tweezers, and balance are cleaned using isopropyl alcohol and lint-free tissues to mitigate the effect of dust contaminates on the weighing process. Powder-free latex gloves are worn during the weighing process to prevent detritus from contaminating the filter. For each test, four filters were pre-weighed on a microbalance with 1ug precision. Each filter is weighed three times, and an average of the three measurements is used for all calculations. Static charges are mitigated by exposing the filter to a Polonium 210 (PO-210) alpha particle source (Model 2U500 Staticmaster Alpha Ionizing Cartridge, NRD Advanced Static Control, LLC., Grand Island, NY, USA) between each mass measurement. After the pre-weighing is complete, each filter is placed in a Delrin filter cassette, and then the filter cassette is placed in a cleaned, sealed container for transport and storage prior to use during the test. The first filter is placed in the filter holder attached to the cyclone and then removed as a blank filter to compute limits of detection (LOD) and limits of quantification (LOQ). The each of the three remaining filters is used in one phase of the test.

Once the PM system is prepared for use the NDIR CO and CO_2 analyzers were calibrated using zero air and a calibration gas consistent with the expected concentration range. For the CO analyzer, the calibration range was 0-500 ppm CO. For CO_2 a calibration gas was typically 6%. All calibration gases were acquired from Airgas in Fort Collins Colorado and have a precision of ±2% of the measured calibration gas concentration.

Test Structure

The experimental procedure was designed to reproduce user behavior observed in the field under laboratory conditions. The traditional testing protocol like the water boil test does not currently address the different operating modes of TLUD semi-gasifier Cookstoves; as such do not adequately represent user exposure and stove performance.

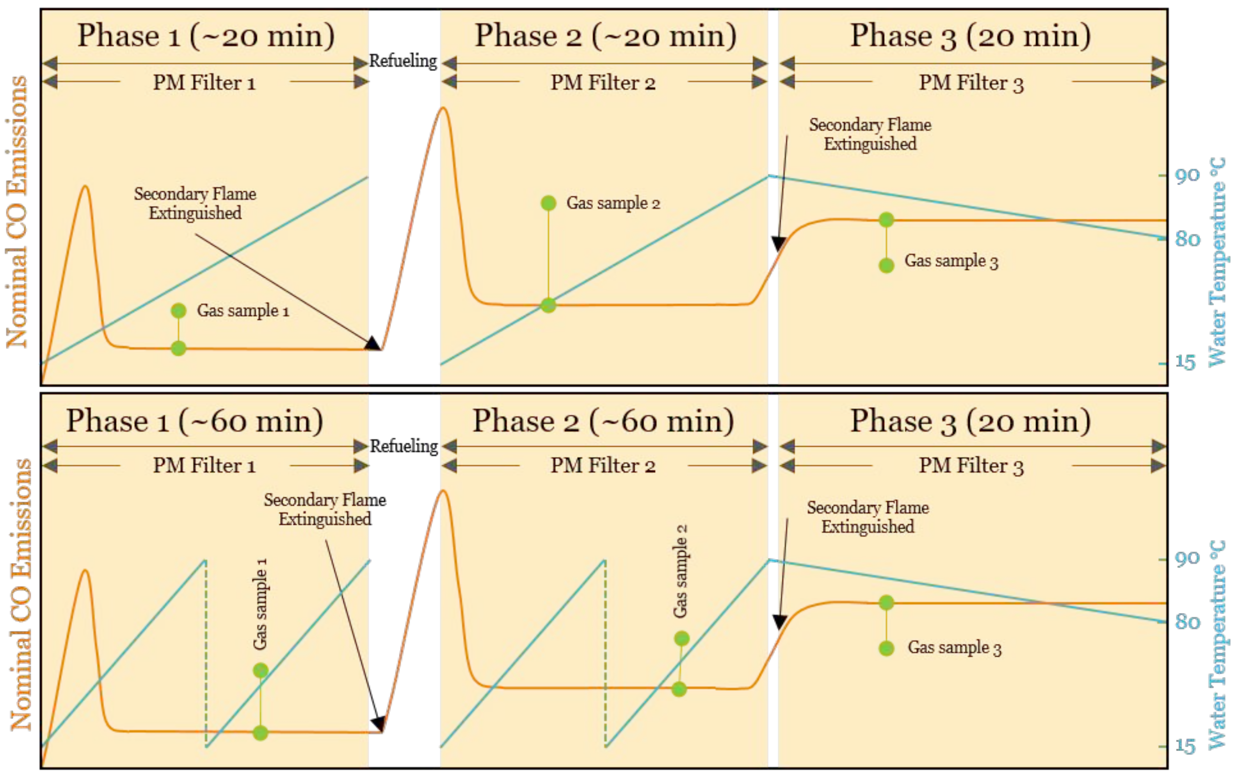

Figure 9 - Diagram of test procedure with refueling and emissions sampling events overlaid with plots of approximate water temperature and CO emissions versus time.

The test procedure is comprised of three distinct segments or phases, which replicate the three primary usage profiles expected in field stove usage. Phase 1 is a cold start phase, which tested the room temperature stove with a fresh load of fuel. Phase 2 was a refueling event in which fresh fuel was added to the top of the char bed that remains from phase 1. Finally, phase 3 was a char burnout phase wherein the remaining char from phase 1 and phase 2 was oxidized using the primary air. Minimal secondary combustion occurs during phase 3.

Prior to each test, the stove is configured according to the requirements of the test case. Configuring the stove includes installing the correct secondary air inlet geometry, placing any additional test hardware including orifices, the chimney, insulation, and setting up pre-secondary air injection if required. Once the hardware is in place, the stove cart is moved into the fume hood. Primary and secondary airflows are set via a pair of rotameters, and if installed, presecondary airflow is set using the third rotameter. Flow through the rotameters is corrected for altitude in accordance with the manufactures requirements. The PID controllers for secondary combustion stage air temperature are also set in accordance with the test case requirements. Finally, all thermocouples are checked for functionality prior to testing.

During test cases where sample gas was drawn from the top of the fuel bed prior to the secondary air inlet, the fuel gas sampling cart is also placed in the hood, and the sample line is connected to the probe on the stove. The water and tar condenser bath is filled with ice water, and the desiccant column is cleaned as needed.

For secondary air, parameter tests, phase 1 began with 300g of chipped Douglas fir (Pseudotsuga menziesii) placed in the combustion chamber of the stove. This fuel was chosen based on a number of parameters including test duration, availability, and how well it represented fuel used in the field. Once the stove is set up for testing, NDIR emissions, gravimetric PM, stove mass, and temperature data acquisition was initiated. The stove was started using 10g of wood chips soaked in 2ml of kerosene placed on top of the fuel bed just prior to ignition. Kerosene soaked fuel was chosen because it can be easily replicated and produced a consistent startup. The same starting procedure was use for every test to normalize the effects of kerosene on emissions and performance. A match is used to ignite the stove. Once ignition was confirmed a stainless steel pot containing 2.5L of water at 15°C +- 2°C and the gravimetric PM measurement was begun. Phase 1 terminated when the pot reached 90°C or the stove extinguished. The end of phase one also marked the end of the first gravimetric sample. The pot was removed and weighed and the fuel bed depth measured using a stainless steel rule lowered to the level of the char bed.

Phase 2 was begun when 200g of fresh fuel was added on top of the char bed. Ignition is again accomplished using 10g of wood chips soaked in 2ml of kerosene and a match. Once ignition was confirmed, a fresh pot of 15 °C water was placed on the stove, and the gravimetric PM system was again activated, and the test was allowed to run until the water reached 90°C or the stove extinguished. The mass of water was again measured, and the hot water was placed back on the stove. The third phase was begun as soon as possible after the stove extinguished. This simmer was allowed to run for 20 minutes.

For the primary air parameter tests, the same procedure was followed except that a pyrolysis gas sample was taken at 10 minutes after the start of the 1st phase and 5 minutes after the start of the 2nd and 3rd phases.

Once the simmer phase was complete, the stove was shut down by turning off the primary and secondary air supply and shutting off the secondary air pre-heater. The remaining char was removed from the stove, and the stove was allowed to cool to ambient temperature prior to beginning the next test.

The test cases selected for this study, covered in more detail below, explore the effects of fuel type, primary and secondary air delivery, and other stove properties on the performance of the modular stove. The test cases represent a wide range of stove design and operating parameters found in commercial stove designs and real field use, as well as some experimental configurations not currently used widely in the field.

Fuels

A number of fuel properties and types are evaluated for their influence on stove emissions and performance. The chemical and bulk properties of the fuels tested are displayed in Table 3.

Table 3 – Properties of the fuels evaluated[2]

	Units	**Value**	**Lodgepole Pine Pellets**	**Douglas fir chips**	**Eucalyptus Chips**	**Corncobs whole, cut, and chipped**
-	-	Species	Pinus contorta	Pseudotsuga menziesii	Unknown	Zea mays
-	Weight % wet basis	Moisture Content	6.84	7.37	7.18	6.38
-	Weight % dry basis	Ash	0.68	0.19	0.69	2.14
Biochemical Analysis *	%	Cellulose	48	48	50	53
		Hemicellulose	24	23	24	32
		Lignin	28	29	27	15
Proximate Analysis	Weight % dry basis	Volatile matter	85.42	87.48	78.82	82.88
		Fixed carbon	13.91	12.32	20.49	14.99
Ultimate Analysis	%	C	51.99	52.17	52.39	48.39
		H	6.09	6.11	5.83	5.89
		N	0.10	0.09	0.20	0.40
		S	0.00	0.00	0.03	0.04
		O	41.61	41.44	40.85	43.15
Heating Values	J/g	Higher heating value	19,980	19,120	17,600	17,090
		Lower heating value	20,120	19,320	17,700	16,980
Density	Wet basis kg/m^3 95% CI	Density	1,100±70	580±40	660±20	250±20
		Bulk Density	636±4	160±1	230±2	174±2
Porosity	-	Particle Porosity	0.32	0.64	0.59	0.84
		Bed porosity	0.42	0.72	0.65	0.31

*data extracted from literature [52,53]

[2] Table data reproduced from the supporting information for The effects of air flow rates, secondary air inlet geometry, fuel type, and operating mode on the performance of gasifier cookstoves[41]

The moisture content, proximate analysis, and lower heating value were completed in-house in accordance with applicable ASTM standards for evaluation of biomass. Moisture content is determined by analysis of the fuel in accordance with ASTM E871-82 (2013)[54]. The volatile content of the fuel is determined in accordance with ASTM E872-82[55]. The ash content of the fuels is determined in accordance with ASTM E1755. The Biochemical composition was obtained from literature[52,53,56]. Higher heating values were measured directly using a bomb calorimeter (C200, IKA, Wilmington, NC, USA) and the results were used to compute the lower heating value in accordance with ASTM-D5865-13[57]. A third party laboratory (Hazen Research, Golden, CO, USA) performed the ultimate analysis for each of the fuels.

Air Delivery

Primary air delivery geometry is not varied for this test but was held constant and delivered through four holes at the base of the combustion chamber. The secondary air delivery geometry is varied through the replaceable secondary air inlet rings as discussed above. Eleven separate inlet geometries divided into three classes, diameter, swirl, and downward angle, are used to vary the inlet velocity and orientation. Four different total airflow rates and four secondary to primary airflow ratios are evaluated. Four different secondary air inlet temperatures are also evaluated. An additional fixture for air injection between the fuel bed surface and the secondary combustion zone termed early secondary air injection is also evaluated. When in use, 10% of the secondary air is sent to the early secondary air injection ports. There are a total of 21 separate stove configurations which affect the secondary and primary air delivery.

Other Features

In addition to the fuels and the air delivery variables, there are several additional features and configurations to evaluate. An orifice plate located between the primary combustion stage and the secondary combustion stage and an orifice plate located just downstream of the secondary combustion stage were added to the baseline configuration. An insulated chimney is also evaluated. A detailed list of the test variables is presented in Table 4 .

Table 4 – Test variables

No.	Variable (units)	Values Tested	Baseline
1	The diameter of the secondary combustion stage air injection holes (mm)	2 , 4, 6, 8, 10	4
2	Swirl angle of the secondary air injection holes (°)	0, 15, 30, 45	0
3	The downward angle of the secondary air injection holes (°)	0, 10, 20, 30	0
4	Secondary Air Temperature (°C)	100, 150, 200, 250, 300	200
5	Secondary to primary air flow ratio	2, 3 ,4 ,5	3
6	Primary air flow rate (g/min)	15, 20, 25, 30	20
7	Orifice location	None, pre-secondary combustion, post-secondary combustion	None
8	Pot gap	15 mm, 30 mm, 45 mm	15 mm
9	Insulated 100-mm chimney	100-mm height	None
10	Early Secondary air injection (% of total secondary air injection)	0, 10	0
11	Insulated Chimney	None, 100mm tall	None
12	Fuel Type	Corncob chips Eucalyptus chips Douglas fir chips Lodgepole pine pellets	Douglas fir chips
13	Fuel moisture content (weight based % wet basis)	0, 7, 15, 25	7
14	Corncob fuel bulk density (kg/m^3)	174, 137, 126	-

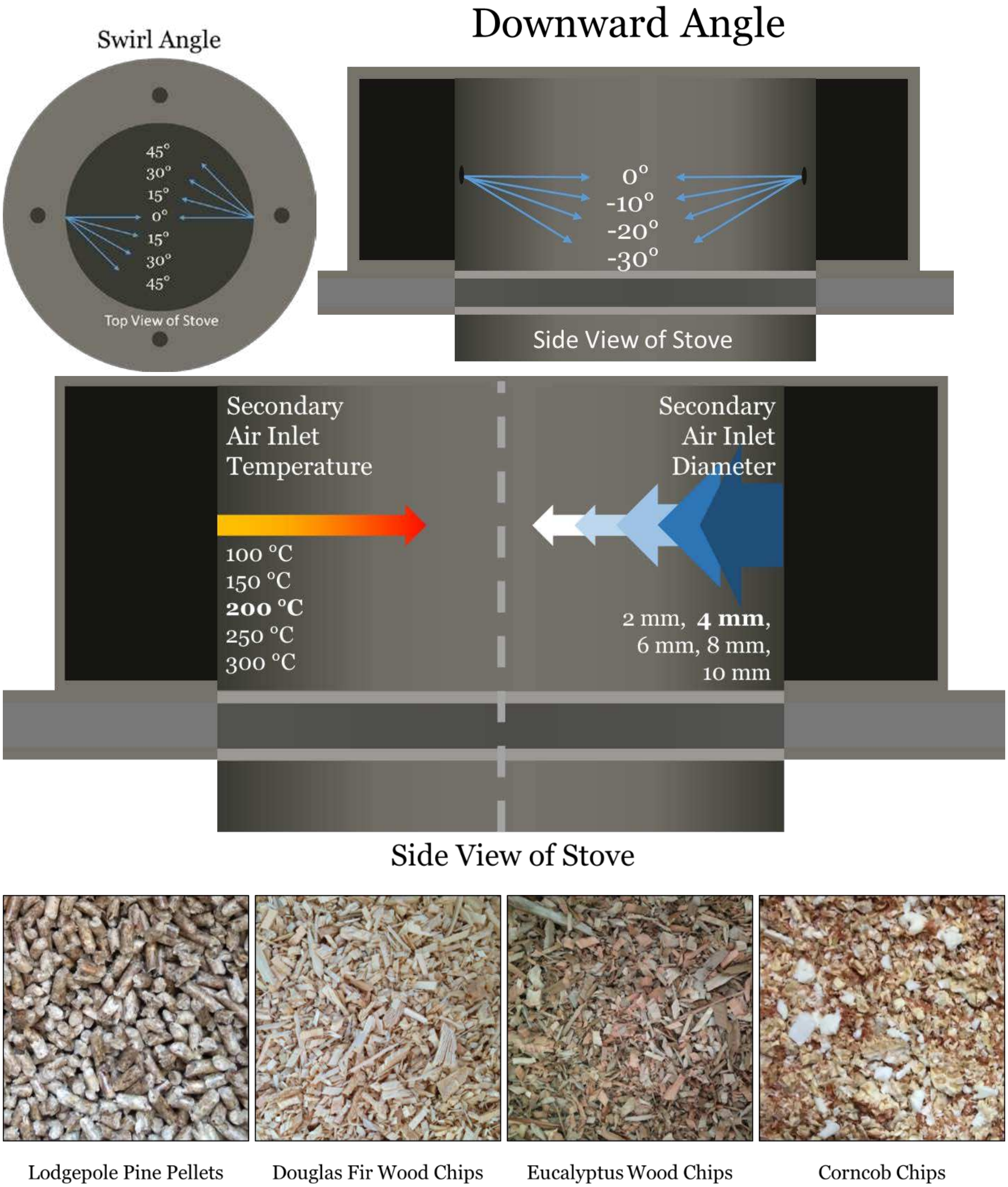

Figure 10 - P0 test parameters. (top left to bottom right) Swirl angle, downward angle, secondary air temperature, secondary air inlet diameter (and subsequently velocity), and fuel stocks.

Analysis of data and Results

All data is post-processed using code written in MatLab™. Raw CO and PM2.5 emissions data are post processed to generate the normalized integrated emissions needed to compare the performance of the stove to the ISO-IWA emissions tiers using Equation 1 and Equation 2 below.

Equation 1: Integrated CO emissions normalized for energy delivered to the cooking pot

$$CO_{HP,Normalized} = \frac{\int_0^t X_{CO}\left(\frac{M_{CO}}{M_{air}}\right)\dot{V}\rho_{air}dt}{m_{H_2O,i}C_{H_2O}\left(T_f - T_i\right) + h_{fg,H_2O}\left(m_{H_2O,f} - m_{H_2O,i}\right)}$$

Equation 2: Gravimetric PM2.5 emissions normalized for energy delivered to the cooking pot

$$PM_{2.5\ HP,Normalized} = \frac{\Delta m_{filter}\left(\frac{A_{probe}}{A_{duct}}\right)}{m_{H_2O,i}C_{H_2O}\left(T_f - T_i\right) + h_{fg,H_2O}\left(m_{H_2O,f} - m_{H_2O,i}\right)}$$

The numerator of Equation 1 is the total mass flow of Carbon Monoxide exhausted from the stove during a phase. X_{CO} was defined as the mole fraction of CO in the exhaust, M_{CO} and M_{air} are the molecular weights of CO $\left(28.01\frac{kg}{kmol}\right)$ and air $\left(28.97\frac{kg}{kmol}\right)$ respectively. $\dot{V}$ was the total volumetric flow through the hood in $\frac{m}{s}$, ρ_{air} is the density of air in in the hood. Moreover, the entire term was integrated from the start of the phase to the end of the phase to determine the entire mass of CO generated during the phase.

The numerator of Equation 2 defined the total mass of $PM_{2.5}$ generated by the stove during the phase. Δm_{filter} was the total change in mass of the 47-mm Teflon filter during the phase. $\left(\frac{A_{probe}}{A_{duct}}\right)$ was the ratio of isokinetic probe area to duct area, where A_{probe} was the cross sectional area of the tip of the PM probe located in the exhaust and A_{duct} was the cross sectional area of the exhaust duct on the laminar fume hood.

The denominator for both Equation 1 and Equation 2 are the useful power. Useful power was defined as the change in energy of the water in the cooking pot. The total change in energy of the water in the cooking pot was the sum of the energy addition, which increased the temperature of the water in the pot from the starting temperature to the ending temperature, and the energy addition, which resulted in a change in phase of the water, which vaporized during the test. In this case, the first half of the denominator,$m_{H_2O,i}C_{H_2O}\left(T_f - T_i\right)$ is the energy required to change the temperature of the starting mass of water $m_{H_2O,i}$ from the initial temperature T_i to the final temperature T_f, where C_{H_2O} is the specific heat of water $\left(4.179\frac{kJ}{kgK}\right)$. The second half, $h_{fg,H_2O}\left(m_{H_2O,f} - m_{H_2O,i}\right)$ is the energy required to vaporize the water that was evaporated during the phase, where h_{fg,H_2O} is the specific heat of vaporization of water $\left(2257\frac{J}{kg}\right)$, and $\left(m_{H_2O,f} - m_{H_2O,i}\right)$ is the mass loss of water during the test, wherein $m_{H_2O,f}$ and $m_{H_2O,i}$ were the ending mass and starting mass of liquid water in the pot respectively.

Average useful power output is calculated using equations similar to those used by Huangfu et al. Average useful power output was calculated using Equation 3

Equation 3: Useful power output from the cookstove

$$P_{useful} = \frac{m_{H2O_{initial}} * C_{H2O} * (\Delta T_{water}) + h_{fg_{H2O}}(\Delta m_{water})}{t_{elapsed}}$$

Where $m_{initial}$ was the initial mass of the liquid water in the pot measured in g, C_{H2O} is the specific heat of water in $J * (g * K)^{-1}$, ΔT_{water} was the change in temperature in ΔK of the water from the beginning of the test phase to the end of the test phase, $h_{fg_{H2O}}$ is the heat of vaporization of water in $J * g^{-1}$, $t_{elapsed}$ is the time elapsed from the start of the test phase to the end of the test phase in seconds.

The average rate of dry sold fuel consumption was calculated using Equation 4.

Equation 4: Average dry solid fuel consumption rate during operation.

$$\dot{m}_{solid\ dry\ fuel} = \frac{m_{solid\ fuel} * (1 - MC_{fuel})}{t_{elapsed}}$$

Where $m_{solid\ fuel}$ was the total mass of fuel at the start of the test phase in g, MC_{fuel} is the moisture content of the fuel as weight % on a wet basis, and $t_{elapsed}$ is the time elapsed between the beginning of the test phase and the end of the test phase.

Carbon Monoxide Results

The modular TLUD stove test data are analyzed to explore the effect of each variable on the carbon monoxide emissions during each phase. CO emissions are normalized against energy delivered to the pot with units of g/MJ_d. In the figures below the baseline test case is noted by black symbols, triangles correspond to phase 1 results and circles correspond to phase 2 results. The results grouped by the parameters varied. It is important to note that phase 1 and phase 2 data shown in the plots below are jittered around the nominal test values to ensure that the error bars and symbols from one phase do not obscure the symbols of the second phase. Error bars represent 90% confidence interval.

The data shown in the left plot of

Figure 11 are normalized CO emissions as the primary airflow rate varies from 15 g/min to 30 g/min. The data in the right plot of

Figure 11 are the normalized CO emissions for test cases where the secondary to primary airflow ratio varies from two (2) to five (5).

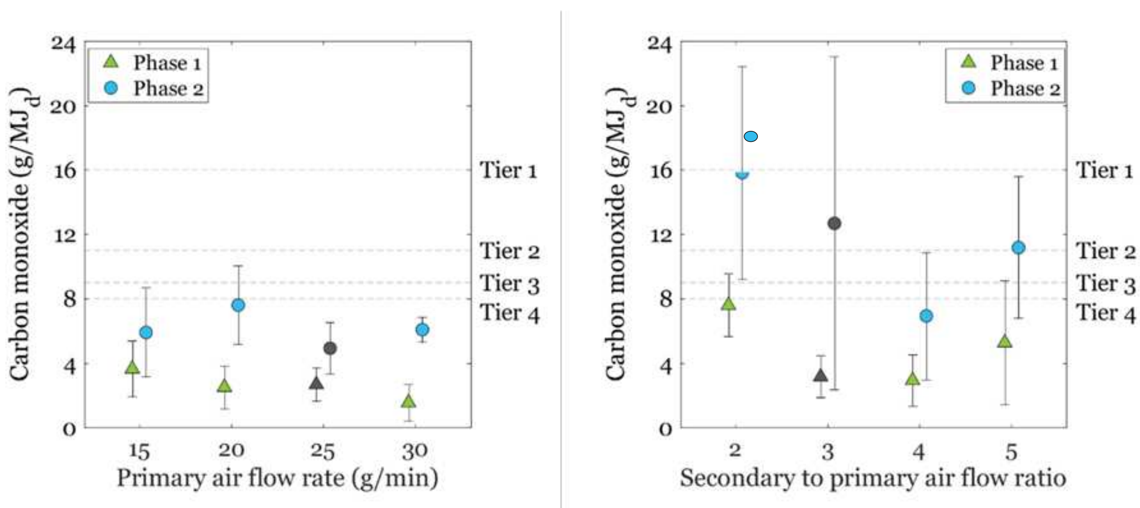

Figure 11 - Normalized CO emissions vs. Primary airflow and secondary to primary airflow ratio rate in a modular laboratory TLUD semi-gasifier cookstove. Baseline test case data indicated by the gray symbols. Jitter added to the x-axis data to increase legibility. CI=90%.

For tests where primary airflow rate varies, the baseline condition is 25g/min. For all test cases where the primary flow rate is varied, the secondary to primary airflow ratio is maintained at the baseline value of three (3). All other test variables are at baseline values.

No significant differences in the CO emissions data for flow rates from 15 g/min to 30 g/min in either Phase 1 or Phase 2 are here measured. All phase 1 data exceed the tier 4 guideline, and the mean values for all phase 2 data also exceed the tier 4 guidelines though the variation in test data make a significant conclusion for tests cases where the primary air flow was 15 and 30 g/min difficult.

Based on the analysis of this data secondary to primary airflow ratio may influence the mean CO emissions during both phase 1 and phase 2. For both phases, the trend of the mean data is a bathtub curve with a minimum being located between the primary airflow ratio of 2:1 and 5:1 with the baseline being located at 3:1. Phase 1 data yields significant differences between the ratios of 2:1 and 3:1. Phase 2 normalized CO emissions results trend with, but are generally higher than, phase 1 emissions. There is considerably more variability in the data generated during phase 2 than in phase 1. Observed variance in the mean for both phases show the minimum CO emissions located between secondary to primary airflow ratios of 3:1 and 4:1. Between the secondary to primary airflow ratios of 3:1 and 4:1 tier 4 performance was achieved in phase 1 and phase 2.

The effects of the secondary air injection angle, varied radially and axially, on normalized CO emissions are investigated using data displayed in

Figure 12. The plot on the left shows the effect of secondary air swirl angle. Swirl angle is the angle of the secondary air injection hole as measured from the radial direction of the secondary air injection ring in the plane perpendicular to the body of the stove. Injection angles varied from 0° to 45° in 15° increments are investigated. All other controlled variables are maintained at the baseline values for these experiments.

Changing the swirl angle from 0° to 15° had no statistically measurable effect on the CO emissions from the stove for both phase 1 and phase 2. The increase in swirl angle from 15° to 30° resulted in a significant increase in CO emissions during phase 1 but no statistically significant affect on the emissions during phase 2 compared to baseline emissions or 15° swirl. Increasing the swirl from 30° to 45° resulted in a slight reduction in emissions during phase 1 but had no statistically significant affect on the emissions during phase 2.

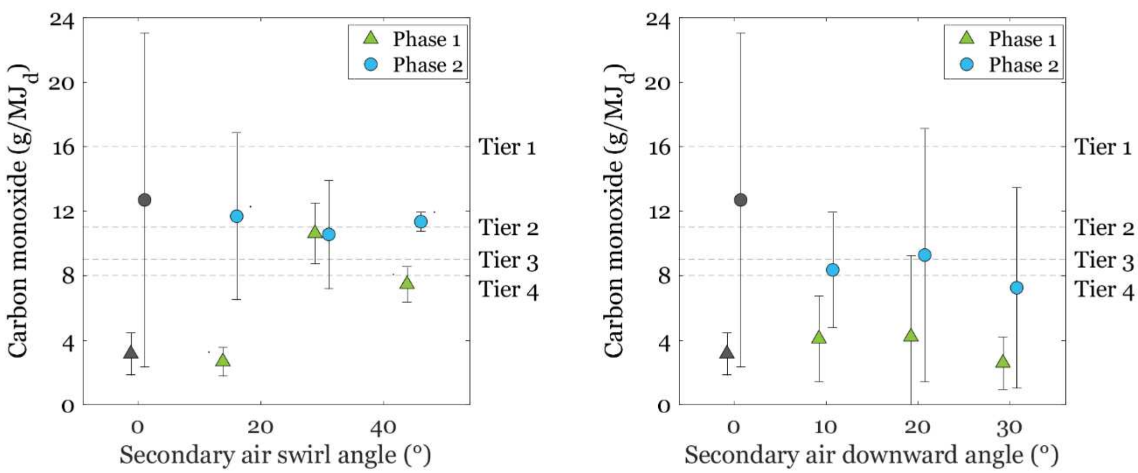

Figure 12 – Normalized CO emissions vs. radial and axial secondary air inlet angle in a modular laboratory TLUD semi-gasifier cookstove. Baseline test case data indicated by the gray symbols. Jitter added to the x-axis data to increase legibility. CI=90%

The injection angle varies from horizontal 0° to 30° down from horizontal in 10° increments. The plot on the right side of Figure 12 is the relationship between the downward angle of the secondary air injection and CO emissions. No statistically significant relationship between the downward angle and Phase 1 CO emissions or Phase 2 CO emissions was detected. In nearly all test cases, regardless of the injection angle the mean emissions of CO were observationally lower than those CO emissions measured during phase 2.

Both fuel type and moisture content are evaluated to determine the effect those variables have on the emissions and performance of the stove. The effect of fuel type and moisture content of the fuel on the normalized CO emissions are shown in the left and right plots of Figure 13 respectively.

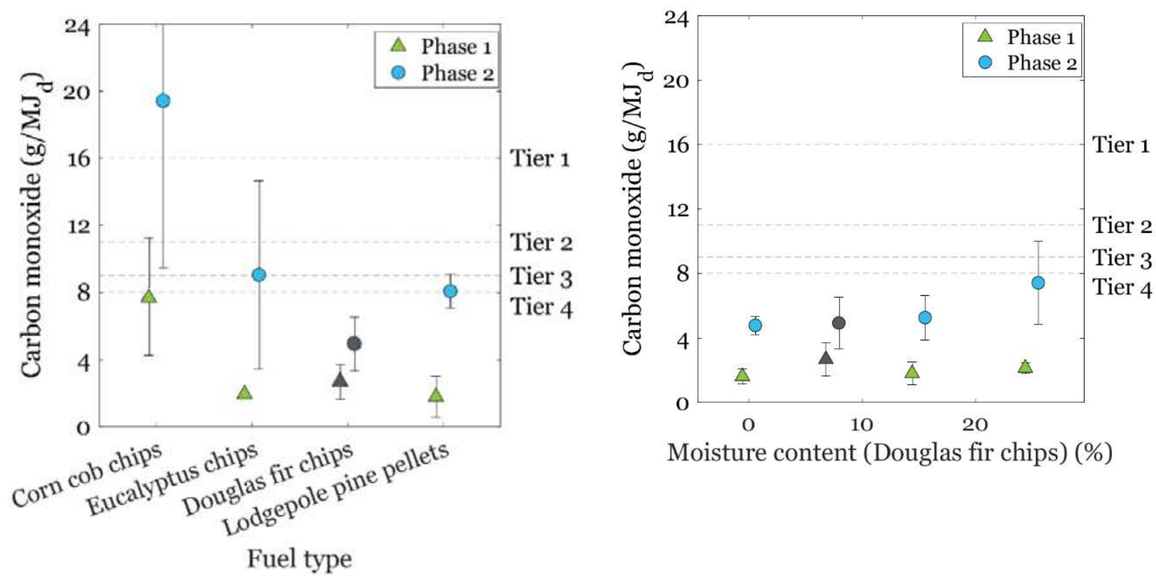

Figure 13 - Normalized CO emissions vs. fuel type and moisture content for Phase 1 and Phase 2, with ISO-IWA Tier levels indicated. Baseline test case data indicated by the gray symbols. Jitter added to the x-axis data to increase legibility.

The data indicate that normalized emissions of CO can be dependent on fuel type. The plot of Normalized CO emissions versus fuel type demonstrates the statistically significant differences in CO emissions during tests with corncob chips compared to tests with wood fuels during Phase 1. No statically significant CO emissions are detected between wood fuel types during Phase 1. As with Phase 1, the corncob chips produce significantly higher emissions when compared to most of the wood fuels. The exception being the Eucalyptus chips which produce more CO emissions than other wood fuels and is subject to more variability as well. Another interesting point is that, while Lodgepole pine pellets perform similarly to Douglas fir wood chips and Eucalyptus wood chips during phase 1, the pellets performed significantly worse than the Douglas fir chips under phase 2 conditions.

The effect that the moisture content of Douglas fir wood chips varied from 0% to 25% on a dry basis has on the normalized CO emissions is estimated using data displayed in the plot on the right side of Figure 13. No significant difference in CO emissions is detected for Phase 1 as moisture content was varied. However, Phase 2 moisture content CO emissions results yield a potential trend of increasing emissions with increasing moisture content.

The normalized CO emissions with respect to changes in secondary air inlet temperature and secondary air inlet velocity (area) are displayed in the left and right plots of Figure 14 respectively. No statistically significant difference in normalized CO emissions are observed for phase 1 conditions where the inlet temperature of the secondary air is varied from $100°C$ to $300°C$ in 50℃ increments.

For test configurations where the flow rate of the secondary is held at constant, the variation in hole size resulted in a variation in a change in the velocity of the air entering the secondary combustion stage of the stove. Test cases where the stove was equipped with the 10-mm diameter secondary air inlet jets and subsequently the lowest secondary air jet velocity, had the highest CO emissions during Phase 1 and Phase 2. Once the velocity is higher than $1\ m/s$ in test cases with the hole size of 8 -mm and smaller, there are no statistically significant dependency of the CO emissions on hole size or jet velocity for either phase.

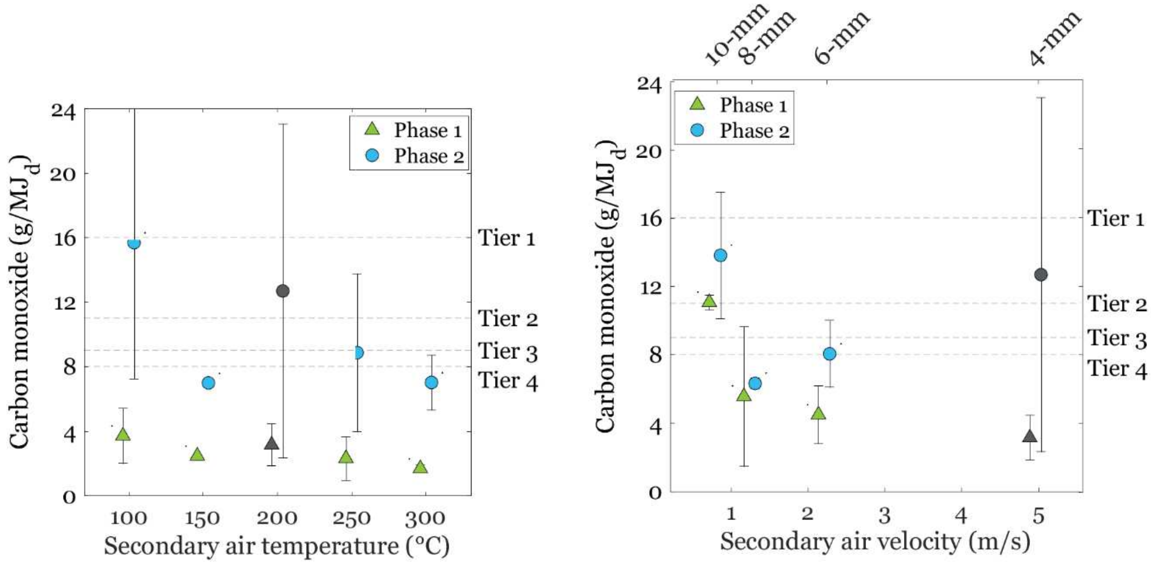

Figure 14- Normalized CO vs. Secondary Air Temperature, and CO vs. secondary air injection velocity in a modular laboratory TLUD semi-gasifier cookstove. Baseline test case data indicated by the gray symbols. Jitter added to the x-axis data to increase legibility.

Pot gap is the distance between the cooking pot and the top of the stove and defines the flow path of combustion gases as they pass out of the stove and transfer energy to the cooking pot. In this experimental setup, the pot is suspended over the stove using independent pot support to prevent the mass change of the pot due to evaporation during the test from affecting the real-time mass measurement of the fuel consumption. There is no integrated pot supports thermally connecting the pot and stove. The only obstruction in the flow path between the top of the stove and the pot are four ¼ - 28 stainless steel hex head screws which hold the bare thermocouples used to measure the exhaust gas temperature in the flow path. The pot gap varies between 15-mm and 45-mm in 15-mm increments. As observed in the data in Figure 15 no statistically significant difference in CO emissions is detected between the three tested pot gaps. However, as in many other test cases, there is an observed difference between the emissions of CO in Phase 1 with the CO emissions in Phase 2 for each test case.

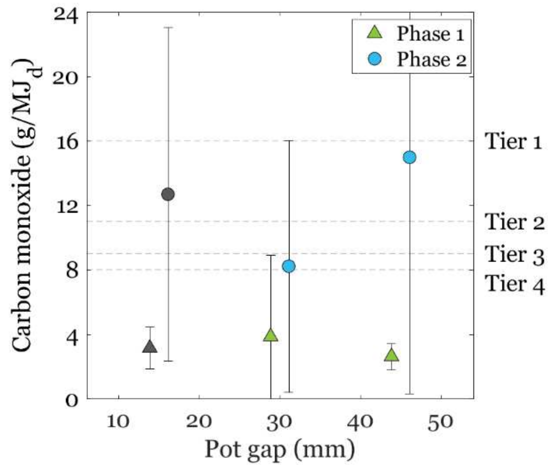

Figure 15 – Normalized CO Emissions vs. Pot Gap in a modular laboratory TLUD semi-gasifier cookstove. Baseline test case data indicated by the gray symbols. Jitter added to the x-axis data to increase legibility.

In addition to the previously discussed variables, several other variables are evaluated for their effect on CO emissions. The additional configurations here evaluated are secondary air holes reduced to 2 -mm in diameter, an insulated chimney section the same diameter as the inner combustion chamber and 100 -mm in height, insulated with a ½ -inch thick calcium silicate insulation and an aluminum radiation shield encapsulating the insulation. Early secondary air injection, which introduced 10% of the secondary airflow 2 inches below the primary combustion stage to induce mixing and turbulence in the rising pyrolysis gases before they entered the secondary combustion stage. A 2.5" constriction located between primary combustion stage and the secondary combustion stage, and a 2.5" constriction located after the secondary combustion stage. As with the other test cases, only one variable of the stoves configuration is changed at a time, and all other test variables are set to the baseline values.

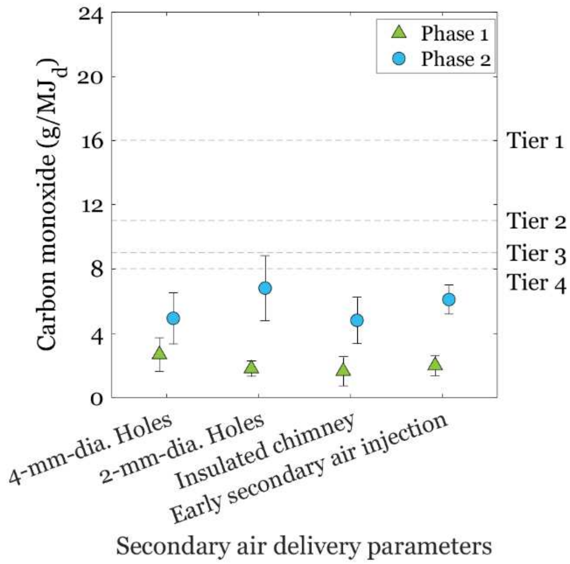

Figure 16- Normalized CO emissions vs. other stove configurations including 2-mm secondary air inlet holes, insulated chimney section following the secondary combustion region, early secondary air injection holes, and constriction rings located between the fuel bed and the secondary combustion zone, as well as a constriction ring located after the secondary combustion zone. Baseline test case data indicated by the gray symbols. Jitter added to the x-axis data to increase legibility.

The effect of each of these variables on the normalized CO emissions are here evaluated using the data displayed in Figure 16 . No statistically significant difference in CO emissions when compared to the baseline in either Phase 1 or Phase 2. The addition of a constriction either before or after the secondary combustion stage makes the stove significantly more difficult to use as it reduces access to the fuel bed making ignition more difficult as well as cleaning.

Particulate Emissions Results

The modular TLUD stove test data are analyzed to explore the effect of each variable on the particulate matter ($PM_{2.5}$) emissions. As with the CO emissions discussed in the previous section, $PM_{2.5}$ emissions are normalized against energy delivered to the pot as mg/MJ_d. In the figures below the baseline test case is noted by black symbols, triangles correspond to phase 1 results and circles correspond to phase 2 results. The results are grouped by the parameters varied. It is important to note that Phase 1 and Phase 2 data shown in the plots below are jittered around the nominal test values to ensure that the error bars and symbols from one phase do not obscure the symbols of the second phase. Error bars represent 90% confidence intervals and the asymmetry seen in the error bars stems from the Logarithmic scaling of the Y-axis not asymmetric error bounds.

The effect of fuel type and the effect of moisture content on $PM_{2.5}$ emissions are shown in the left and right plots of Figure 17 respectively. A statistically significant difference in $PM_{2.5}$ emissions result from different fuel types. Corn chips being the fuel with the highest mean emissions of $PM_{2.5}$ and Lodgepole pine pellets with the lowest. In both phase 1 and phase 2, a statistically significant difference between the emission of $PM_{2.5}$ when operating the TLUD on corn chips, and operating the TLUD on Lodgepole pine pellets is observed. With the exception of the Lodgepole pine pellets phase 1 resulted in lower PM emissions when compared to phase 2 emissions of the same fuel type. The difference between the emissions of Douglas fir wood chips and Lodgepole pine pellets lacks statically significant resolution. As with most other test cases, the data generated from Phase 2 also lacks statistic resolution, stemming from large distributions of test emissions during Phase 2 stove operation.

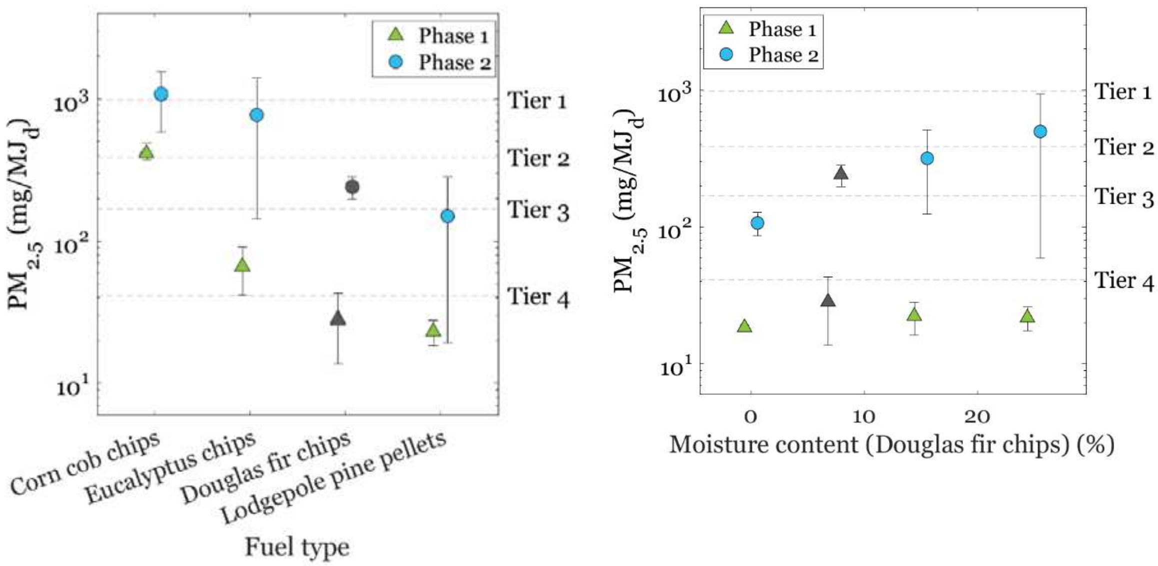

Figure 17 - $PM_{2.5}$ emissions vs. fuel properties in a modular laboratory TLUD semi-gasifier cookstove. Fuel type and moisture content vary and the effect of the changes on $PM_{2.5}$ emissions are quantified. Baseline test case data indicated by the gray symbols. Jitter added to the x-axis data to increase legibility.

The plot on the right side of Figure 17 is normalized $PM_{2.5}$ data for test cases where the moisture content of the Douglass fir varies. The 0% nominal moisture case was Douglas fir chips which were kiln dried and preserved in an airtight container until immediately prior to use. The test case with a nominal moisture content of 7% was the moisture content of the Douglass fir chips stored at laboratory ambient conditions. The cases with moisture contents of 15% and 25% were prepared by immersing the chips in liquid water and then kiln drying the chips to the desired moisture content using mass to compute the moisture content. These data indicate that moisture content does not affect the mean phase 1 emissions of $PM_{2.5}$ with any resolvability. Phase 2 data also lacks resolution between the data, there is an observed correlation between the moisture content of the fuel and the rate of emissions of $PM_{2.5}$. The phase 2 results indicate that 0% moisture content produces lower $PM_{2.5}$ emissions than does the 7% case with good resolution. Increasing the moisture content to 15% and 25% causes a significant increase in variability in the test data, which prevents further confidence in the trend of increasing $PM_{2.5}$ emissions with increasing moisture content.

While data indicate that fuel type and moisture content play a role in $PM_{2.5}$ emissions other factors lacked significant measureable affect on the emissions of $PM_{2.5}$ from the modular TLUD stove. The data in Figure 18 are Normalized $PM_{2.5}$ emissions data for test cases where different stove configurations and varying primary airflow rate were used.

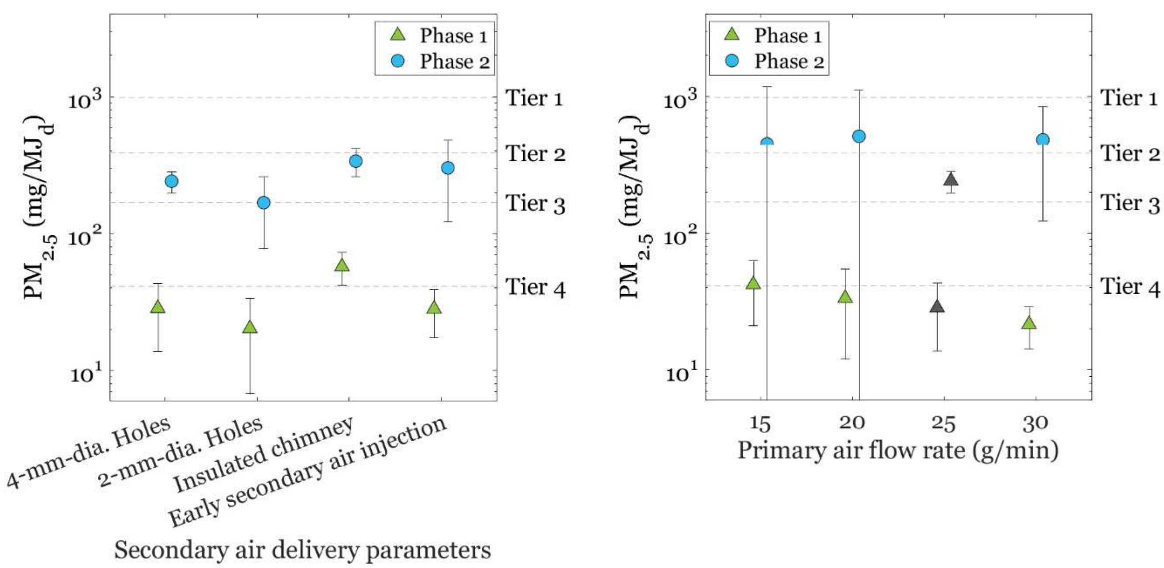

Figure 18 - The effect of stove design and operating parameters on $PM_{2.5}$ emissions in a modular laboratory TLUD semi-gasifier cookstove. Baseline test case data indicated by the gray symbols. Jitter added to the x axis data to increase legibility.

With the exception of the additional chimney, stove configuration and primary airflow rate did not affect the normalized $PM_{2.5}$ emissions. The addition of the insulated chimney, increases the normalized $PM_{2.5}$ emissions from the stove. As before, except where obscured by unusually large confidence intervals, the emissions of $PM_{2.5}$ is measurably lower in Phase 1 than that of Phase 2.

Power Output Results

Power output is another significant result because it is indicative of the stoves emissions performance and stability during different cooking tasks. There are two different cooking tasks, high power cooking, and low power simmer. During high power cooking tasks, the user is generally attempting to bring the cooking pot to temperature as quickly as possible while a simmer operation intends to hold the cooking pot at a constant temperature. Turndown on gasifier stoves is typically achieved by adjusting the flow rate of primary air flow while attempting to hold the secondary to primary air flow ratio constant. There are other factors which can influence power output from a stove including fuel type and composition, the bulk density of the fuel bed. And the surface area of the fuel used. It is also important to note that power output is not the only factor in achieving a high useful power performance from a stove; other factors include stove efficiency and time to steady-state operations.

Figure 19 contains plots of the effect of fuel type and moisture content on useful power output from the modular laboratory TLUD semi-gasifier stove. The plot on the left side of

Figure 19 shows the influence of fuel type on the power output. As fuel quality increases the power output generally increases as well. Corn chips which produced the worst emissions, also produce the lowest power outputs, followed by eucalyptus chips, Douglas fir chips, and finally Lodgepole pine pellets. For all cases except the very dense Lodgepole pine pellets, the difference between phase 1 and phase 2 power output is not statically resolvable. Generally, a cold start will have slightly lower useful power output due to the thermal losses associated with heating up the stove from ambient temperature to operating temperature. The thermal losses to the stove body are less significant during the hot start portion of the test because the starting temperature of the stove is significantly higher than the ambient temperature.

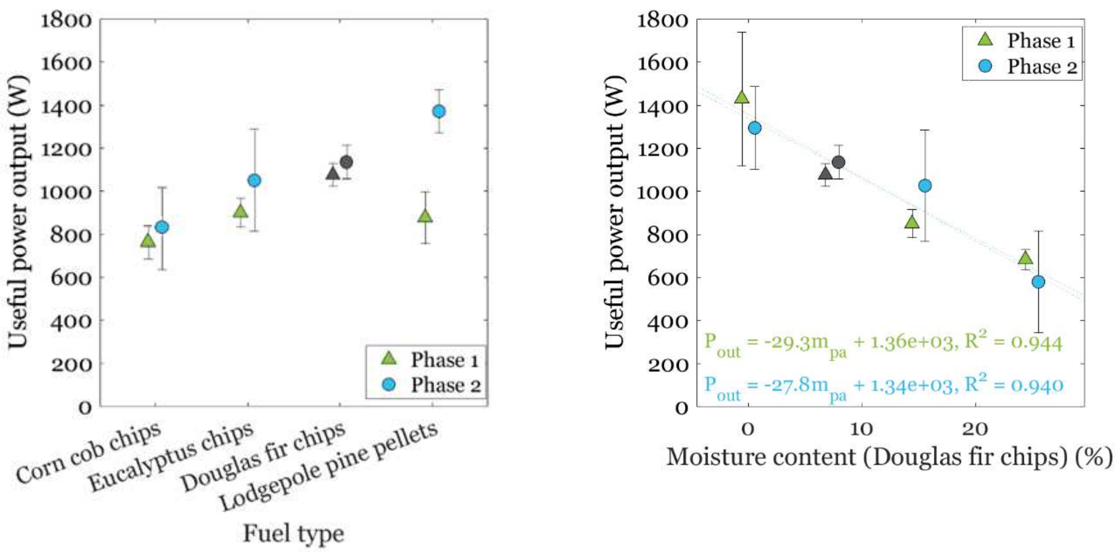

Figure 19 - The effect of fuel type and moisture content on useful power output in a modular laboratory TLUD semi-gasifier Cookstove . Linear regression is applied to Phase 1 and Phase 2 moisture content data. Baseline test case data indicated by the gray symbols. Jitter added to the x-axis data to increase legibility.

In the case of Lodgepole pellets, it is observed that phase 1 has a significantly lower useful power output than in phase 2. This is likely due to the much longer time to steady state operations when using the very dense Lodgepole pellets when compared to the less dense chipped fuels. During phase 2 of tests with the Lodgepole pine pellets the stove and fuel bed is preheated before adding the fresh fuel, reducing the time to steady state operations and producing higher useful power outputs. The plot of useful power output vs. moisture content on the right side of

Figure 19 shows that there is statistic relationship between the moisture content of the fuel and the useful power output. The relationship between moisture content and useful power is nearly identical for both phase 1 and phase 2. The fit has an r^2 of 0.94 for both cases, increasing the moisture content from 0% to 25% results in a reduction of the power output by approximately 50%.

Though fuel type and moisture content played a significant role in power output from the stove, examining data in Figure 20 suggests that stove configuration and pot gap do not.

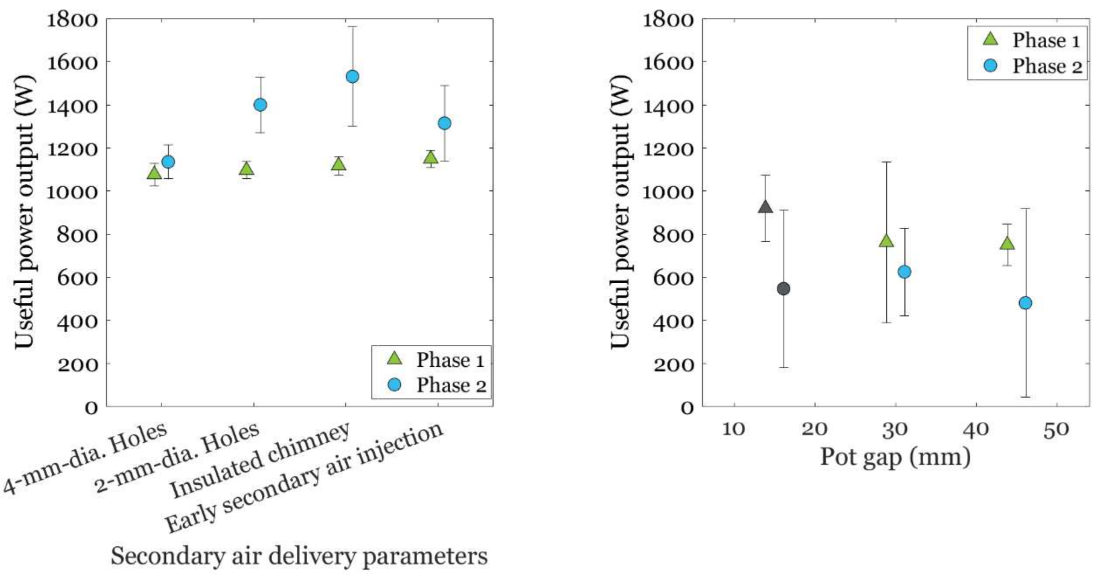

Figure 20 - Useful power output vs. stove configuration and pot gap in a modular laboratory TLUD semi-gasifier Cookstove. Baseline test case data indicated by the gray symbols. Jitter added to the x-axis data to increase legibility.

The plot on the left side of Figure 20 indicates that there is little observed variation in the phase 1 power output between the stove configurations, while there is a 22% and 30% increase in useful power output between baseline and the 2-mm hole test case and the insulated chimney case respectively during phase 2. There also exists a well-defined difference between phase 1 and phase 2 for the test cases using the 2-mm secondary air inlet holes and the insulated chimney, but no strong difference between phase 1 and phase 2 for the other stove configurations.

From the data plotted on the right side of Figure 20, it can be observed that adjusting the pot gap from 15 -mm to 45-mm in 15-mm increments has no measurable effect on the power output of the stove under these conditions.

The most important plot in the useful power output dataset is displayed in Figure 21. The primary airflow is the main user input in controlling gasifier stove power output. The turndown ratio, which is defined as the ratio between maximum and minimum firepower is the design parameter which makes the stove useful in a wide range of cooking applications.

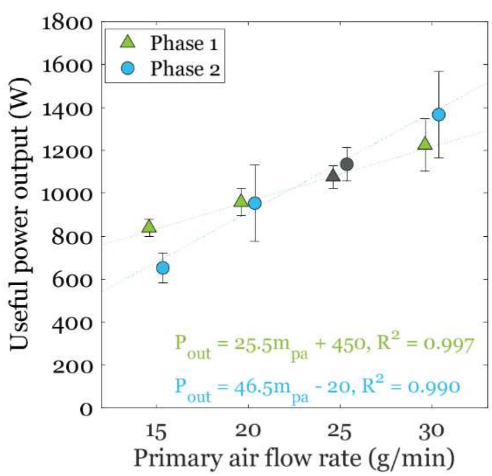

Figure 21 - Useful power vs. primary air flow rate in a modular laboratory TLUD semi-gasifier Cookstove. Phase 1 and Phase 2 are fitted with linear regressions. Baseline test case data indicated by the gray symbols. Jitter added to the x-axis data to increase legibility.

The primary airflow varies between 15 g/min and 30 g/min in 5 g/min incremets. The results indicate a strong dependence in primary airflow rate and the output of the stove. Power output for both Phase 1 and Phase 2 responded approximately linearly to changes in primary airflow rate over the range tested. Phase 1 has a slightly slower response rate than does Phase 2 as indicated by the shallow slope of Phase 1 (25.5) when compared to the more aggressive Phase 2 slope (46.5). The linear fits for both datasets have a strong statistical power as indicated by the r^2 value of 0.99 for both phases.

Equation 5 and Equation 6 are the results of a linear fit of the data and are useful for stove TLUD semi-gasifier Cookstove design. Once the power output requirement is determined, a similar equation can be used to calculate the airflow rate, which will provide the required output.

Equation 5: Phase 1 useful power output vs. mass flow rate of primary air in a modular laboratory TLUD semi-gasifier Cookstove.

$$\mathrm{P1_{UPO}} = 25.5\,\dot{\mathrm{m}}_\mathrm{p} + 450, \mathrm{r}^2 = 0.997$$

Equation 6 Phase 2 useful power output vs. mass flow rate of primary air in a modular laboratory TLUD semi-gasifier Cookstove.

$$\mathrm{P2_{UPO}} = 46.5\mathrm{m_p} - 20, \dot{r}^2 = 0.990$$

Equation 5 and Equation 6 are only relevant to the modular laboratory TLUD stove operating on chipped Douglas fir fuel. Other empirically derived relationships need to be produced for different stove configurations and fuel types.

Laboratory Modular TLUD Conclusions

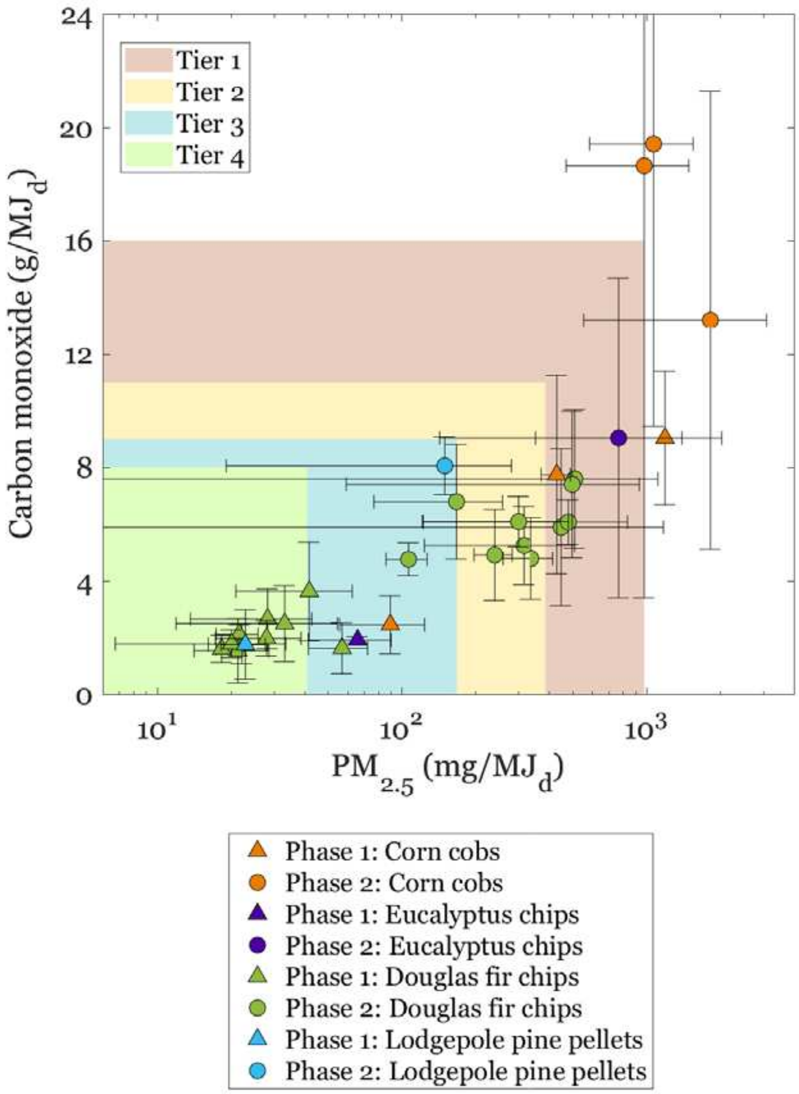

Figure 22 - Normalized CO vs. Normalized $PM_{2.5}$ with ISO-IWA tier boxes. A visual summary of high power emissions results from the Laboratory Modular TLUD semi-gasifier cookstove.

Figure 22 is a visual summary of the emissions results from the testing completed on the Laboratory Modular TLUD. It is critical to note that the author does not intend to show that there is any correlation between the emissions of CO and $PM_{2.5}$, this plot was chosen to display a larger picture of trending in emissions with different factors as they relate to the ISO-IWA tier system.

The colored boxes in the background define the boundaries of the ISO-IWA Tiers. Tier 4 is shown in green, followed by tier 3 in blue, phase 2 in orange, phase 1 in red, and phase 0 is white. The triangular symbols indicate Phase 1 results, while circular symbols indicate phase 2 results. Results shown in gray are those from tests using corn chips, results shown in purple are those from eucalyptus chips, green indicates the test cases using Douglass fir wood chips, and finally, the test cases shown in gold are tests which used Lodgepole Pine pellets.

There are several significant trends which should be noted. The first is the test cases which attained Tier 4 emissions in both CO and $PM_{2.5}$. All of the tests which fall in to this category used Douglass fir wood chips or Lodgepole Pine pellets. Note that all tests located inside the Tier 4 box are Phase 1 results. Even when using high quality fuel stock, Phase 2 never attained Tier 4 results for $PM_{2.5}$. Most Phase 2 results using wood fuels fall between Tier 2 and Tier 1 for $PM_{2.5}$ even when the CO emissions is Tier 4. Finally, test cases using corn chips had very poor performance with most test cases falling in the Tier 0 to Tier 1 range and even the best case for corn chips was still Tier 3 for $PM_{2.5}$.

These results lead to several conclusions, which influence stove design, and stove program development. The TLUD stove is capable of meeting the ISO tier 4 emissions targets under laboratory testing conditions in a number of stove configurations and operating conditions. It is worth noting here that laboratory test results may not be indicative of real world performance as it is a highly controlled environment and has some different objectives than that of preparing food. Under laboratory conditions, the researcher has additional control over the operating environment as well as instrumentation providing information to aid in stove operation.

There are a number of noteworthy and applicable conclusions, which may be drawn from the dataset generated from the Modular Laboratory TLUD Semi-Gasifier Cookstove. These conclusions have application in stove design, as well as informing the creation and management of cookstove programs intent on reducing indoor air pollution and improving global health.

One of the primary objectives of this work is determining the feasibility of a stove design that can meet the stringent ISO-IWA Tier 4 emissions guidelines. The results discussed above indicate that for a variety of stove operating conditions and fuel types Tier 4 emissions can be achieved using a TLUD semi-gasifier cookstove. When the stove is operating on Douglas fir chips or Lodgepole Pine pellets during Phase 1, CO and $PM_{2.5}$ emissions were tier 4 compliant, even when the stove configuration varied to include other, off the baseline stove configuration, such as smaller secondary air holes and early secondary air injection. Figure 22 illustrates the feasibility of a stove which can meet the tier 4 guidelines for emissions. A large number of test cases produced results that fall inside the tier 4 box in green.

If the stove is operating on off design fuels such as corncob chips, or eucalyptus chips the emissions fall well outside the Tier 4 guidelines, in the worst case, nearly 3 orders of magnitude higher than the cleanest fuels. The higher emissions associated with off design fuels indicated by orange and purple markers in Figure 22 fail to meet the tier 4 guidelines in either phase 1 or phase 2.

Another significant finding is that stove-operating procedure plays a significant role in stove performance. If the stove is operating in phase 1 where the stove is consuming fuel from the top down, and pyrolysis products pass through the hot fuel bed prior to entering the secondary combustion stage, the stove emissions generally meet the Tier 4 guidelines. However if fresh fuel is added to the top of a combusting fuel bed, and the hot pyrolysis gas passes through a cold fuel bed prior to entering the secondary combustion region, the emissions are, in some cases as much as 2 orders of magnitude worse than the same test configuration operating under phase 1. The variation between triangular markers generally clustered near the tier 4 and tier 3 boxes indicating phase 1 tests in Figure 22 and circular markers clustered in tier 2 through tier 0 boxes in Figure 22 indicates that the user has a significant role to play in ensuring low emissions cooking when using a gasifier cookstove.

Another significant finding from Figure 21 is that the TLUD Semi-gasifier stove design is capable of significant turndown, without compromising emissions performance. The test results show that CO emissions remained constant regardless of the primary airflow rate, even though there was a significant change in useful power output from the stove over the same primary air flow rates. It was also determined that there is a strong correlation between the primary airflow rate and useful power output (see Equation 5 and Equation

6). Thought these correlations only apply to the Laboratory Modular TLUD Semi-gasifier used in this study; a similar data set could be derived from data on any stove design to inform the primary airflow rate to meet the useful power output design criteria.

It should here be noted that phase 3 data is not considered in the context of this work. There are two reasons why the data collected during phase 3 are excluded from this text. Firstly, there was minimal effect on the emissions and performance of the P0 Laboratory Modular TLUD during phase 3 for all test cases evaluated. And secondly, fresh fuel rather than char burnout is used when evaluating the P1 and P2 prototype the simmer performance. This allows more control over the simmer phase initial conditions and the evaluation of the stove turndown ratio.

3. FIELD USABLE PROTOTYPES

P1 Transitional Laboratory TLUD

Testing the Modular Laboratory TLUD created a significant body of work identifying and quantifying variables that affect the performance characteristics of top-lit up-draft semi-gasifier stoves. The knowledge gained through testing the P0 modular stove must be translated to a standalone stove, which can be used for cooking to achieve relevance to the lives of those most affected by the hazards of cooking with solid fuels. Prototype stoves bridge the gap between the laboratory testing and real cooking practicality. The prototypes used for this work fall into two iterative categories defined as P1 and P2 prototypes. The P1 prototypes are tools for developing functionality similar to that of the Modular Laboratory TLUD, but using fewer supporting instruments, and components that are more mobile. While P2 prototypes are tools for assessing stove performance, specifically emissions and efficiency in addition to iterating the design aesthetic for production.

The first experiment is intended to explore the effect of moving from a pressurized air system to a fan-driven system. The modular test bed stove requires a source of pressurized air to drive flow through the primary and secondary air holes. This system is not practical for a stove suitable for use in the field. A field ready stove must contain a mechanism for providing air to the primary and secondary stages of the stove during operation.

There are two motivating techniques used to drive airflow through a gasifier stove. The first is buoyancy driven flow where a density gradient created by heat generated from combustion in the stove motivates airflow through the primary and secondary combustion stages of the stove. The second technique is a mechanically driven system relying on an electric blower or fan, which forces air through the primary and secondary combustion stages of the stove. The advantages and disadvantages of each method must be evaluated when considering a stove design.

The buoyancy driven method is straightforward and durable. It relies on fluid dynamics and heat transfer rather than mechanical systems to motivate airflow through the stove. A buoyancy driven system reduces cost because there are no electronics, a critical consideration when designing products for the developing world. It also improves the durability of the final stove by reducing the number of components in the stove. The disadvantage of the buoyancy-driven system is that a feedback loop exists between the thermally driven flow and the combustion process. If the heat generated by combustion is insufficient to drive the airflow required, there is no external forcing mechanism to provide the additional airflow. The user can manually reduce the airflow through a buoyancy-driven system using a louver, valve, or similar restriction as required for the cooking task.

A mechanically forced stove is more complicated and expensive than a similar buoyancy-driven stove. To mechanically force air through the stove a fan, blower or pump and the associated hardware for power and control are necessary. There are additional moving parts which must be factored into the overall system reliability as well. Generally, a mechanically forced system requires an external supply of power which may limit the market size and increase the cost of use. In spite of the cost and complexity, there are some distinct advantages over the buoyancy motivated airflow designs. In a mechanically forced system, the combustion process and the forcing mechanism are decoupled. The decoupling of the combustion process and the mechanically forced airflow simplifies the engineering to achieve specific airflow rates. Airflow through a mechanically forced stove is less transient than the buoyant stove designs. Mechanical systems are capable of producing greater pressure differentials, and as a result, higher flow rates and air inlet velocities when compared to buoyancy-driven counterparts. For both P1 and P2 prototypes, a mechanically forced design is chosen, as it will provide a more stable and controlled platform to evaluate stove designs. It is also capable of providing the pressure differential required to drive flow through the stove.

There are several options for electrical power. The first is a battery pack, which can power the fan, or blower and any other systems integrated into the stove. A battery is a reliable, robust, and relatively low-cost method of providing electrical power to the stove hardware. A battery requires an external electrical supply to charge after it has been depleted, which may be a wall plug, hand crank or solar panel. The fan hardware may also receive power directly from the electrical grid. Depending on the electrical access and power distribution reliability of the target market electrical grid, a wall plug may be an acceptable design decision. A third common option is a Peltier device or thermoelectric generator (TEG) This system is found on some stoves already available in the market such as the BioLite Homestove[58]. This device uses heat from combustion to generate electrical charge via the Peltier effect. TEG's do not require an external power supply but can be challenging to implement, as they are inefficient without a sufficient temperature differential across the device and are expensive to implement compared to battery packs and external power supplies.

A fan powered by a wall plug is has been chosen for both the P1 and P2 prototypes. The fan and wall plug offers the control required to develop the technology without adding significant complexity to the device. The wall plug is superior to the other options for this case because it provides the most reliable source of electrical power for development, eliminating battery charging and the required hardware and packaging constraints of integrating a battery into a final P2 prototype. A wall plug is preferred to a TEG in this application because the heatsink to source heat from combustion to power the electronics requires significant engineering, and if required can be incorporated into the design at a later time. The TEG heatsink may also interfere with fluid dynamics and heat transfer in the combustion chamber potentially influencing the repeatability of stove test data.

Experimental Setup

The first step in the design process is to establish plenum pressure maps for the desired flow rates. Then a fan can be specified which is capable of meeting those pressure specifications at the desired airflow rate. The P1 prototype is primarily used to generate this data and validate the feasibility of this design. A cross-sectional view with subsection and component callouts is displayed in Figure 23. The Modular Laboratory TLUD design strongly influences the geometry of the P1 prototype. The components of the stove are manufactured from 20g 304 stainless steel sheet, which was cut on a CNC waterjet formed, and assembled using TIG or spot welding except for the drip pan and the fan and compressed air adaptor plate, which were affixed using stainless steel screws. The two sealing surfaces, one at the top and one at the bottom are manufactured from high-temperature resistant graphite sheet. These seals prevent leakage from the common pressurized plenum. The P1 combustion chamber is 289-mm in height and has a diameter of 109-mm. The P1 prototype has nine primary, six early secondary, and 32 secondary air holes, all of which are 2-mm in diameter. The resulting secondary to primary air hole ratio is 4.2 to 1. The primary and secondary stages are supplied air by a common pressurized plenum formed by the space between the combustion chamber and the outer shell of the stove. A compressed air source or a fan can pressurize the common plenum. A mass flow controller (MCP-250SLPM-D, Alicat Scientific, Tucson AZ, USA) regulates the flow of compressed air when a compressed air source is used.

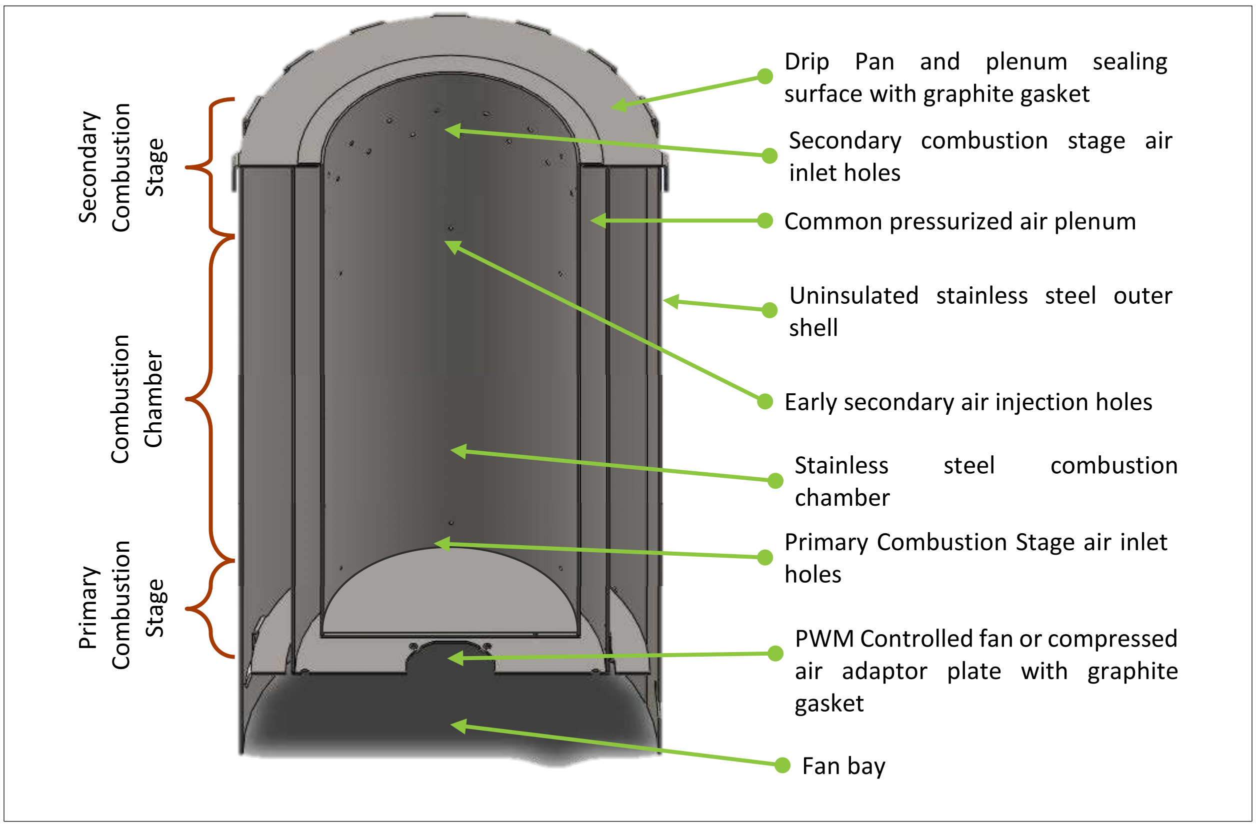

Figure 23 - *P1 TLUD cookstove cross-section with component callouts. Labels on the left side of the figure show the three subsections of the P1 TLUD cookstove prototype. Labels on the right side indicate the components of each subsection.*

A static pressure probe for making plenum pressure measurements is mounted in the bottom of the stove. Pressure measurements were made using a digital pressure calibrator (APC030C, Ametek, Berwyn, Pa, U.S.A).

Results

The initial test to map the plenum pressure of the P1 prototype to the airflow rate was completed using the P1 compressed shop air adaptor and varying the mass flow rate through the stove using an Alicat mass flow controller. The results of this test, shown here in Figure 25, are used to create a function, which allows the selection of a suitable fan and the calculation of flow rate from a known pressure. The tests were conducted under ambient laboratory conditions of 26°C and 86.74 kPa.

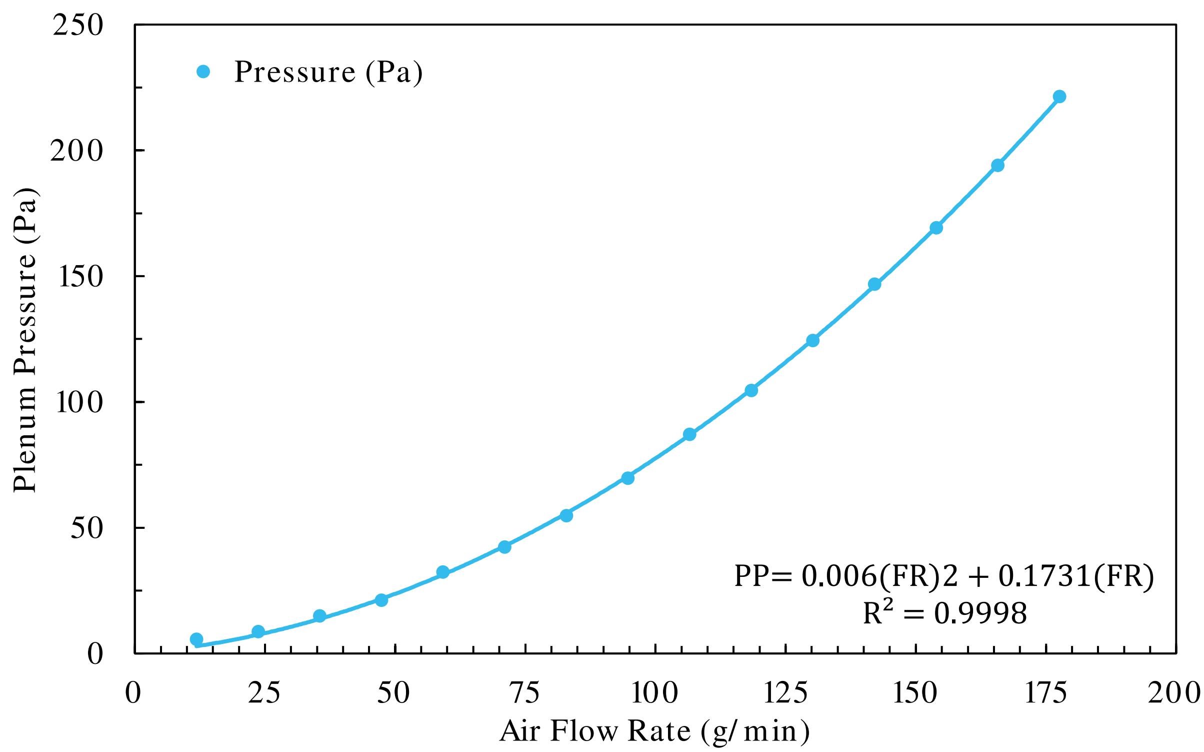

Figure 24 - P1 Prototype Plenum Pressure vs. Air Flow Rate

The fan-selected based on this data is a 12 VDC 40 by 40 by 28 –mm axial fan with integrated 5V PWM input and fan speed output (04028DA-12R-AUF, Nippon Miniature Bearing (NMB), Nagano, Japan). Several other fans were also evaluated but were deemed either underpowered or too loud for practical use.

The second function maps plenum pressure to the fan speed, controlled via a PWM signal. To generate this function, the NMB 04028DA-12R-AUF replaced the compressed air adaptor on the bottom of the P1 prototype using the 40-mm by 40-mm fan adaptor plate. The fan speed, varied using PWM to change the duty cycle, was mapped to the plenum pressure. A function of plenum pressure with respect to the duty cycle generated from this data is displayed in Figure 26.

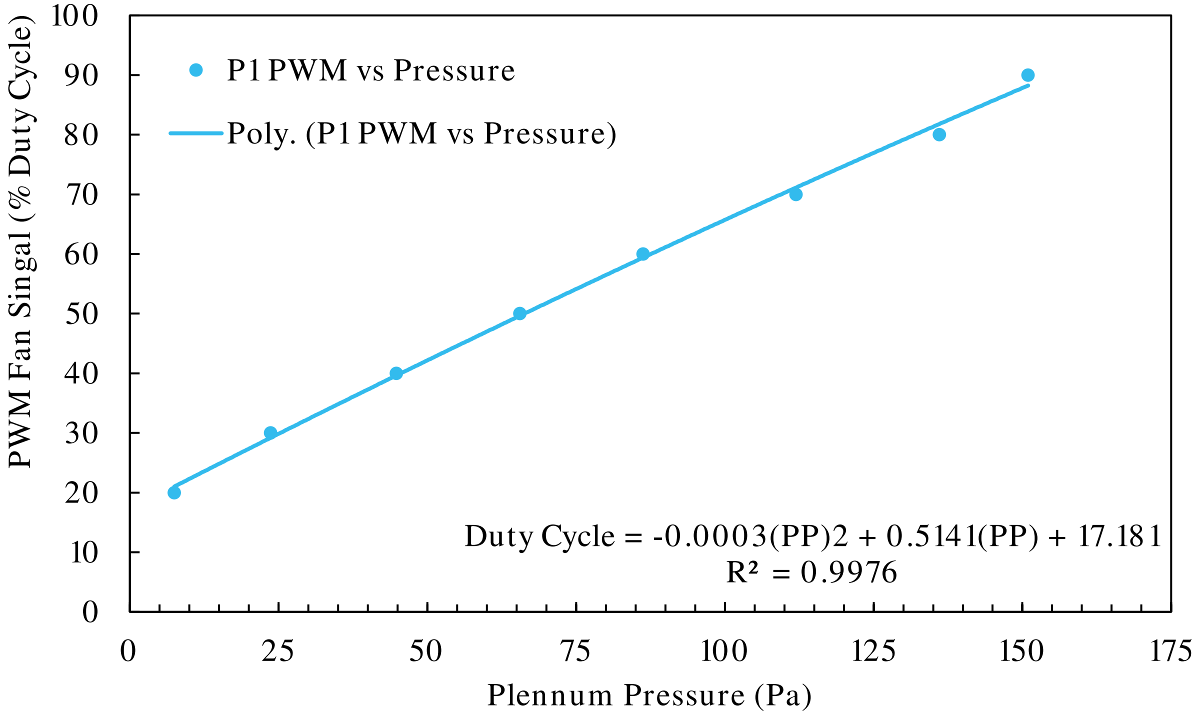

Figure 25 – P1 prototype plenum pressure vs. fan duty cycle

The PWM equation derived from the data in Figure 24 and the pressure equation derived from the data in Figure 25 solved as a system yield Equation 7, which can be used to set PWM to determine flow rates for this specific stove and fan combination.

Equation 7 - Flow equation derived from pressure and PWM maps

$$Duty\ Cycle = -0.0003\left(0.006(Flow^2) + 0.1731(Flow)\right)^2 + 0.5141(0.006(Flow^2 + 0.1731(Flow)) + 17.181$$

This equation is unique to each stove iteration and adjustments to the geometry will influence the terms of the equation

For this work P1 and P2 were developed in parallel with P1 being complete approximately 1 month before P2, therefore stove development proceeded using the P2 prototype as soon as it was available.

P2 Field Ready Prototype TLUD

The objective of the P2 prototype design is a stove that is ready for evaluation by end users. The P2 meets the criteria of a standalone device that does not require any external equipment beside power for the integrated fan and control electronics, is capable of performing cooking tasks with reasonable safety, and is aesthetically pleasing. Figure 25 is a cross-sectional view of the P2 prototype with component and design callouts. The P2 design is near production ready and has a number of design elements, which distinguish it from the simpler P1 prototype. It has integrated pot supports, CNC milled from aluminum billets. The pot supports are similar in design to what would be acceptable on a production stove. With the exception of the pot supports, all other steel components are cut from sheet steel on a waterjet. The sheet metal components are then formed and welded or riveted. The drip pan is a stamped sheet metal part, manufactured in-house. The original P2 prototype fuel chamber is assembled using spot welding rather than TIG welding as in previous prototypes to reduce the number of complex assembly procedures required to make the stove. The bottom of the combustion chamber is also an in-house stamped sheet metal component. All components in the combustion chamber and the path of combustion gasses are manufactured from 304 stainless steel. 304 stainless steel was chosen for its availability formability and for its high-temperature and corrosion resistance. Further cost reductions may be achieved by incorporating a lower cost material with acceptable corrosion and temperature resistance such as FeCrAl. A number of different fuel chamber designs were evaluated during the P2 development process. The baseline fuel chamber is similar to the P1 and P0 chamber geometries, except that the overall height of the fuel chamber is reduced to shorten the stove.

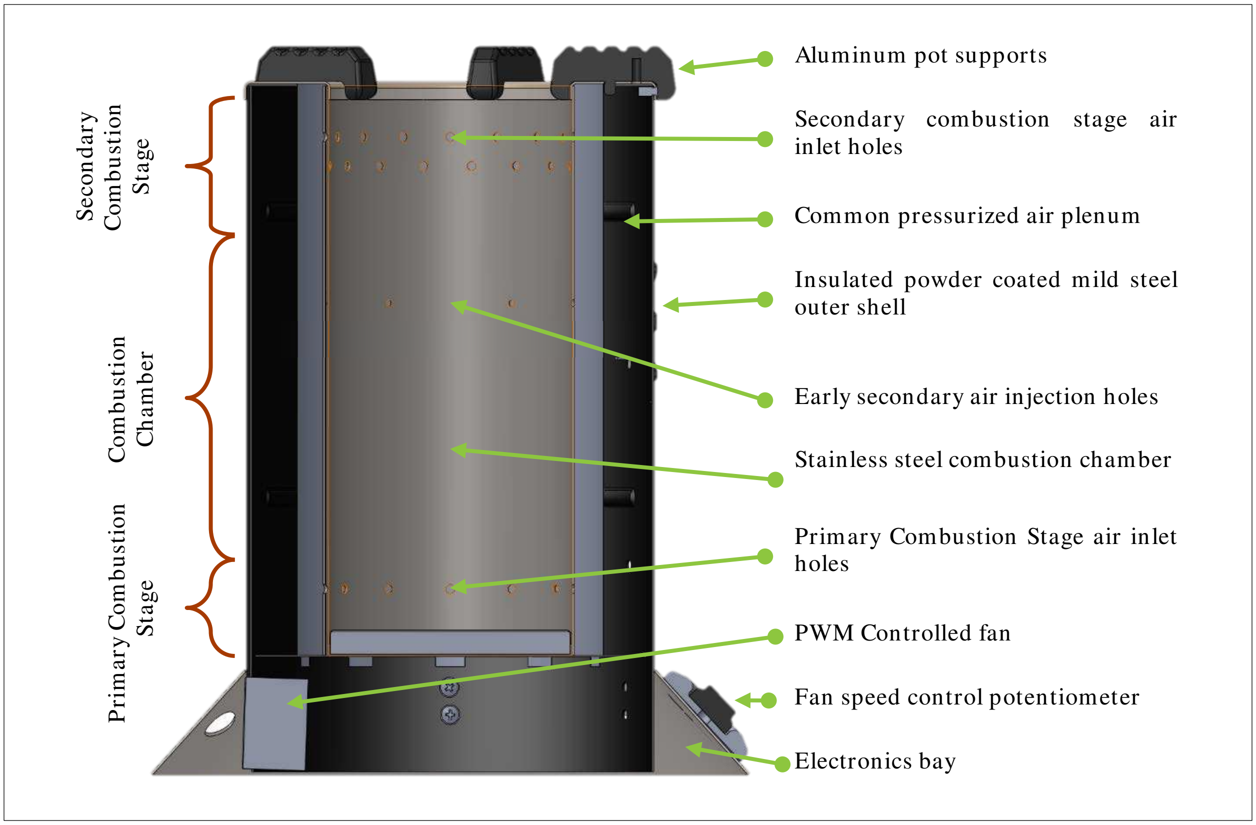

Figure 26 – P2 TLUD cookstove cross-section with component callouts. Labels on the left side of the figure show the three subsections of the P2 TLUD cookstove prototype. Labels on the right side indicate the components of each subsection.

The final version of the P2 fuel chamber is composed of two discreet chamber diameters, known hereafter as a varying geometry chamber (VGC) to aid in low power combustion stability without compromising the high power performance of the stove. Dimensions for both the baseline chamber and the VGC are found in Table 6 on page 129 .

The stove exterior is manufactured from 20ga mild steel and powder coated, reducing cost compared to an all stainless steel construction like the P1 prototype. A two-layer insulation system reduces heat transfer from the combustion chamber to the outer body of the stove improving safety and potentially reducing thermal losses that negatively affect thermal efficiency. This insulation system is made of a layer of 0.5” Insulfrax® Alkaline

Earth Silicate (ASE) low bio-persistence fiber blanket sandwiched between the inner surface of the outer shell of the stove and a polished aluminum radiation shield that makes up one of the walls of the plenum. Handles mounted to the body of the stove make moving and positioning the stove easier even when the stove is hot. Rolled features in the outer body of the stove provide a visual cue for where to handle the stove, keeping the user's hands away from the hot drip pan area, and above the center of gravity, as well as providing a more tactile grip when moving the stove. Unlike previous iterations, the base of the stove is larger in diameter than the main body of the stove improving stability. A frustum blends the larger base diameter to the main body of the stove and provides a place to mount the electronics package where radiant heat emitting from the fuel chamber during operation is less likely to damage the electronics.

The electronics package is schematically represented in Figure 27. AC wall power enters the circuit from a wall AC to DC converter (WSU120-1000, Triad Magnetics, Perris, CA, USA). The incoming DC power supply has a 10μF bypass capacitor to suppress high-frequency RF noise from the power supply. In addition to the 12VDC power required to drive the fan, a 5-VDC supply is required to power the microcontroller.

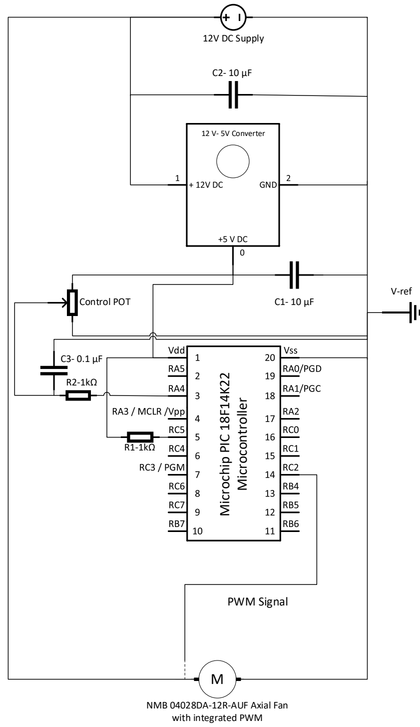

Figure 27 - P2 prototype electronics package schematic diagram.

For the purpose of powering the microcontroller, the incoming 12-VDC supply is converted to 5-VDC using a DC-to-DC converter (OKI-78SR-5/1.5-W36-C, Murata Power Solutions Inc., Mansfield MA., USA). The output from the DC-to-DC converter provides a 5VDC differential to pin 1(Vdd) and Pin 5 (RC5) across a 1kΩ regulating resistor on the PIC microcontroller (PIC18F14K22-I/P-ND, Microchip Technology, Chandler, AZ, USA). A 10kΩ linear response rotary potentiometer (POT) in series with a 1kΩ resistor provides the user input signal to pin 3 (RA4) on the PIC microcontroller. A 0.1μF bypass capacitor provides high-frequency RF noise suppression on the input signal from the POT. A 5-VDC square wave PWM signal generated by the PIC microcontroller is fed to the fan control terminal. The fan is a 12-VDC 40-mm by 40-mm by 28-mm axial fan with integrated 5-VDC PWM input and fan speed output (04028DA-12R-AUF, Nippon Miniature Bearing (NMB), Nagano, Japan) as specified from the P1 experiments.

All the components except the fan power supply jack and POT are soldered to a (50.0-mm by 35.0-mm) general-purpose through-hole breadboard for mounting inside the electronics bay of the stove. Once assembled the entire breadboard is shrink-wrapped for electrical insulation, vibration resistance, and affect protection. The 12-VDC Power supply jack and POT are mounted in the frustum at the base of the stove.

This electronics and control package allows great flexibility in the control scheme at a low cost. The stove can be configured to allow continuously variable fan speeds, or discrete settings based on the design requirements. There is significant room for future development including the addition of pressure and temperature transducers to provide operating condition feedback for automated control of the stove. In this application, the fan is assigned three discrete settings to simplify use and ensure test-to-test repeatability in the fan speed setting. Currently, there are no feedback signals processed by the microcontroller.

Figure 28 is a photograph of the completed P2 Prototype. Development of the P2 prototype was funded in part by Envirofit International (Envirofit International, Inc. Fort Collins, CO, USA). In addition to funding Envirofit International engineers aided in the design of the stove body, including mechanical and aesthetic design assistance, CAD and drawings, and initial field evaluation of the final product. A stamped Envirofit branding plaque was also generated for the P2 Prototype. The field surveys were conducted in India to assess the market appeal of the stove's aesthetics and functionally. Three P2 prototypes were manufactured. One for field trials with Envirofit, one initial prototype for testing at CSU and one final prototype for testing at CSU and at LBNL.

Figure 28 - Photographs of complete P2 Prototype. Images from left to right are the side profile, front, and rear of the stove

P2 Prototype Testing

The P2 prototype stove is designed with a common pressurized plenum which provides the pressure gradient to drive flow to the primary combustion stage and the secondary combustion stage, similar to the P1 prototype. An adaptor allows mass flow controlled compressed air to be supplied to the stove, which was used to map the plenum pressure with respect to the net mass flow rate of air through the stove. The tests were conducted under ambient laboratory conditions of 25.61℃ and 86.74 kPa.

The flow rate form 10 SLPM to 150 SLPM in increments of 10 SLPM. Triplicate measurements of the plenum pressure were recorded using a digital pressure transducer calibrator (APC030C, Ametek, Berwyn, Pa, U.S.A) measured in inH_2O gauge. Unit conversion from SLPM to g/min and are applied to the averaged data. Figure 29 is a plot of the four averaged and converted datasets fitted with a second-order polynomial with the intercepts forced to zero.

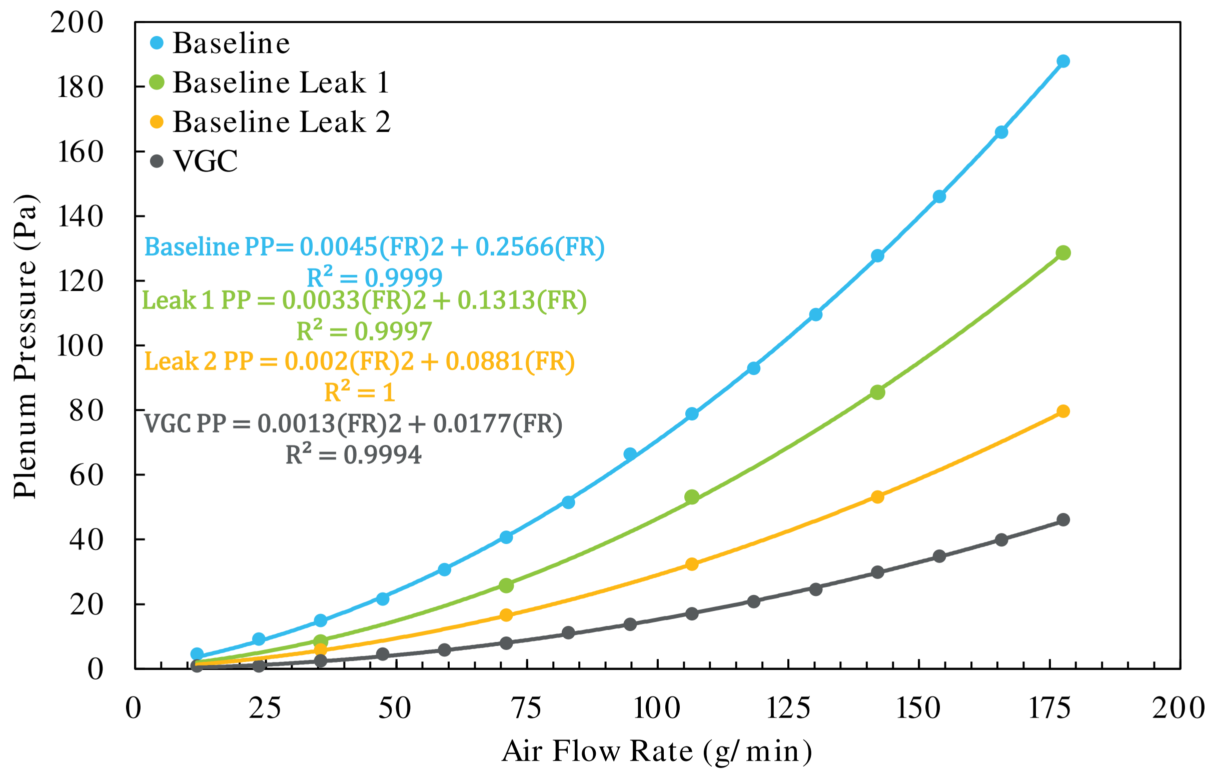

Figure 29 – The P2 Prototype plenum pressure vs. airflow curves for the baseline and final VGC combustion chambers as well as two controlled leak conditions.

The flow rate form 10 SLPM to 150 SLPM in increments of 10 SLPM. Triplicate measurements of the plenum pressure were recorded using a digital pressure transducer calibrator (APC030C, Ametek, Berwyn, Pa, U.S.A) measured in inH_2O gauge. Unit conversion from SLPM to g/min and inH_2O to kPa are applied to the averaged data. Both the original chamber and the final VGC chamber were tested. The baseline test cases with two different controlled leaks were also tested to illustrate the importance of a design that has a robust seal on the common plenum. Leak 1 was an opening with an area of 63.3-

mm^2 increasing the total outlet area of the plenum by 43%. Leak 2 had an opening with an area of 126.6-mm^2 which increases the total outlet are of the plenum by 86%. A leak one resulted in a 32% reduction in plenum pressure, while a leak two resulted in a 58% reduction in plenum pressure at a flow rate of $106.6\frac{g}{min}$. At the full scale mass flow rate of 177.6 $\frac{g}{min}$ leak one and leak two resulted in a 31% and 58% reduction respectively.

Next, the fan replaces the compressed air adaptor, and a map of the fan duty cycle with respect to the plenum pressure is created for all four test cases. The data from the map of the fan duty cycle with respect to plenum pressure is shown here in Figure 29. The fan is powered using a laboratory power supply (VB-8012, National Instruments, TX. USA). A 5-VDC square wave is generated using a laboratory signal generator (VB-8012, National Instruments, TX. USA) and applied to the PWM lead on the fan. The duty cycle of the 5-VDC square wave varies from 10% to 100% in increments of 10%. At each duty cycle, the steady state pressure inside the common plenum is measured using the digital pressure calibrator in units of inH_2O. The total number of replicates is three for the baseline and VGC test cases and one for the leak test cases. For the test cases with replicates, the data are averaged. All data points are converted to SI pressure units of Pa. The results of this study are plotted with a second-order polynomial fits in Figure 29. Here the plot of the independent variable is on the y-axis, and the dependent variable is on the X-axis counter to the convention. The objective of plotting this way is to make the process of solving the airflow rate vs. PWM duty cycle simpler in the next step. The second-order polynomial curve fits from Figure 28, and Figure 29 can be solved to yield an equation for each of the four stove configurations tested which can be used to determine the PWM duty cycle required to obtain a specific flow rate.

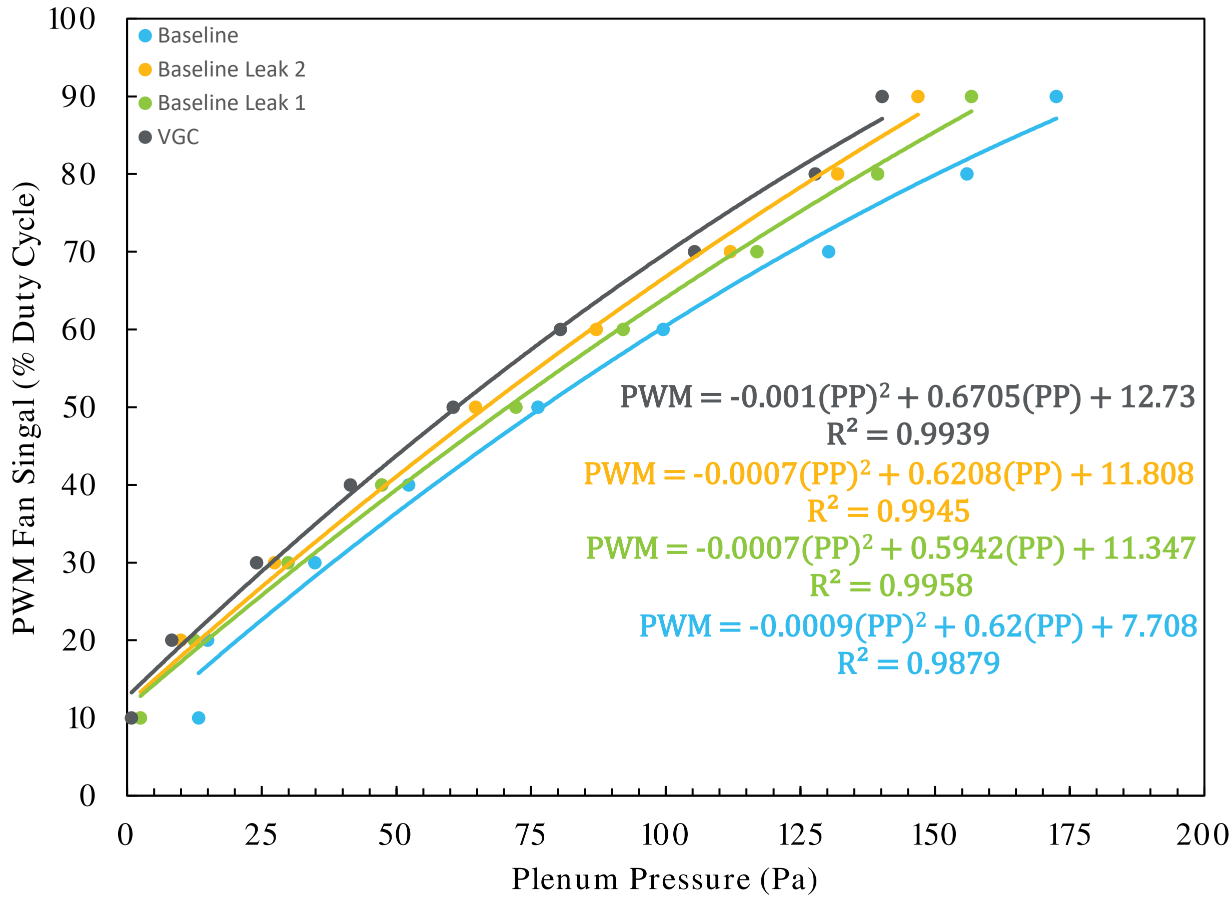

Figure 30 - P2 prototype PWM fan signal vs. plenum pressure for the baseline combustion chamber, two leak sizes and the final VGC combustion chamber.

Equations 10, 11, 12, and 13 are the duty cycle equations derived from the experimental data in Figure 29 and Figure 30.

Equation 8 - Baseline fan duty cycle equation

$$Duty\ Cycle = -0.0009\left(0.0045(Flow^2) + 0.2566(Flow)\right)^2 + 0.62(0.0045(Flow^2) + 0.2566(Flow)) + 7.708$$

Equation 9 – Baseline leak 2 fan duty cycle equation

$$Duty\ Cycle = -0.0007(0.002(Flow^2) + 0.0881(Flow))^2 + 0.6208\left(0.002(\mathrm{Flow}^2) + 0.0881(\mathrm{Flow})\right) + 11.808$$

Equation 10 - Baseline leak 1 fan duty cycle equation

$$Duty\ Cycle = -0.0007\big(0.0033(Flow^2) + 0.1313(Flow)\big)^2 + 0.5942\big(0.0033(Flow^2) + 0.1313(Flow)\big) + 11.347$$

Equation 11 - VGC fan duty cycle equation

$$Duty\ Cycle = -0.001\big(0.0013(Flow^2) + 0.0177(Flow)\big)^2 + 0.6705\big(0.0013(Flow^2) + 0.0177(Flow)\big) + 12.73$$

The equation for the pressure generated from the data displayed in Figure 29 into the pressure term for the associated PWM duty cycle equation generated in Figure 30. The PWM duty cycle output of these four equations are plotted from 10 g/min 150 g/min in Figure 31.

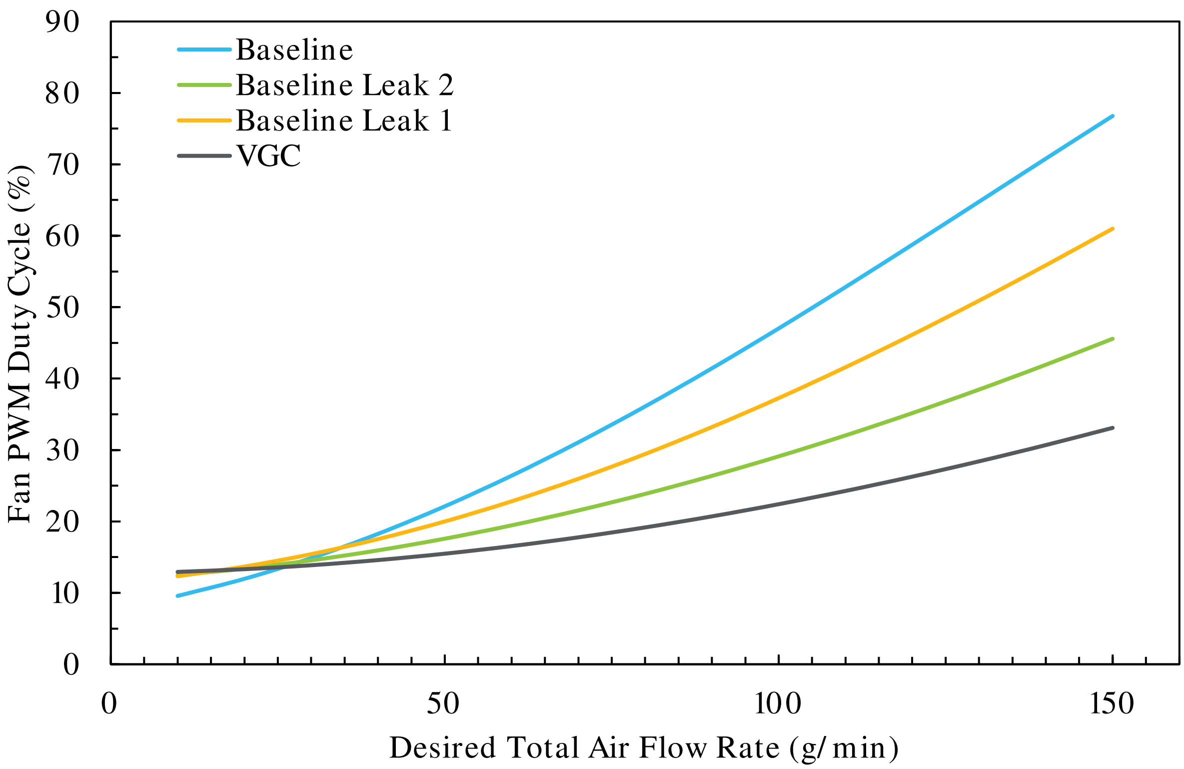

Figure 31 - Fan PWM duty cycle vs. desired total air mass flow rate

The output from Equation 10, 11, 12, and 13, which define the curve fits for PWM fan duty cycle vs. flow rate through the stove are used to set the fan speed PWM output on the microcontroller to attain the desired flow rate. This system provides some control over the mass flow of oxidizer through the stove, but there are still a number of variables that are uncontrolled. The initial ambient air temperature and pressure, as well as the porosity of the fuel bed, may affect the net flow rate through the stove. Moreover, any leakage can result in lower flow rates through the primary and secondary combustion stages as well as illustrated by the plenum pressure and flow test cases where intentional leaks are introduced seen in Figure 29, Figure 30, Figure 31.

The hypothesis that the ratio of the area of the secondary combustion stage holes to the primary combustion stage holes would be proportional to the mass flow rate of air into the secondary and primary combustion stages respectively proved to be false. Initial testing showed that the density of the air at the secondary air holes was substantially lower than expected due to higher air temperatures. During P0 Modular laboratory TLUD testing this was not an issue because the secondary and primary air flows are controlled separately at rotameters which were at the same temperature. In the P1 and P2 prototypes, the flow is driven by the plenum pressure. The mass flow rate of air to the primary and secondary combustion stages is governed by plenum pressure and by the density of the air in the plenum at the height of primary and secondary air holes. To better understand this phenomenon and make appropriate design changes, thermocouples installed in the common plenum at the primary and secondary air hole inlet height provide temperature feedback to calculate the density difference between the two stages.

Table 5 contains the results for calculating the density effect from the temperature differential between the two combustion stages.

Table 5 – Density effect on the primary to secondary air flow ratio.

Stove	**P2 (Baseline)**	**P2 (VGC Final)**
Total primary combustion stage air inlet area (mm^2)	28.27	21.99
Total secondary combustion stage air inlet area (mm^2)	119.38	337.33
Secondary to primary combustion stage air inlet ratio	4.22	15.34
Secondary to primary air density difference measured during operation **average (max)**	0.770 (0.660)	0.770 (0.660)
Secondary to primary mass flow ratio without density correction **average**	4.22	15.34
Secondary to primary mass flow ratio with density correction **average (max temp)**	3.21 (2.15)	11.81 (7.80)
Secondary to primary mass flow ratio with density correction and early secondary air contribution to primary combustion (VGC only) **average (max temp)**	-	7.71 (5.01)

For this experiment, the average secondary air inlet temperature is 289.63 ℃ with a maximum of 406.24℃ while the average primary air inlet temperature is 157.39℃ with a maximum 277.33℃. This leads to a computed average and maximum secondary to primary air density ratio of 0.77 and 0.66 respectively. The lower density of the secondary inlet air, when compared to the primary inlet air, reduces the secondary to primary airflow ratio. Combining the density difference and the ratio of inlet area of the air entering the primary and secondary combustion stages an approximate secondary to primary mass airflow ratio can be computed. The average secondary to primary mass airflow ratio for the baseline test case is 3.21 with a minimum of 2.15. From P0 modular TLUD testing we know that at ratios lower than 4 an increase in CO emissions is observed. To counteract the effect of the density difference in an attempt to reduce emissions, additional secondary inlet area is added and a slight reduction in primary inlet area is applied to ensure that the stove was always operating with enough secondary air. The reduction in primary inlet area is also motivated by a need to reduce the simmer CO emissions as seen in the following section. With the modifications to the stove, the final secondary to primary airflow ratio is an average of 11.81 with a minimum of 7.80. However, it is thought that some of the early secondary air is recirculated to the surface of the fuel bed especially during the first half of the high power tests resulting in higher emissions that lower the overall ratio to as low as 7.71 and 5.01 for the average and minimum secondary to primary air flow ratio. This trend is observed in the Figure 32. The test cases shown in Figure 32 is the final P2 VGC chamber with pine pellets. A significant CO emissions is measured on startup for all three phases. Once the fuel recedes from the early secondary air inlet further down into the stove, the CO emissions drop off.

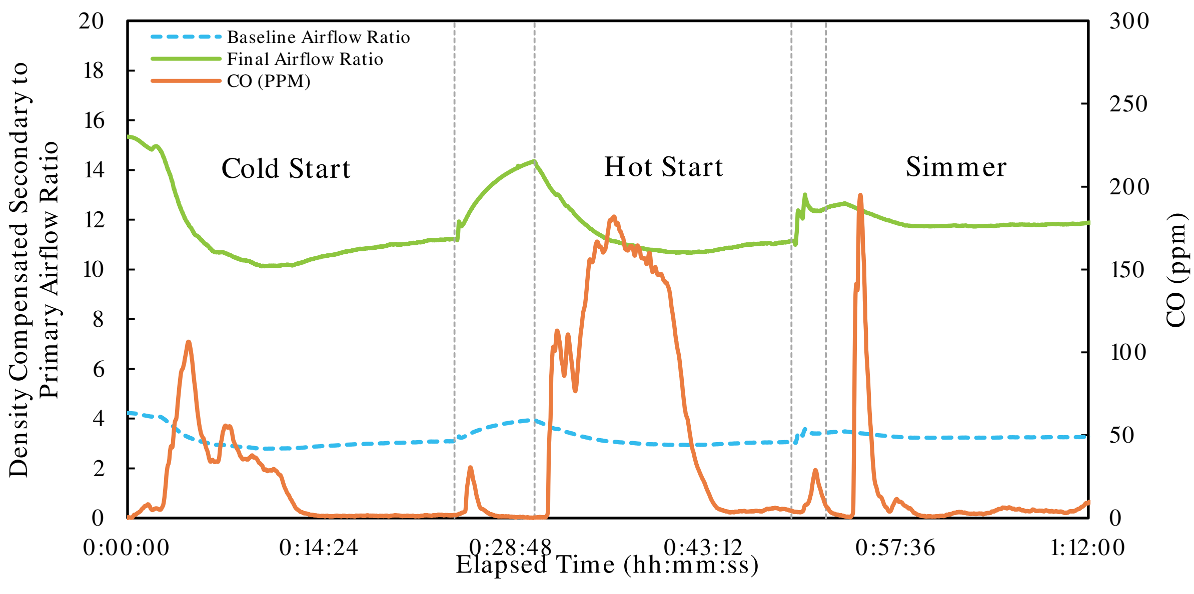

Figure 32 - Test case evaluating the secondary to primary airflow ratio (green) during different phases of the test.

Early testing established that the prototype stove can achieve acceptable CO emissions rates during normal operation with the modified air inlets, as demonstrated by the data plotted in Figure 33.

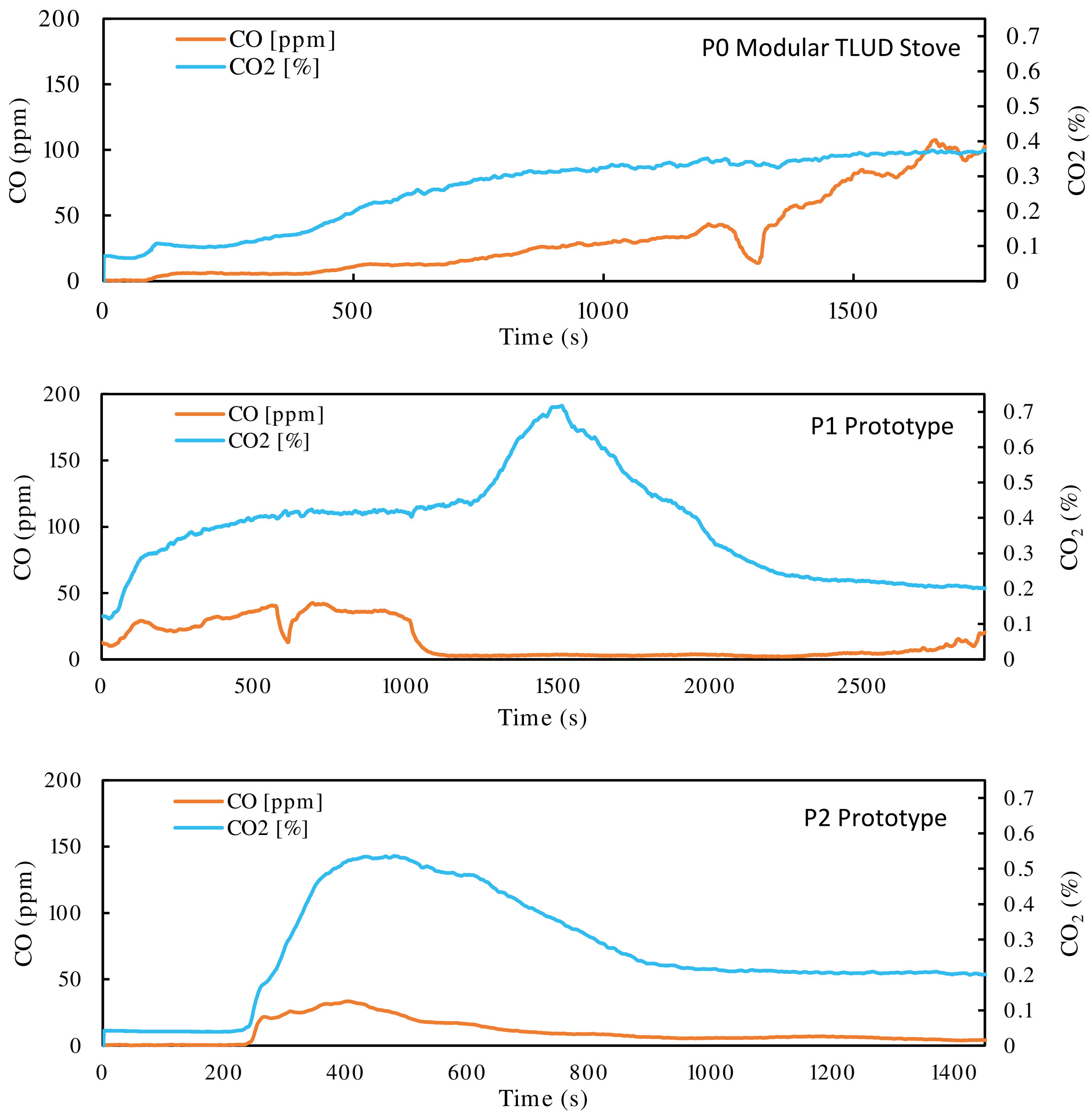

Figure 33 – Nominal CO and CO_2 Emissions for high power cold start tests for each of the three stove designs. From top to bottom are the emissions from the P0 Modular TLUD, P1 transitional prototype, and the P2 production intent prototype

These trends show that for the P0 modular stove, the P1 transitional prototype with the baseline chamber geometry, and for the P2 production intent prototype with the modified VGC chamber geometry and the enlarged air inlets, there is no significant differences in high power nominal CO emissions. This was not the case for the low power simmer emissions. A low power simmer flow sweep was conducted using the P1 prototype with the mass flow controller. The stove was ignited, and a steady state operating condition was achieved. The stove was then turned down to reduce the power output for a simmer cooking test. With each turndown, the CO emissions rose sharply and reached near steady state.

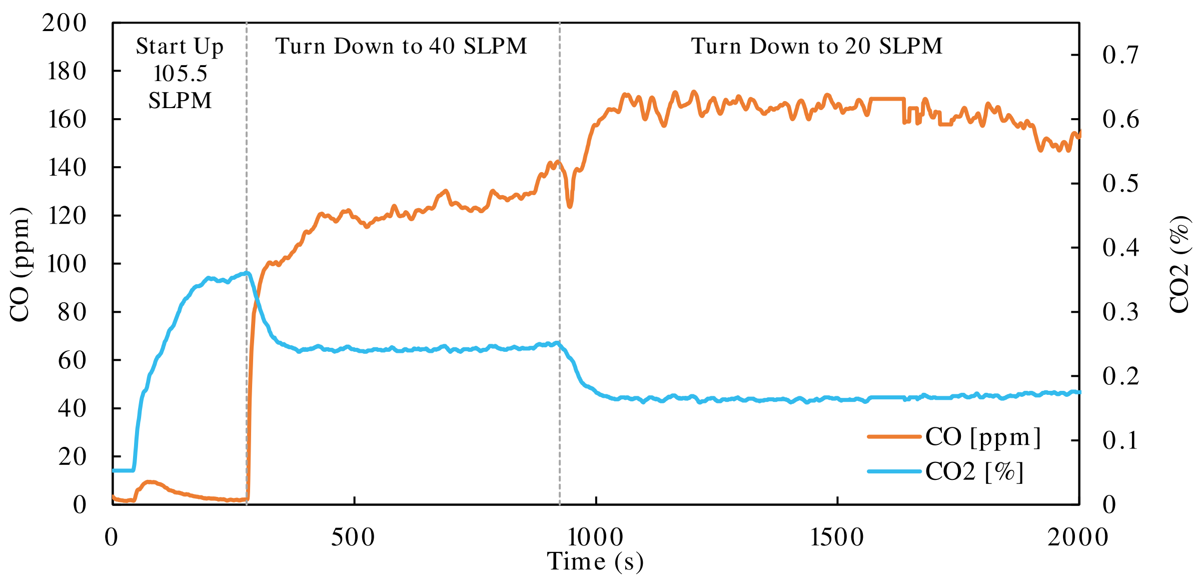

Figure 34 - P1 prototype low power flow sweep with CO and CO_2 emissions trends.

A new stove chamber geometry is needed to address the higher emissions in low power simmer tests. The chamber designed to meet this need is known hereafter as the varying geometry chamber (VGC) and is illustrated in Figure 35. The VGC consists of two discrete diameters connected by a frustum that gradually transitions from the larger diameter to the smaller diameter. This design allows a larger turndown ratio to be achieved for simmering tests while maintaining the higher output capabilities of the full diameter stove. Initial proof of concept prototyping was conducted using an insert placed in the P1 prototype, followed by a full P2 prototype chamber. This solution was efficacious in reducing the simmer CO emissions.

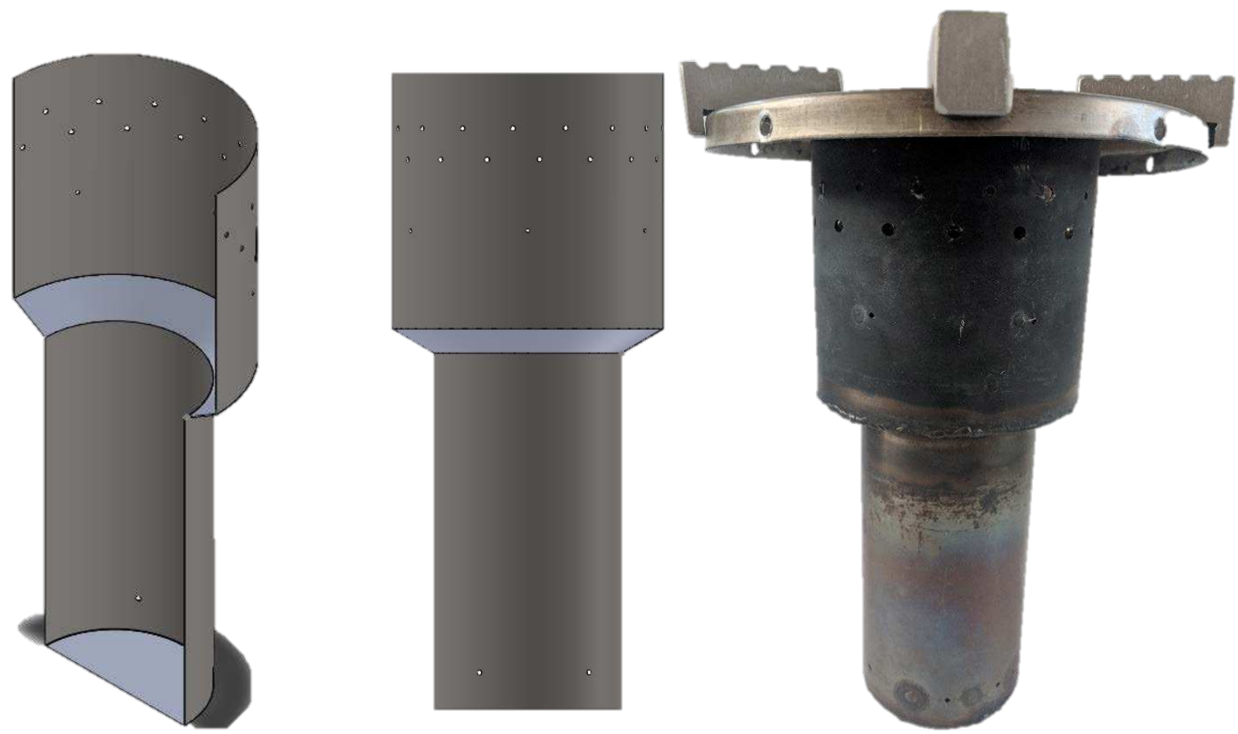

Figure 35 - Varying geometry combustion chamber (VGC) CAD cross-section, CAD side profile, and Photograph of the final VGC design.

With the significant technical challenges to getting a standalone TLUD gasifier cookstove operational testing to improve and evaluate the design against the ISO IWA tiers can commence.

Final WBT Testing

All of the P2 emissions and performance test cases use the final P2 VGC configuration of the P2 prototype stove. The fuel for all test cases is Lodgepole pine (Pinus contorta) pellets except for the test case where corncob pellets (Premium Horse Bedding, BestCob, IA, USA) are used. Two different water-boiling tests are used to evaluate the performance of the stove. A diagram showing the two distinct test procedures used for P2 prototype evaluation is located in Figure 36.

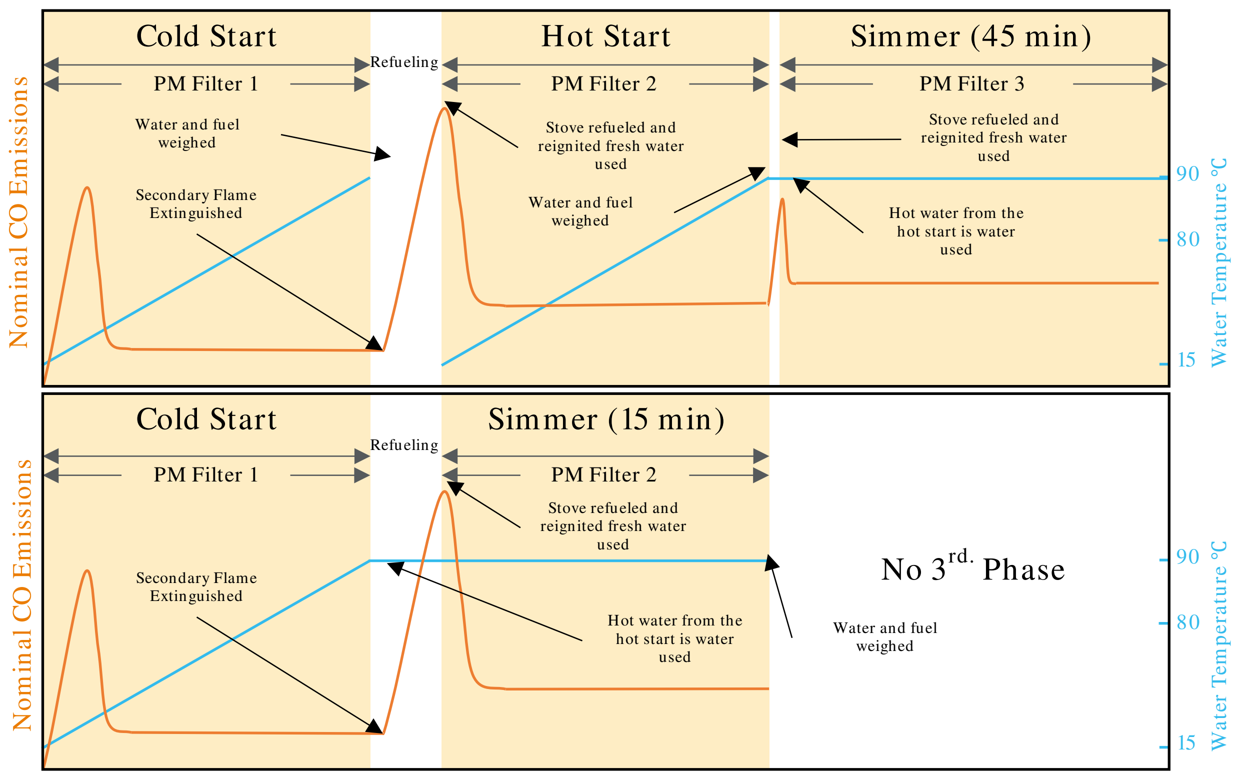

Figure 36 – Water boiling test procedures used for tests designated CSU and LBNL for the upper diagram and lower diagram respectively.

The top diagram of Figure 36 is a full-length water boil test consisting of a cold start, hot start, and a 45 minute simmer phase. The bottom diagram of Figure 36 is an abridged water boil test in which a cold start is followed by a shortened simmer phase. The longer test procedure, hereafter denoted as the CSU procedure, is a modified water boil test beginning with a cold start where a room temperature stove is ignited using 10 ml of kerosene and a match. A 5-L pot of water with at 15°C ±2°C, is covered with a floating foam lid to minimize evaporation, and heated to 90°C. Once the water reaches 90°C the mass of the pot with the water is weighed to account for the evaporated water, and the fuel is removed from the stove, extinguished, sorted, and weighed to account for the energy released during the test phase. The hot start in follows immediately after the cold start. The stove is refueled as quickly as possible with the same starting mass of fuel as used during the cold start phase. The stove is reignited using 10 ml of kerosene and a match. A second 5-L pot of water at 15°C ±2°C with the floating foam lid is again placed on the stove. Once again, the water in the pot is brought from 15°C ±2°C to 90°C. The water and pot is again weighed, the floating foam lid is removed, and then placed back on the stove for a 45-minute simmer phase where the water is maintained at 90℃ $\pm$ 3℃. For all phases CO and CO_2 are measured using NDIR instruments. For each of the three phases, a gravimetric filter is used to sample PM.

For tests conducted to replicate the LBNL testing the hot start portion of the test procedure above was forgone, and the simmer was reduced from 45 minutes to 15 minutes. A 15-minute simmer was chosen to shorten the turnaround between tests compared to the standard 45-minute simmer.

The baseline configuration has seven 2-mm diameter primary air holes, six 1.5-mm diameter early secondary air holes, and 32 secondary air holes of which 24 are 2-mm in diameter, and 8 are 4-mm in diameter. The baseline test case is fueled with 600g of fresh

Lodgepole pine pellet fuel for both the cold start and the hot start. 400g of fresh Lodgepole pine pellet fuel is used for all low power simmer tests. A number of variations of the VGC stove are evaluated. Test cases where the fuel load is varied assesses the effect that lowering the height of the fuel bed might have on the performance of the stove. Two different fuel masses, one at 600g and one at 550g, are evaluated based on results from testing using the CSU test procedure and the LBNL test procedure.

A stove configuration with an extended pot deck is evaluated to determine the effect the pot deck has on efficiency and emissions. The pot deck was extended from 7.25 inches to 10.5 inches, a diameter larger than the bottom of the pot used, using the hardware pictured in Figure 37.

Figure 37 – Pot deck extension.

A version of the VGC stove with all 32 of the secondary air inlet holes set at 4mm, increasing the secondary air hole area and by extension the assumed flow rate by 18.3% for a density compensated air flow ratio of between 9.5:1 and 14.5:1 was evaluated to increase the secondary air flow rate. A test of the stove that has had the insulation removed is used to evaluate the effect that insulation has on the performance of the stove.

A smaller pot gap, reduced from 15 -mm to 7 -mm is evaluated. A test with a well-established pot with a significant soot deposit is performed to see if the cooking vessel chosen for the testing had any effect on the performance of the stove. Corncob pellets are evaluated to determine the potential performance using different fuels.

All test cases where the stove configuration and fuel type vary are conducted using the CSU test procedure.

P2 CO Emissions Results

Carbon monoxide emissions are measured using an NDIR instrument (ULTRAMAT 6, Siemens AG, Munich, Germany). The emissions rates are normalized using Equation 12 and Equation 13 for high power cold start and hot start test, while low power simmer CO emissions are normalized using and Equation 14. Finally, high power indoor CO emission rates are evaluated using Equation 15.

Equation 12 - Energy normalized CO emissions in $\frac{g}{MJ_d}$.

$$CO_{\frac{g}{MJ_d}} = \frac{m_{CO}}{(m_{H_2O\ Start} * C_P * (\Delta T_{water}) + m_{steam} * h) * 10^{-6}}$$

Where m_{CO} is the total mass of the CO emitted in g calculated using Equation 13.

Equation 13 - The total CO emissions from a test phase in g.

$$m_{CO} = \sum \Delta t * \dot{m}_{air} * \left(\frac{CO_{\%}}{100}\right) * \left(\frac{\rho_{CO}}{\rho_{Air}}\right) * 1000$$

Where $CO_{\frac{g}{MJ_d}}$ is the CO emissions for a test normalized by the energy delivered to the cooking vessel. m_{CO} is the summed mass of the CO emitted in g. Δt is the time step, $\dot{m}_{air}$ is the mass flow rate of air, $CO_{\%}$ is the measured CO concentration in the hood exhaust as measured in %. ρ_{CO} and ρ_{Air} are the densities of CO and air respectively. The starting mass in g of the water in the cooking vessel is m_{H_2O}. C_P is the specific heat in J/gC. ΔT_{water} is the temperature change of the water in the cooking vessel. m_{steam} is the mass of water vaporized from the pot during the test in g. The specific enthalpy of vaporization, denoted by h is the in J/g for water

Equation 14 - Normalized low power (simmer) CO emissions in $g/min/L$.

$$CO_{LP} = \frac{m_{CO}}{\frac{T_{simmer}}{L_{H_2O}}}$$

Where CO_{LP} is the low power CO emissions normalized by the length of the test and the volume of water boiled. m_{CO} is the total mass in g of CO emitted during the low power simmer phase of the test. The total length of time in minutes for the low power simmer test is T_{simmer}. L_{H_2O} is the volume of water used in the test in liters.

Equation 15 - Indoor CO emissions rate in $\frac{g}{min}$

$$CO_{indoor} = \frac{\dot{m}_{CO_{\max}}}{TTB}$$

Where $\dot{m}_{CO_{\max}}$ is the greater of the average of the cold start and hot start CO emissions rate in $\frac{g}{min}$ or the simmer CO emissions rate in $\frac{g}{min}$. TTB is the time to boil in minutes.

For high power tests where both a cold start and hot start are conducted the CO emissions results are averaged. The cold start is a worst case scenario and for the abridged LBNL testing only the cold start data is displayed.

The results contained in Figure 38 are test cases for both CSU testing and LBNL testing where the starting fuel mass for the test varied. Gray indicators in Figure 38 denote test cases where 600g of fuel was used while yellow points are data were 550g of fuel was used. CSU test cases are the averaged emissions results from the hot start and cold start testing. LBNL test cases are cold start data. There is no statistically significant difference between the high power CO emissions where 600g of fuel is used and cases where 550g of fuel is used for CSU and LBNL test procedures.

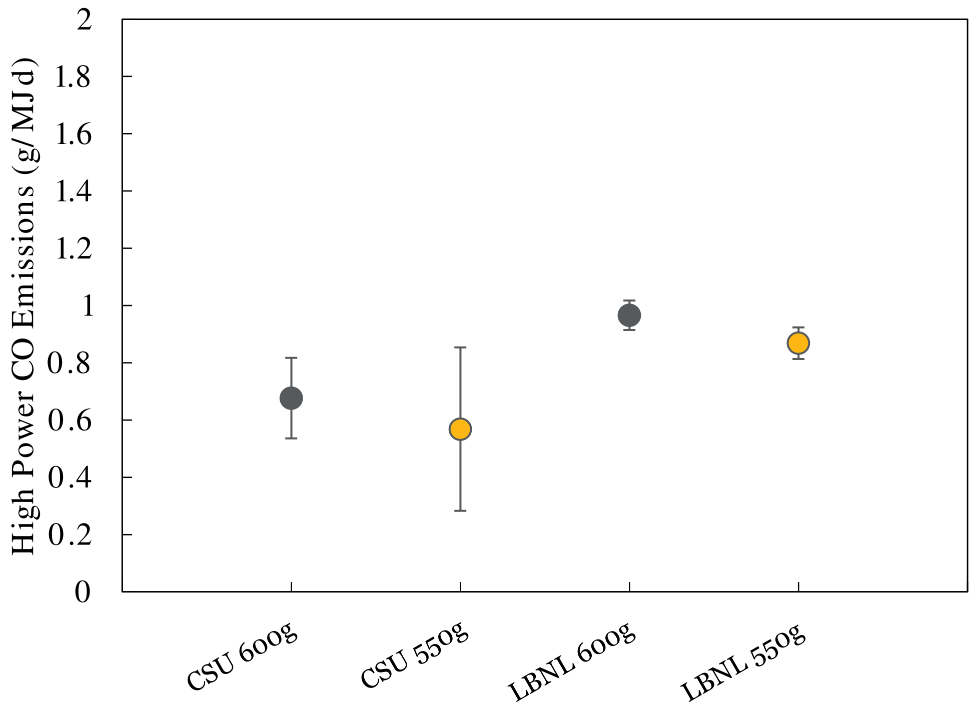

Figure 38 - P2 high power CO results from test cases where the starting mass of fuel varied. Error bars indicate a 90% CI.

There is a large difference between the high power CO emissions testing using the CSU procedure compared to emissions testing using the LBNL procedure. CSU and LBNL test cases using 600g of fuel produces 0.68 g/MJ_d and 0.97 g/MJ_d at CSU and LBNL respectively for a difference of approximately 30%. Test cases using the smaller initial fuel load of 550g produces 0.57 g/MJ_d and 0.87 g/MJ_d at CSU and LBNL respectively for a difference of 35%.

High power CO emissions results for test cases where the stove configuration and fuel type vary are shown here in Figure 39. All test cases have a sample size of N=1 and therefore lack statistical power. Despite the lack of statistical power, several observations are made.

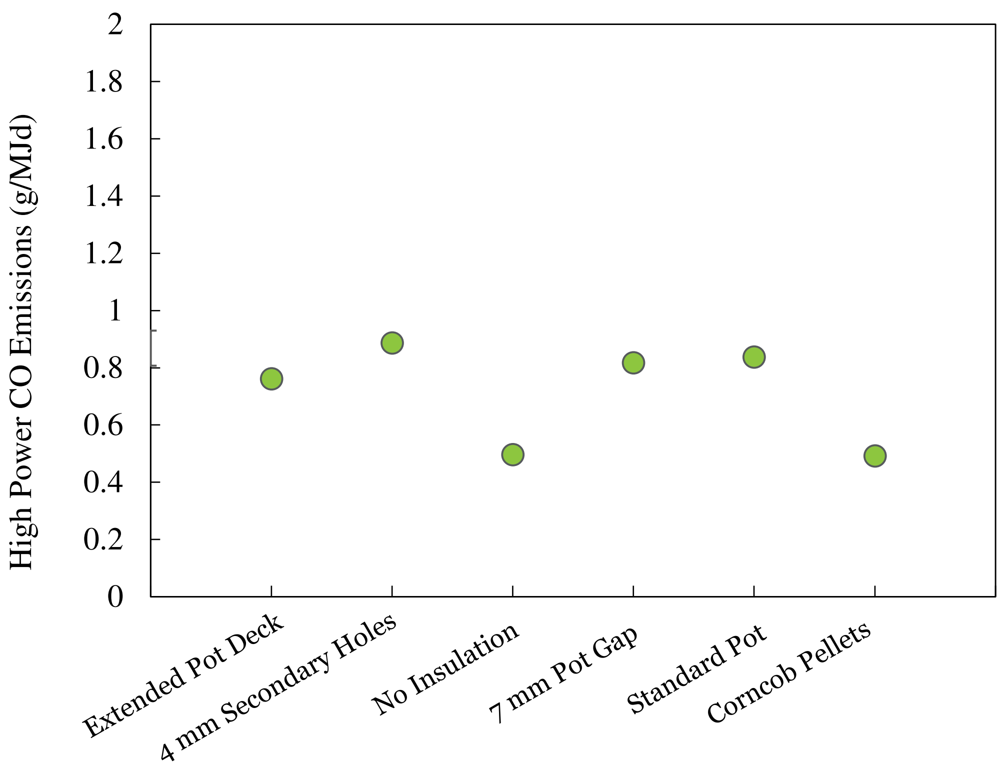

Figure 39 - P2 high power CO emissions results for test cases with different stove configurations and corncob pellets. N=1

All tests cases exceed the tier 4 guideline for the high power CO emission rate regardless of the stove configuration. The test case with the corn pellets also exceed the tier 4 guideline for the high power CO emission rate. The span of the results is 0.49 g/MJ_d for the test case where corn pellets are used to 0.89 g/MJ_d where 4-mm secondary air inlet holes are used. A similar to the spread of results observed in the test cases where the starting mass of the fuel varies 0.57 g/MJ_d to 0.97 g/MJ_d. Thus without statistical power from replicate testing it can be concluded that there is likely minimal difference between the baseline test case using 600g of fuel and any stove configuration changes that are here evaluated. Additionally, the corncob pellets do not likely result in a significant difference in CO emissions compared to the baseline test case. It is also important to note that the Cold start and Hot start for the test case where the pellets are used is not capable of completing the boiling task as all the fuel is consumed prior to the 90℃ test termination point.

Simmer or low power CO emissions results are shown in Figure 40 and Figure 41, for test cases where starting fuel mass varied and where the stove configuration varied respectively.

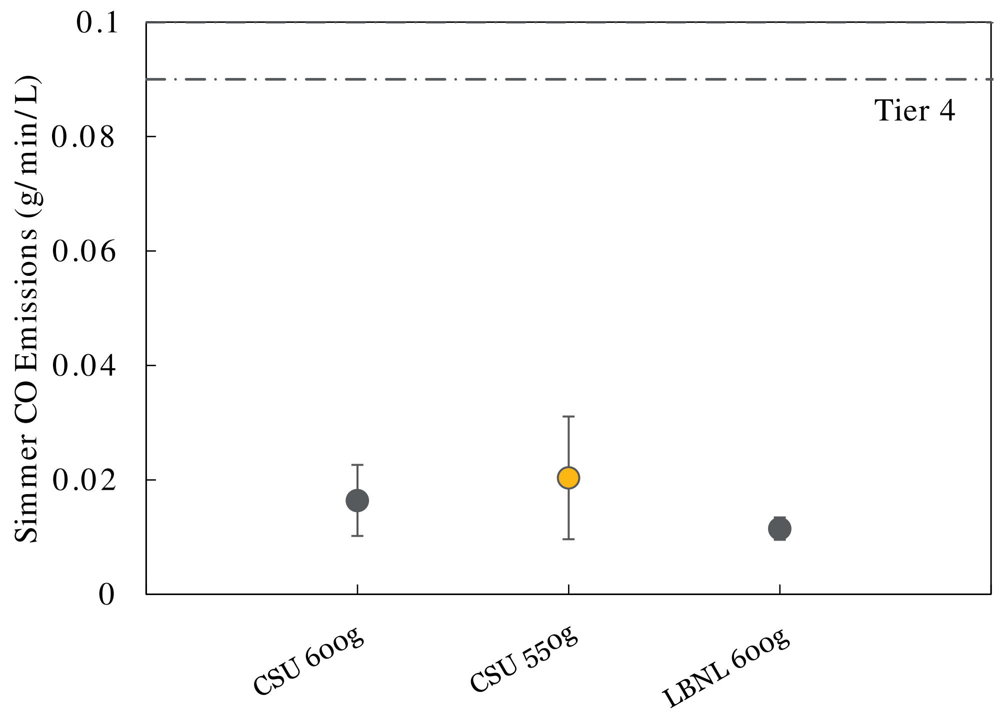

Figure 40 – P2 prototype low power (simmer) CO emissions results for test cases where starting fuel mass varied. Error bars represent 90% CI.

Figure 40 is a plot of data for test cases with 600g and 550g initial fuel loads, indicated by gray markers and yellow markers in respectively. All test cases exceeded the guideline for tier 4 low power emissions.

There is no statistically significant difference between testing were 600g, and 550g of initial fuel is used. There is also no statically significant difference between low power CO emissions measured using the CSU and the LBNL procedures. No statistically significant difference between the baseline test case where 600g of fuel is used and test cases where the stove configuration includes an extended pot deck, 4-mm secondary holes, and no insulation exist.

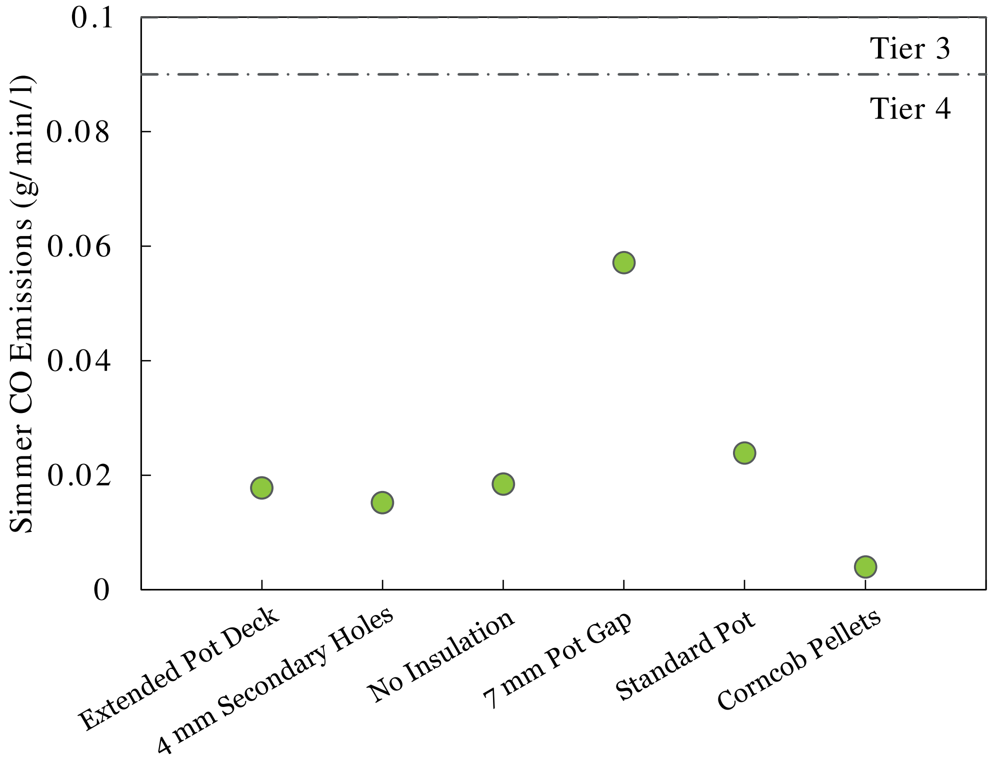

Figure 41 - P2 prototype low power CO emissions results with different stove configurations and corncob pellets. N=1.

A statistically significant difference between the baseline and test cases were 7-mm pot gap, the standard pot, and corn cob pellets are detected. With the 7-mm pot gap emitting 3.6 times more CO than the baseline test case and the corn pellets emitting 4 times less CO than the baseline test case.

Indoor CO emissions rates for test cases where starting fuel mass was varied and where stove configuration varied are shown in Figure 42 and Figure 43 respectively. Error bars in Figure 42 indicate 95% CI; gray markers are test cases conducted at CSU, and yellow markers are conducted at LBNL. No significant difference is observed between the test cases conducted at CSU and LBNL.

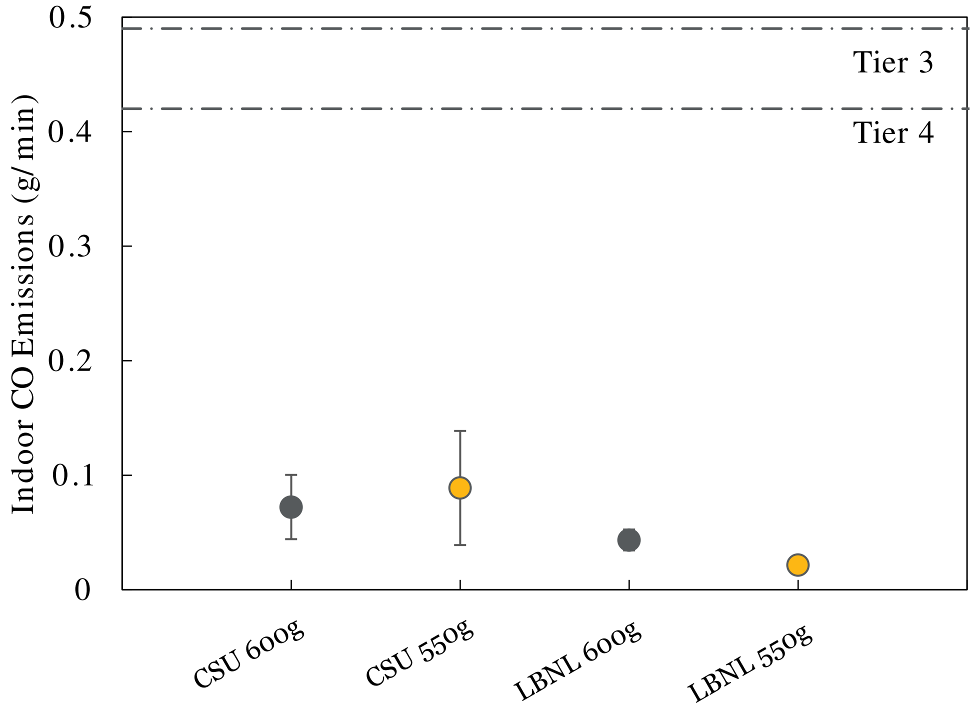

Figure 42 - P2 prototype Indoor CO emissions results for test cases where starting fuel mass varied. Error bars represent 90% CI.

A difference larger than one standard deviation exists between the test cases where 600g of fuel is used to start the stove compared to test cases where 550g of fuel is used to start the stove.

Test cases where the stove configuration is varied, as shown in Figure 43, are all test cases where only a single replicate is available. No confidence can be had from the results based on the data. There is little difference between the extended pot deck, 4-mm secondary holes, and no insulation test cases and the baseline test case where 600g of fuel is used. There is a significant difference in the test case where a smaller 7-mm pot gap, and the baseline test case.

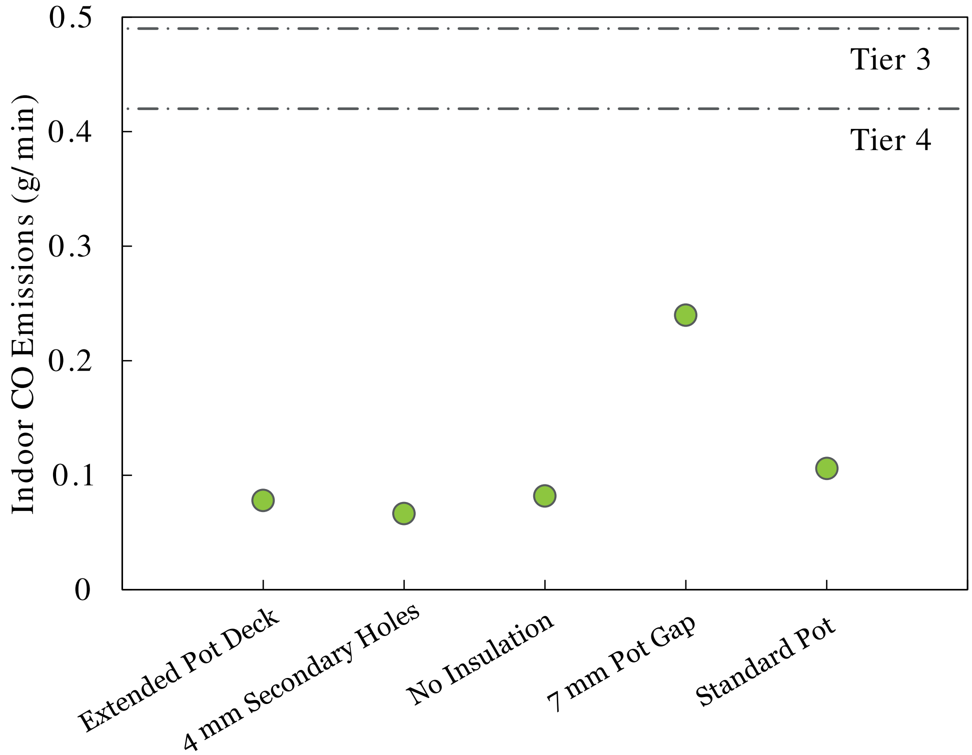

Figure 43 - P2 prototype indoor CO emissions results with different stove configurations. N=1.

The indoor CO emissions for the test case using the 7-mm pot gap is 11.33 standard deviations higher than the baseline case, and the test case where the standard pot is used is 6.5 standard deviations higher than the baseline case.

All test cases evaluated here meet the tier 4 guidelines for high power, low power simmer, and indoor emissions rates. Varying fuel load and stove configuration have minimal effect on the energy normalized or time normalized CO emission rate. Provided that the stove is operated correctly and reasonably high quality fuel is available to the user, the ISO-IWA tier 4 emissions guidelines for CO are attainable under laboratory control conditions and should be further evaluated for efficacy with field trials.

P2 particulate Emissions Results

Particulate emissions ($PM_{2.5}$) are measured gravimetrically. $PM_{2.5}$ emissions rates are normalized by the energy delivered to the cooking vessel using Equation 16 for high power cold start and hot start tests, Equation 17 for low power simmer tests, and Equation 18 for indoor emissions rates.

Equation 16- Energy normalized PM emissions in $\frac{\mu g}{MJ_d}$

$$PM_{2.5\frac{\mu g}{MJ_d}} = \frac{m_{PM_{2.5}}}{(m_{H_2O\ Start} * C_P * (\Delta T_{water}) + m_{steam} * h) * 10^{-6}}$$

Where $PM_{\frac{\mu g}{MJ_d}}$ is the gravimetric $PM_{2.5}$ emissions for a test, normalized by the energy delivered to the cooking vessel. $m_{PM_{2.5}}$ is the total mass of the $PM_{2.5}$emitted in μg. The starting mass of the water, in g, in the cooking vessel is m_{H_2O}. C_P is the specific heat in J/g℃. ΔT_{water} is the temperature change of the water in the cooking vessel. m_{steam} is the mass of water vaporized from the pot during the test in g. h is the specific enthalpy of vaporization in J/g for water.

Equation 17 - Normalized low power PM emissions in $\mu g/min/L$.

$$PM_{LP} = \frac{\frac{m_{PM_{2.5}}}{t_{simmer}}}{L_{H_2O}}$$

Where PM_{LP} is the low power gravimetric $PM_{2.5}$ emissions normalized by the length of the test and the volume of water boiled. $m_{PM_{2.5}}$ is the total mass in μg of PM emitted during the low power simmer phase of the test. The total length of time in minutes for the low power simmer test is t_{simmer}. L_{H_2O} is the volume of water used in the test in liters.

Equation 18 - Indoor PM emissions rate in $\frac{g}{min}$

$$PM_{indoor} = \frac{\dot{m}_{PM_{max}}}{TTB}$$

Where $\dot{m}_{PM_{\max}}$ is the greater of the average high power $PM_{2.5}$ emissions rate in $\frac{\mu g}{min}$ computed as the average of the cold start and hot start $PM_{2.5}$ emissions rates or the simmer PM emissions rate in $\frac{\mu g}{min}$. TTB is the time to boil in minutes.

The test cases where initial fuel load is varied are displayed in Figure 44.

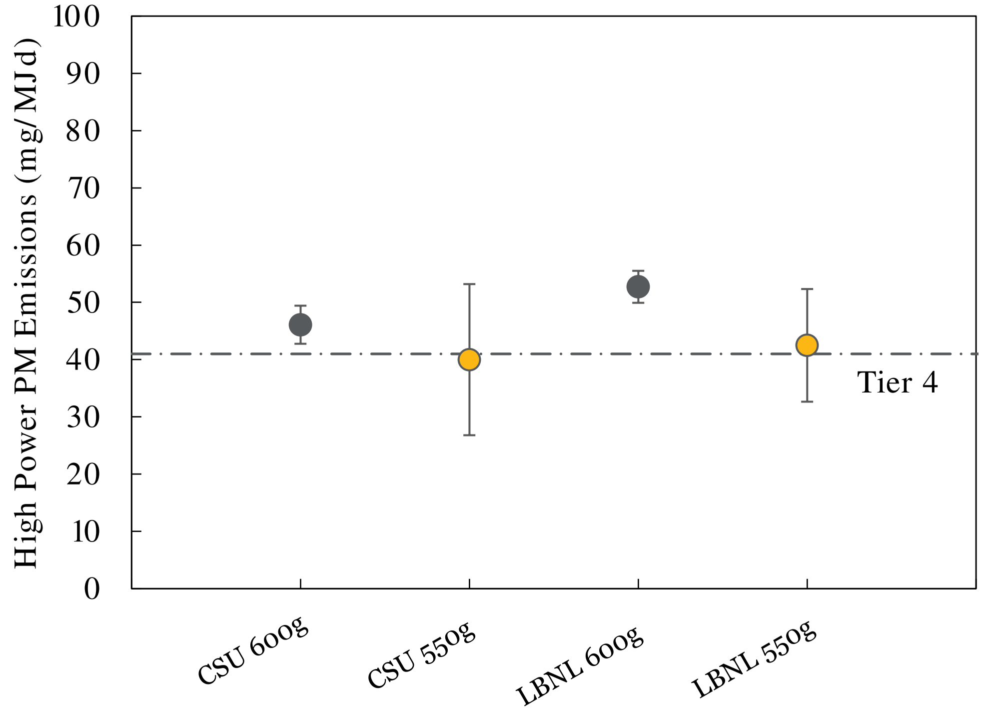

Figure 44 – P2 prototype high power PM results from test cases where the starting mass of fuel varied. Error bars indicate a 90% CI.

Test cases indicated by gray markers in Figure 44 are tests where the initial fuel mass is 600g. Test cases indicated by yellow markers are the test cases where 550g of fuel is used. Error bars indicate a 90% confidence interval.

The mean energy normalized CSU 600g $PM_{2.5}$ emission is 46.09 mg/MJ_d Twith a standard deviation of 1.82 mg/MJ_d. There is no significant difference observed between high power $PM_{2.5}$ emissions measurements made using the CSU and the LBNL test procedure when 550g of fuel is used. A statistically significant difference in the mean PM emissions for measurements made using the CSU and LBNL procedures does exist for test cases where 600g is used. The CSU procedure yielded a mean $PM_{2.5}$ emissions of 46.09 mg/MJ_d and the LBNL procedure produced 52.72 mg/MJ_d of $PM_{2.5}$ emissions when 600g of fuel is used for a 12.6% difference. Test cases where 600g of fuel is used produced results that are tier 3. Where test cases where 550g of fuel is used are between tier 3 and tier 4 but stochastic variation prevents a definitive statement.

Data for test cases where the stove configuration and fuel type vary are shown in Figure 45. Conclusions that are drawn from this dataset are tentative as only one replicate is available. The following observations are made based on the available data.

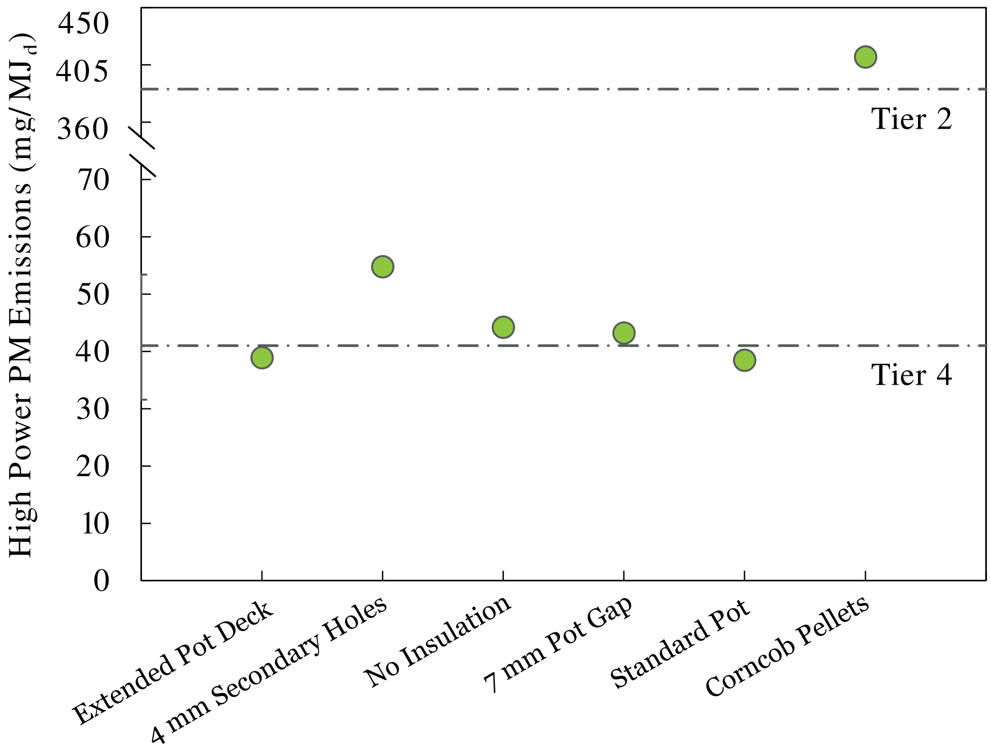

Figure 45 – P2 high power PM emissions results for test cases with different stove configurations and corncob pellets. N=1.

The extended pot deck, no insulation, 7-mm pot gap and standard pot test cases have lower $PM_{2.5}$ emissions during high power operation than the mean baseline test case (CSU 600g). The 4-mm secondary air hole case and the corncob pellet test cases produced more high power $PM_{2.5}$emissions than the baseline test case. The corncob pellet test case is ISO-IWA tier 1 for high power $PM_{2.5}$ emissions (note the broken axis in Figure 45) and produces an order of magnitude more $PM_{2.5}$emissions than the baseline test cases though again statistically significant data are not available. It is also important to note that the cold start and hot start for the test case where the pellets are used is not capable of completing the boiling task as all the fuel is consumed prior to the 90℃ test termination point. All test cases except the corncob pellet test case are near tier 4 high power $PM_{2.5}$ emissions under laboratory conditions. Only a few of the tests produced mean emissions capable of meeting the ISO-IWA tier 4 high power $PM_{2.5}$ emissions guidelines, single replicate data sets means that conclusions lack confidence in any statement indicating that the stove is compliant with tier 4 high power $PM_{2.5}$ emissions guidelines. However, low power simmer $PM_{2.5}$ emissions results are much more definitive.

The low power emissions results are plotted in Figure 46 and Figure 47. Low power $PM_{2.5}$ emissions data for test cases where the starting fuel mass is varied during high power operation are found in Figure 46. The gray markers indicate test cases where the high power initial fuel load is 600g; yellow markers indicate test cases where the high power initial fuel load was 550g. Error bars indicate a 90% confidence interval. It is important to note that for all simmer tests 400g of fresh fuel was used, the nomenclature of 600g and 550g tests only applies to the high power portions of the CSU and LBNL test procedures. A low power simmer test is not shown using the corncob pellet fuel because the simmer phase failed, nor is a simmer test performed for the LBNL 550g test case.

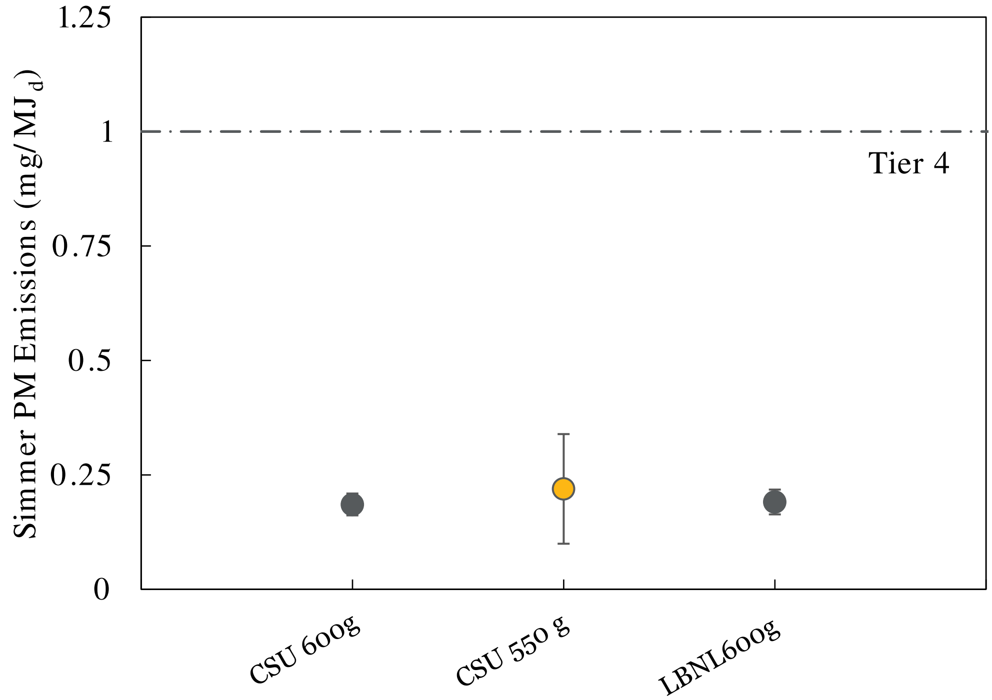

Figure 46 - P2 prototype low power PM emissions results for test cases where starting fuel mass varied. Error bars represent a 90% CI.

Several conclusions are drawn from the data in Figure 46. There is little difference in the mean low power $PM_{2.5}$ data acquired using the CSU procedure and the mean low power $PM_{2.5}$ emissions acquired using the LBNL procedure for the test case where the starting fuel mass was 600g. Nor is there a difference between the mean low power $PM_{2.5}$ emissions for the 600g test case and the 550g test case conducted using the CSU procedure. All three test cases in Figure 46 exceed the tier 4 low power PM emissions guidelines.

Shown in Figure 47 are the test cases where the stove configurations vary. As with the other data sets for different stove configurations, the data in Figure 46 lacks power, so qualitative observations are the only conclusion possible. Based on the data displayed in

Figure 47, all but the 7-mm pot gap test case, meet the tier 4 guideline for low power PM emissions.

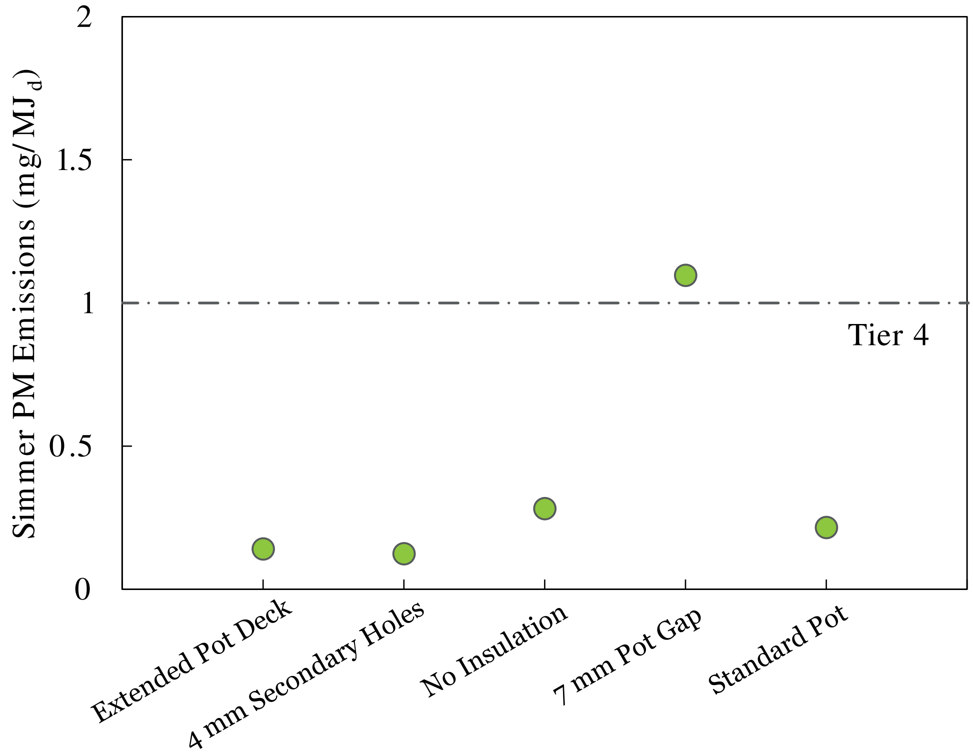

Figure 47 - P2 prototype low power PM emissions results with different stove configurations.N=1.

Figure 48 and Figure 49 are plots of the highest mean indoor PM emissions rate for test cases where the initial fuel mass, and stove configuration and fuel type varied respectively. All three phases, cold start, hot start, and simmer are considered for each test case, and the highest emissions rate during that phase is shown in the figure. The baseline test case is the CSU test case using 600g of fuel for the hot start and the cold start. The maximum baseline mean PM emissions rate is 3.45. Error bars represent a 90% confidence interval.

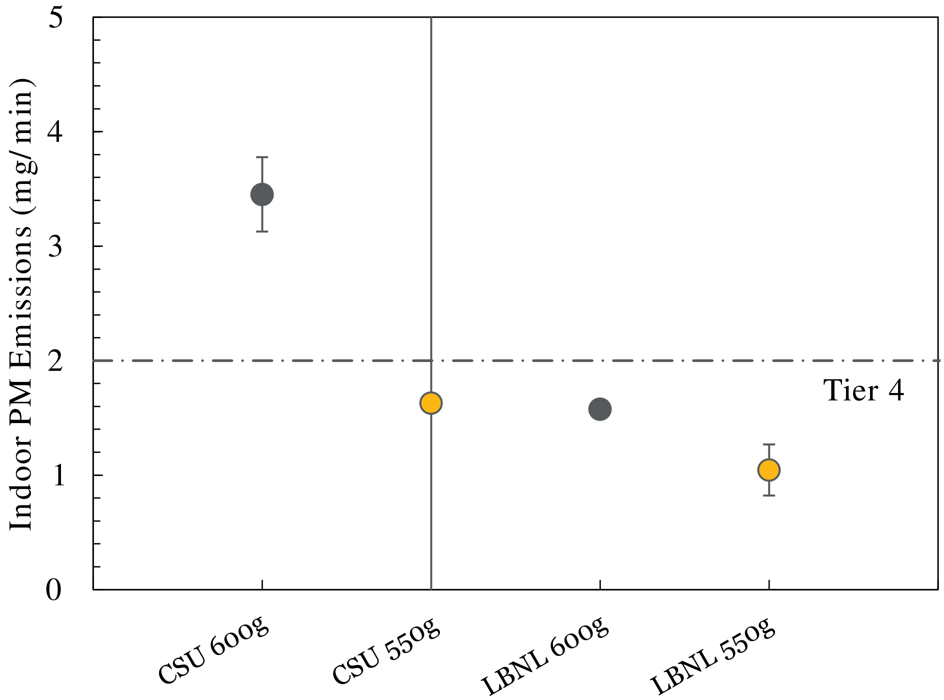

Figure 48 - P2 prototype indoor PM emissions results for test cases where starting fuel mass varied. Error bars represent a 90% CI.

For the test cases conducted using the CSU procedure and 550g of fuel, only two replicates exist, resulting in large error bars. Based on the data displayed in Figure 48, test cases using 550g of fuel have lower mean $PM_{2.5}$ emissions rates compared to test cases using 600g of fuel under the same test procedure and conditions. The 550g test case conducted using the LBNL procedure is statistically lower than the test case using 600g of fuel under the LBNL procedure. Test cases using the LBNL procedure have lower emissions rates than test cases using the CSU procedure. The baseline test case meets the ISO-IWA tier 3 indoor PM emissions rate guidelines but not tier 4. The mean CSU 550g and both 600g and 550g tests completed using the LBNL procedure meet the tier 4 guideline for indoor PM emission rates, as do all of the various stove configuration tests. The test cases where the stove configuration is varied are plotted in Figure 49. The mean baseline indoor $PM_{2.5}$ emissions rate is a minimum of 2.6 standard deviations greater than all the test cases in Figure 49. Additionally, all test cases in which the stove configuration is varied exceeded the tier 4 emissions requirement for indoor PM emissions rates. The test case where corncob pellets are used produced two orders of magnitude more PM emissions that the test result which produced the least PM emissions and approximately one order of magnitude more emissions than the baseline test case.

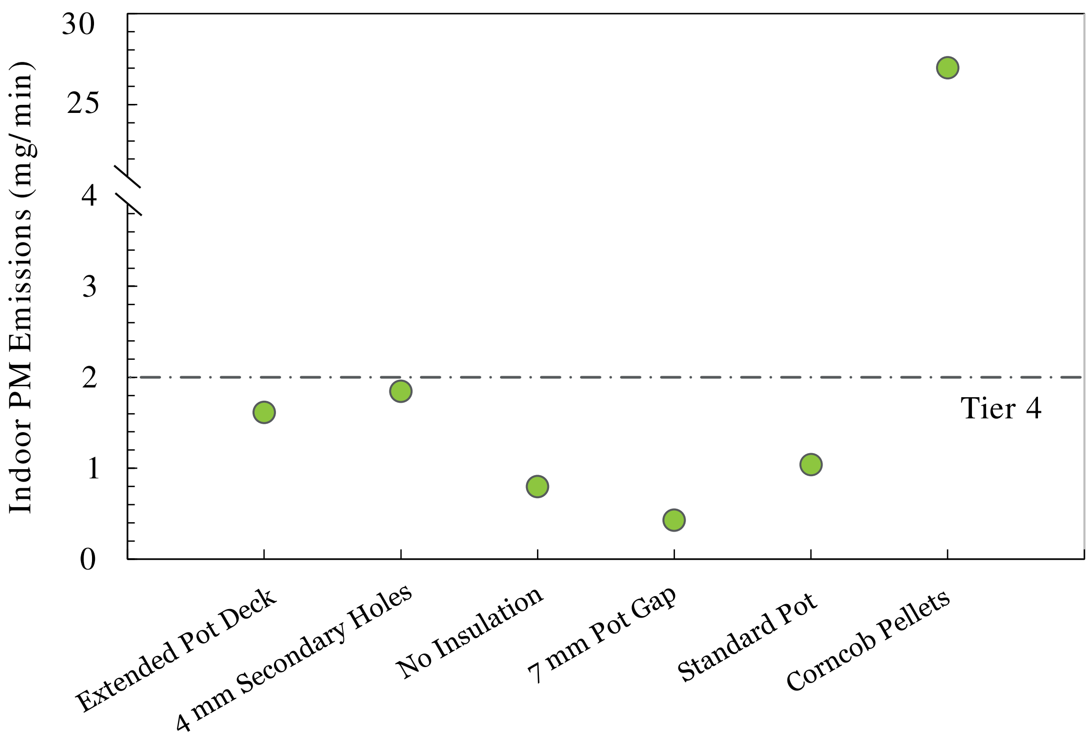

Figure 49 - P2 prototype indoor PM emissions results with different stove configurations and corncob pellets. All test cases that are shown here have one replicate.

The test cases where the pot gap was reduced from 15-mm to 7-mm produced the lowest indoor emissions rate at 0.427 mg/min. Further investigation of this test case may be useful as it emitted PM at a rate 8 times lower than the baseline test case and 2.5 times lower than the LBNL 550g test case.

P2 Power output results

Power output or firepower is the total thermal energy liberated by the combusted mass of fuel used during a test. P2 prototype power output is computed using Equation 19.

Equation 19 - Firepower in w based on the energy content of the fuel consumed during the test phase.

$$P_{total} = \frac{\left(\frac{m_{Fuel_{dry}} * LHV}{1000}\right)}{TTB * 60}$$

Where P_{total} is the average power output in w calculated from the energy released during combustion of the fuel. $m_{fuel_{dry}}$ is the total mass in g of the fuel consumed during the test on a dry basis. LHV is the lower heating value of the fuel in J/g. TTB is the time to boil in minutes.

A difference between the cold start firepower and the hot start firepower indicates that thermal losses to stove mass may be inhibiting stove performance as the stove heats up during the cold start absorbing thermal energy that would otherwise be delivered to the cooking vessel. The difference in power output computed for high power tests and low power simmer tests is defined as the turndown ratio. The turndown ratio an essential factor when evaluating a stoves ability to perform real-world cooking tasks where the end user desired the rapid addition of heat until the desired temperature is reached followed by the maintenance of that desired temperature for a period of time.

The calculated power output values are here published in Figure 50 and Figure 51 respectively. The average of the cold start and hot start power output for the baseline (CSU 600g) test case is 4.08 kW of thermal power. The difference between cold and hot start tests are not statistically significant. The baseline low power simmer output for the same test case is 1.79kw. The difference between the high power and low power baseline power output is significant and results in a turndown ratio of 2.28:1. The comparative test case conducted using the CSU test procedure using 550g of fuel yielded a cold start and hot start power output of 3.11 kW and 3.45 kW the difference between the mean cold and hot start is not statistically significant.

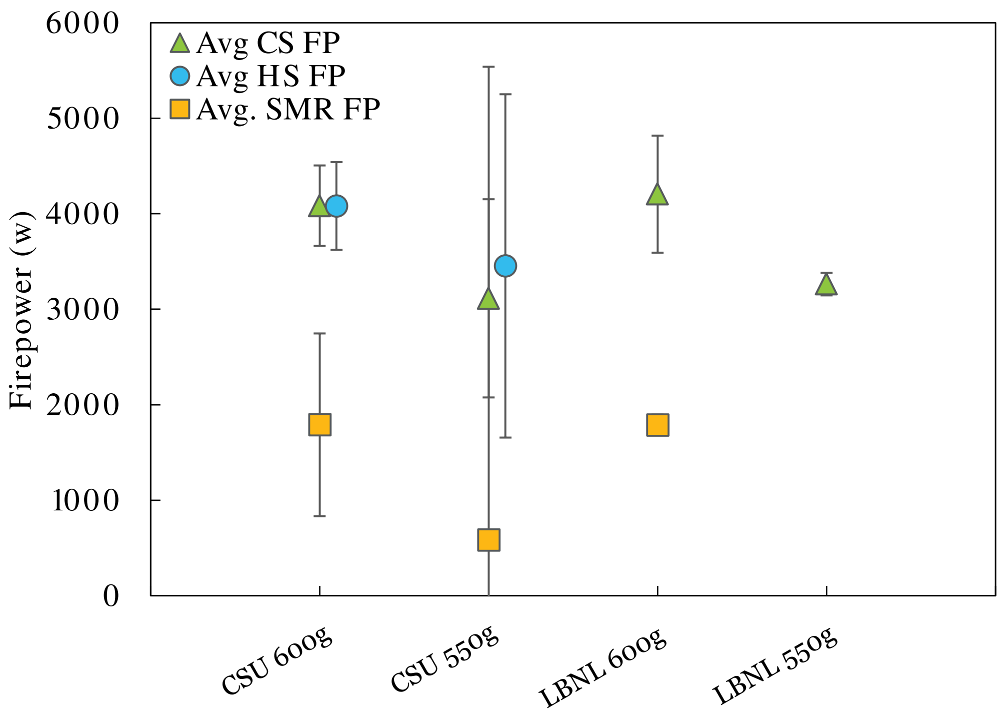

Figure 50 - P2 prototype average thermal power output for high power cold start, hot start, and low power simmer tests where initial fuel mass varied. Jitter added to test case axis to clarify data points. Error bars represent 90% CI.

The low power output for the CSU 550g test case is 0.58 kW for a total turndown of 5.66:1 though large error bars prevent confidence in this conclusion. The turndown ratio is 2.48 times higher for the test case where 550g of fuel is used compared to the test case where 600g of fuel is used. Tests conducted with 600g of fuel under the LBNL test procedure result in a cold start 4.21kw. The low power output for the LBNL 600g test case is 1.79 kW resulting in a turndown ratio of 2.35:1. Hot start and low power tests with an initial fuel load of 550g using the LBNL test procedure have not yet been conducted. The LBNL 550g cold start test yielded an output of 3.26kw, which is not significantly different from the same test condition using the CSU test procedure.

P2 prototype test cases where the stove configuration is varied Figure 51. All the test cases shown in Figure 51 are single test replicates and lack any test repetition. The test case with the bigger secondary air holes produced the highest power output for all three test phases The 4-mm secondary air hole test case power outputs are 3.97kw, 4.67kw, and 1.81kw for cold start, hot start, and low power simmer respectively. The lowest power outputs of 2.95kw, 2.93kw, and 0.1kw for cold start, hot start, and low power simmer respectively are produced by the extended pot deck test case. The extended pot deck test case produced the largest turndown ratio, 29.3:1, of all the test configurations. The 7 -mm pot gap test case produced the smallest turndown ratio of 1.95:1.

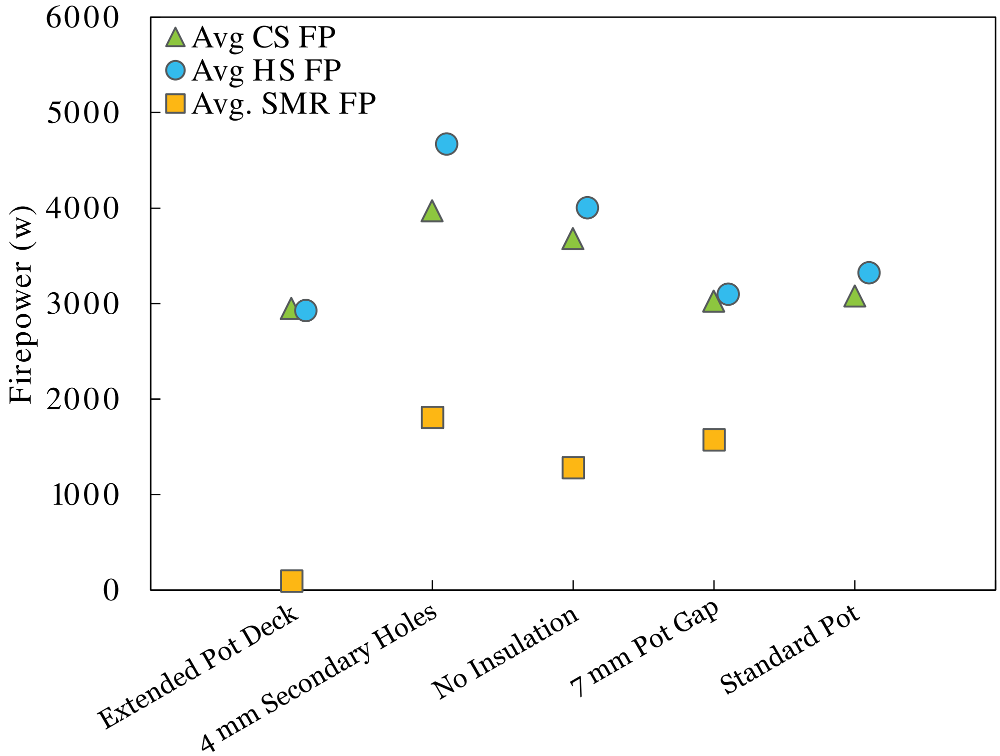

Figure 51 - P2 prototype average thermal power output for high power cold start, hot start, and low power simmer tests where stove configuration is varied. N=1.

Only a fraction of the thermal energy liberated by the pyrolysis and combustion of the fuel as the calculated firepower seen in the previous section is absorbed by the cooking vessel, heating up the water. The remainder of the released energy is lost as heat absorbed into the stove, waste heat in the exhaust and radiant losses to the environment. The useful power output is calculated using Equation 20 to find the energy absorbed by the cooking vessel during the test cycle.

Equation 20 – Useful power output for cold start and hot start tests.

$$P_{useful} = \left(m_{H_2O\ Start}\right) * C_P * (\Delta T_{water})) + m_{steam} * h$$

Where P_{useful} is the useful power output in w, m_{H_2O} is the starting mass of water in g, C_P is the specific heat in J/gC, ΔT_{water} is the temperature change of the water in the cooking vessel. m_{steam} is the mass of water vaporized from the pot during the test in g, and h is the specific enthalpy of vaporization in in J/g for water. The results of this calculation for test cases where the initial fuel mass is varied and for test cases where the stove configuration and fuel type is varied are plotted in Figure 52 and Figure 53 respectively.

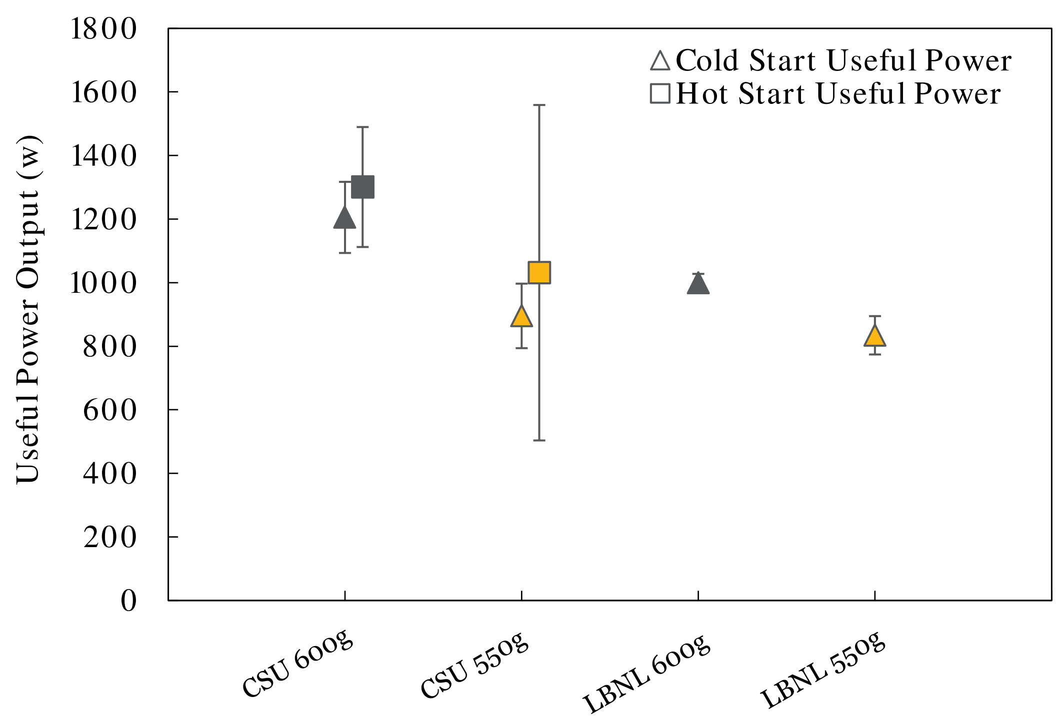

Figure 52 - P2 Prototype average useful power output for high power cold start and hot start tests where initial fuel mass varied. Error bars represent 90% CI.

The data in Figure 52 indicate that there is little difference between the useful power output of cold start and hot start test cases. There is an observed trend of lower useful power output for test cases where less fuel is used. Significant differences are observed between cold start test cases where different starting fuel masses were used. Both CSU

EPTP and LBNL test procedures yield higher useful power outputs during the cold start test phase for cases where the stove is initially fueled with 600g of pellets compared to test cases where the stove was initially fueled with 550g of fuel.

Test data generated from testing where the stove configuration and fuel type are shown in Figure 53.

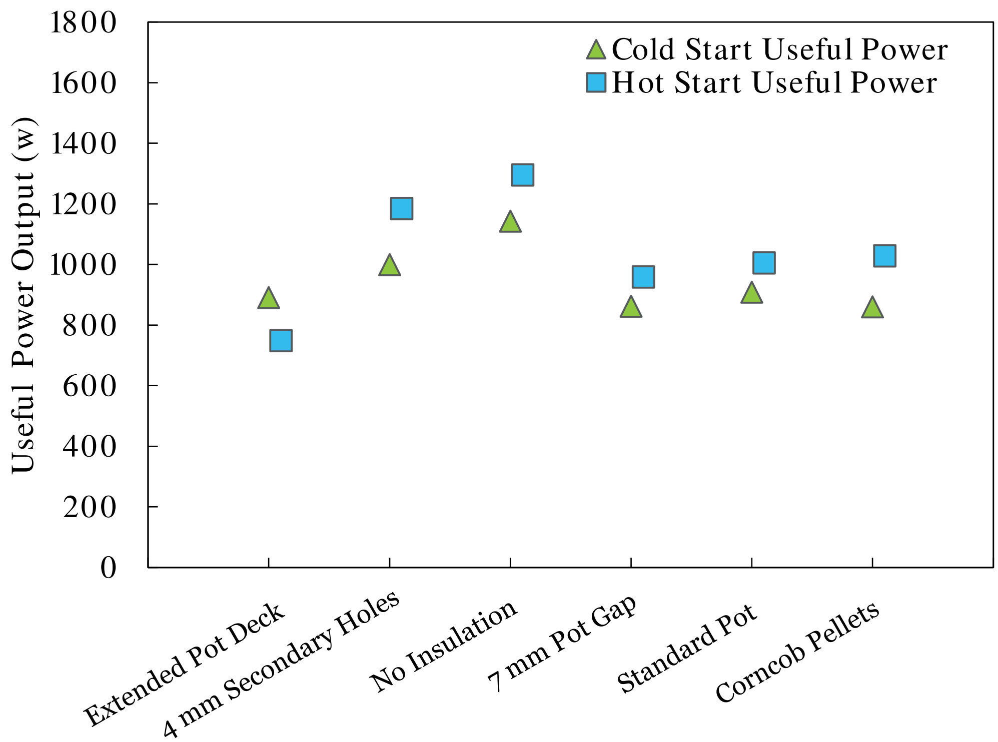

Figure 53 – P2 prototype useful power output for high power cold start and hot start, where stove configuration and fuel type varied. N=1.

These data consists of a single replicate for each test case. However, some hypotheses can be generated from the data. Comparing the individual test points to the baseline test case and the 550 g test cases in Figure 52 it can be seen that the baseline test cases have a higher useful power than most of the test cases where the stove configuration varied. The exception is the test case where no insulation was used, which fell inside the 90% confidence interval for the baseline test case. The test case with larger secondary combustion stage inlet holes and the test case with no insulation both produced more useful power output than the 550g CSU confidence bounds, all other test configurations produced a result which falls between the 90% confidence interval bounds of the 550g test case. The results are the same when comparing the 550g test case using the LBNL test procedure except that the datum for the cold start using the standard pot falls just above the 90% confidence interval.

P2 Thermal Efficiency Results

The fraction of the total power output that is captured in the cooking vessel as useful power is summarized as thermal efficiency. Thermal efficiency results are computed as the fraction of thermal energy liberated by the combustion process, which is used to raise the temperature of the water. Thermal efficiency is computed using Equation 21.

Equation 21 - Thermal Efficiency for cold start and hot start tests

$$\eta_{\mathrm{th}} = \frac{\left(m_{H_2O\ Start}\right) * C_P * (\Delta T_{water})) + m_{steam} * h}{m_{dry\ fuel} * LHV}$$

Where η_{th} is the thermal efficiency, m_{H_2O} is the starting mass of water in g, C_P is the specific heat in J/gC, ΔT_{water} is the temperature change of the water in the cooking vessel. m_{steam} is the mass of water vaporized from the pot during the test in g, h is the specific enthalpy of vaporization in in J/g for water, $m_{dry\ fuel}$ is the total fuel mass in g consumed during the test on a dry basis. The LHV is the lower heating value of the fuel inJ/g.

In order to generate an accurate assessment of the energy liberated during the test, the analysis of the remaining fuel is required. The fuel remaining at the terminus is sorted into char and unburned fuel. The char mass is assumed to have an LHV of 29,500 $\frac{J}{g}$ and 0% moisture content while the unburned fuel is assumed to have an LHV of 19,001 $\frac{J}{g}$ and 6.84% moisture content. These values come from the evaluation of representative samples of the char and the fresh fuels and were not measured for the fuel and char mixture remaining from each test.

The resulting efficiency analysis for test cases where the starting mass of fuel is varied and for test cases where the stove configuration and fuel type is varied are plotted in Figure 54 and Figure 55 respectively. The data in Figure 54 indicate that there is little difference in thermal efficiency between the baseline test case of 600g and the test case where 550g is used. All four of the test cases shown meet the ISO-IWA tier 1 and tier 2 guidelines. CSU test cases have higher thermal efficiency than do test cases using the LBNL techniques. The CSU 600g test case was slightly more efficient than the CSU 550g test case, and there is no robust difference between the 600g and the 550g LBNL test cases.

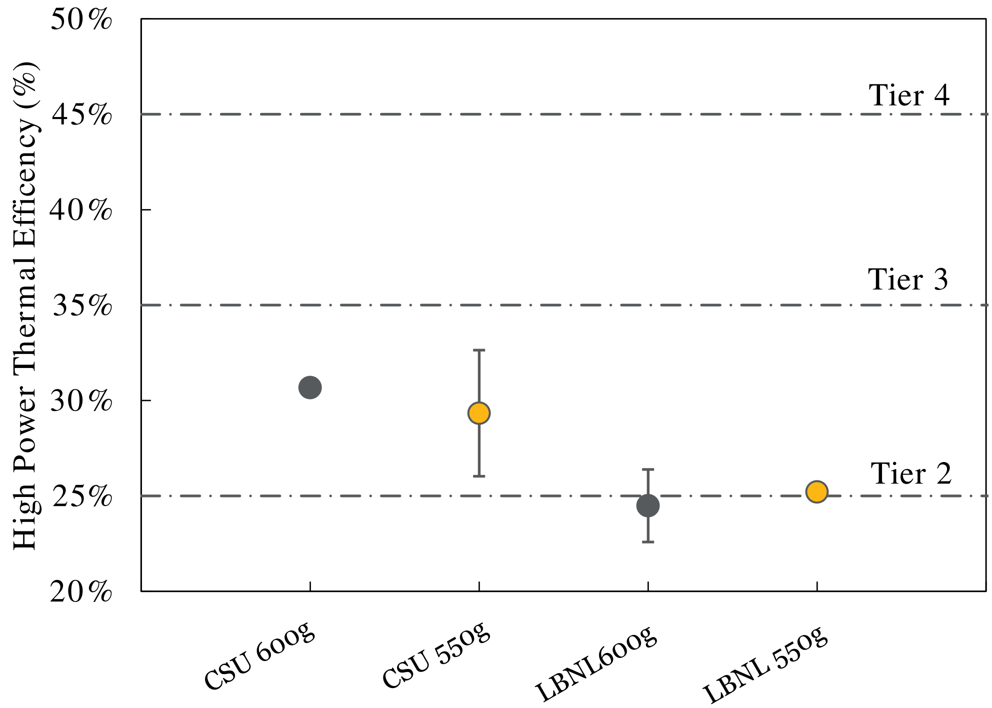

Figure 54 - P2 prototype high power thermal efficiency results for test cases where starting fuel mass varies. Error bars represent a 90% CI.

The data in Figure 55 fall between the ISO-IWA tier 2 and tier 3 for efficiency. The lowest efficiency measured is the test cases with the larger secondary air inlet area. The highest efficiency measured is the test case with no insulation. The no insulation test case is also the only test case to produce an efficiency result higher than the baseline CSU 600g test case. The baseline test case is 30.68% efficient with a standard deviation of 0.253%, and the no insulation test case is 31.71% efficient. The mean efficiency of the baseline test case is 4 standard deviations below the test case with no insulation.

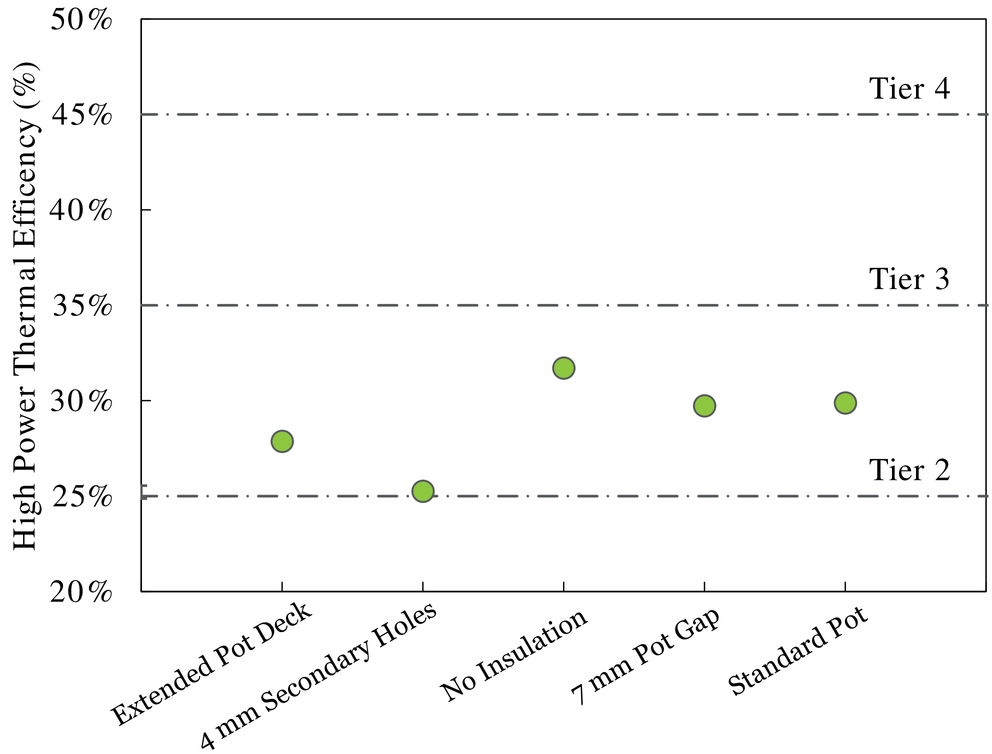

Figure 55 - P2 prototype high power thermal efficiency results for different stove configurations. N=1.

Low power specific fuel consumption results for test cases where the initial fuel mass is varied and test cases where the stove configuration is varied are plotted in Figure 56 and Figure 57 respectively. There is little difference between the test cases using the CSU testing procedure and the LBNL testing procedure for the baseline condition of 600g of fuel. There is an observed difference between the test cases where 600g of fuel is used and cases where 550g of fuel is used, though large error bars suggest that further study should be conducted. The notable exception is the test case where the extended pot deck is used. The mean baseline ISO-IWA low power specific fuel consumption of $0.024 MJ/min/L$ is 3.4 standard deviations higher than the test case where the extended pot deck is used which was measured at $0.0013 MJ/min/L$.

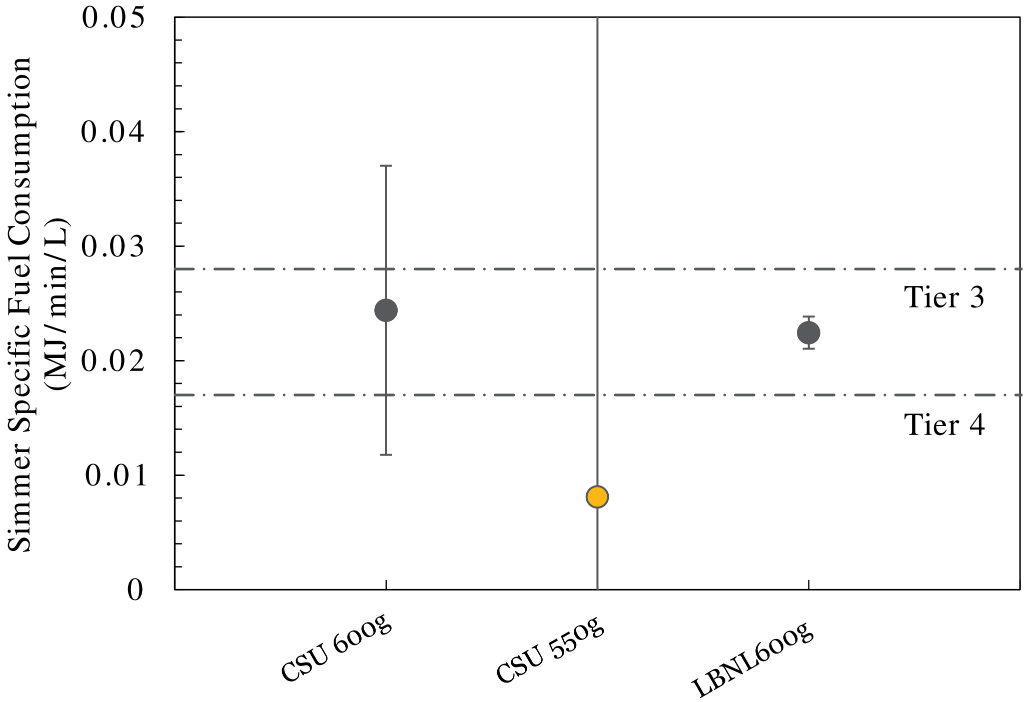

Figure 56 – P2 prototype low power (simmer) specific fuel consumption for test cases where starting fuel mass varies. Error bars represent a 90% CI.

All the low power specific fuel consumption results fall between ISO-IWA tier 3 and tier 4 guidelines. The lowest measured value is 0.0013MJ/min/L, and the highest measured value is 0.036MJ/min/L.

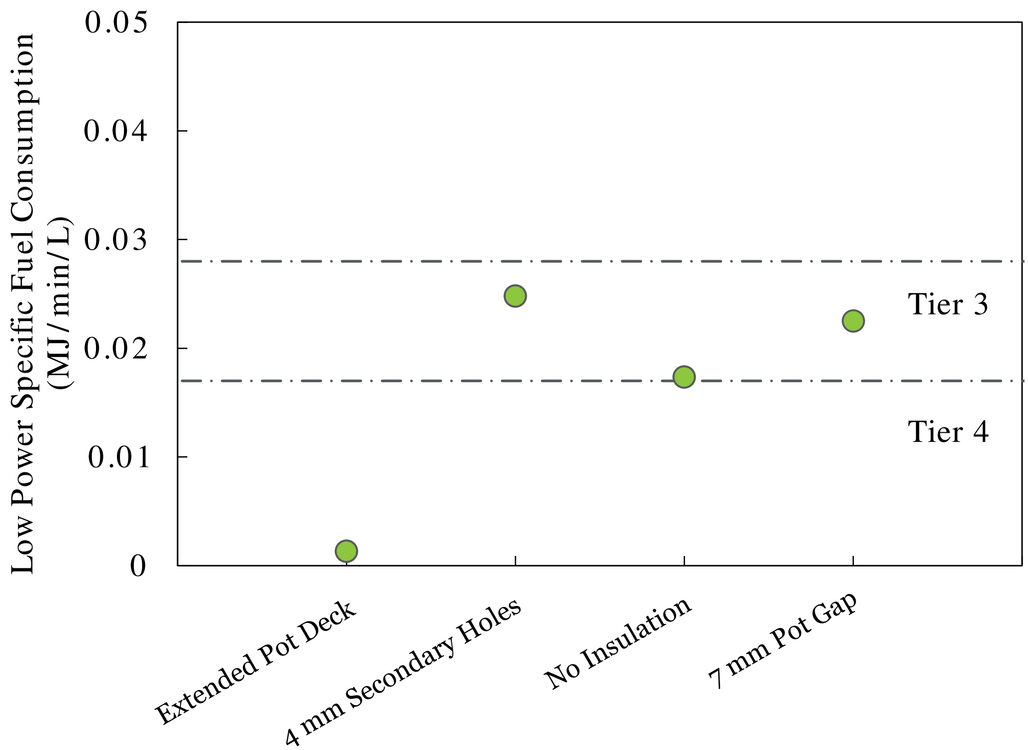

Figure 57 - P2 prototype low power (simmer) specific fuel consumption results for test cases where starting fuel mass varies. N=1.

P2 Time to Boil Results

Time to boil is another critical metric to consider when evaluating a stove for use in the field. If the end user is not satisfied with the time it takes for the stove to complete the cooking task, it is unlikely the stove will be regularly used, if at all. As a comparative measurement to evaluate the stoves ability to heat the content of the cooking vessel a standard metric of temperature-corrected time to boil is used here in this work.

This metric is a measurement of the time it takes to heat the water from the starting temperature to the ending temperature of the test normalized by the delta temperature of 75 C defined by the ideal starting and ending temperatures for the water-boil test. Equation 22 is the equation for normalizing the time to boil.

Equation 22 - temperature corrected time to boil.

$$TTB_{TC} = TTB * \frac{75}{\Delta T_{water}}$$

Where TTB_{TC} is the temperature corrected time to boil in minutes, TTB is the measured time to complete the test cycle in minutes, $\Delta T_{water}$is the change in the water temperature in ℃.

The data plotted in Figure 58 and Figure 59 are temperatures corrected time to boil for tests conducted with different initial fuel mass, and different stove configuration and fuel type respectively.

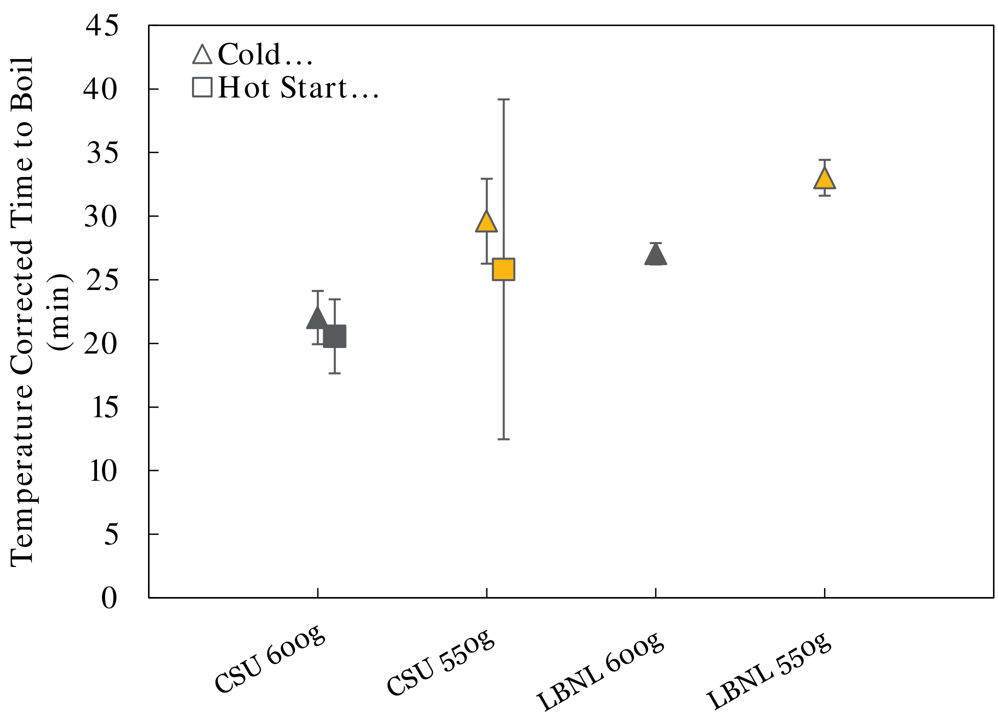

Figure 58 - P2 prototype cold start and hot start high power temperature corrected time to boil results for test cases where starting fuel mass varied. Jitter added to test case axis to clarify data points. Error bars represent 90% CI.

Figure 58 data demarcated by triangular indicators are cold start tests, and square indicators are hot start tests. Error bars indicate a 90% CI. The cold start and hot start time to boil are not significantly different for test cases using 600g of fuel. Compared to the test cases using 550g of fuel the cold start and hot start temperature corrected time to boil for test cases using 600g of fuel are 31.91% and 25.58% faster respectively.

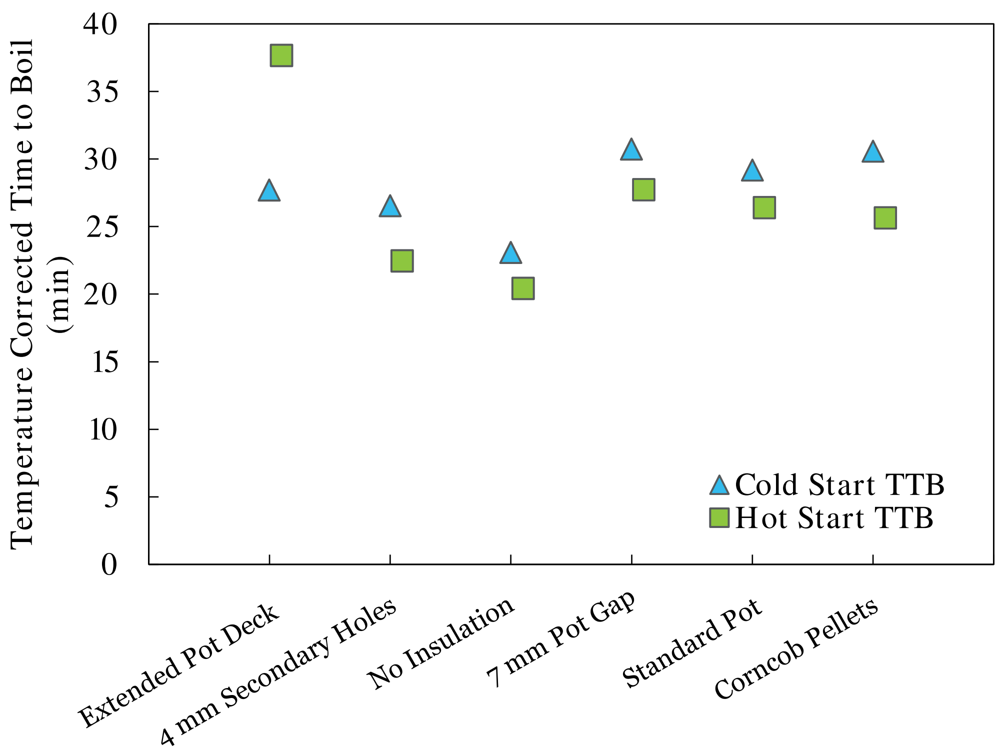

Figure 59 - P2 prototype cold start and hot start high power temperature corrected time to boil results for test cases where stove configuration and fuel type varied. N=1.

P2 prototype test cases where the stove configuration and fuel type varied, shown in Figure 59, show trends similar to those identified in the data from Figure 58. With the exception of the test case where the extended pot deck is used, all stove configurations showed that a cold start takes approximately 14.22% longer than a hot start under the same stove configuration. The exceptional case is the test case where the extended pot deck was used. In this test case, the hot start takes 37.65 minutes which is longer than the baseline hot test at 20.56 minutes and the average hot start using 550 grams of fuel at 24.66 minutes.

CONCLUSIONS AND FUTURE WORK

Carbon Monoxide emission for the final P2 prototype with the VGC chamber is excellent. Every test conducted with the P2 VGC prototype stove using the CSU and the LBNL test procedures yielded a result exceeding the tier 4 guidelines for CO emissions. This includes the high power results, simmer results and the indoor emissions rate results. There is little variation between different test configurations and no strong patterns emerge from the evaluation of the data. The only test cases to fall far from the baseline 600g result measured at CSU are the 7-mm pot gap test case and the standard pot test case. Without replicate tests little can be stated with certainty about these two results. The results do warrant future investigation. It can be hypothesized that the smaller 7-mm pot gap reduces ambient air entrainment in the secondary combustion stage and increase incomplete combustion products while moving the pot into more significant contact with the flame further cooling exhaust gasses and allowing more CO to pass from the stove un-oxidized.

PM emissions do not generally meet the ISO-IWA guidelines for tier 4 high power $PM_{2.5}$ emissions for this prototype. A number of individual test cases for a wide range of stove configurations did meet the tier 4 guidelines, and with additional refinement, the tier 4 guidelines appear in reach. One notable exception is the test case using corncob pellets. The suboptimal corncob pellet fuel produced significant $PM_{2.5}$ emissions during high power operation, highlighting the importance of proper fuel selection and the critical nature of providing a quality fuel to the end user for efficacious emissions reduction. Low power $PM_{2.5}$ emissions for all test cases except the 7-mm pot gap meet the ISO-IWA tier 4 guidelines for low power $PM_{2.5}$ emissions. The lack of replicate data for the 7-mm pot gap test case mean that the difference between the baseline and the 7-mm pot gap low power $PM_{2.5}$ emissions cannot be used to draw a stochastic conclusion. However, it is possible that the reduced pot gap may be cooling the hot exhaust gas and allowing the condensation of greater numbers of particulates than the baseline 15-mm pot gap. Thus further investigation as to the effect of the pot gap on $PM_{2.5}$ emissions may considered for future work.

Indoor PM emissions rates for the P2 prototype is also promising. Most test cases meet the ISO-IWA tier 4 guidelines for indoor PM emissions rates. Notably, the baseline test case using 600g of fuel to start the high power portions of the testing produced significantly more emissions than the test cases where 550g of fuel is used, indicating that the lower fuel bed improves the PM emissions rates. The likely cause of this improvement is not due to a lower total $PM_{2.5}$ mass emission for test cases where 550g of fuel is used but rather a longer time to boil as seen in Figure 58, which results from a lower power output as seen in Figure 50.

Stove configuration did not seem to have any significant influence over the PM emissions rates for the P2 prototype stove, operating under ideal laboratory conditions, by skilled users, fueled with high-quality pellets may achieve the ISO-IWA tier 4 emissions guidelines for high power, low power, and indoor CO and PM emissions. If the stove is operated under non-ideal conditions, or in a manner not consistent with best practices, then the stove may produce considerably more emissions than is allowed.

High power thermal efficiency is the metric which has the worst performance as measured against the ISO-IWA guidelines. No test cases produced tier 4 or tier 3 performance results. Test cases where the initial fuel load is varied from 550g to 600g produce a minimal difference in thermal efficiency. Out of the stove configurations evaluated for future testing the test where the insulation was removed performed the best for both high power thermal efficiency and low power specific fuel consumption. It may, therefore, be worth future evaluation to verify that the result is reliable. There is a measurable difference between the test which used the CSU EPTP test procedure and test cases using the LBNL test procedure.

Future Work

While this body of work has resulted in strides forward in the design and implementation of a field ready fan powered gasifier cookstove, additional research questions have also been uncovered. Additional evaluation of the effect that stove diameter has on emissions, efficiency, and power output performance warrants further evaluation. Specifically, evaluating if a dual diameter chamber such as the VGC here tested is required to provide the high power and low power performance required to complete high power and simmer operations, or if a single intermediate diameter is sufficient.

High power thermal efficiency and low power specific fuel consumption also remains a significant area of interest as the stove design is refined to comply with the ISO-IWA tier 4 guidelines. Honing the global secondary combustion stage air to fuel ratio may be significant in achieving higher thermal efficiency values. It may also be necessary to implement heat recovery devices into the cooking vessel such as heat transfer fins, or a pot skirt.

Based on the P0 Modular Laboratory TLUD results, fuel type and user ability are the most critical factors in determining the efficacy of a stove in reducing harmful emissions.

Therefore, additional P2 fuel type evaluation is also of interest as a full breadth of fuel types expected to be used in the field. It may be useful to couple laboratory fuel evaluation in stove design with a field campaign that studies what common fuel types are available in the target market.

Improved combustion stability of the stove, especially during transient events such as startup and shutdown, and when using sub-optimal fuels may have a significant effect on real-world emissions. The implementation of sensor feedback to the stove fan could play a role in improving stove stability. A plenum pressure sensor can be used to map the PWM signal to a specific flow rate through the primary and secondary inlets. Using a pressure sensor feedback control would make the stove more ambivalent to leakage as the stove ages and can allow altitude compensation as well. Temperature feedback, especially in the secondary combustion stage air inlet, can be used to further compensate for density differences and also act as a safety feature in the event that the secondary combustion is extinguished while pyrolysis gas is still being released by the primary combustion stage thus preventing the release of harmful gases and particles into the ambient environment.

Another critical area of research that is currently being explored but must be well understood before any confident statement on human health improvements is the effect that modern improved stoves have on particle size and number count. Preliminary research indcates that smaller more numerous particles may have a stronger negitive influence on human health than fewer larger particles. And improved stoves may produce more of those ultrafine particles than the unimproved stoves they replace[59].

Another area of further exploration which is critical to a stove programs success is the ability of an improved stove design to meet the cooking needs of the end user. For example is the stove astheticly pleaseing to the user (something that is culturally dependent), does the stove prevent burns and tips, is the stove durable and reliable, can it compleately replace the traditional stove for all cooking tasks? If the stove fails in any of these design requirements the stove may not be used with enough regularity to acomplish the goal of improving human health and quality of life.

There are a vast number of engineering, human health, and social variables to consider for each stove design and each culture. A successful stove program is far more than a well engineered stove and carful research and implimentation are critical to the long term success of any stove program, and to the altruistic objectives of reducing human suffering through improved human health and quailty of life. The heart of every improved stove program is a stove that can reduce emissions, improve efficency and do so safely, but the design of such a stove, as challanging as that may be is only the beginning.

REFERENCES

1. Turns, S. R. *An introduction to combustion: concepts and applications. System* **499,** (2000).

2. Bonjour, S. *et al.* Solid fuel use for household cooking: Country and regional estimates for 1980-2010. *Environ. Health Perspect.* **121,** 784–790 (2013).

3. Naeher, L. P. *et al.* Woodsmoke health effects: a review. *Inhal Toxicol* **19,** 67–106 (2007).

4. Hinds, W. C. *Aerosol Technology: Properties. Behavior, and Measurement of airborne Particles.* (1999).

5. Oberdörster, G. Pulmonary effects of inhaled ultrafine particles. *Int. Arch. Occup. Environ. Health* **74,** 1–8 (2001).

6. HEI Review Panel. Understanding the Health Effects of Ambient Ultrafine Particles. *Heal. Eff. Inst.* 122 (2013).

7. J., G. *et al.* Comparisons of ultrafine and fine particles in their associations with biomarkers reflecting physiological pathways. *Environ. Sci. Technol.* (2014).

8. Donaldson, K., Stone, V., Clouter, A., Renwick, L. & Macnee, W. Ultrafine Particles. 211–216 (2001).

9. Fullerton, D. G., Bruce, N. & Gordon, S. B. Indoor air pollution from biomass fuel smoke is a major health concern in the developing world. *Trans. R. Soc. Trop. Med. Hyg.* **102,** 843–851 (2008).

10. Smith, K. R., Samet, J. M., Romieu, I. & Bruce, N. acute lower respiratory infections in children Indoor air pollution in developing countries and Topic collections Indoor air pollution in developing countries and acute lower respiratory infections in children. *Thorax* **55,** 518–532 (2000).

11. Kurmi, O. P., Semple, S., Simkhada, P., Cairns S Smith, W. & Ayres, J. G. COPD and chronic bronchitis risk of indoor air pollution from solid fuel: A systematic review and meta-analysis. *Thorax* (2010). doi:10.1136/thx.2009.124644

12. Boy, E., Bruce, N. & Delgado, H. Birth weight and exposure to kitchen wood smoke during pregnancy in rural Guatemala. *Environ. Health Perspect.* **110,** 109–114 (2002).

13. Raspanti, G. A. *et al.* Household air pollution and lung cancer risk among never-smokers in Nepal. *Environ. Res.* **147,** (2016).

14. Zhao, Y., Wang, S., Aunan, K., Martin Seip, H. & Hao, J. Air pollution and lung cancer risks in China-a meta-analysis. *Sci. Total Environ.* (2006). doi:10.1016/j.scitotenv.2005.10.010

15. Martoni, A. A. in *Clinical Handbook of Air Pollution-Related Diseases* (2018). doi:10.1007/978-3-319-62731-1_24

16. Ezzati, M. & Kammen, D. M. Indoor air pollution from biomass combustion and acute respiratory infections in Kenya: An exposure-response study. *Lancet* **358,** 619–624 (2001).

17. Mishra, V. Indoor air pollution from biomass combustion and acute respiratory

illness in preschool age children in Zimbabwe. *Int. J. Epidemiol.* **32,** 847–853 (2003).

18. Bruce, N. *et al.* Impact of improved stoves, house construction and child location on levels of indoor air pollution exposure in young Guatemalan children. *J. Expo. Anal. Environ. Epidemiol.* **14,** S26–S33 (2004).

19. WHO. Indoor Air Quality Guidelines: Household Fuel Combustion. *World Heal. Organ.* 1–172 (2014).

20. Bruce, N. *et al.* WHO indoor air quality guidelines on household fuel combustion: Strategy implications of new evidence on interventions and exposure-risk functions. *Atmos. Environ.* **106,** 451–457 (2015).

21. WHO. *the Energy Access Situation in Developing Countries. UNDP WHO New York* (2009).

22. Forouzanfar, M. H. *et al.* Global, regional, and national comparative risk assessment of 79 behavioural, environmental and occupational, and metabolic risks or clusters of risks, 1990–2015: a systematic analysis for the Global Burden of Disease Study 2015. *Lancet* **388,** 1659–1724 (2016).

23. Forouzanfar, M. H. *et al.* Global, regional, and national comparative risk assessment of 79 behavioural, environmental and occupational, and metabolic risks or clusters of risks in 188 countries, 1990-2013: A systematic analysis for the Global Burden of Disease Study 2013. *Lancet* **386,** 2287–2323 (2015).

24. Lim, S. S. *et al.* A comparative risk assessment of burden of disease and injury

attributable to 67 risk factors and risk factor clusters in 21 regions, 1990-2010: A systematic analysis for the Global Burden of Disease Study 2010. *Lancet* **380,** 2224–2260 (2012).

25. Output, H. L. *et al.* Millions dead: how do we know and what does it mean? Methods used in the comparative risk assessment of household air pollution. *Biomass and Bioenergy* **20,** 3–12 (2014).

26. Abajobir, A. A. *et al.* Global, regional, and national comparative risk assessment of 84 behavioural, environmental and occupational, and metabolic risks or clusters of risks, 1990–2016: a systematic analysis for the Global Burden of Disease Study 2016. *Lancet* **390,** 1345–1422 (2017).

27. Bond, T., Venkataraman, C. & Masera, O. Global atmospheric impacts of residential fuels. *Energy Sustain. Dev.* (2004). doi:10.1016/S0973-0826(08)60464-0

28. Bond, T. C. & Sun, K. Can reducing black carbon emissions counteract global warming? *Environ. Sci. Technol.* **39,** 5921–5926 (2005).

29. Food and Agricultural Organization of the United Nations. *State of the World's Forests*. (2014). doi:10.1103/PhysRevLett.74.2694

30. Dolisca, F., McDaniel, J. M., Teeter, L. D. & Jolly, C. M. Land tenure, population pressure, and deforestation in Haiti: The case of For??t des Pins Reserve. *J. For. Econ.* **13,** 277–289 (2007).

31. Peduzzi, B. P. Article Tropical cyclones : paying a high price for environmental destruction Tropical cyclones : paying a high price for environmental destruction.

(2005).

32. US Law | LII / Legal Information Institute. *40 CFR Part 89 - CONTROL OF EMISSIONS FROM NEW AND IN-USE NONROAD COMPRESSION-IGNITION ENGINES. may* (2018).

33. Engines, M. *et al.* Electronic Code of Federal Regulations : TITLE 40--Protection of Environment Electronic Code of Federal Regulations. *Clean Air* (2011).

34. *ISO-IWA2012*. (2012).

35. McKendry, P. Energy production from biomass (part 1): overview of biomass. *Bioresour. Technol* **83,** 37–46 (2002).

36. Di Blasi, C. Modeling chemical and physical processes of wood and biomass pyrolysis. *Prog. Energy Combust. Sci.* **34,** 47–90 (2008).

37. Chan, W. C. R., Kelbon, M. & Krieger, B. B. Modelling and experimental verification of physical and chemical processes during pyrolysis of a large biomass particle. *Fuel* **64,** 1505–1513 (1985).

38. Tillman, D. A. *Combustion of Solid Fuels & Wastes. Combustion of Solid Fuels & Wastes* (1991). doi:10.1016/B978-0-08-057112-6.50006-9

39. Institute, S. E. R., Reed, T. B. & of Energy, U. S. D. A Survey of Biomass Gasification. **II,** (1979).

40. Tryner, J., Willson, B. D. & Marchese, A. J. The effects of fuel type and stove design on emissions and efficiency of natural-draft semi-gasifier biomass cookstoves.

Energy Sustain. Dev. **23,** 99–109 (2014).

41. Tryner, J. *et al.* The Effects of Air Flow Rates, Secondary Air Inlet Geometry, Fuel Type, and Operating Mode on the Performance of Gasifier Cookstoves. *Environ. Sci. Technol.* **50,** 9754–9763 (2016).

42. Jetter, J. J. & Kariher, P. Solid-fuel household cook stoves: Characterization of performance and emissions. *Biomass and Bioenergy* **33,** 294–305 (2009).

43. Jetter, J. *et al.* Pollutant emissions and energy efficiency under controlled conditions for household biomass cookstoves and implications for metrics useful in setting international test standards. *Environ. Sci. Technol.* **46,** 10827–10834 (2012).

44. Varunkumar, S., Rajan, N. K. S. & Mukunda, H. S. Experimental and computational studies on a gasifier based stove. *Energy Convers. Manag.* (2012). doi:10.1016/j.enconman.2011.08.022

45. Mukunda, H. S. *et al.* Gasifier stoves - science, technology and field outreach. *Curr. Sci.* (2010).

46. James, R. A. M., Yuan, W. & Boyette, M. D. The effect of biomass physical properties on top-lit updraft gasification of woodchips. *Energies* (2016). doi:10.3390/en9040283

47. Huangfu, Y. *et al.* Effects of moisture content in fuel on thermal performance and emission of biomass semi-gasified cookstove. *Energy Sustain. Dev.* (2014). doi:10.1016/j.esd.2014.05.007

48. Tryner, J., Volckens, J. & Marchese, A. J. Effects of operational mode on particle size and number emissions from a biomass gasifier cookstove. *Aerosol Sci. Technol.* **6826,** 1–11 (2017).

49. Varunkumar, S., Rajan, N. K. S. & Mukunda, H. S. Single particle and packed bed combustion in modern gasifier stoves-density effects. *Combust. Sci. Technol.* (2011). doi:10.1080/00102202.2011.576658

50. Carter, E. M., Shan, M., Yang, X., Li, J. & Baumgartner, J. Pollutant emissions and energy efficiency of chinese gasifier cooking stoves and implications for future intervention studies. *Environ. Sci. Technol.* (2014). doi:10.1021/es405723w

51. Kirch, T., Medwell, P. R. & Birzer, C. H. Natural draft and forced primary air combustion properties of a top-lit up-draft research furnace. *Biomass and Bioenergy* (2016). doi:10.1016/j.biombioe.2016.05.003

52. PETTERSEN, R. C. The Chemical Composition of Wood. 57–126 (1984). doi:10.1021/ba-1984-0207.ch002

53. Demirba, A. 97/02918 Calculation of higher heating values of biomass fuels. *Fuel Energy Abstr.* **38,** 240 (1997).

54. E871-82, A. Standard Test Method for Moisture Analysis of Particulate Wood Fuels 1. *Annu. B. ASTM Stand.* **82,** 2 (2014).

55. ASTM. Standard Test Method for Volatile Matter in the Analysis of Particulate Wood Fuels E872 - 82. *ASTM Int.* **82,** 14–16 (2011).

56. Lenth, R. V. Some practical guidelines for effective sample size determination. *Am.*

Stat. **55,** 187–193 (2001).

57. ASTM D5865. Standard Test Method for Gross Calorific Value of Coal and Coke. *ASTM Int.* (2013). doi:10.1520/D5865

58. BioLite's HomeStove. Available at: https://www.bioliteenergy.com/products/homestove/. (Accessed: 14th April 2018)

59. Just, B., Rogak, S. & Kandlikar, M. Characterization of ultrafine particulate matter from traditional and improved biomass cookstoves. *Environ. Sci. Technol.* **47,** 3506–3512 (2013).

60. Tryner, J. Combustion Phenomena in Biomass Gasifier Cookstoves. (Colorado State University, 2016).

61. Tryner, J. *et al.* The E ff ects of Air Flow Rates, Secondary Air Inlet Geometry, Fuel Type, and Operating Mode on the Performance of Gasi fi er Cookstoves. (2016). doi:10.1021/acs.est.6b00440

62. Tryner, J., Volckens, J. & Marchese, A. J. Effects of operational mode on particle size and number emissions from a biomass gasifier cookstove. *Aerosol Science and Technology* 1–11 (2017). doi:10.1080/02786826.2017.1380779

APPENDIX 1: STOVE DESIGN DATA

Table 6 - Stove Design Parameters

Stove	P0 Modular TLUD (Baseline)	P0 Modular TLUD (Final)	P1 Prototype (Baseline)	P2 Prototype (Baseline)	P2 Prototype (VGC Final)
Height (mm)			289	254	254
Diameter (mm)			109	105	109
Primary Air Hole Number			9	9	7
Primary Air Hole Diameter (mm)			2	2	2
Secondary Air Hole Number			32	32	24
Secondary Air Hole Diameter (mm)			2	2	4
Secondary Air Hole Number (2nd size)			-	-	8
Secondary Air Hole Diameter (2nd size) (mm)			-	-	2
Early Secondary Air Hole Number			6	6	6
Early Secondary Air Hole Diameter (mm)			2	2	1.5
Total Primary Air Hole Area (mm^2)			28.3	28.3	22.0
Total Secondary Air Hole Area (mm^2)			119.4	119.4	337.3
Secondary to Primary Air Hole Area Ratio			4.2	4.2	15.3
VGT					
Height	NA	NA	NA	NA	146
Diameter	NA	NA	NA	NA	75
Transition Frustum Height	NA	NA	NA	NA	10

Table 7: Parametric Testbed Instrument table

No.	Measurement Location	Model Number	Description
1	Fuel Chamber Bottom Temperature 1	KMTSS-125U-6	Ungrounded 6” X 1/8” probe
2	Fuel Chamber Bottom Temperature 2	KMTSS-125U-6	Ungrounded 6” X 1/8” probe
3	Fuel Chamber Middle Temperature 1	KMTSS-125U-6	Ungrounded 6” X 1/8” probe
4	Fuel Chamber Middle Temperature 1	KMTSS-125U-6	Ungrounded 6” X 1/8” probe
5	Fuel Chamber Top Temperature 1	KMTSS-125U-6	Ungrounded 6” X 1/8” probe
6	Fuel Chamber Top Temperature 2	KMTSS-125U-6	Ungrounded 6” X 1/8” probe
7	Fuel Gas Temperature 1 (Sample Probe side)	KMTSS-125U-6	Ungrounded 6” X 1/8” probe
8	Fuel Gas Temperature 2	KMTSS-125U-6	Ungrounded 6” X 1/8” probe
9	Primary Air Temperature	TC-K-1/8NPT-E	1/8” exposed junction
10	Stove body Temperature 1	WTK-8-24	8-24 size Bolt-on
11	Stove body Temperature 2	WTK-8-24	8-24 size Bolt-on
12	Stove body Temperature 3	WTK-8-24	8-24 size Bolt-on
13	Stove body Temperature 4	WTK-8-24	8-24 size Bolt-on
14	Exhaust Gas Temperature 1	HH-K-24-SLE	24 AWG, exposed junction*
15	Exhaust Gas Temperature 2	HH-K-24-SLE	24 AWG, exposed junction*
16	Exhaust Gas Temperature 3	HH-K-24-SLE	24 AWG, exposed junction*
17	Exhaust Gas Temperature 4	HH-K-24-SLE	24 AWG, exposed junction*
18	Water Temperature	KMTSS-125U-6	Ungrounded 6” X 1/8” probe
19	Secondary Air Temperature 1	KMTSS-125U-6	Ungrounded 6” X 1/8” probe
20	Secondary Air Temperature 2	KMTSS-125U-6	Ungrounded 6” X 1/8” probe
21	Carbon Dioxide	Ultramat 6	NDIR CO_2 analyzer
22	Carbon Monoxide	Ultramat 6	NDIR CO analyzer
23	Producer Gas	Custom System	Drying and sampling system

All thermocouples are type K, * Thermocouple junction manufactured in-house using thermocouple welding to reduce the junction size.

APPENDIX 2: EXPERIMENTAL PHOTOGRAPHS

The following appendix is photographs of the experimental setup used in this work.

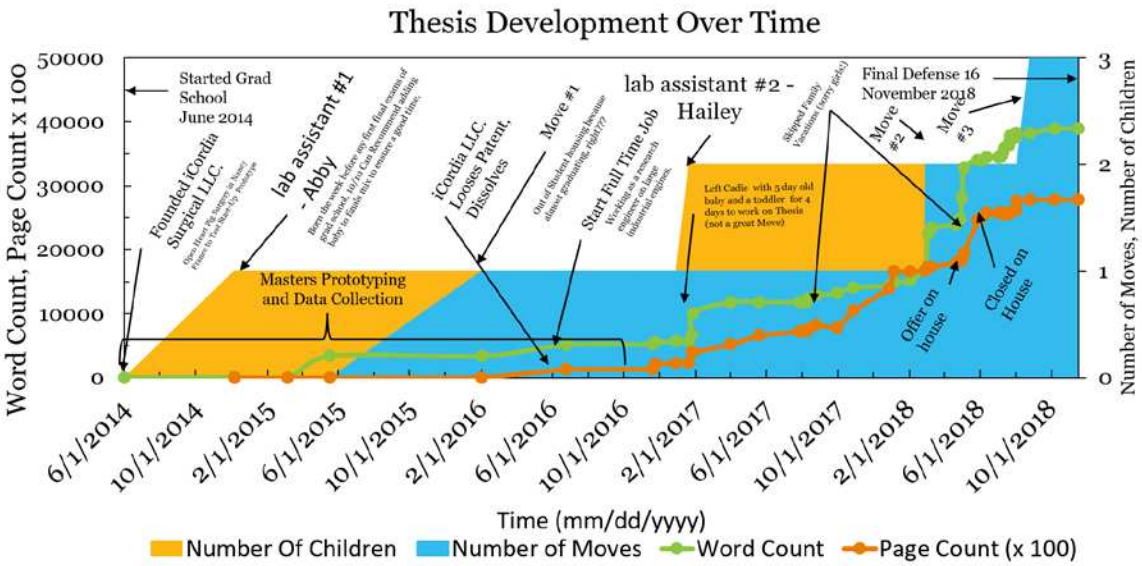

Figure 60 – Plot of thesis development over time with markers indicating major life events.

P0 Modular Laboratory Top-lit Up-Draft Semi-gasifier Cookstove Prototype

The following subsection of appendix 2 contains photos of the P0 TLUD prototype.

Figure 61 – P0 prototype with large secondary flame (not part of actual testing).

Figure 62 – Photographs of the modular secondary air inlet rings. On the left side of the figure are the swirl inlets, 45, 30, and 15 degrees from top to bottom. In the center stack are the varying hole diameter inlets, 2mm, 4mm, 6mm, 8mm and 10mm from the top to the bottom. The right side of the figure are downward angle inlets 30, 20, and 10 degrees from the top to the bottom.

Figure 63 – Visible swirl of the flame in P0 prototype test configuration where swirl secondary air inlet was used

Figure 64 – Image of inverse diffusion flame. Several jets are visible with the largest and clearest being located near the center of the frame. Note the blue flame front and the yellow flame surrounding the blue flame front indicating the present of heated particulates.

Figure 65 – P0 prototype early secondary air inlet combustion chamber

Figure 66 – P0 Prototype 100mm Chimney. Note insulation has been removed for this image.

Figure 67 – P0 post-secondary combustion stage orifice plate

Figure 68 – P0 pre-secondary combustion stage orifice plate

P1 Intermediate Top-lit Up-Draft Semi-gasifier Cookstove Prototype

The following subsection of appendix 3 is photographs of the P1 TLUD prototype

Figure 69 – P1 prototype with electronics package installed.

Figure 70 – P1 prototype TLUD top view.

P2 Production Intent Top-lit Up-Draft Semi-gasifier Cookstove Prototype

The following subsection of appendix 3 are photographs of the P2 TLUD prototype

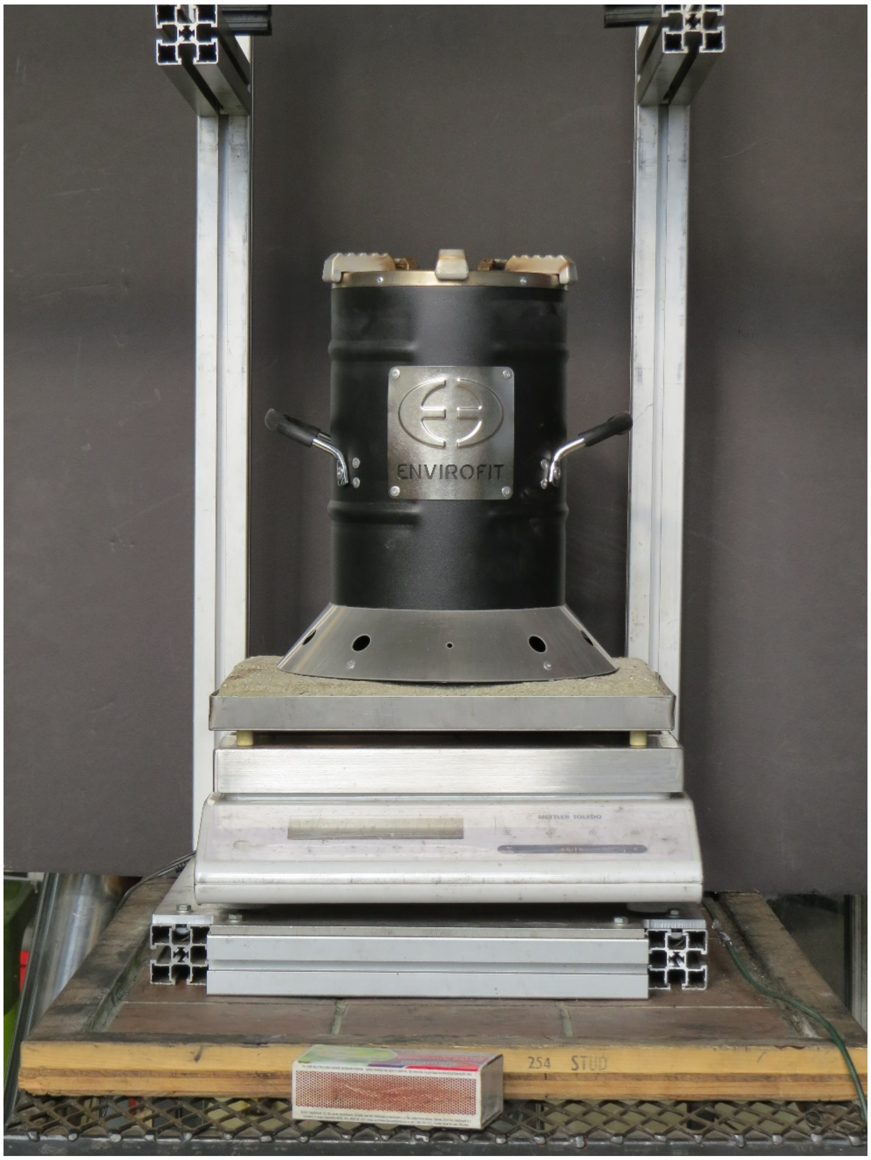

Figure 71 – P2 prototype with early electronics package ready for testin.

Figure 72 – P2 prototype with early electronics package just prior to igniting the stove

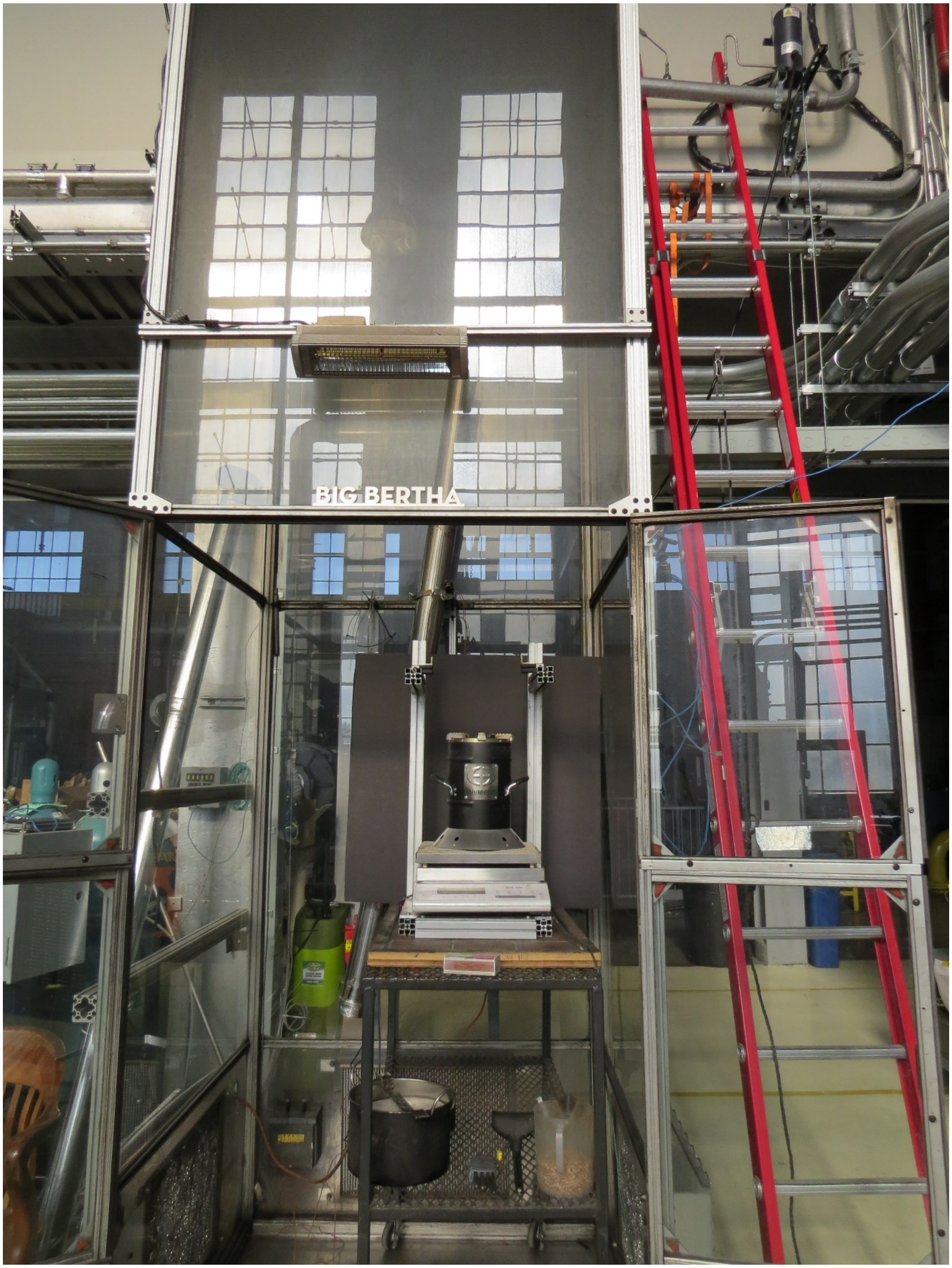

Figure 73 – P2 prototype in the large laminar fume hood "big bertha" ready for testing

Figure 74 – P2 prototype during testing

Figure 75 - A plurality of views of the P2 prototype design aesthetic

Figure 76 – P2 VGC Combustion Chamber side view

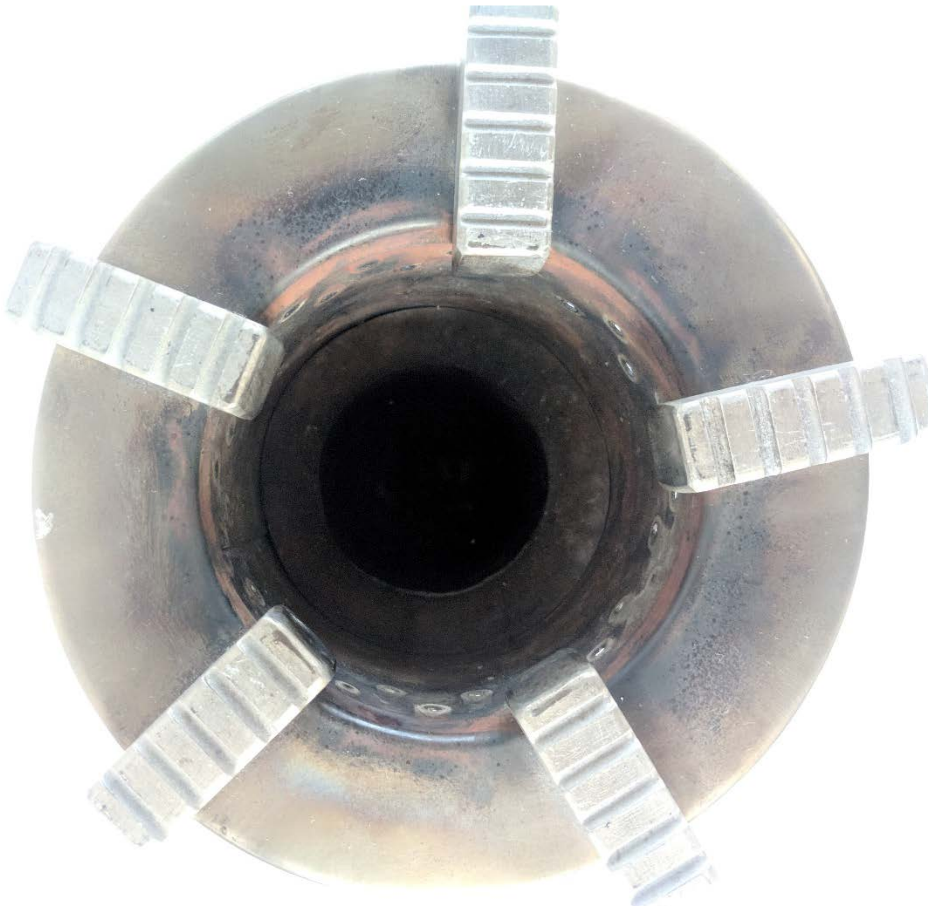

Figure 77 – P2 VGC from the top

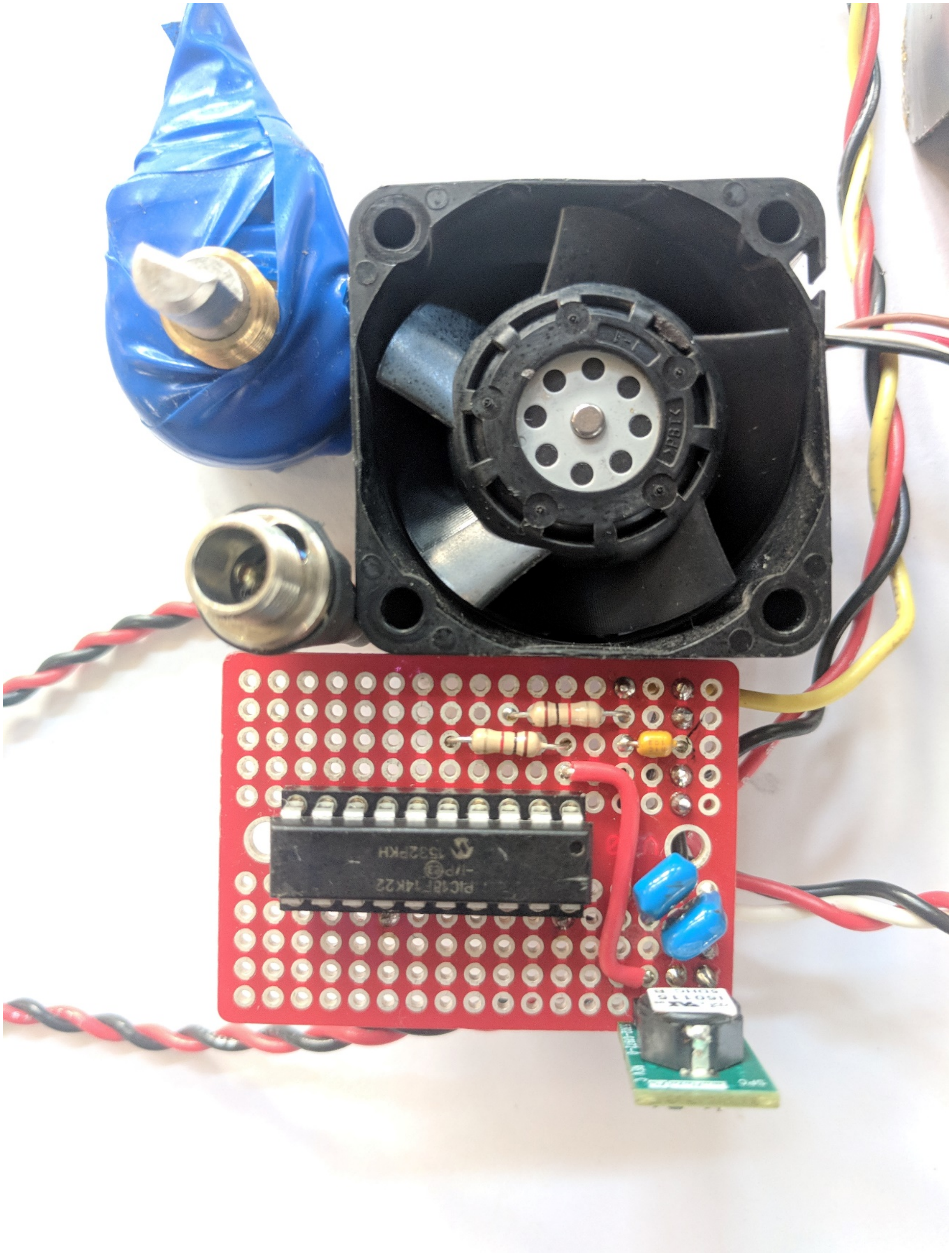

Figure 78 – P2 Final electronics package including NMB fan, microcontroller, and electronic circuitry for integrated fan control.

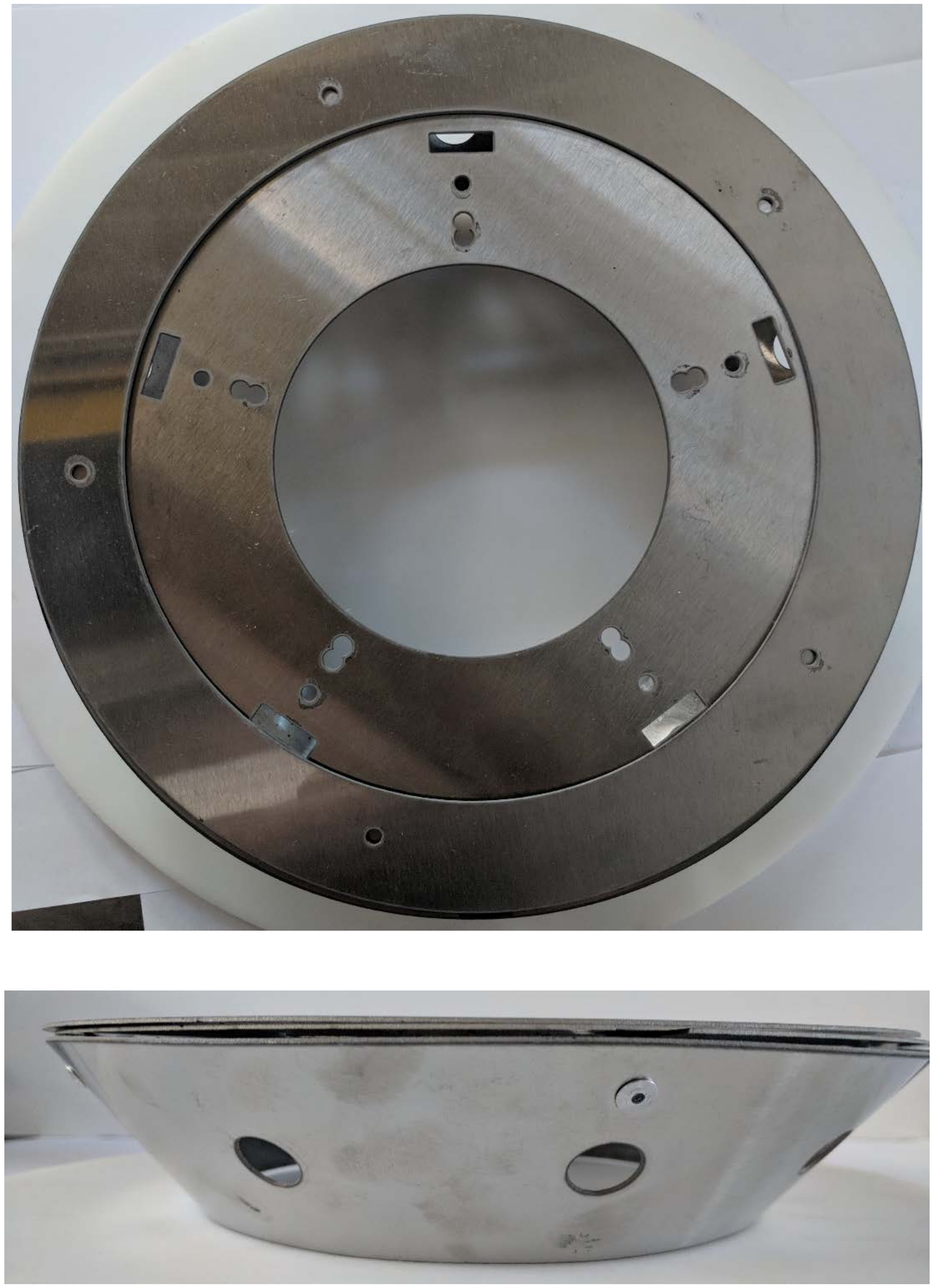

Figure 79 – P2 prototype extended pot deck

Figure 80 – Alternative untested chamber designs.

Appendix 3: P2 prototype Engineering drawings

The following are drawings of the major components of the P2 prototype completed by Envirofit International in cooperation with the Colorado State University Powerhouse Energy Institute Cookstoves team. The initial prototypes were manufactured by the CSU Cookstoves team at the Powerhouse Energy Institute in accordance with the drawings generated in partnership with Envirofit International. Two prototypes were reserved for testing at CSU, and the third was sent to Envirofit International in India for market evaluation.

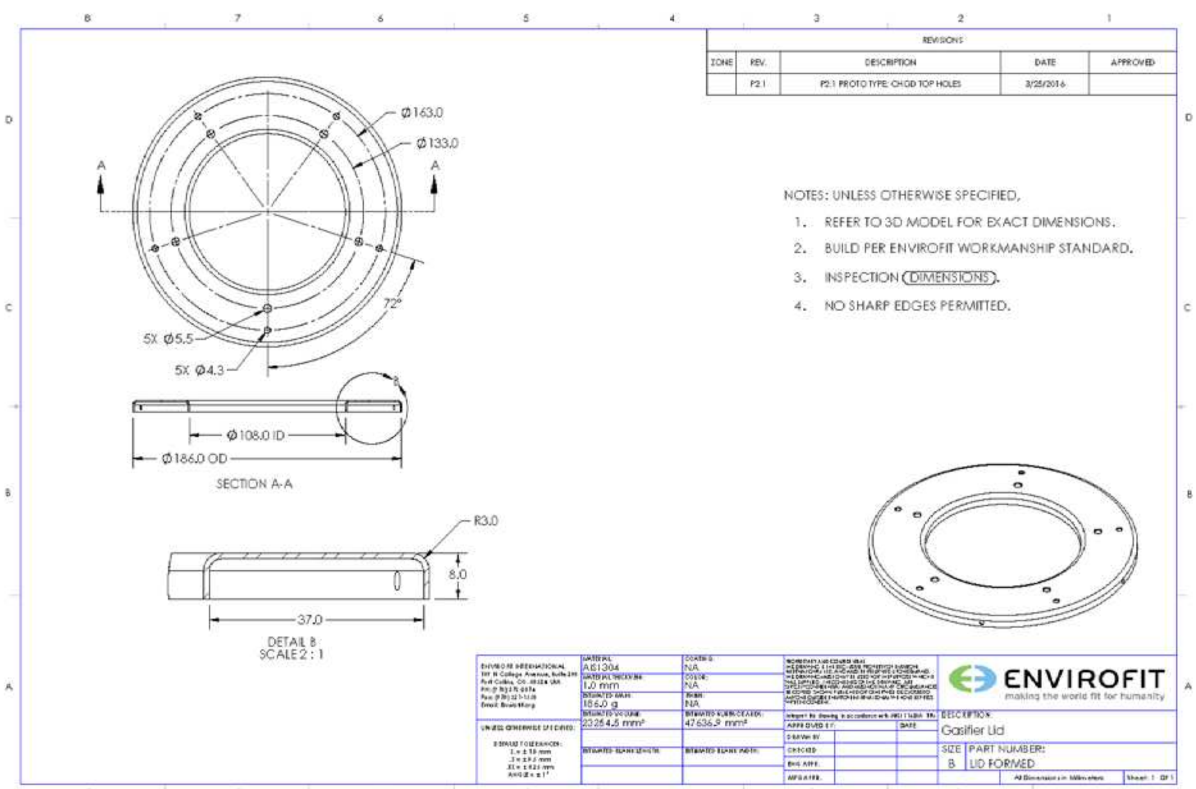

Figure 81 – Sample drawing of top

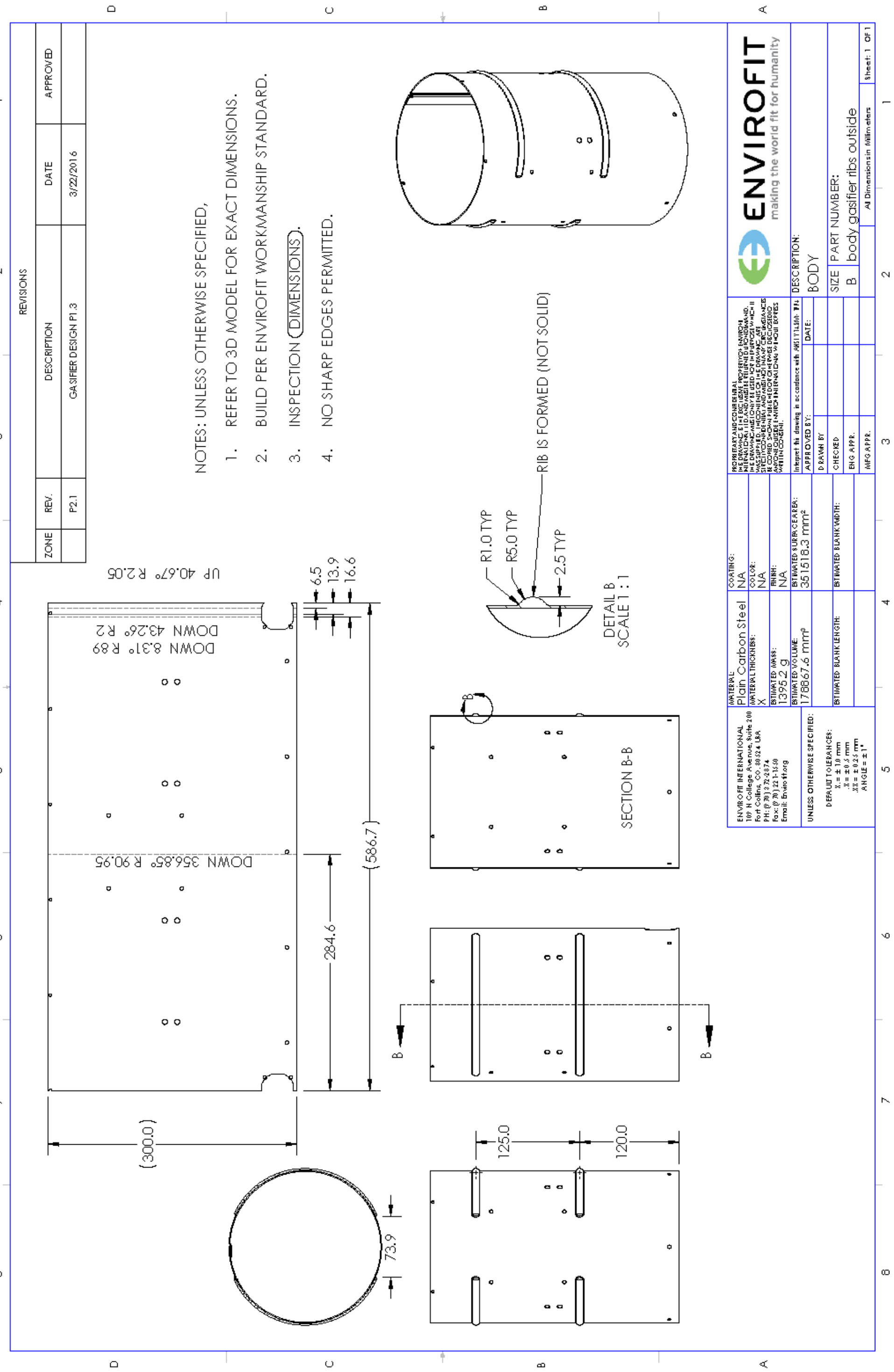

Figure 82 – P2 prototype engineering drawing for the stove body

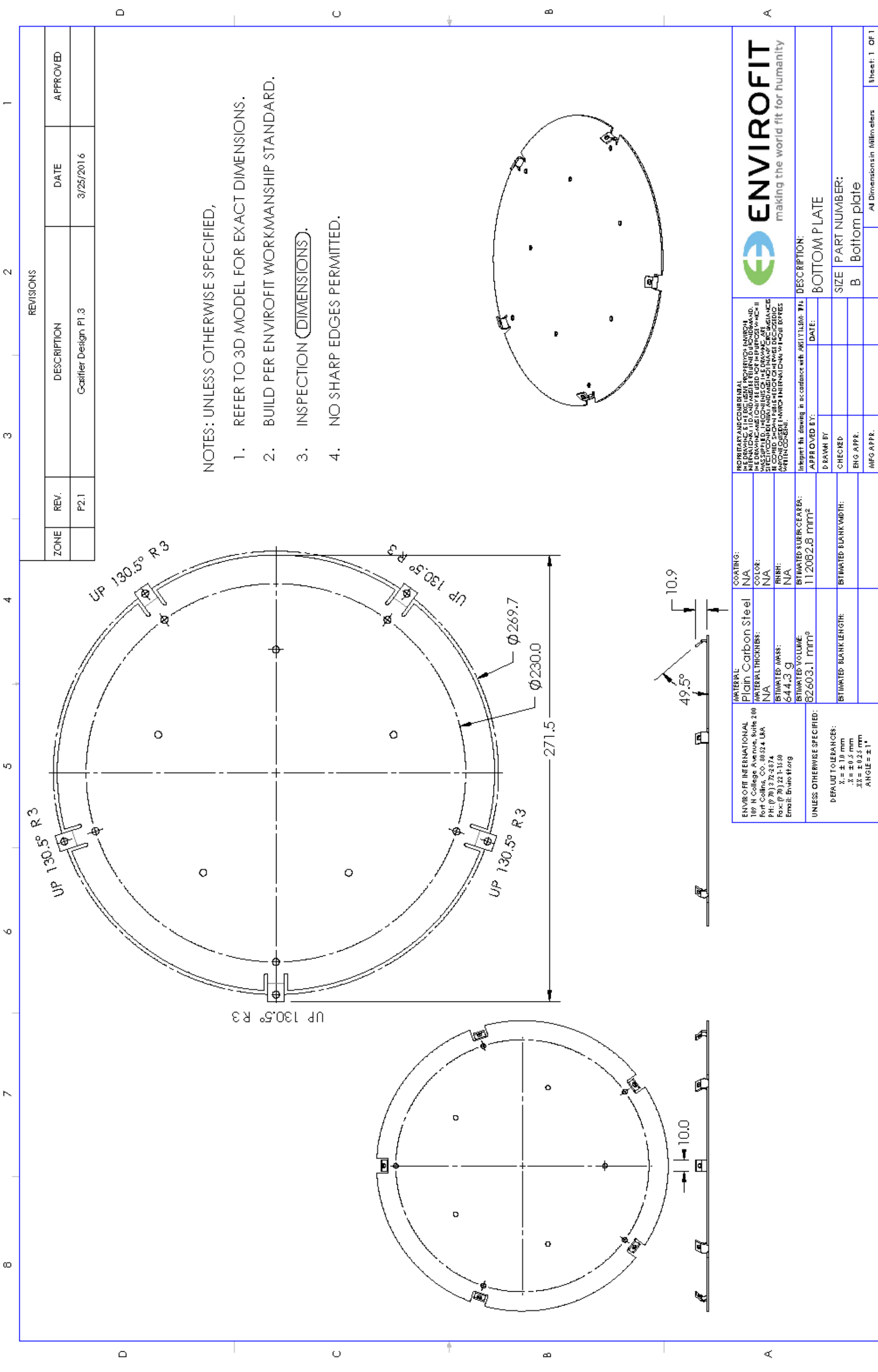

Figure 83 – P2 prototype engineering drawing for the stove base

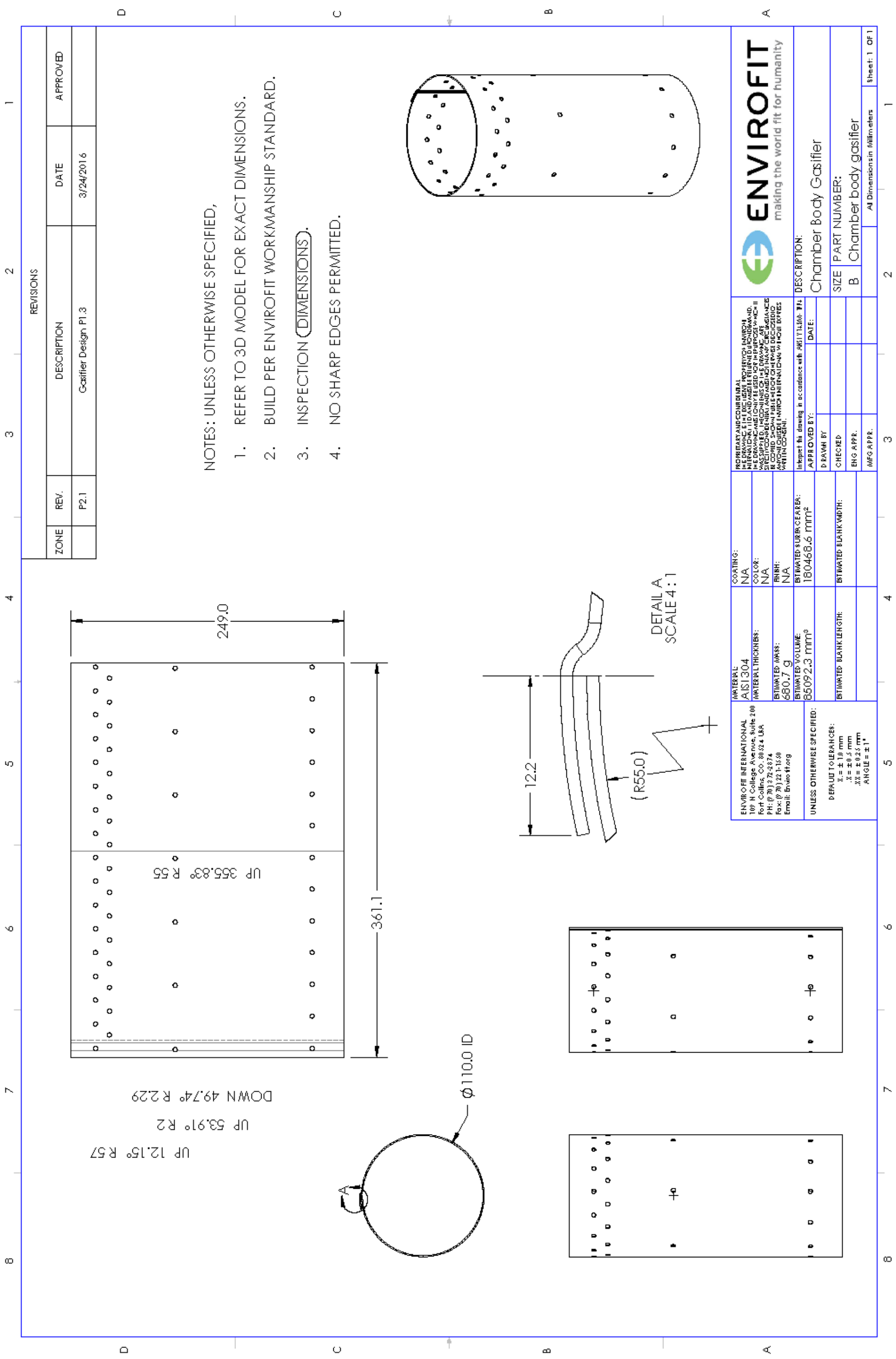

Figure 84 - P2 prototype engineering drawing for the baseline combustion chamber

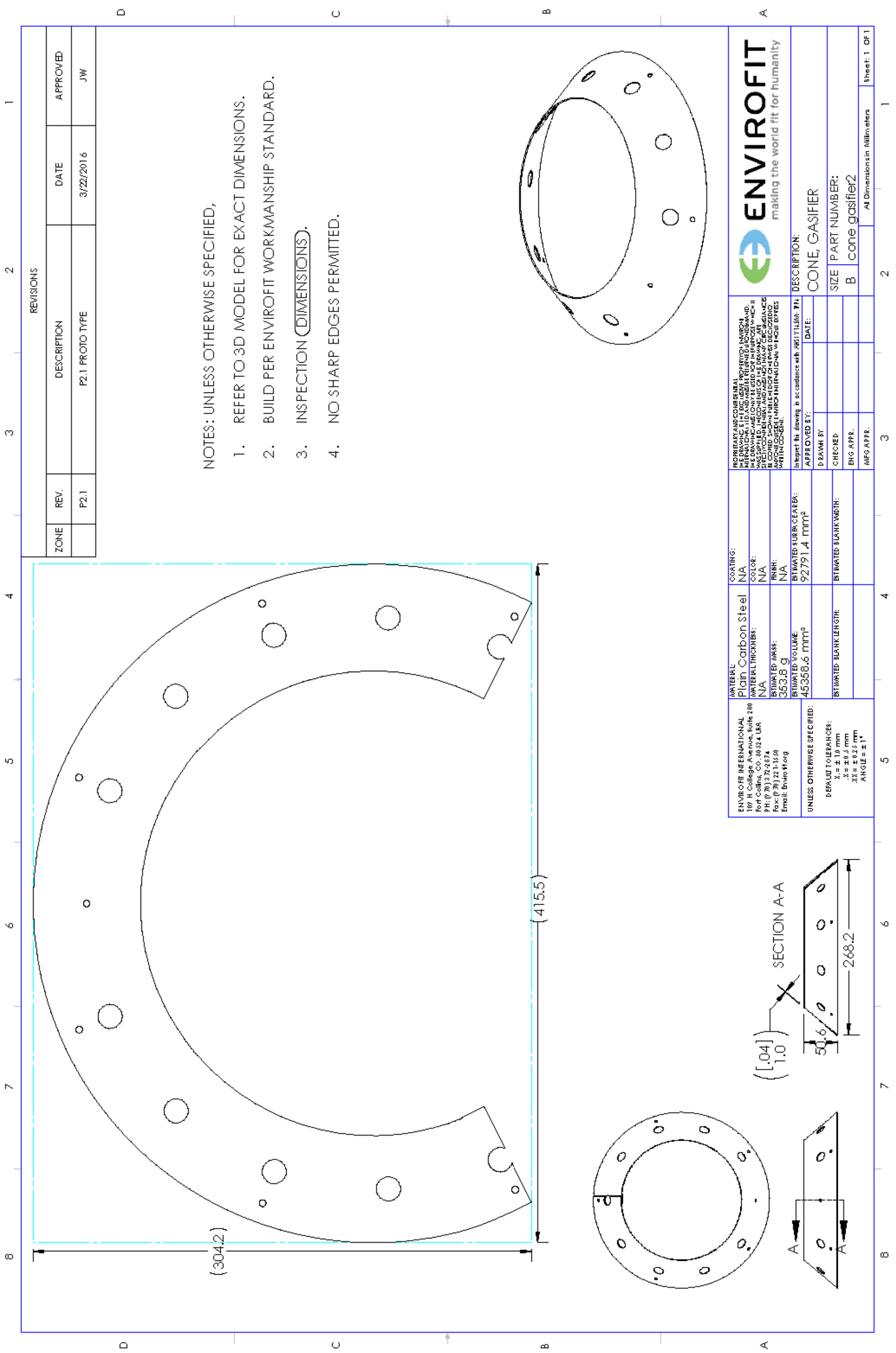

Figure 85 - P2 prototype engineering drawing for the base frustum.

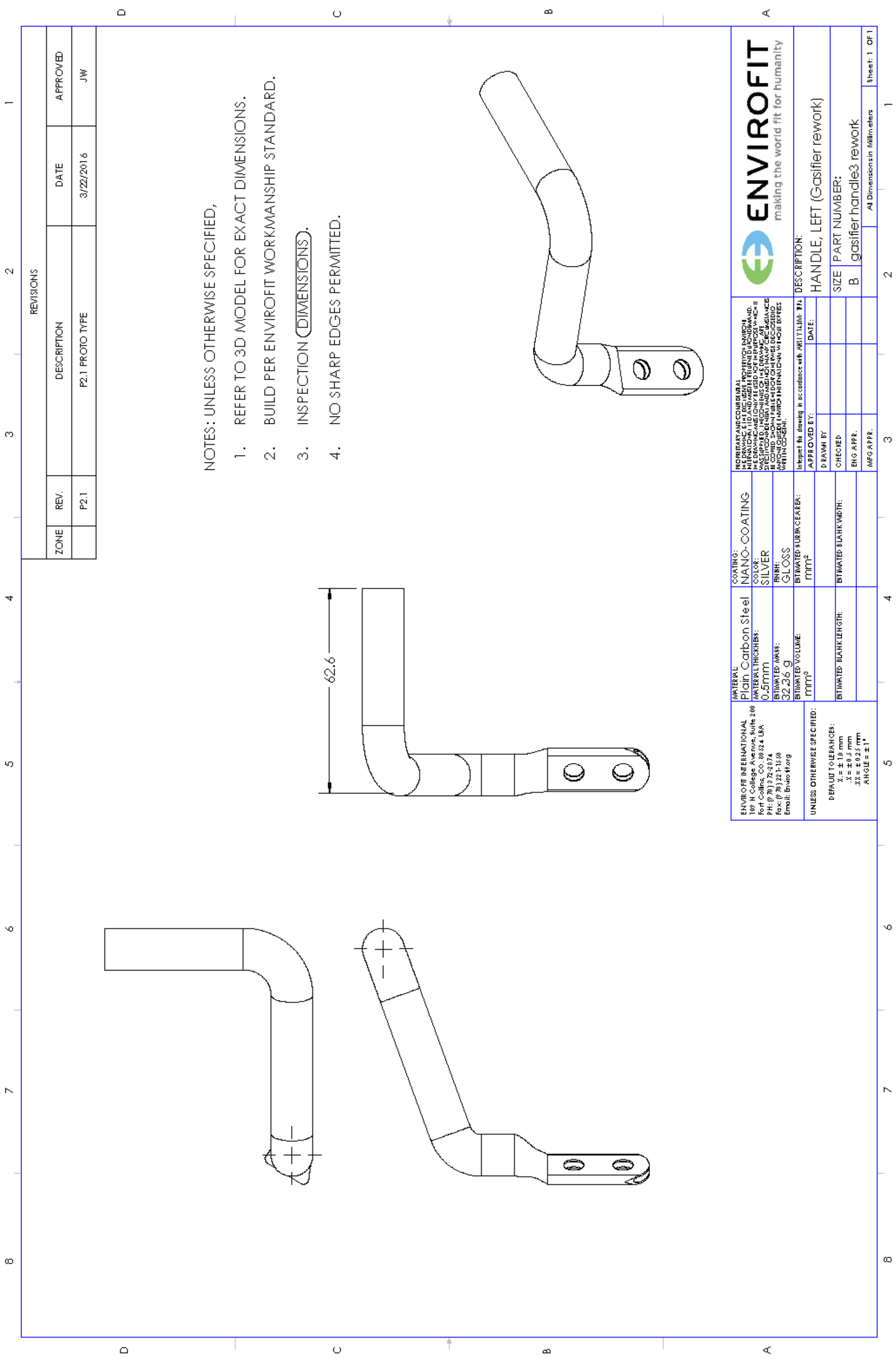

Figure 86 - P2 prototype engineering drawing for the stove handle

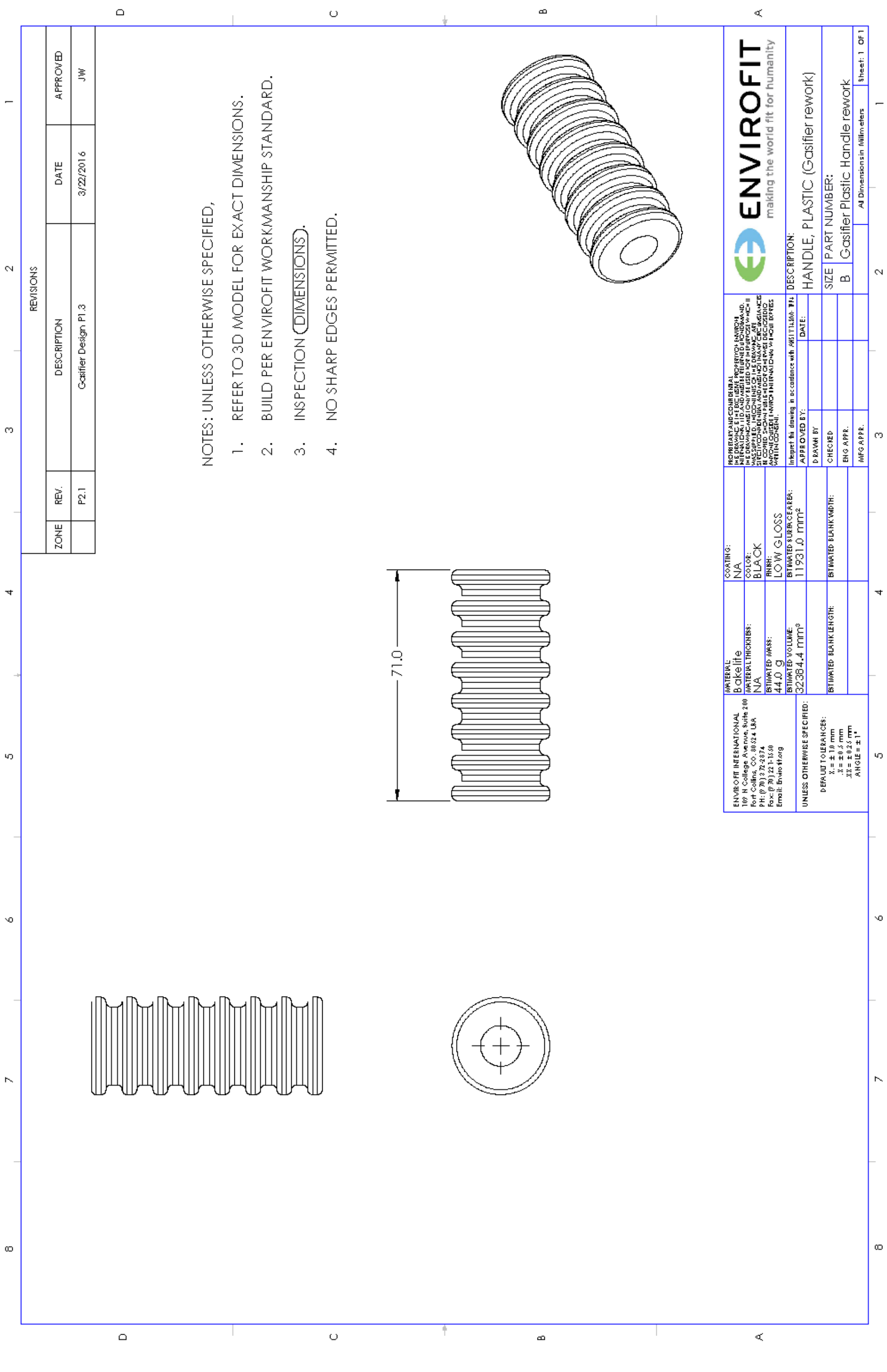

Figure 87 - P2 prototype engineering drawing for the stove handle grip

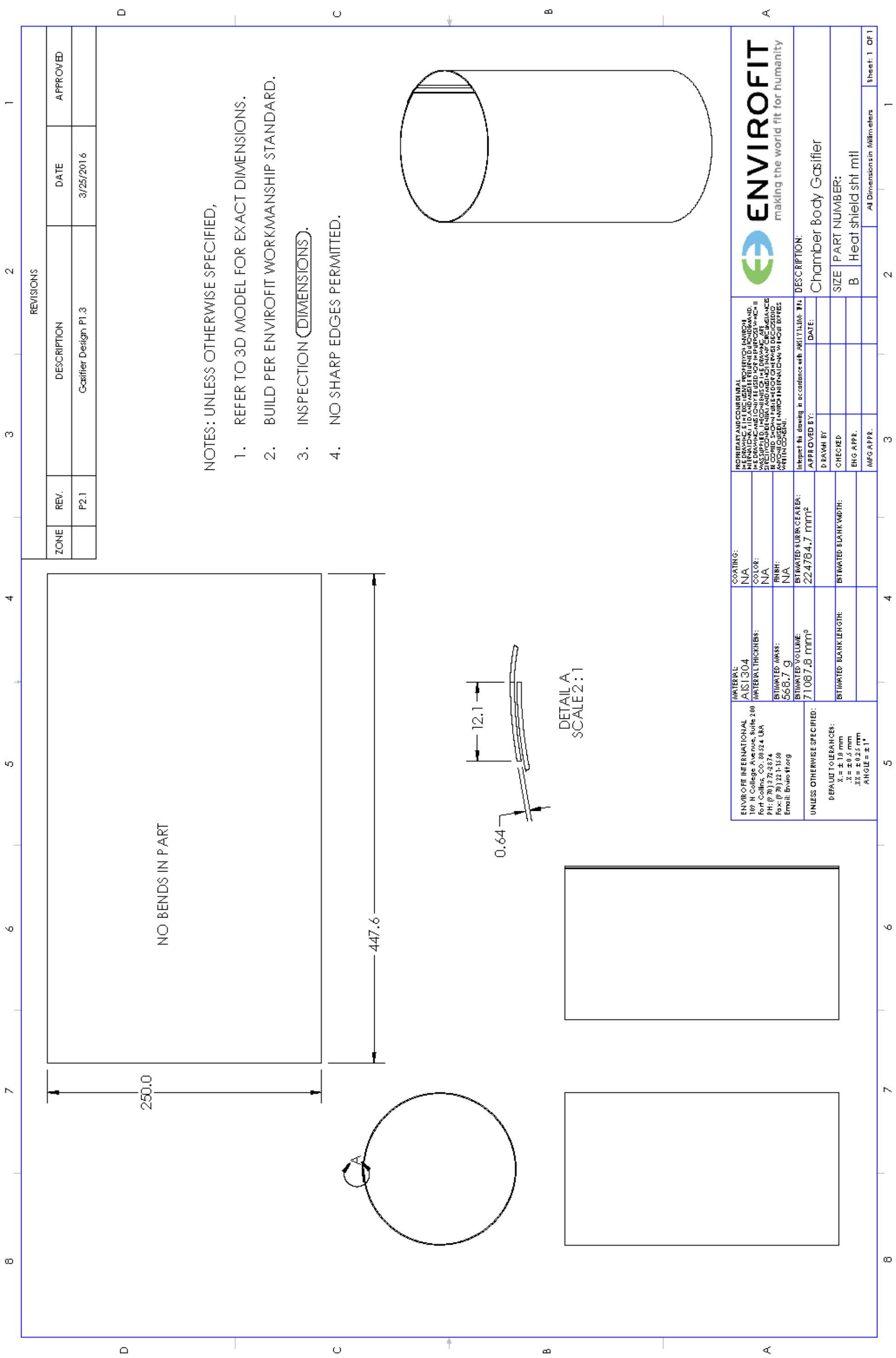

Figure 88 - P2 prototype engineering drawing for the radiation heat shield

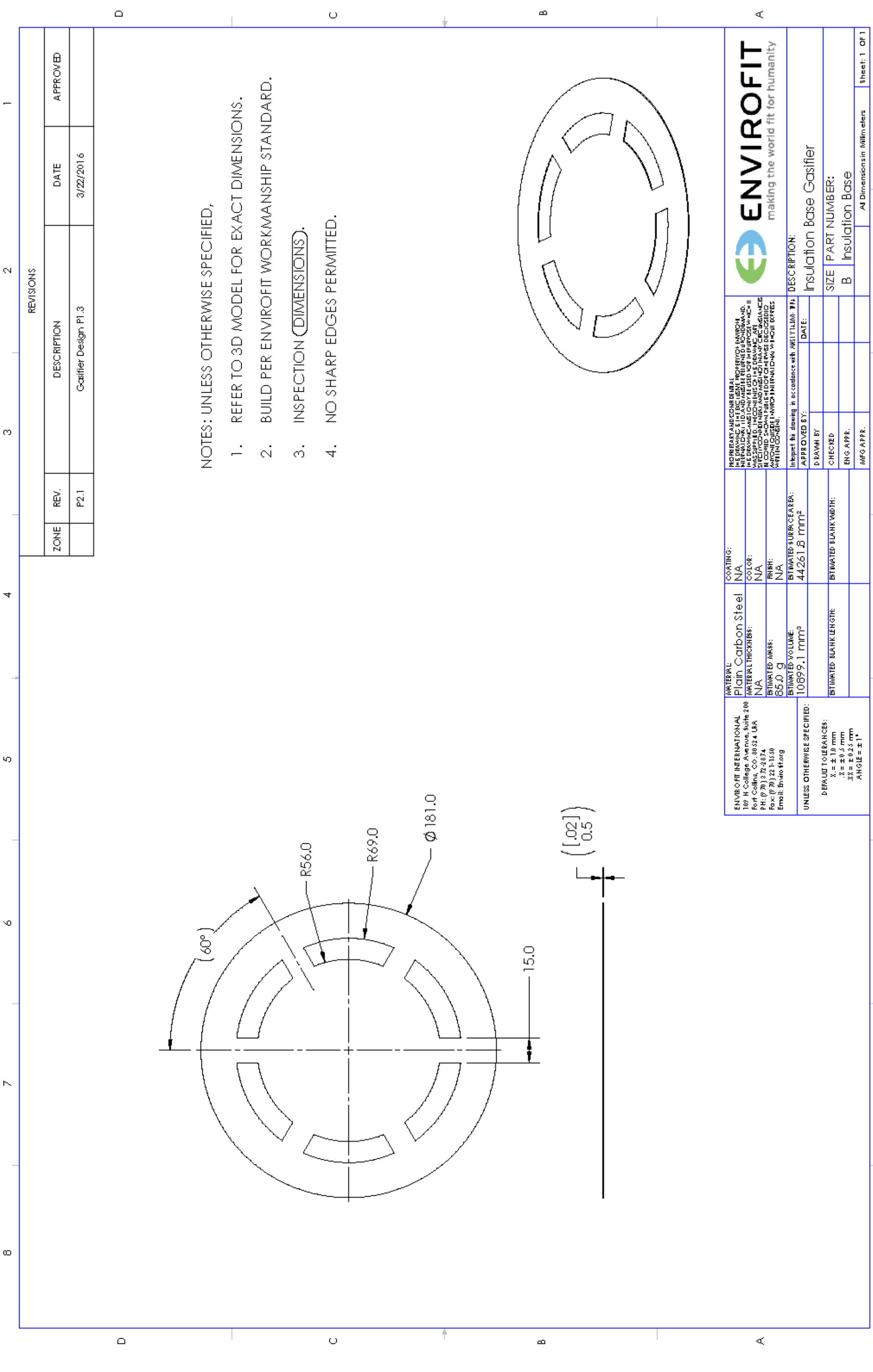

Figure 89 - P2 prototype engineering drawing for the inner insulation support.

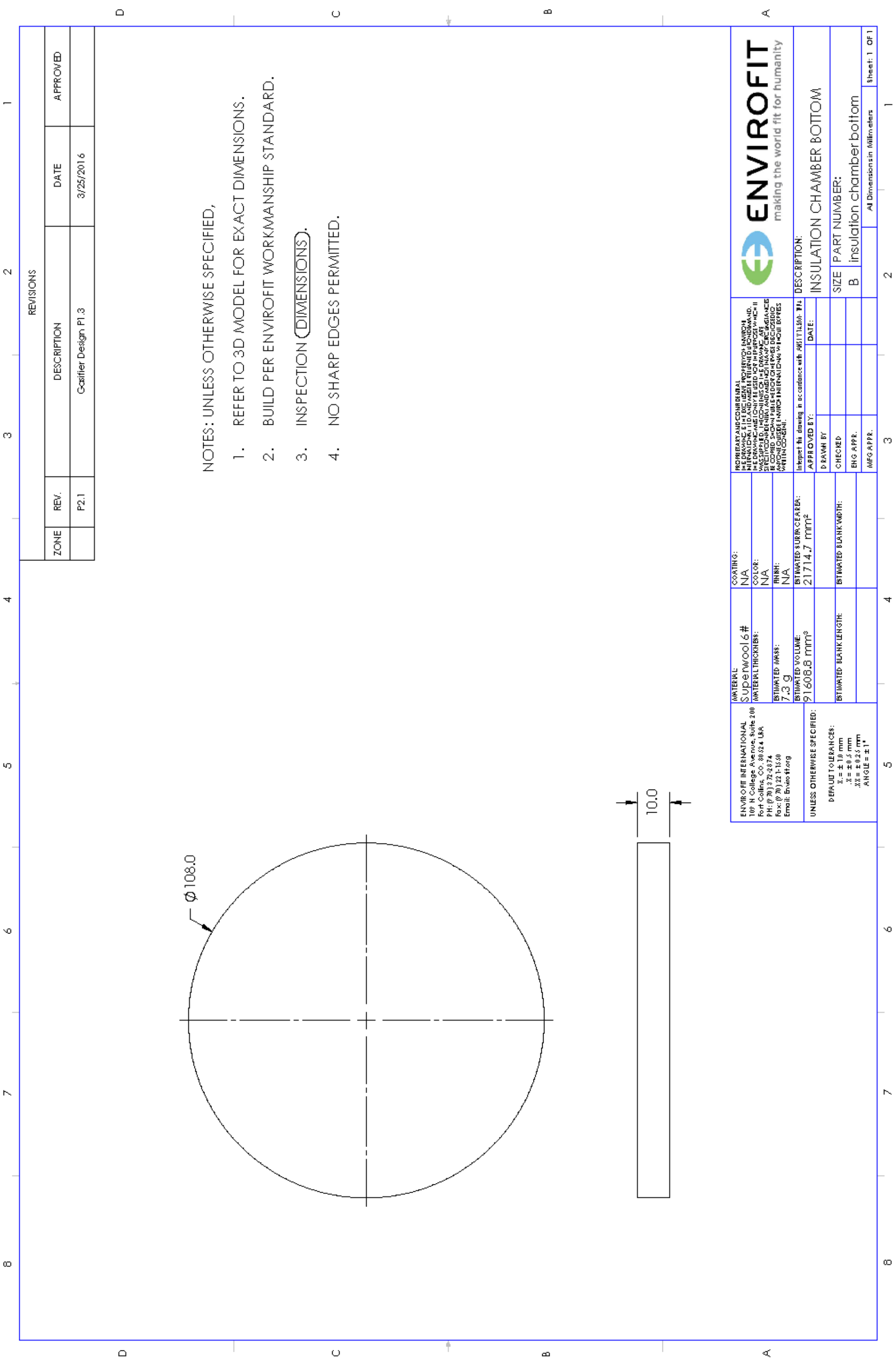

Figure 90 - P2 prototype engineering drawing for the insulation chamber bottom.

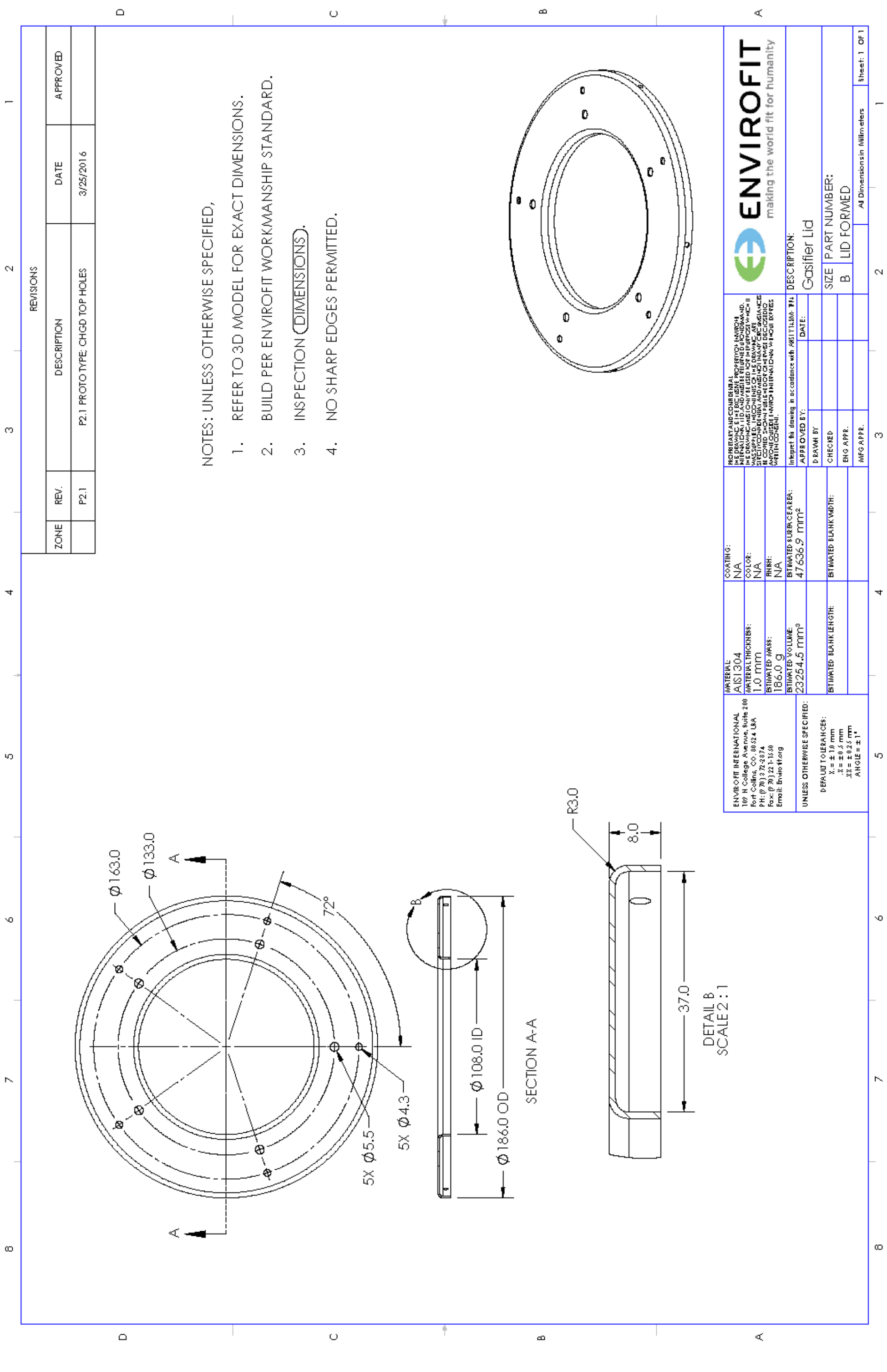

Figure 91 – P2 prototype engineering drawing for the stove top.

APPENDIX 4: APPLICABLE STANDARDS

A number of standards apply to the testing and evaluation of cookstoves. Below is a list of standards used in this work.

1. The Water Boiling Test 4.2.3 Protocol
2. ISO-IWA-2012
3. ASTM International, Standard Test Method for Volatile Matter in the Analysis of Particulate Wood Fuels; E872 – 82; ASTM International: West Conshohocken, PA, DOI: 10.1520/E0872-82R13.
4. ASTM International, Standard Test Method for Determination of Ash Content of Particulate Wood Fuels; D1534 – 93; ASTM International: West Conshohocken, PA, DOI: 10.1520/E1534-93R13.
5. ASTM International, Standard Test Methods for Analysis of Wood Fuels; E870 – 82; ASTM International: West Conshohocken, PA, DOI: 10.1520/E0870-82R06.
6. ASTM International, Standard Test Method for Gross Calorific Value of Coal and Coke; D5865 – 13; ASTM International: West Conshohocken, PA, DOI: 10.1520/D5865-13.

APPENDIX 5: LABORATORY TLUD PROTOTYPE PLOTS

The following appendix is a compendium of plots illustrating data collected during the testing using the P0 Modular Laboratory TLUD stove. Included are descriptions of measurements and calculations required to make each plot at the beginning of each subsection as well as a description and explanation of the data in each plot.

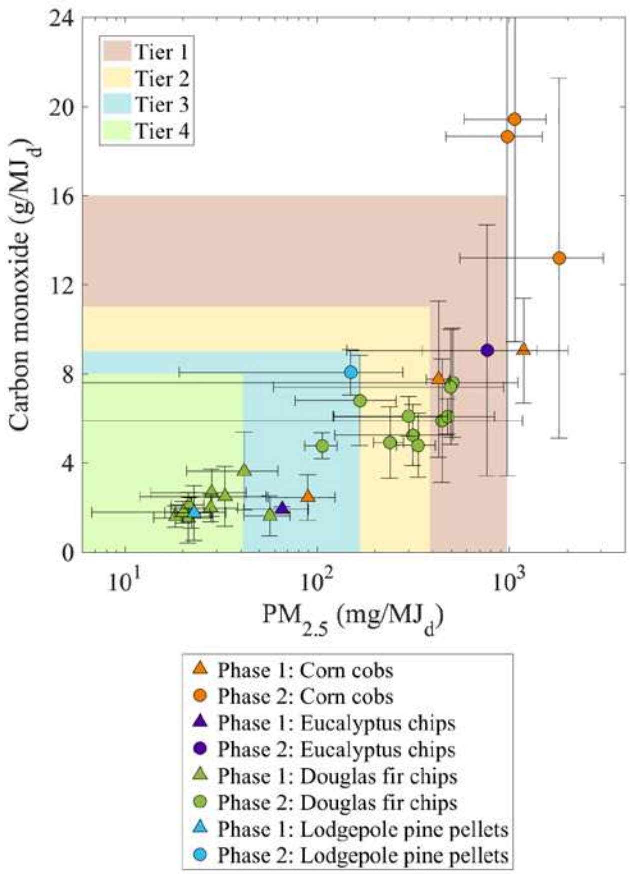

Figure 92: P0 Modular Laboratory TLUD Prototype Testing Data Summary CO vs. PM. Quality fuels and proper usage of the stove had the largest impact as seen in the data presented by the green triangles in the Tier 4 box. If the stove was used improperly (as represented by P2 testing where fuel was added to the top of a lit fuel bed during stove operation) the performance was worse. Finally, the lowest performance was seen when using off design fuels. The effect of usage and fuel type greatly overshadowed any effect from stove design.

Carbon Monoxide Results

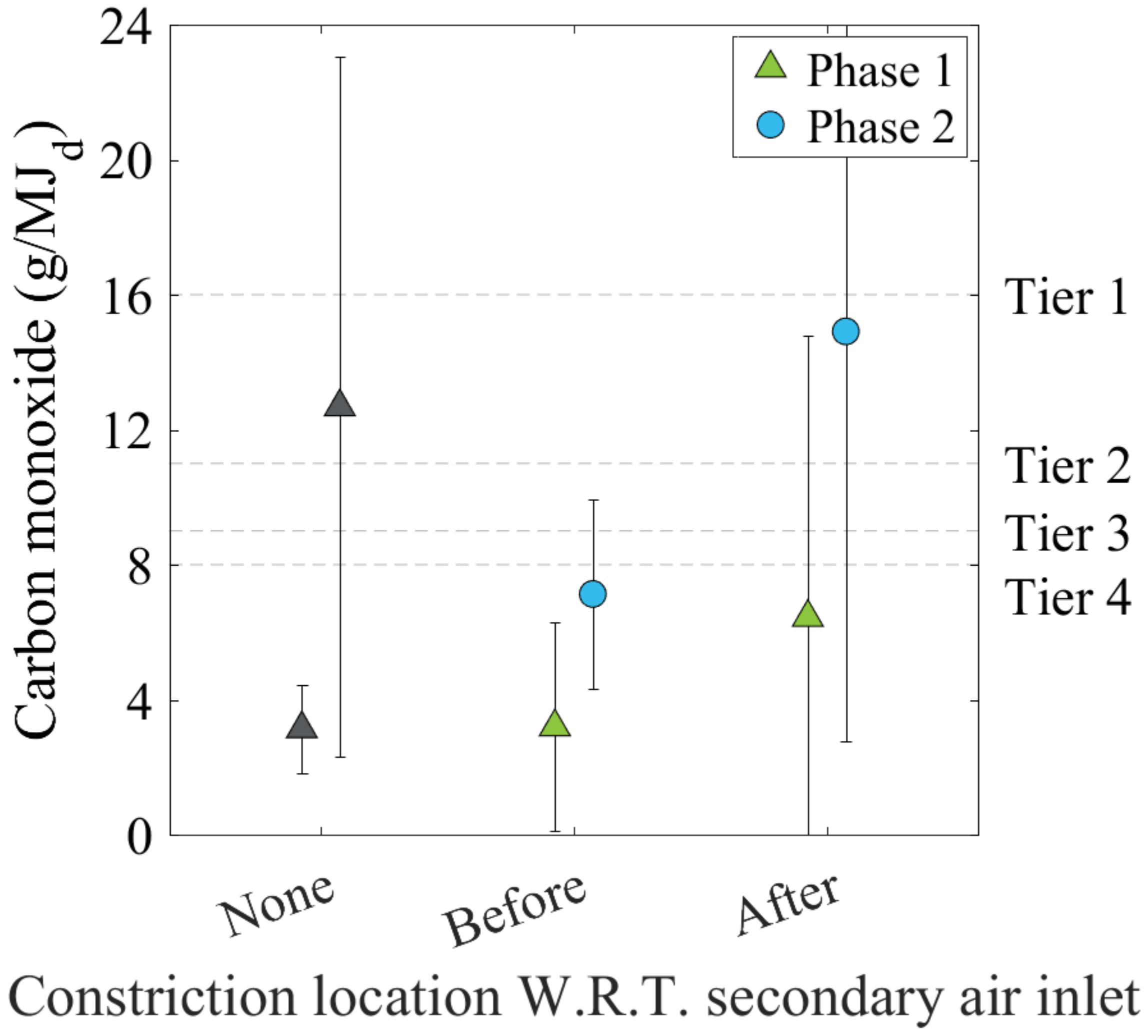

Figure 93: No statistically significant change in CO emissions were measured for stove configurations, which placed a restriction between the primary and secondary combustion zones or after the secondary combustion zone.

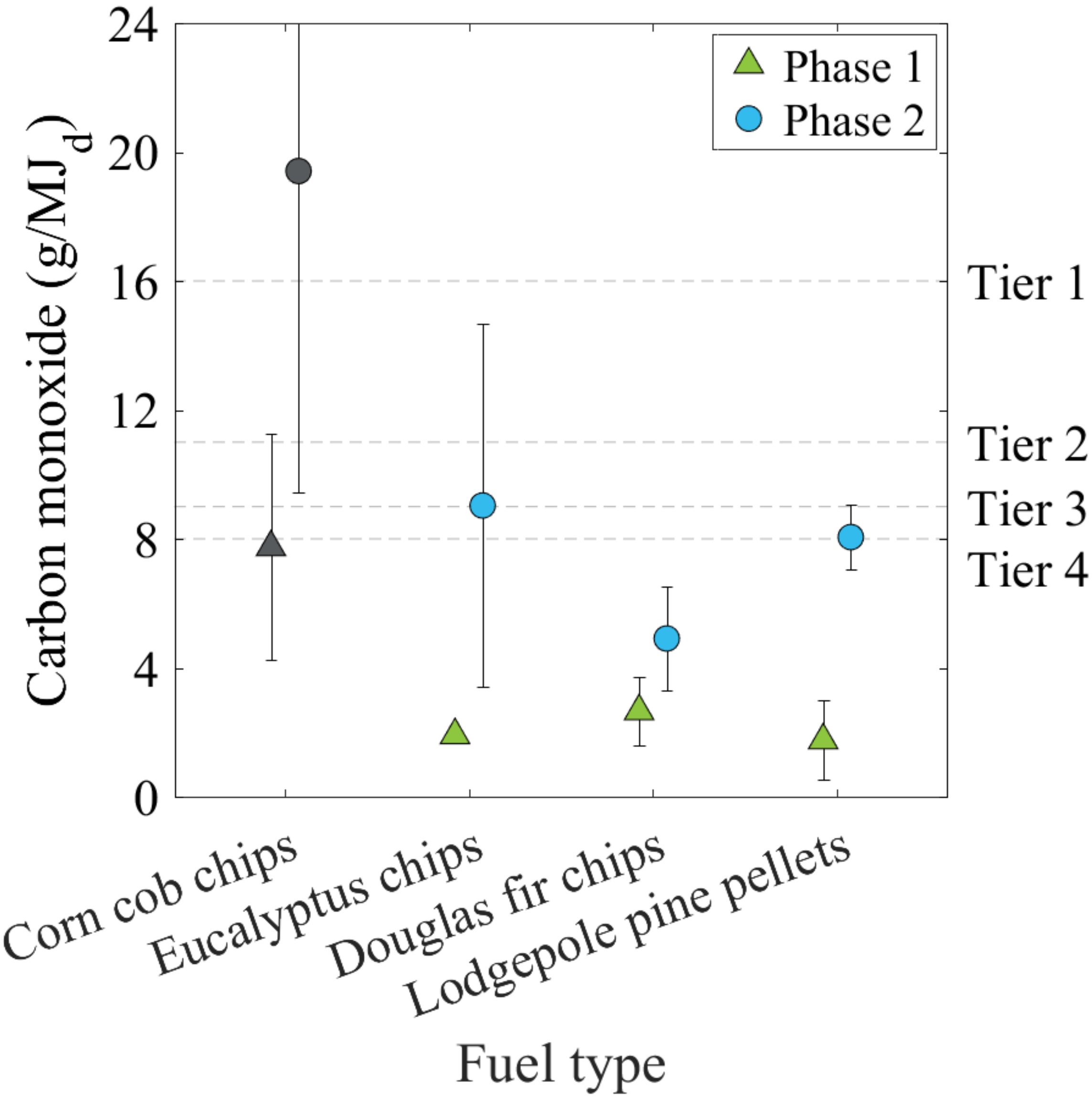

Figure 94 – Fuel type did have a statistically significant impact on carbon monoxide emissions. Corncob chips had significantly more CO emissions than wood fuels used.

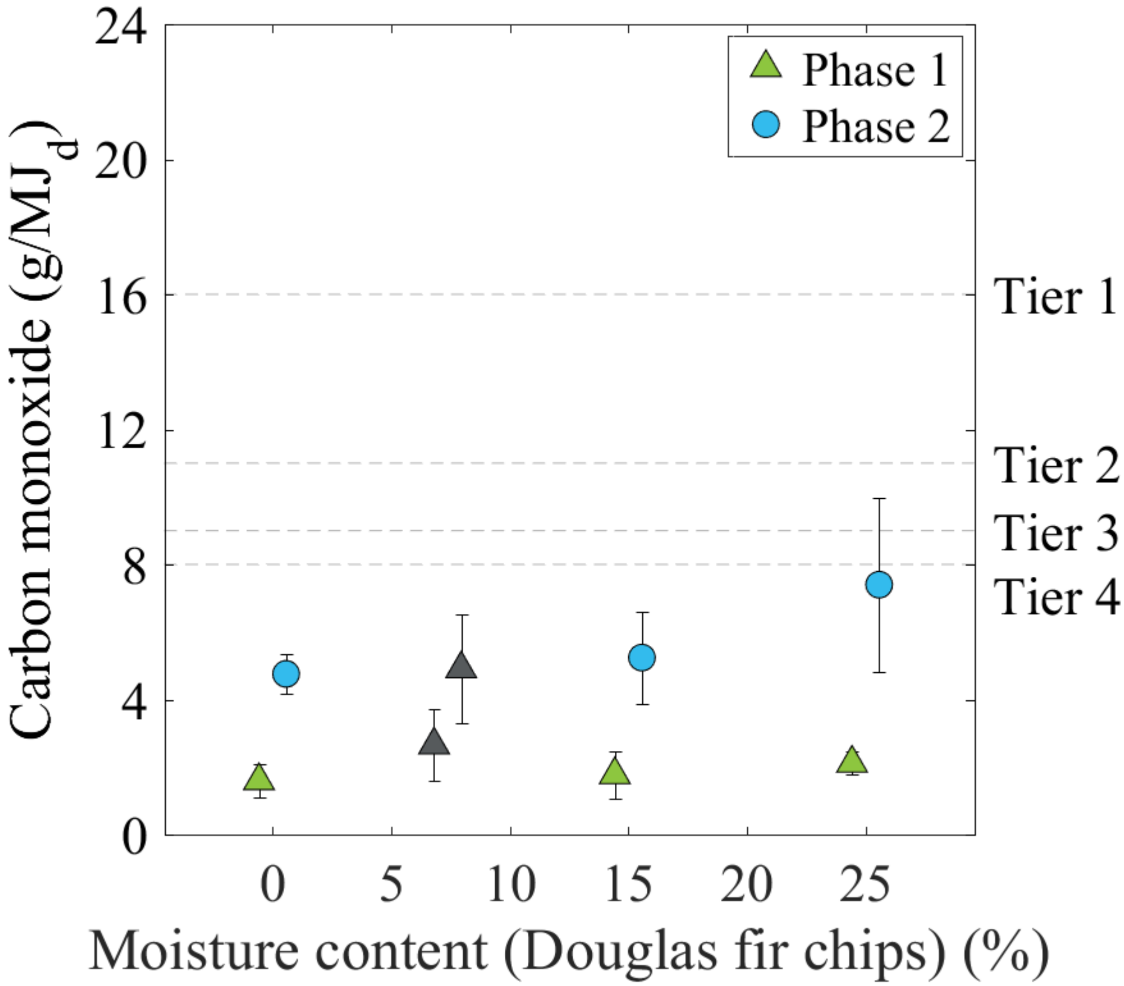

Figure 95 – Fuel moisture content did not have a significant impact on the CO emissions. The moisture content of Douglas fir chips was varied from 0% to 25% by placing the wood chips in a kiln to reduce the moisture or adding liquid water to the wood chips to increase the moisture content.

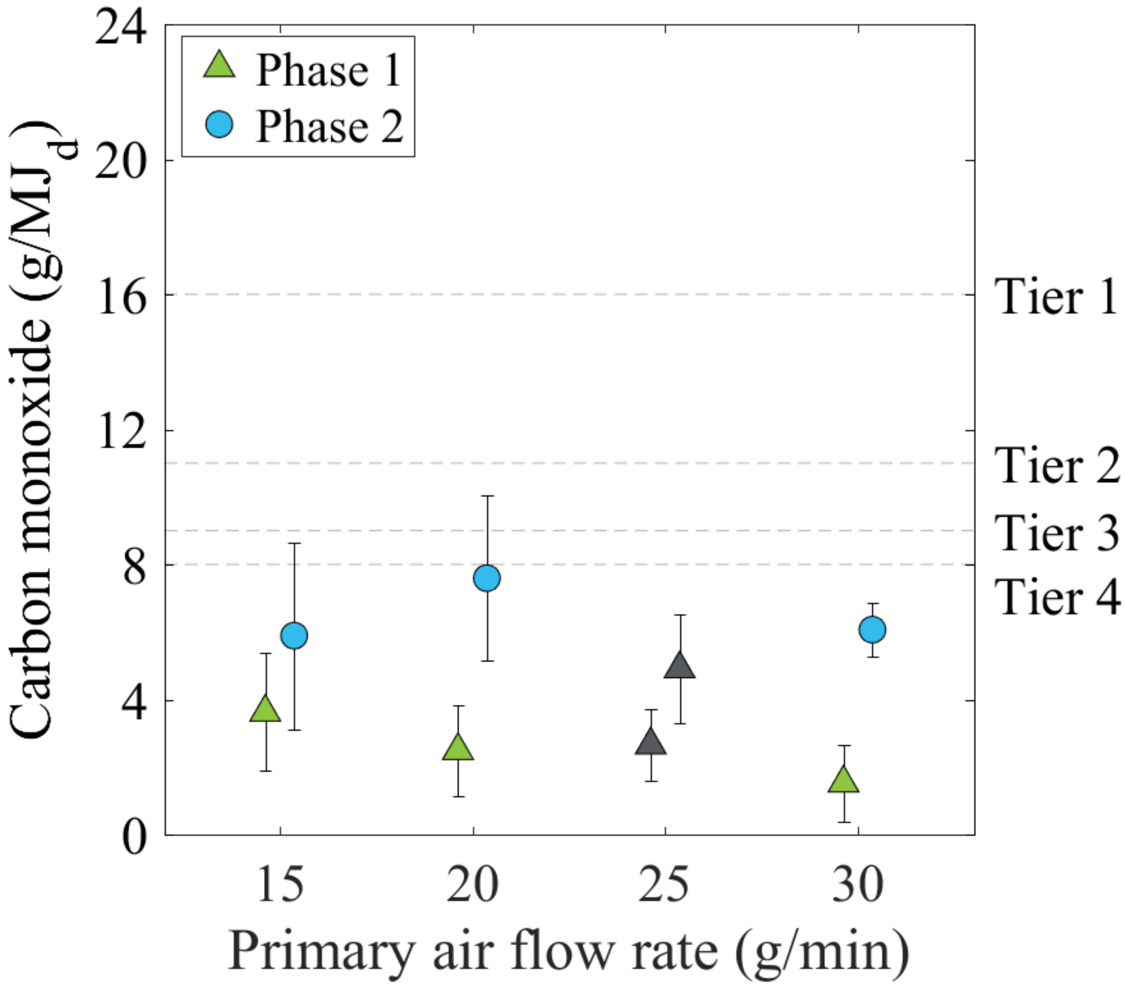

Figure 96 – CO emissions vs. primary airflow rate in g/min. Tier leaves are also noted. All mean CO emissions meet tier 4 guidelines in both phase 1 and phase 2 testing.

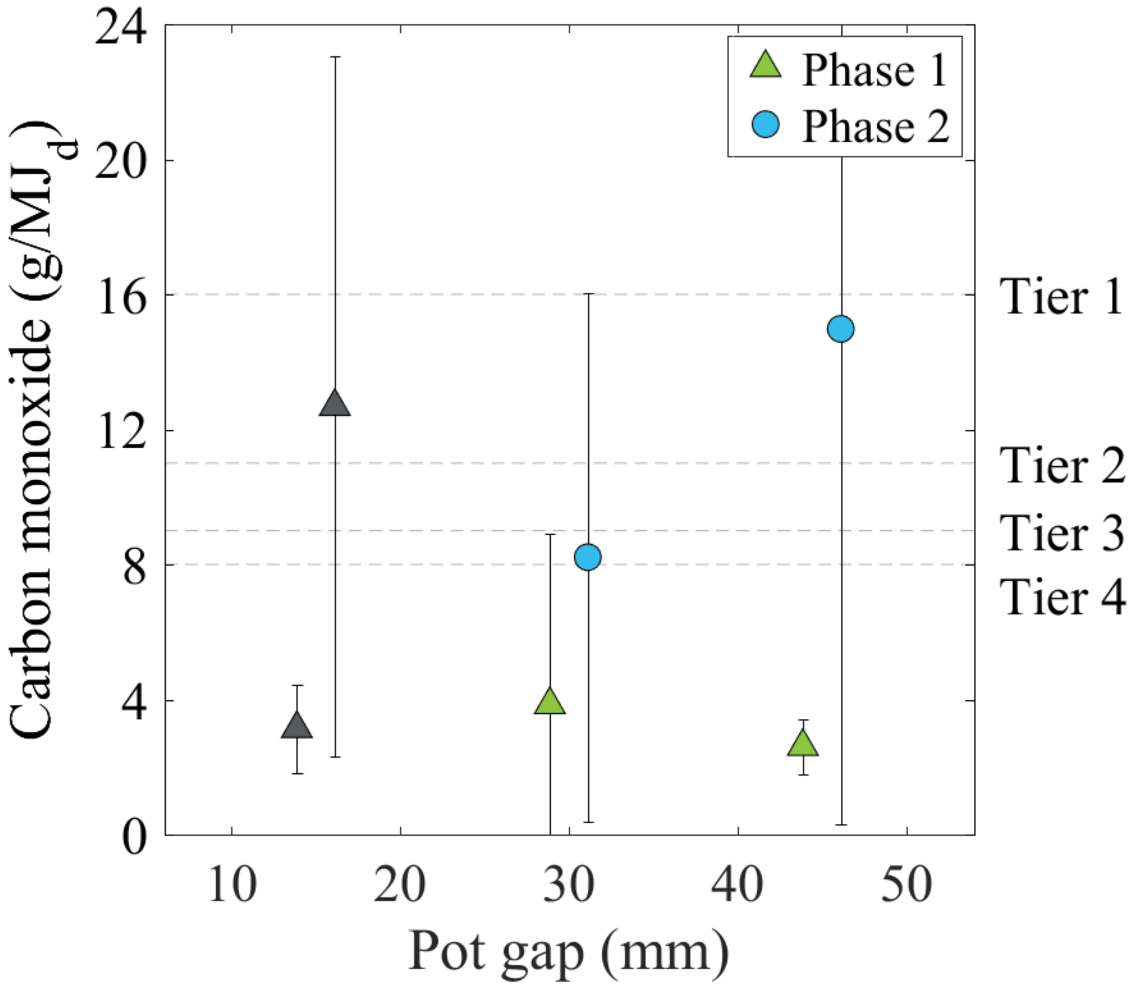

Figure 97 – Carbon Monoxide emissions normalized by power delivered to the cooking vessel vs. pot gap varied from 15 -mm to 45 mm. Error bars are 90% C.I. Note that x-axis jitter is applied to the phase 1 and phase 2 data points at each x value to prevent data overlap.

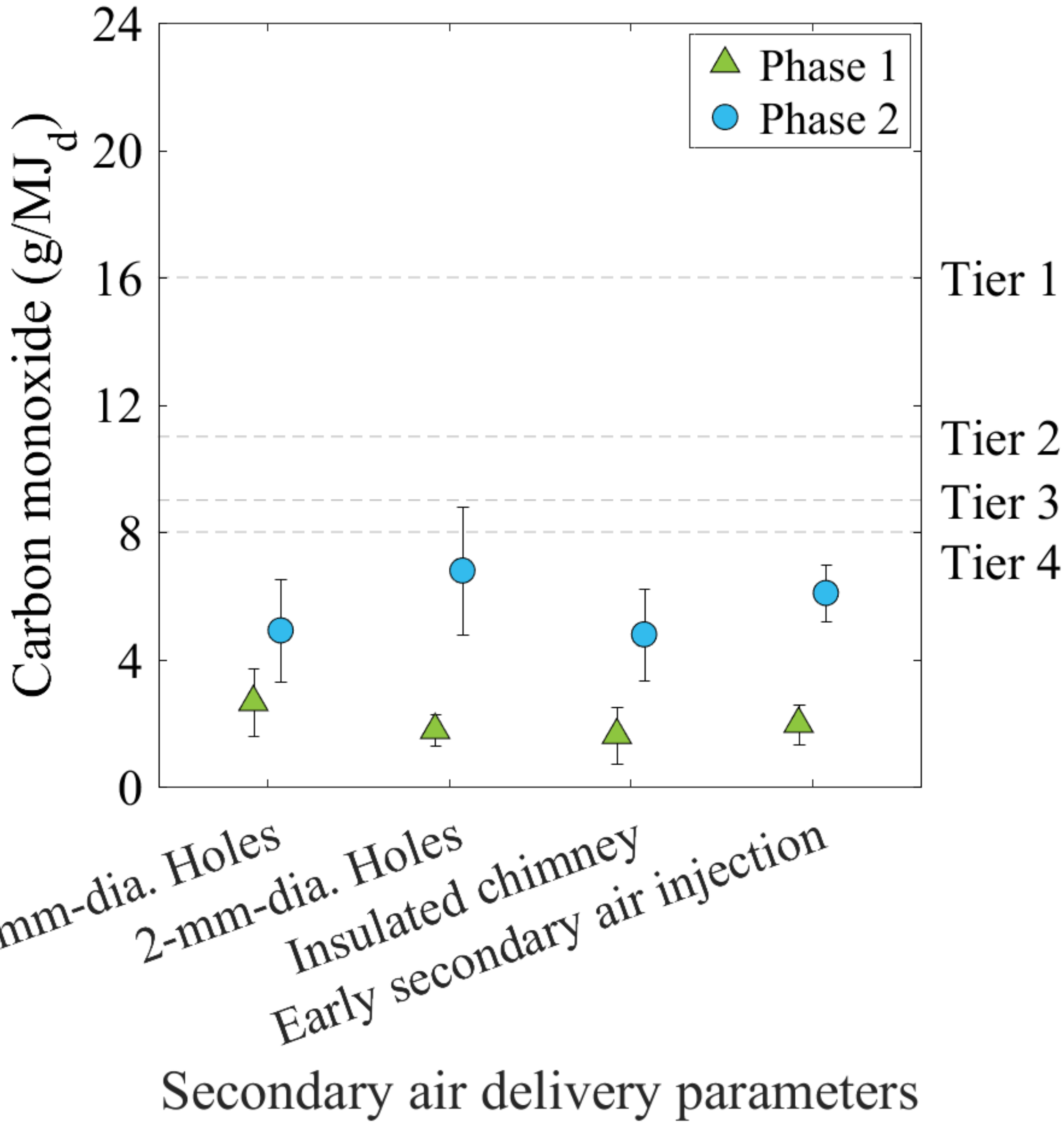

Figure 98 – Carbon monoxide emissions normalized by power delivered to the cooking vessel vs. stove configuration. 4-mm-dia. Holes and 2-mm-Holes are 4 -mm diameter secondary air injection holes and 2-mm diameter secondary air injection holes respectively. The insulated chimney was the baseline stove configuration but with a 100-mm tall insulated chimney added after the secondary combustion stage. The early secondary air was a configuration which had 10% of the secondary air injected just prior to the secondary combustion stage. Error bars are 90% C.I. Note that x-axis jitter is applied to the phase 1 and phase 2 data points at each x value to prevent data overlap.

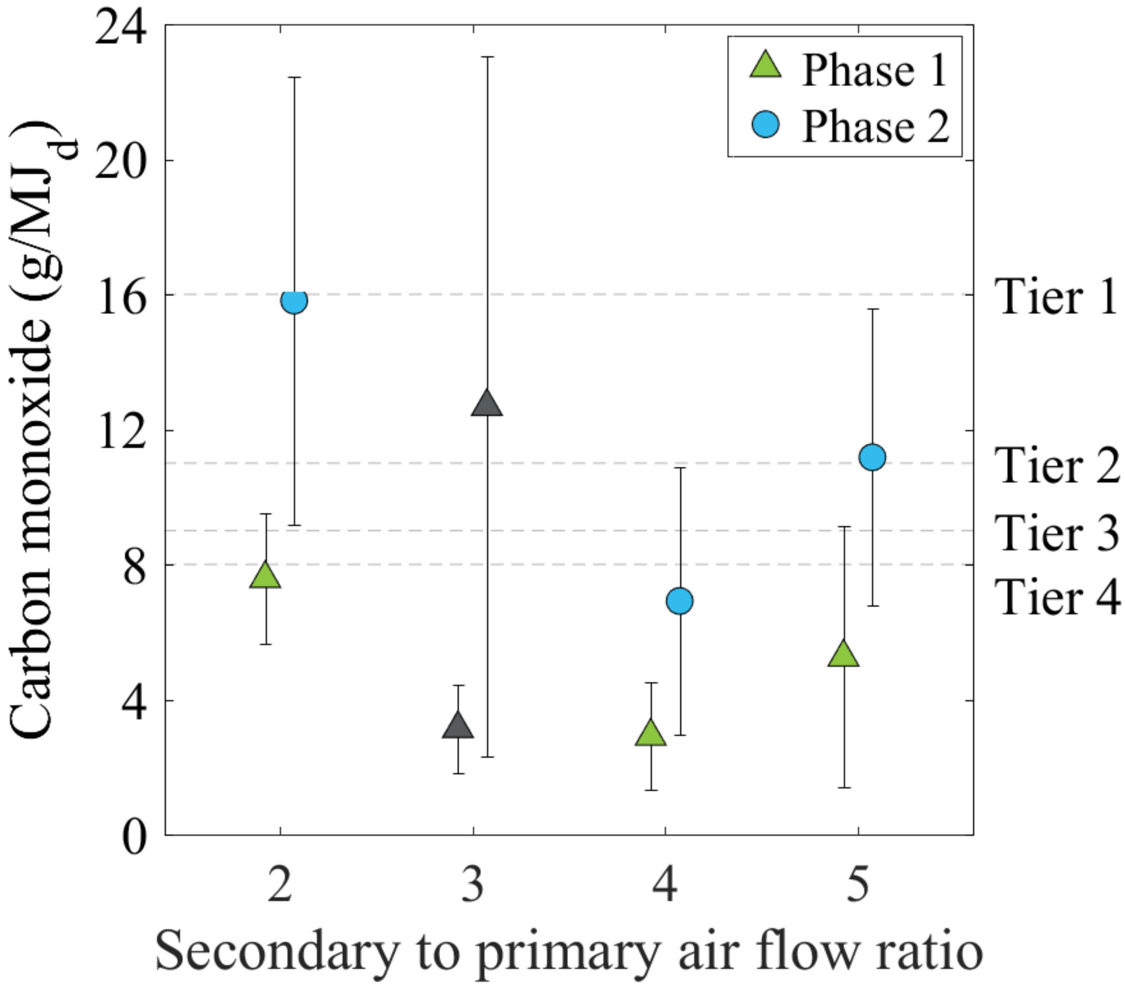

Figure 99 – Carbon Monoxide emissions normalized by the power delivered to the cooking vessel. Vs. secondary to primary air flow ratio varied from 2 to 5. Error bars are 90% C.I. Note that x-axis jitter is applied to the phase 1 and phase 2 data points at each x value to prevent data overlap.

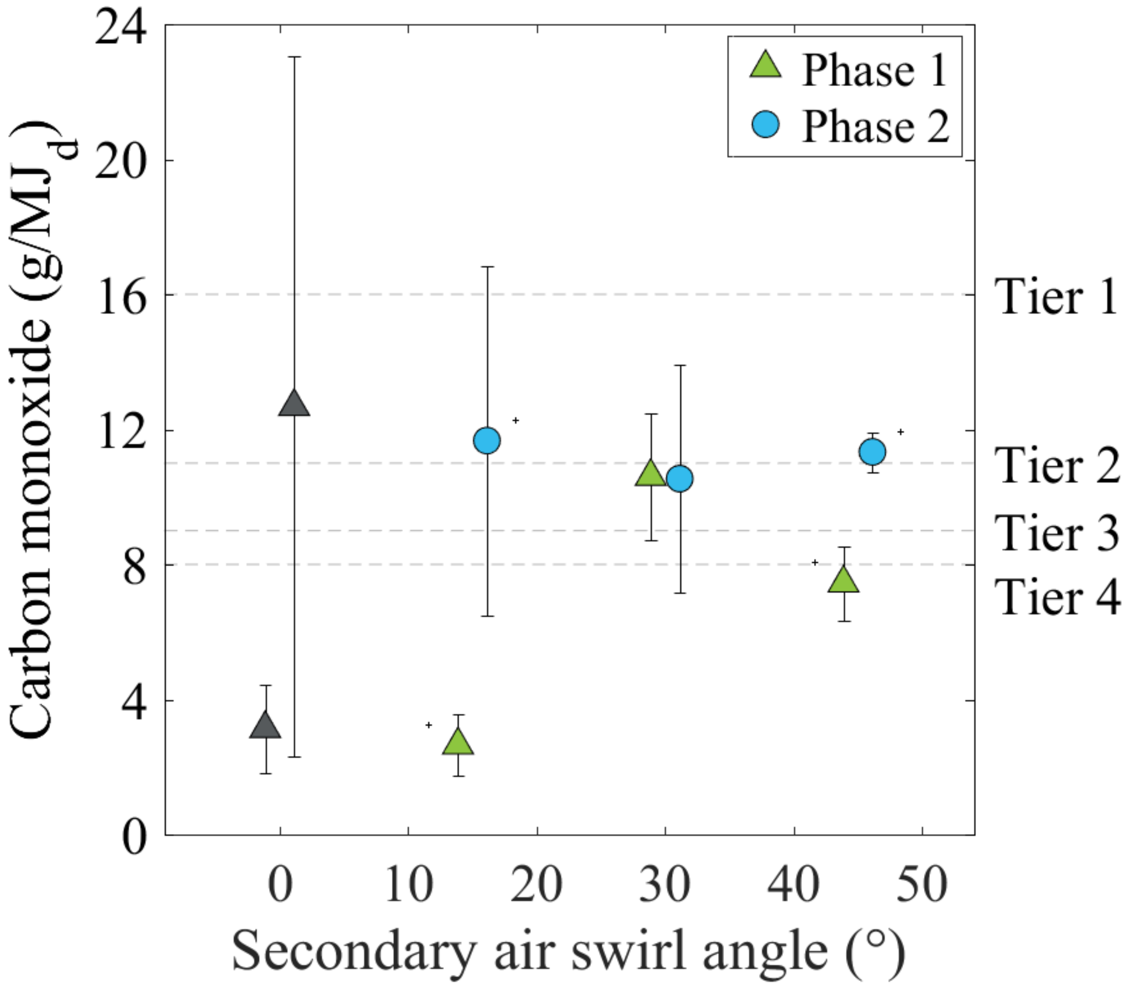

Figure 100 – Carbon Monoxide emissions normalized by power delivered to the cooking vessel vs. the swirl angle of the air injected into the secondary combustion stage varied from 0 ° to 45°. The gray data points (0°) represent baseline data; triangles are phase 1 data and circles are phase 2 data. Error bars are 90% C.I. Note that x-axis jitter is applied to the phase 1 and phase 2 data points at each x value to prevent data overlap.

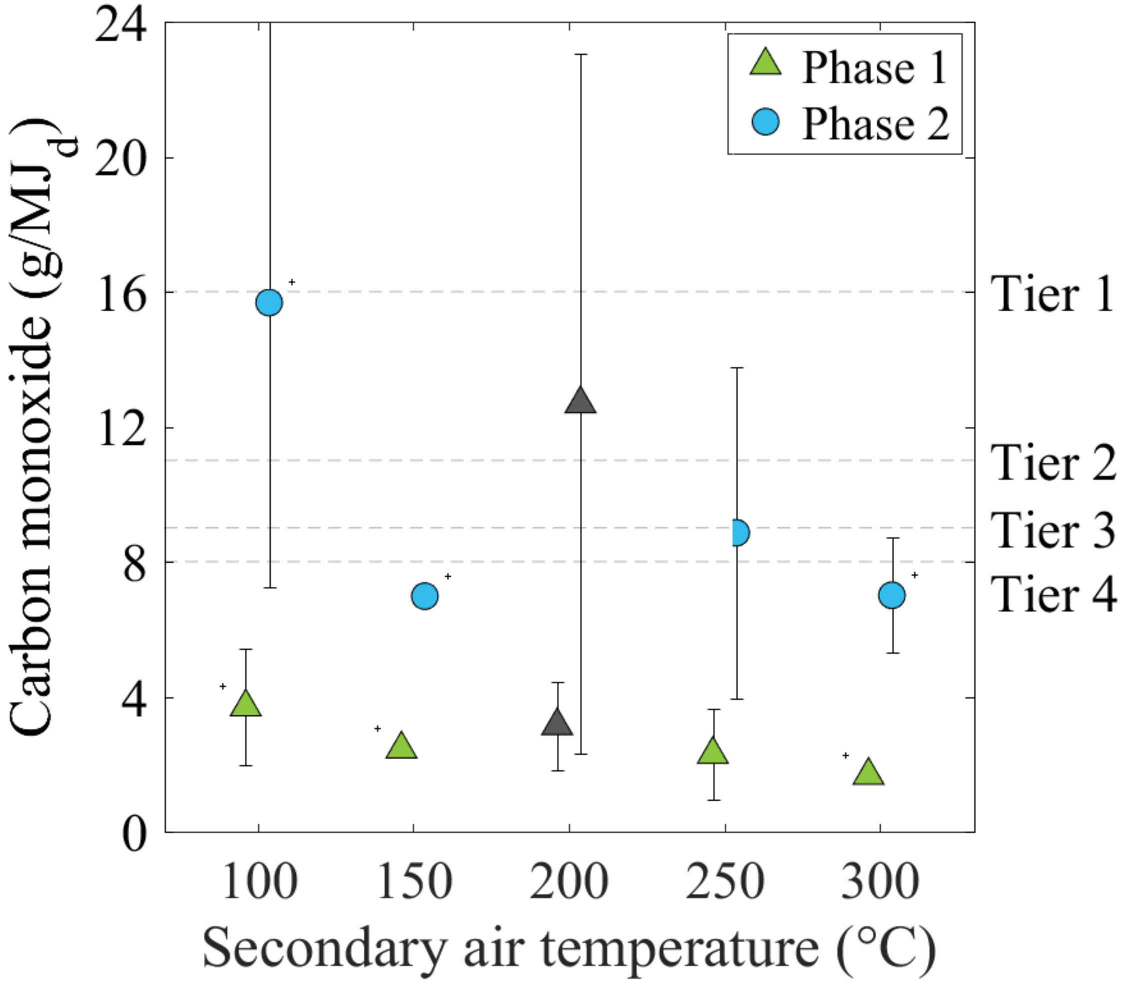

Figure 101 – Carbon Monoxide emissions normalized by the power delivered to the cooking vessel vs. secondary air injection temperature in °C varied from 100 °C to 300 °C.

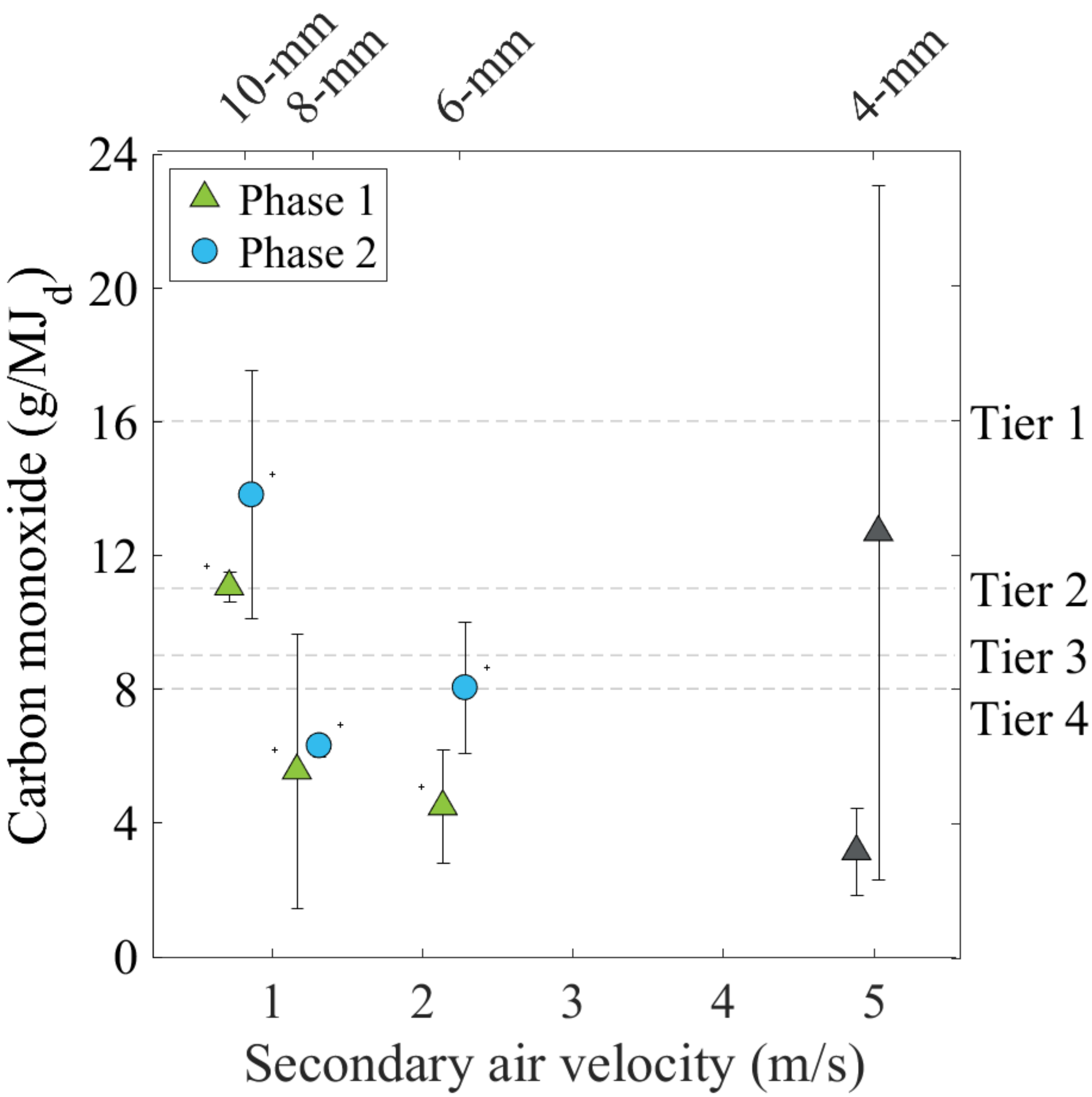

Figure 102 - Carbon Monoxide emissions normalized by power delivered to the cooking vessel vs. secondary air velocity in (m/s) or secondary air injection hole size.

Particulate Emissions

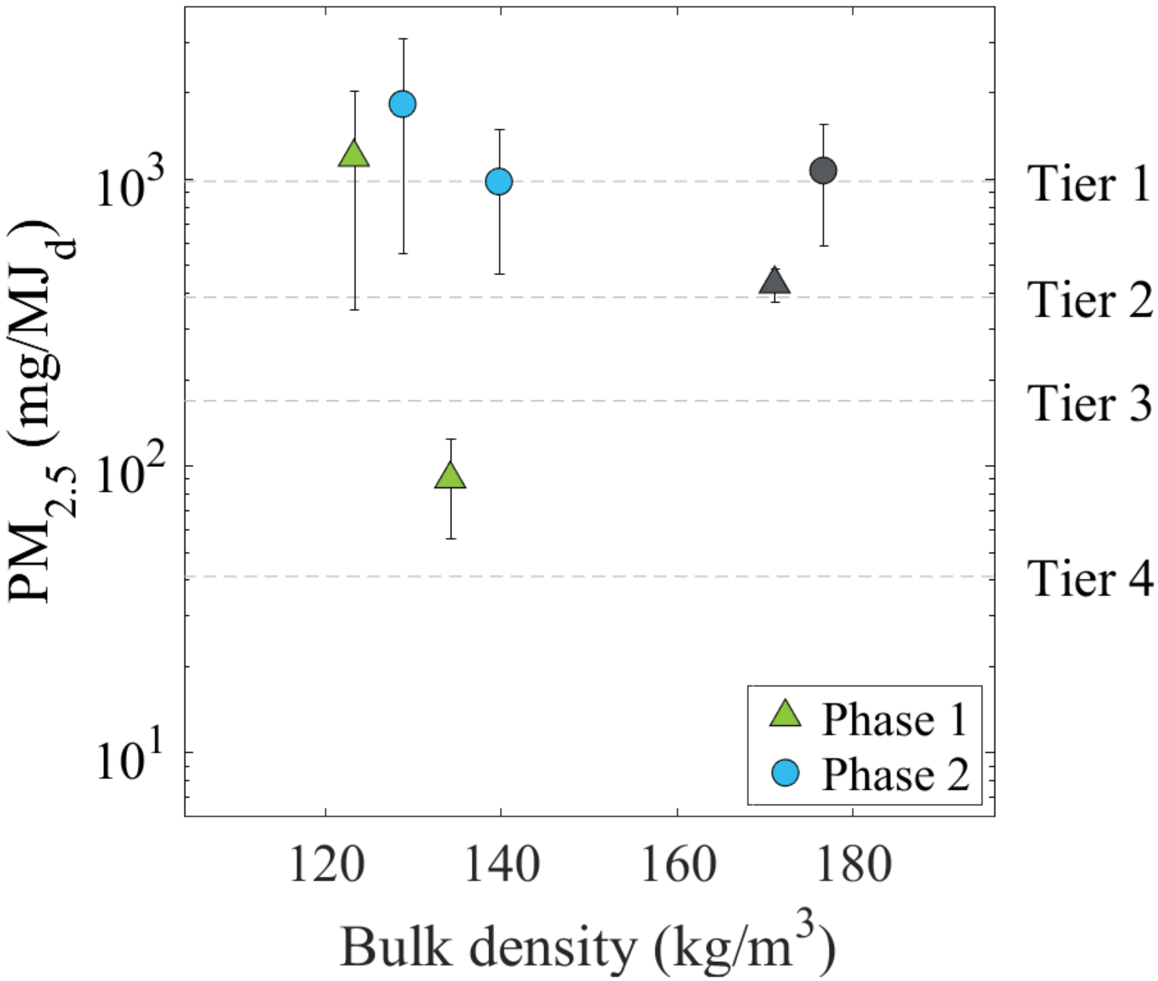

Figure 103 – Particulate emissions ($PM_{2.5}$) normalized by power delivered to the cooking vessel vs. fuel bulk density in (kg/m^3).

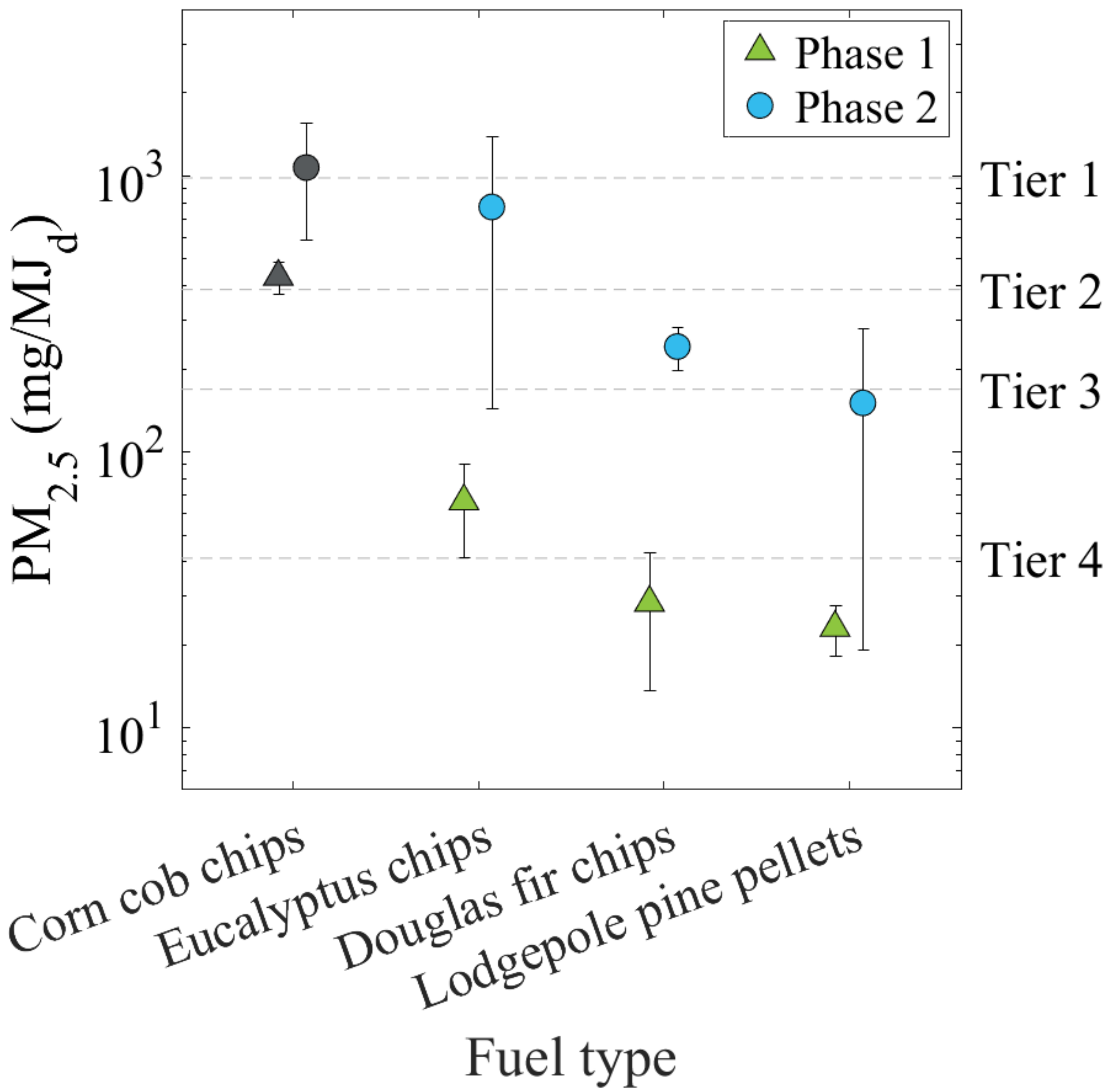

Figure 104 – Particulate emissions ($PM_{2.5}$) normalized by power delivered to the cooking vessel vs. Fuel type.

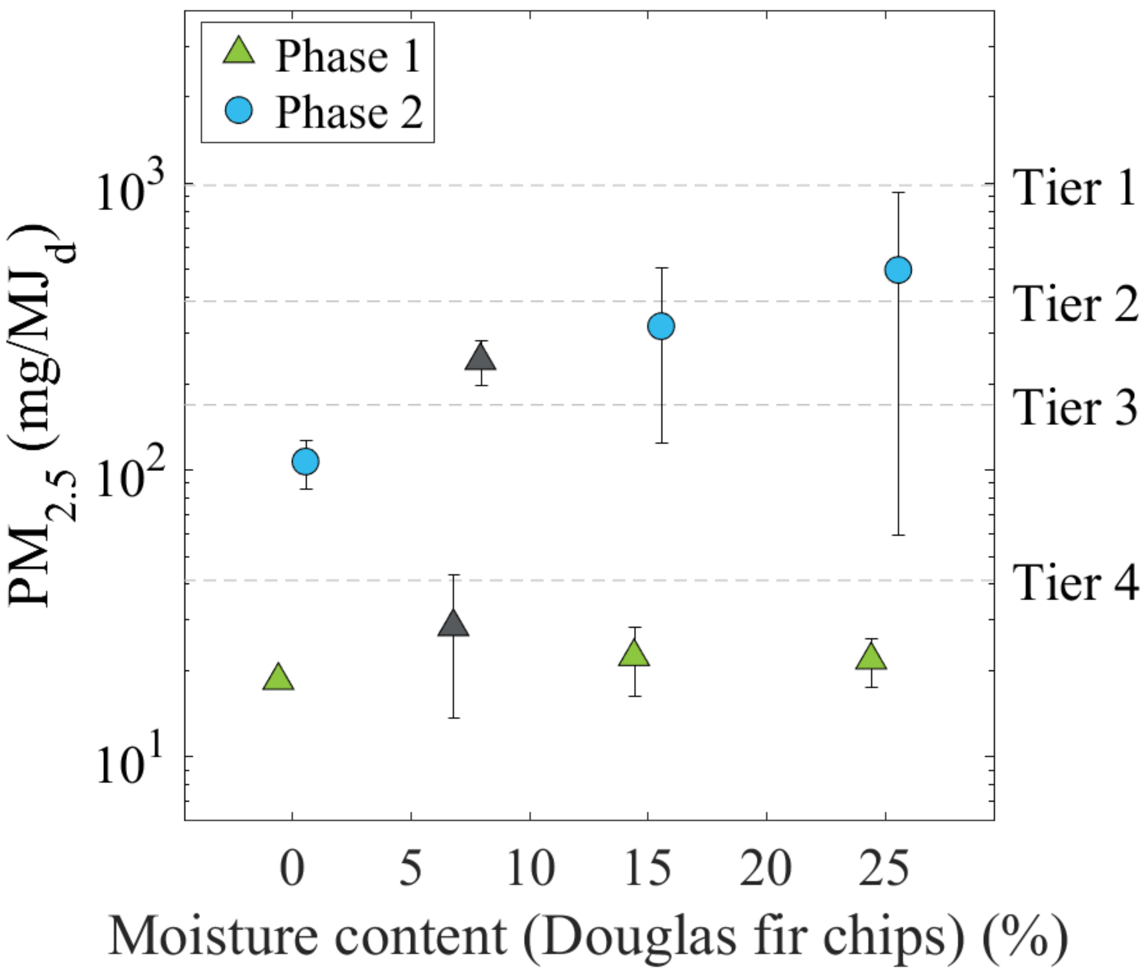

Figure 105 – Particulate emissions ($PM_{2.5}$) normalized by power delivered to the cooking vessel vs. fuel moisture content (%).

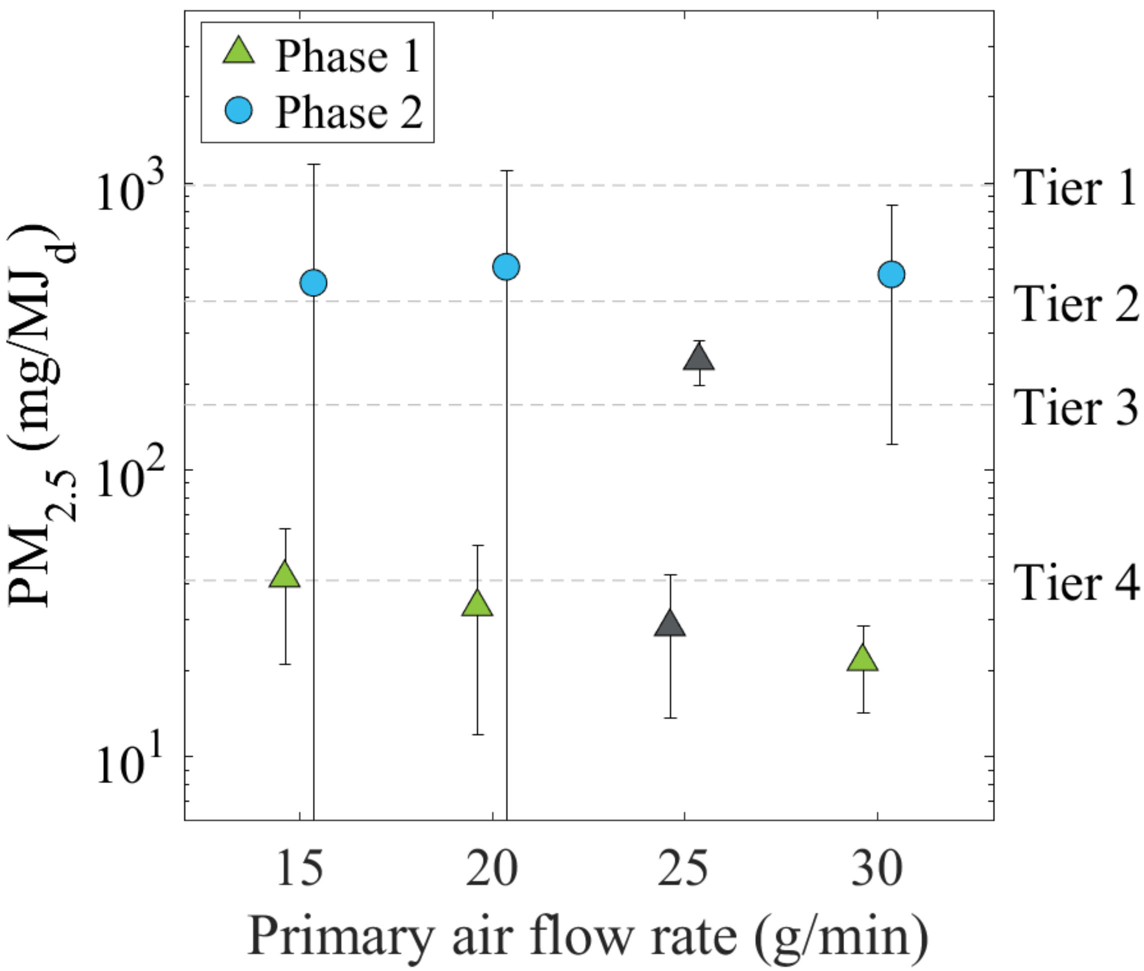

Figure 106 – Particulate emissions ($PM_{2.5}$) normalized by power delivered to the cooking vessel vs. primary air flow rate (g/min)

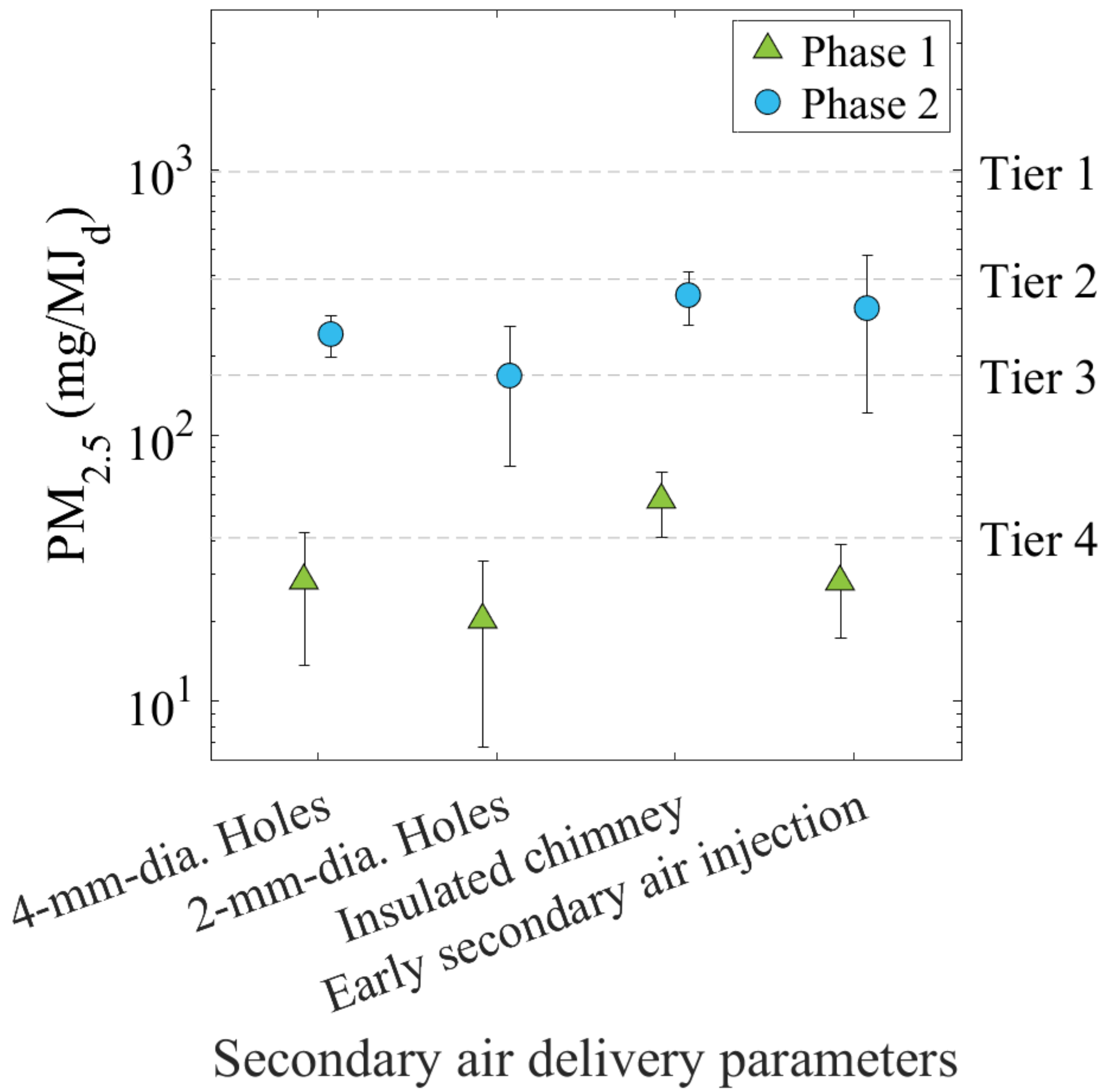

Figure 107 – Particulate emissions ($PM_{2.5}$) normalized by power delivered to the cooking vessel vs. secondary air delivery parameters.

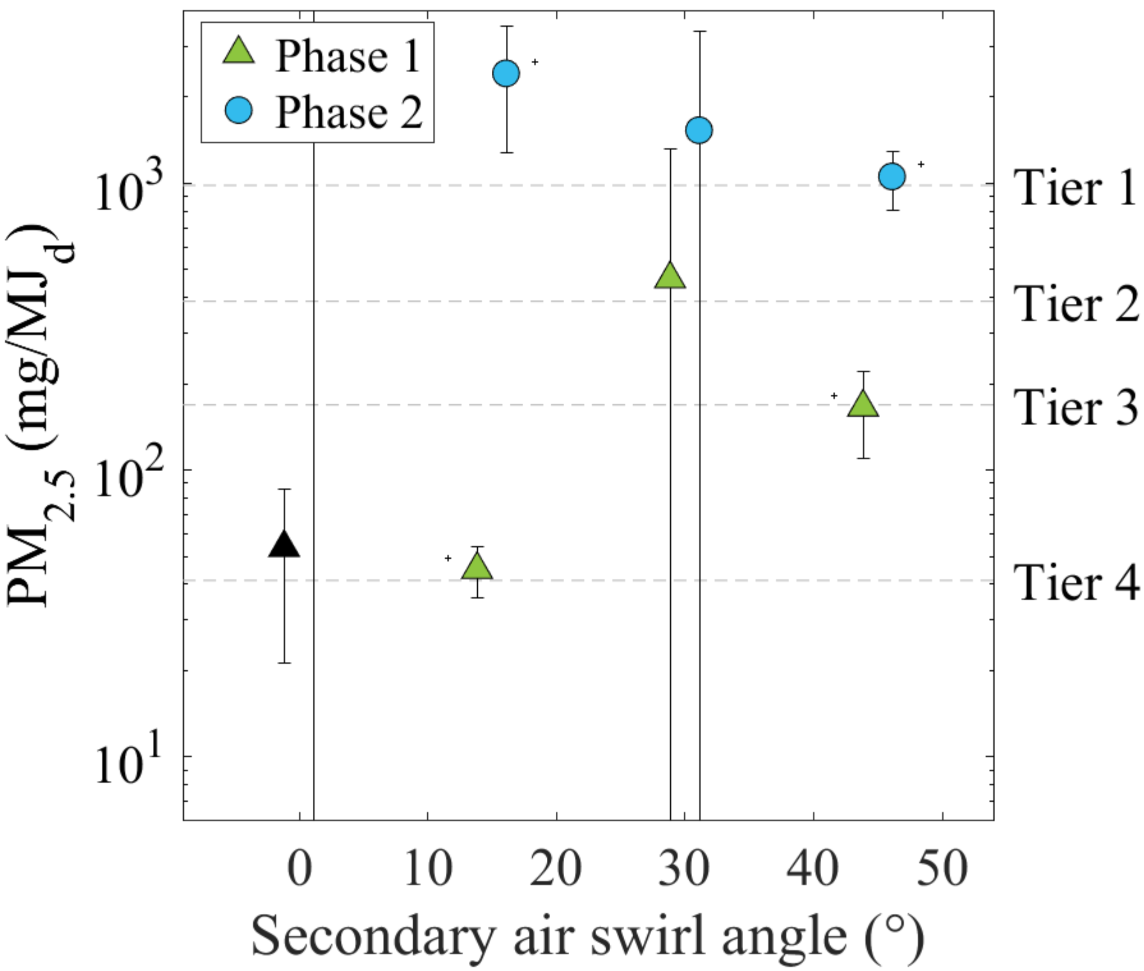

Figure 108 – Particulate emissions ($PM_{2.5}$) normalized by power delivered to the cooking vessel vs. secondary air swirl angle (° from radial)

Fuel Consumption Rate

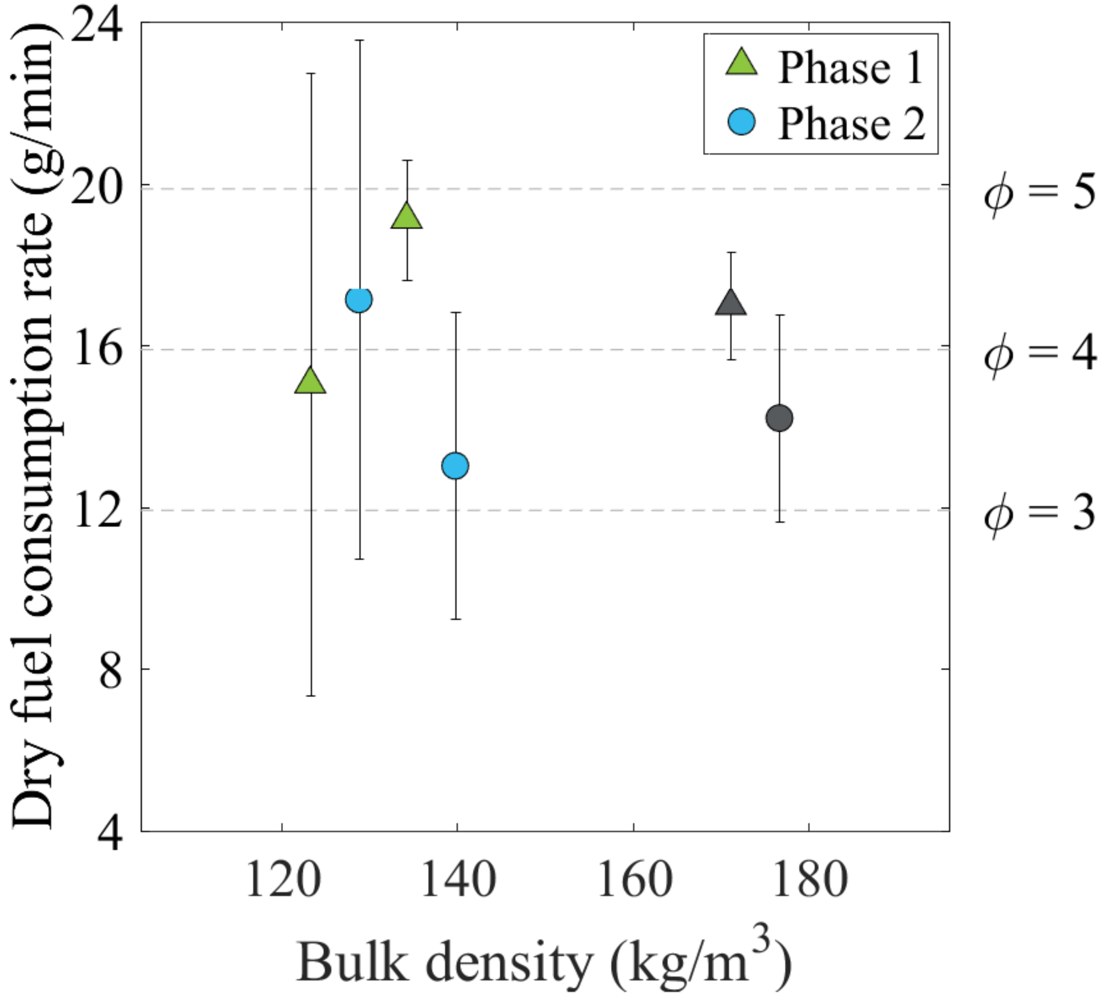

Figure 109 – Dry fuel consumption rate in (g/min) vs. bulk density (kg/m³).

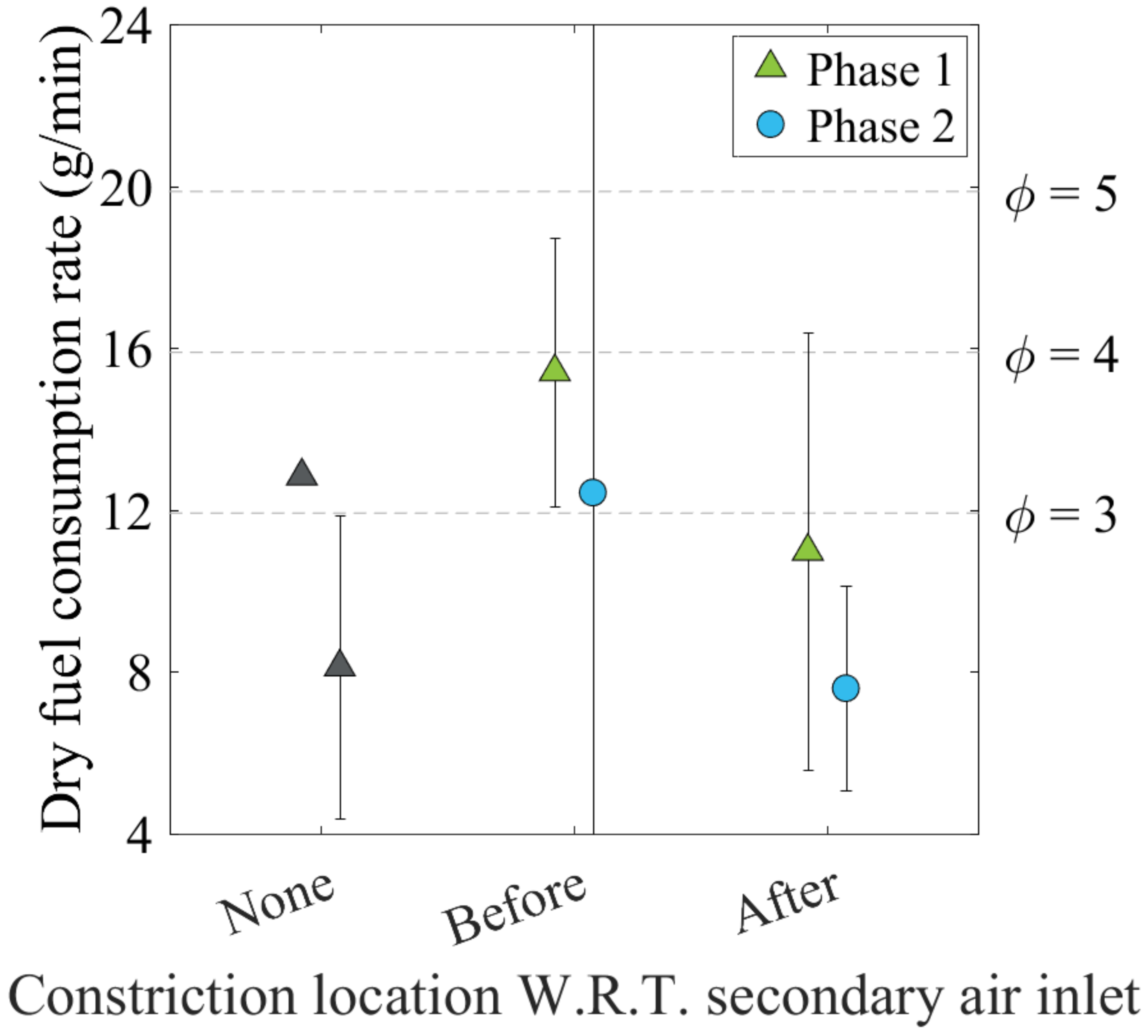

Figure 110 – Dry fuel consumption rate in (g/min) vs. constriction location with respect to the secondary combustion stage air inlet.

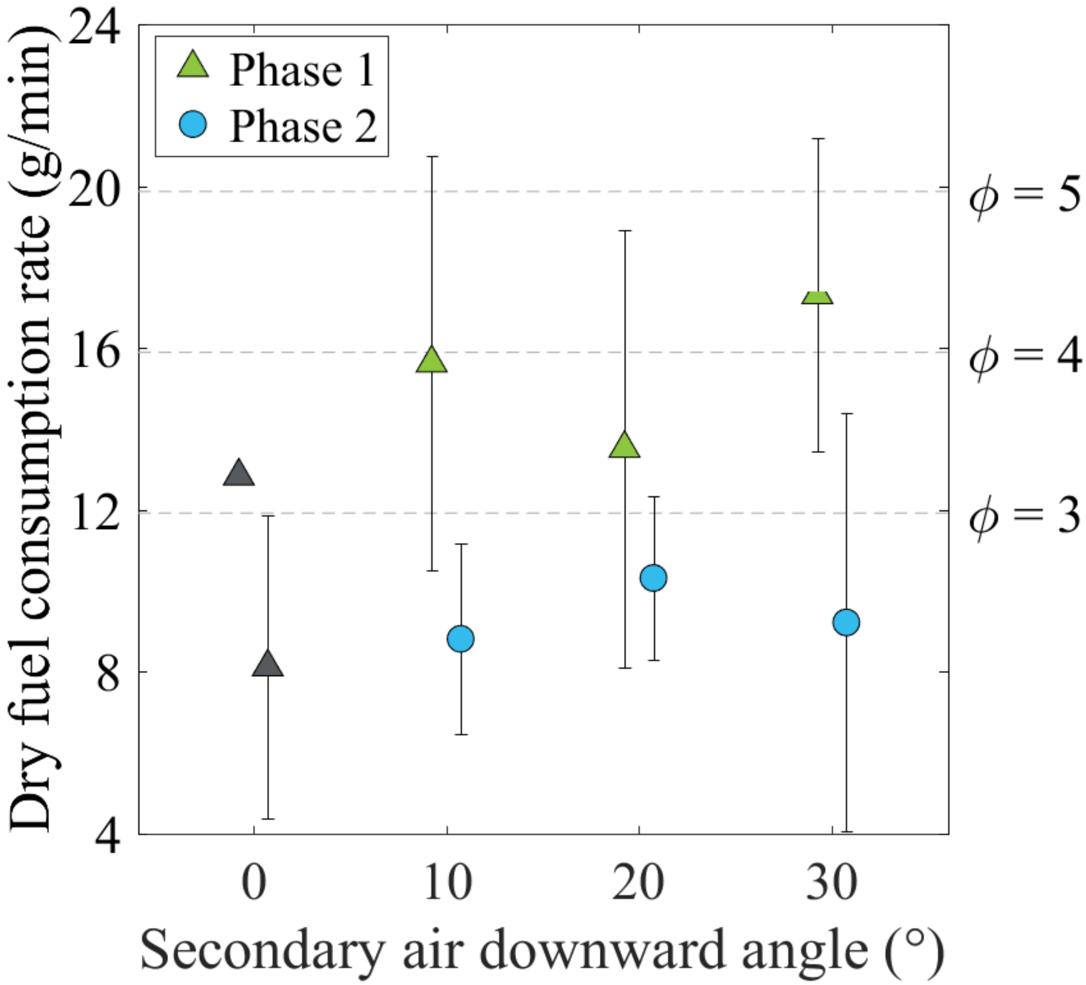

Figure 111 – Dry fuel consumption rate in (g/min) vs. secondary combustion stage downward air injection angle (° downward from the radial axis).

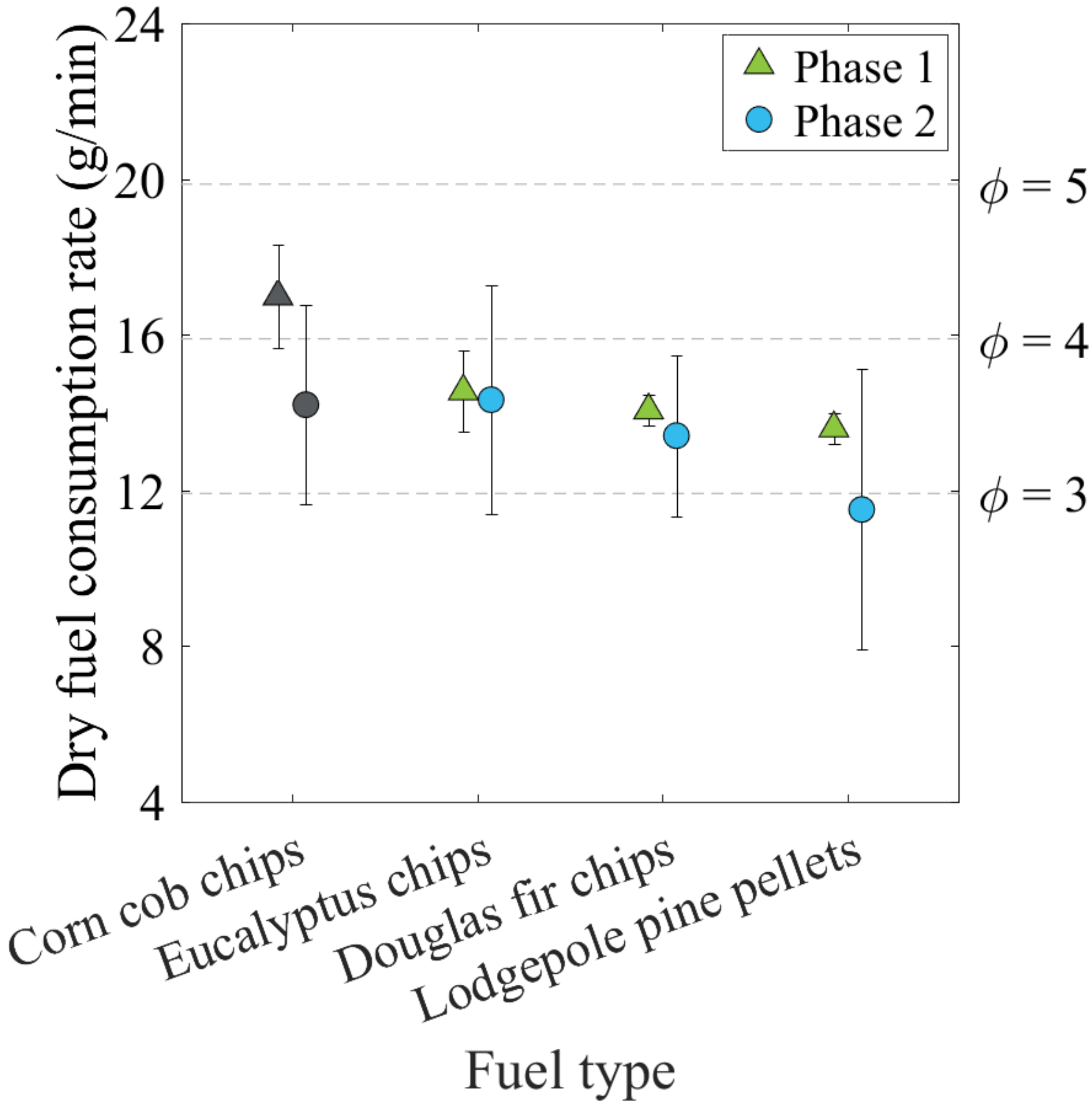

Figure 112 – Dry fuel consumption rate in (g/min) vs. fuel type.

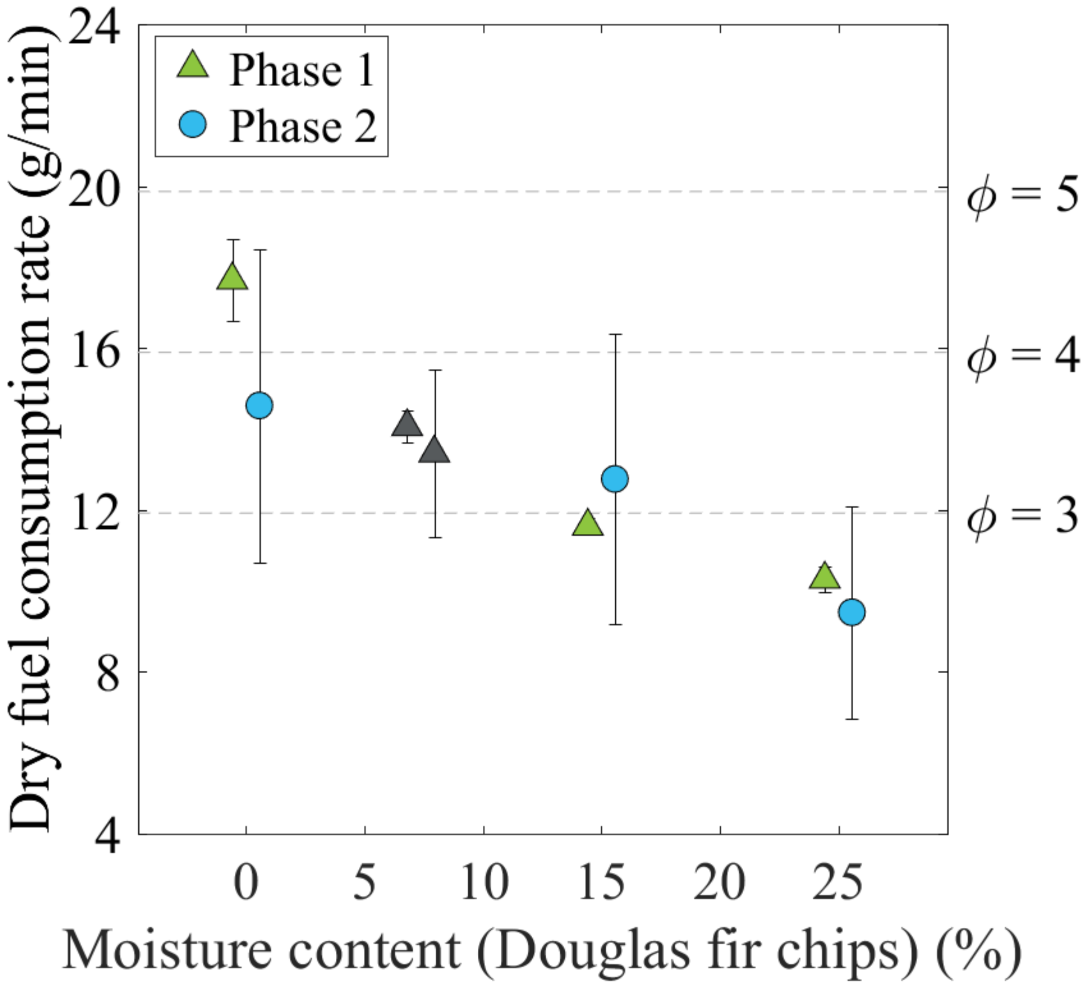

Figure 113 - Dry fuel consumption rate in (g/min) vs. moisture content (%)

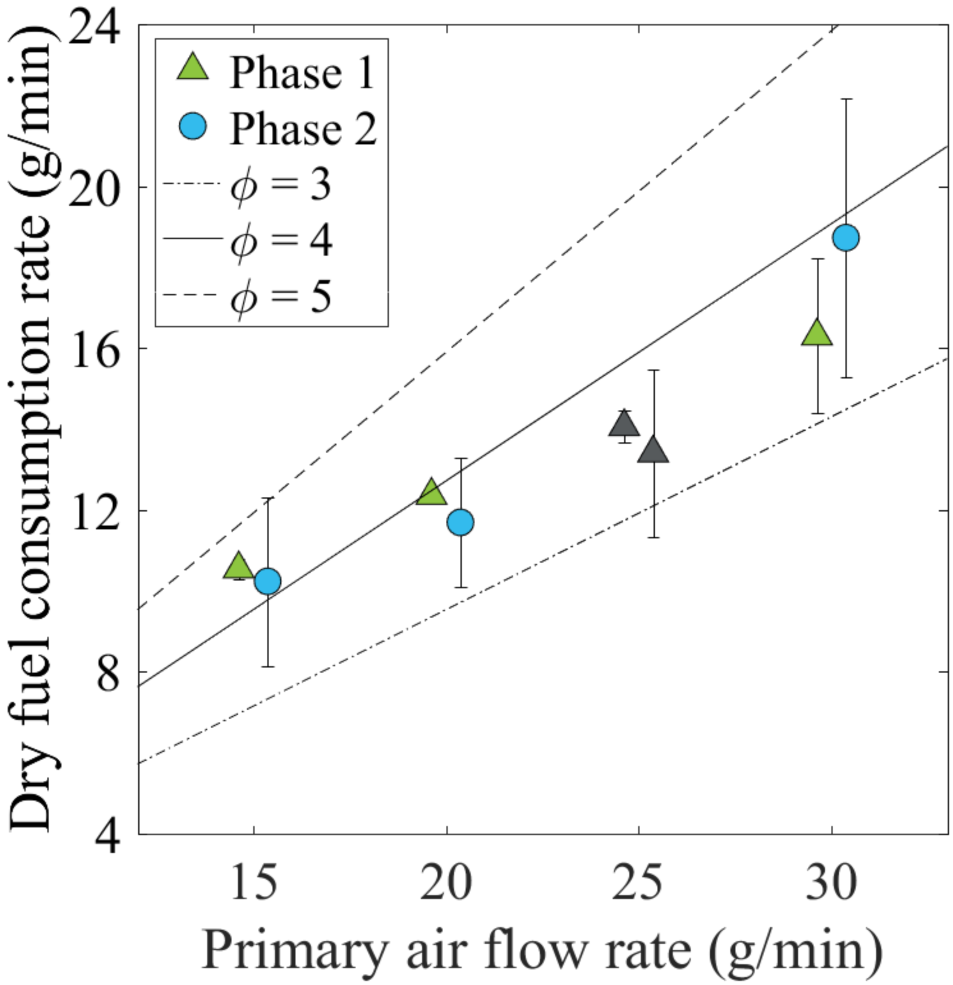

Figure 114 – Dry fuel consumption rate in (g/min) vs. primary air flow rate in (g/min) with fuel to air ratio Φ.

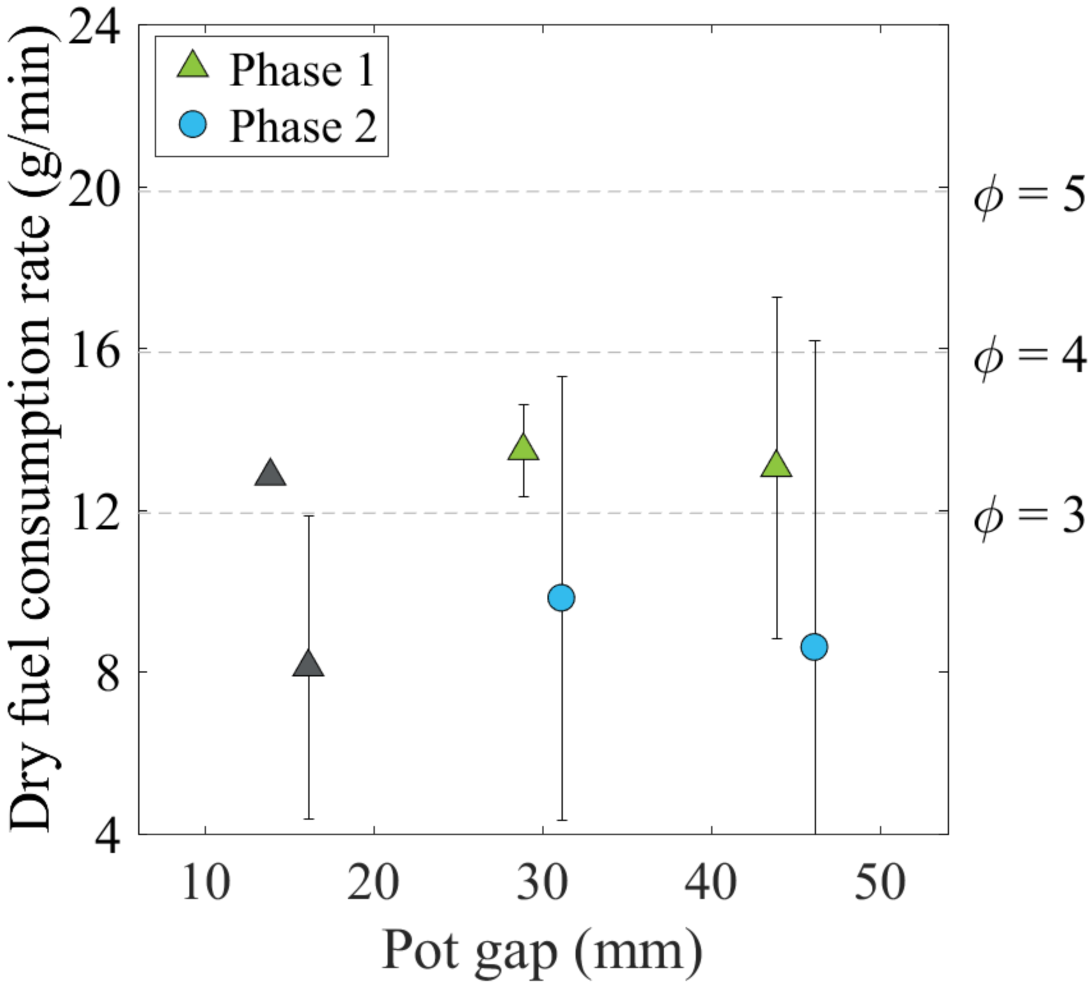

Figure 115 – Dry fuel consumption rate in (g/min) vs. pot gap (mm).

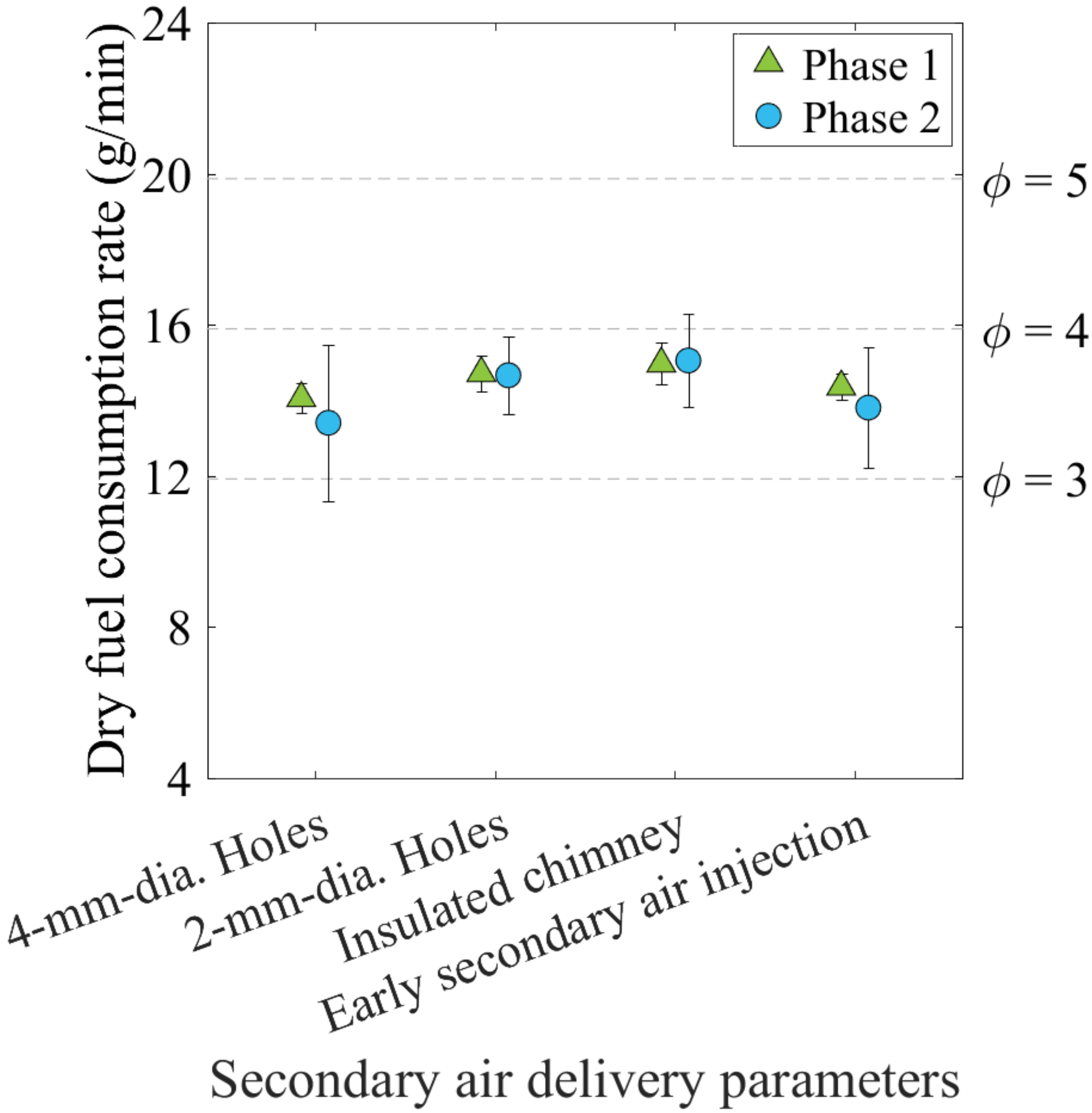

Figure 116 - Dry fuel consumption rate in (g/min) vs. secondary air delivery parameter.

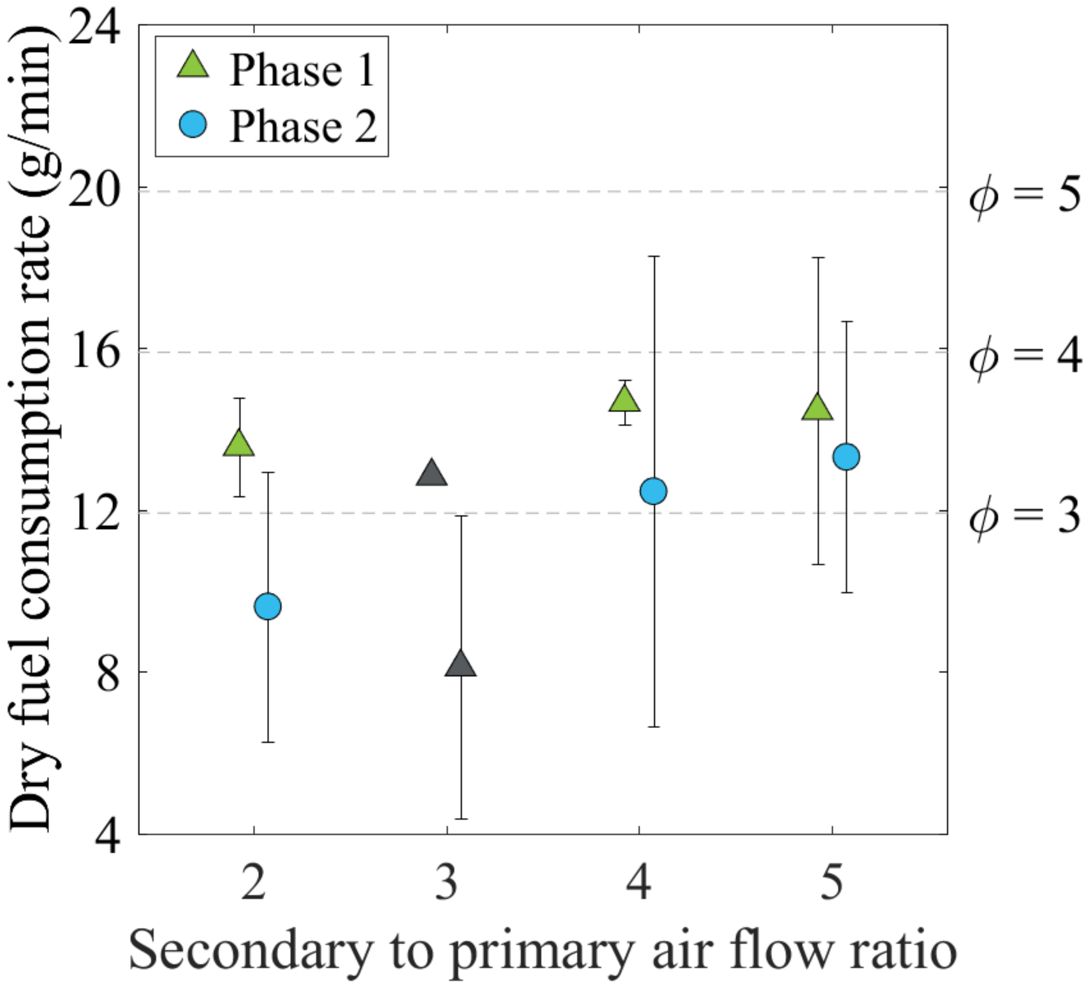

Figure 117 – Dry fuel consumption rate in (g/min) vs. secondary to primary air flow ratio

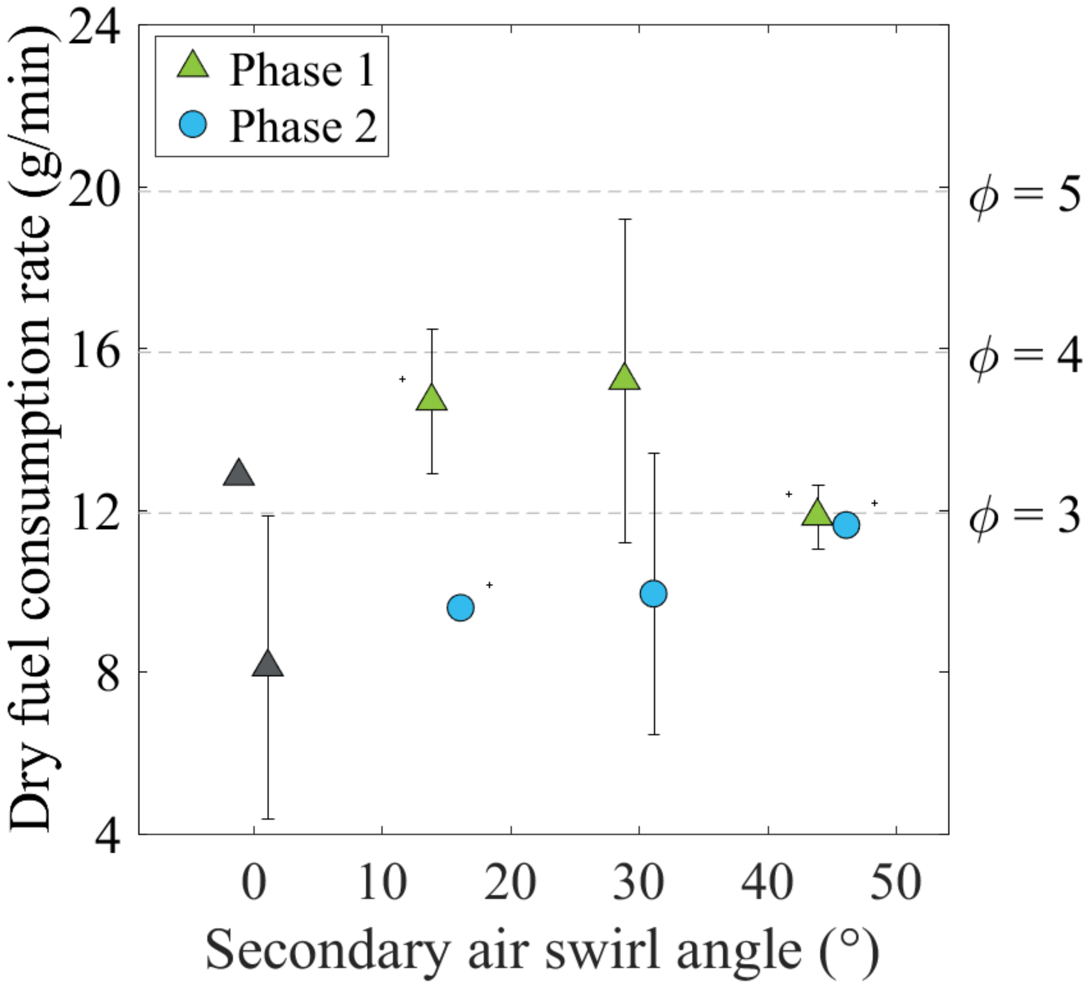

Figure 118 – Dry fuel consumption rate in (g/min) vs. secondary air swirl angle (° with respect to the radial axis)

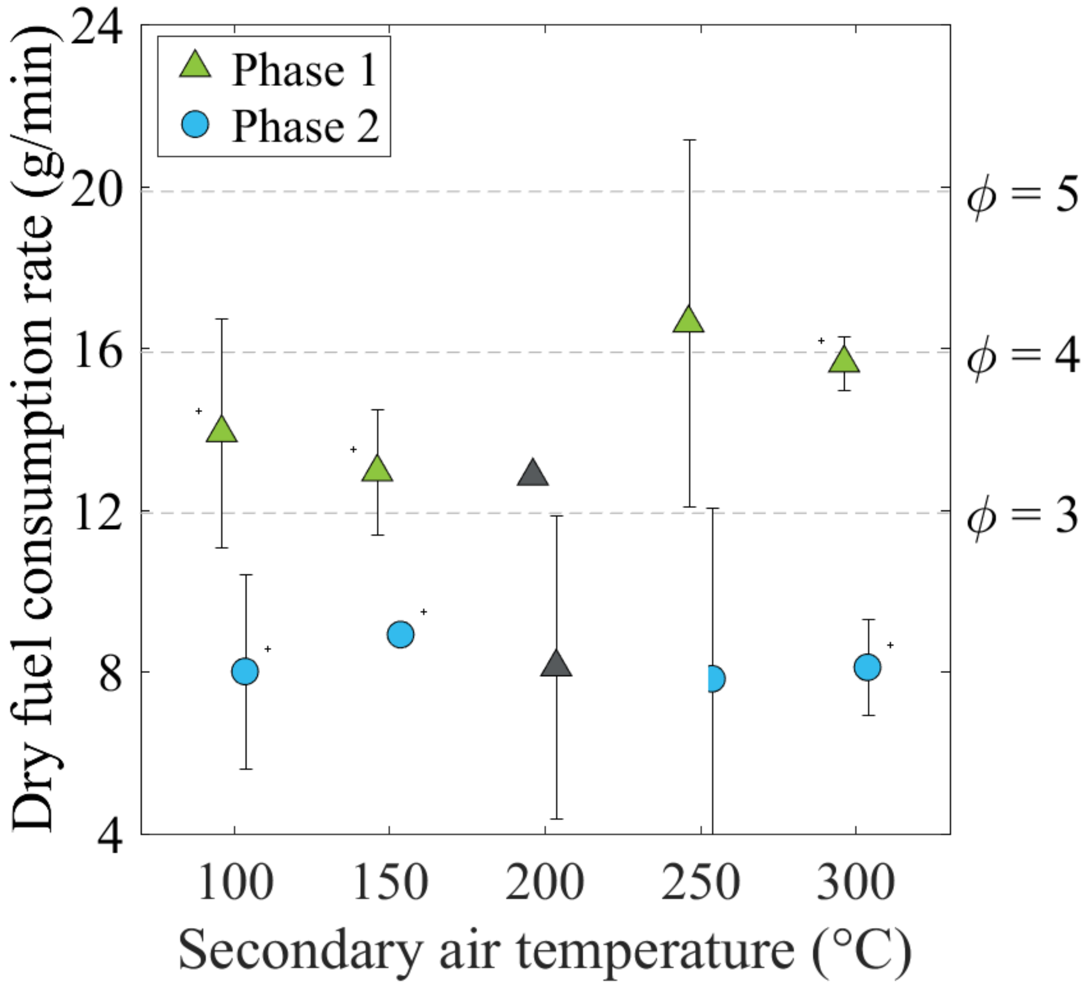

Figure 119 - Dry fuel consumption rate in (g/min) vs. secondary air inlet temperature (°C).

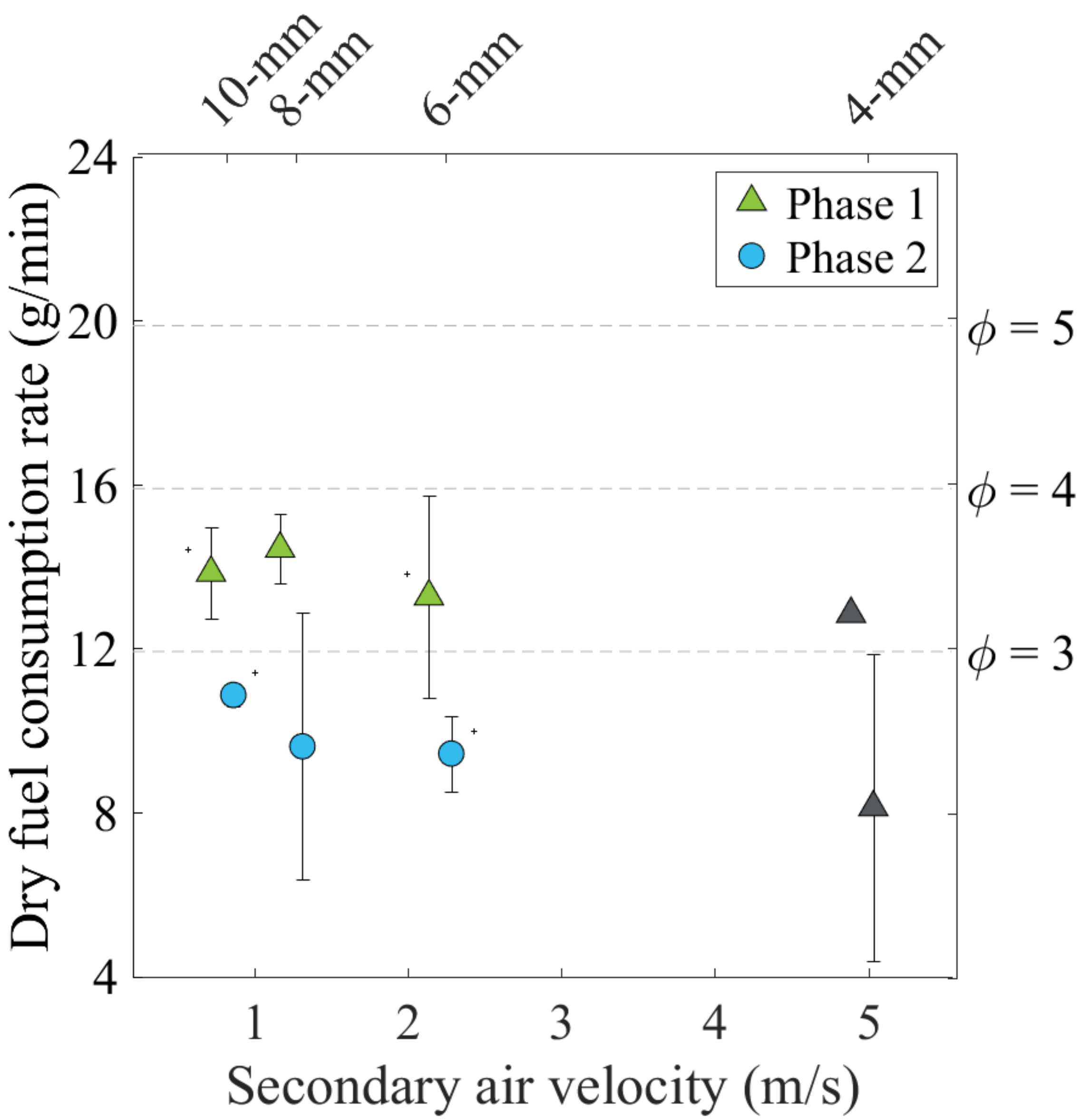

Figure 120 – Dry fuel consumption rate in (g/min) vs. secondary air velocity (m/s) and secondary hole size.

Average Mass Loss Rate

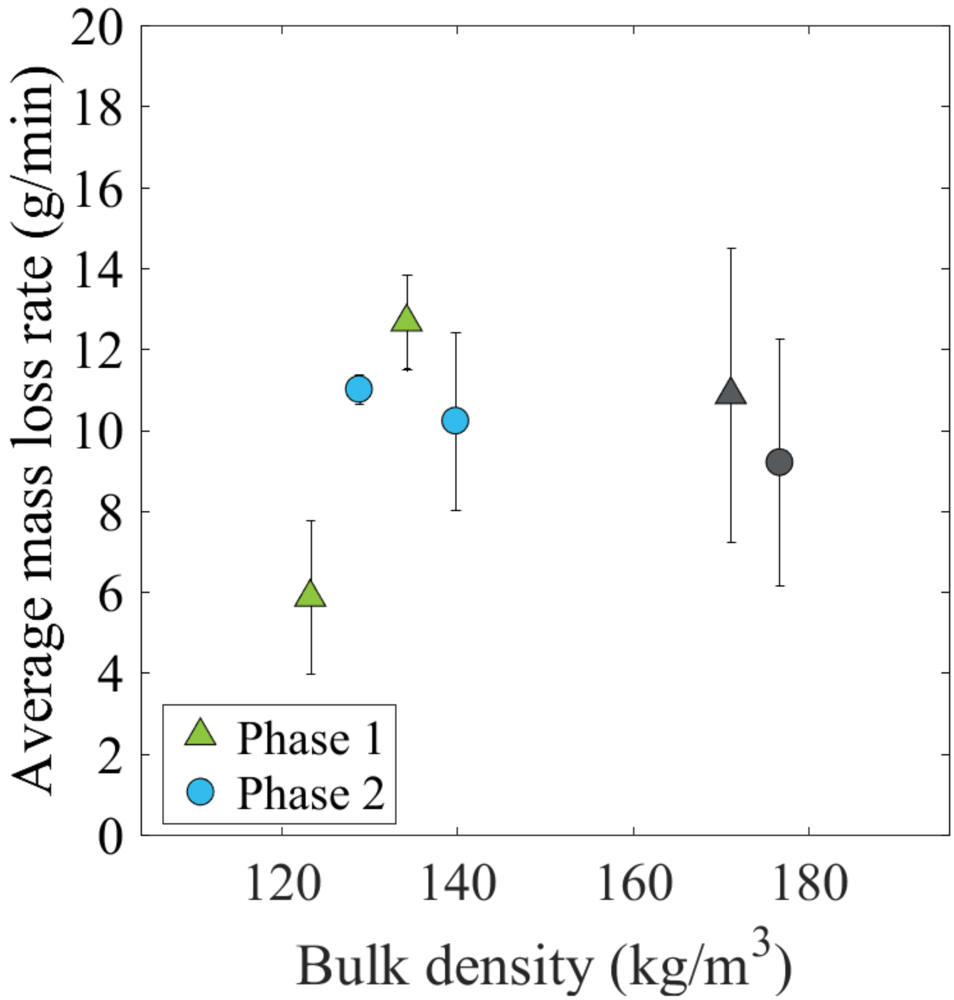

Figure 121 – Average fuel mass loss rate (g/min) vs. fuel bulk density (kg/min).

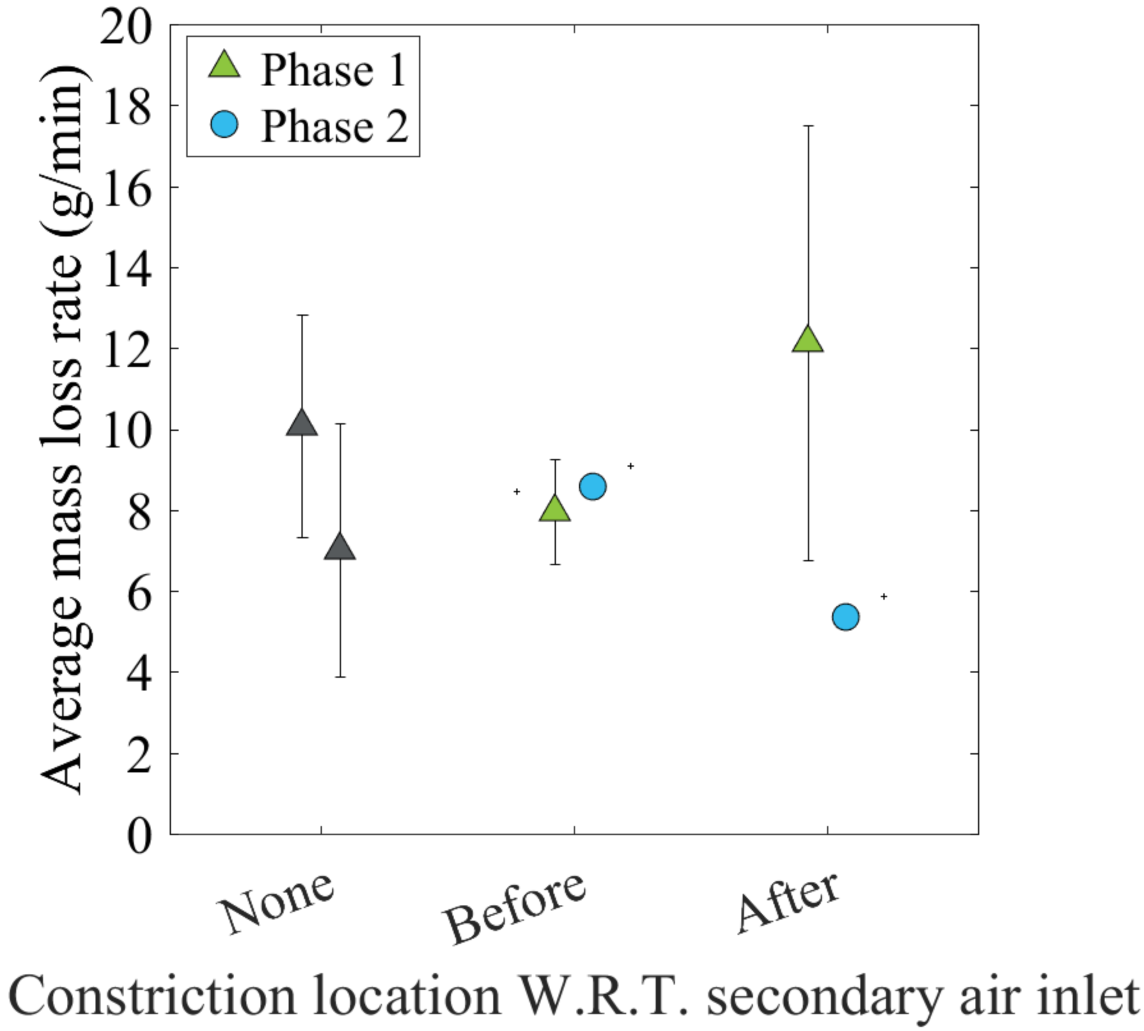

Figure 122 - Average fuel mass loss rate (g/min) vs. constriction location with respect to the secondary combustion stage air inlet.

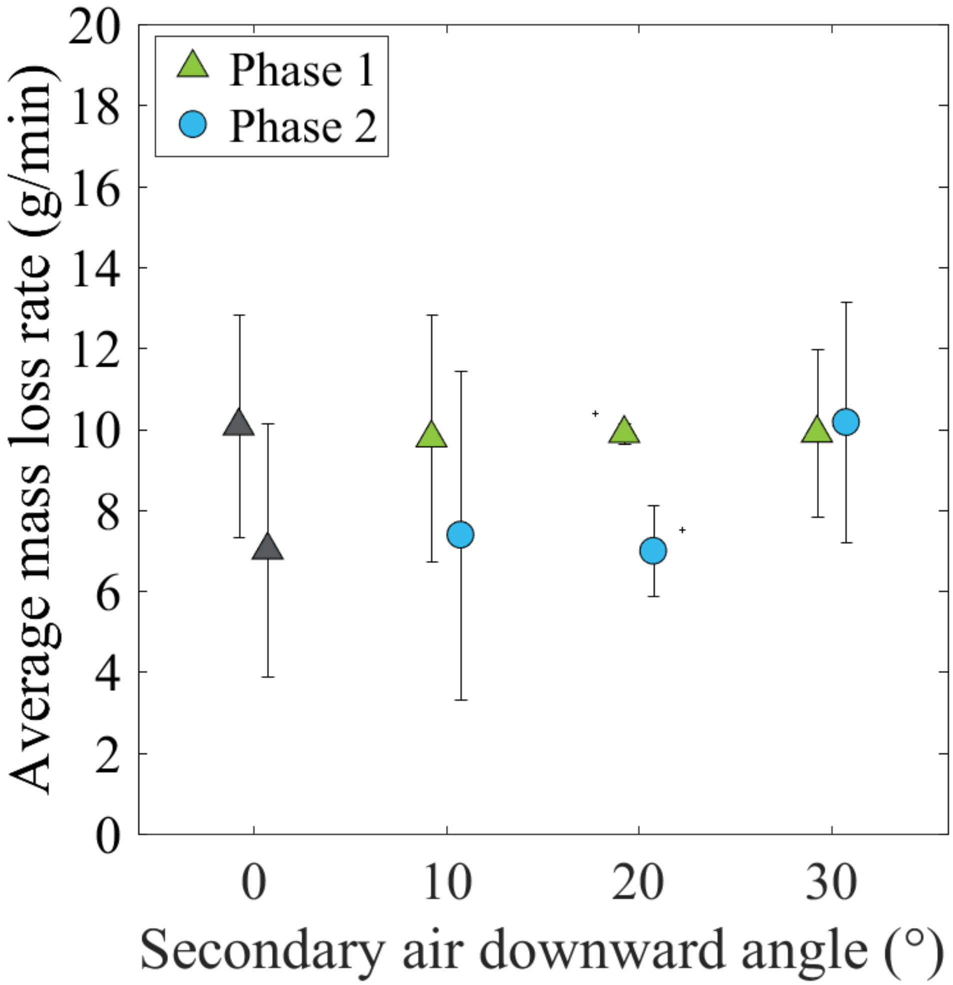

Figure 123 – Average fuel mass loss rate (g/min) vs. secondary air inlet downward angle (°).

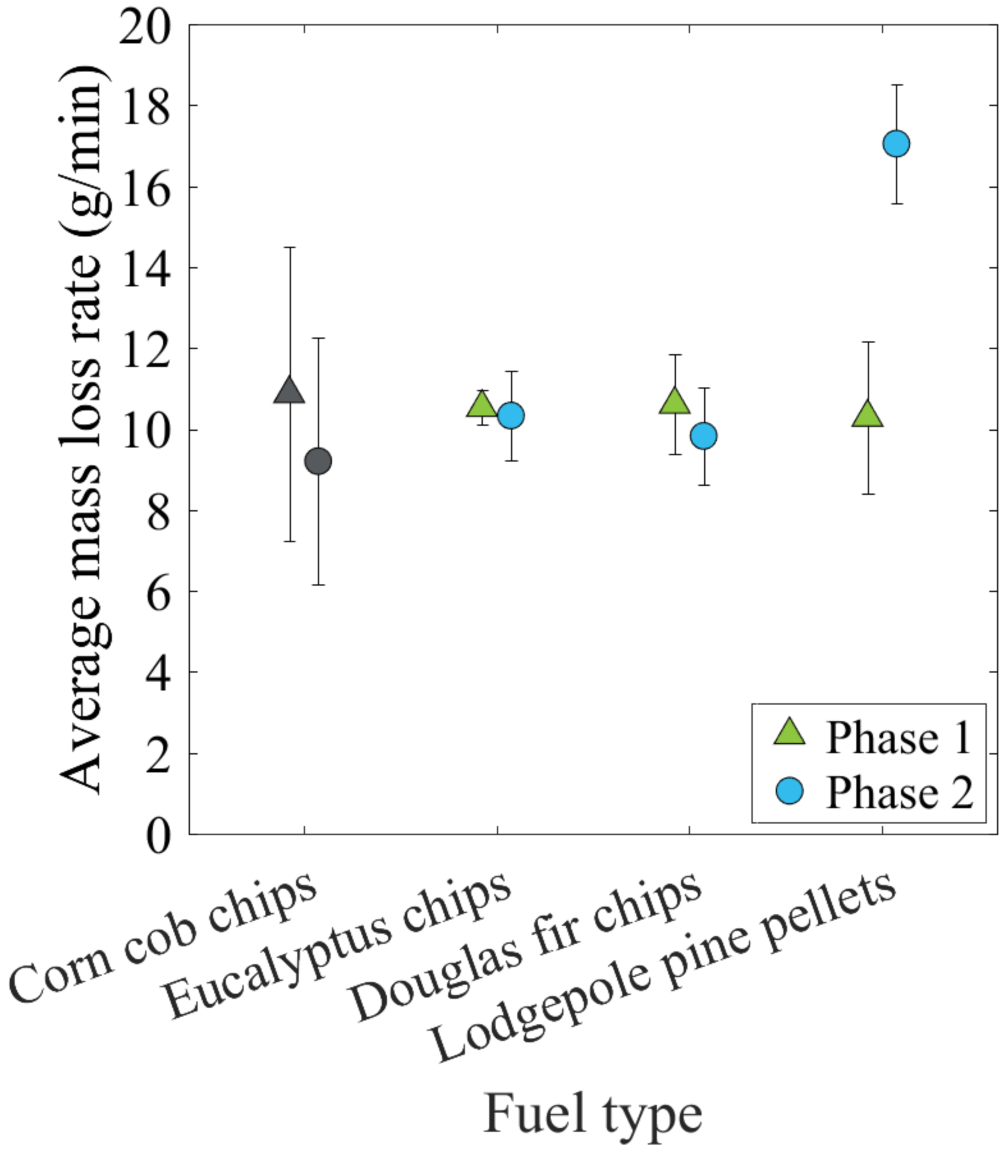

Figure 124 – Average fuel mass loss rate (g/min) vs. fuel type.

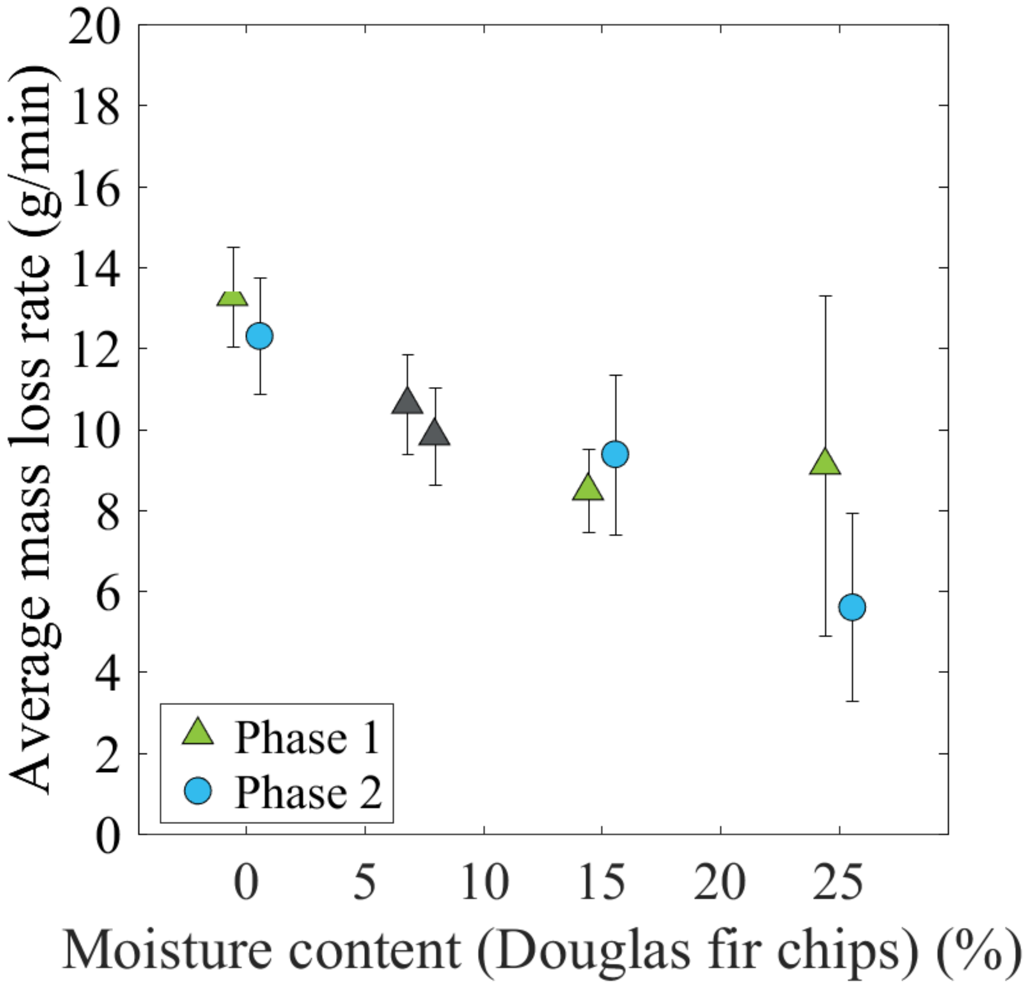

Figure 125 – Average fuel mass loss rate (g/min) vs. moisture content (%)

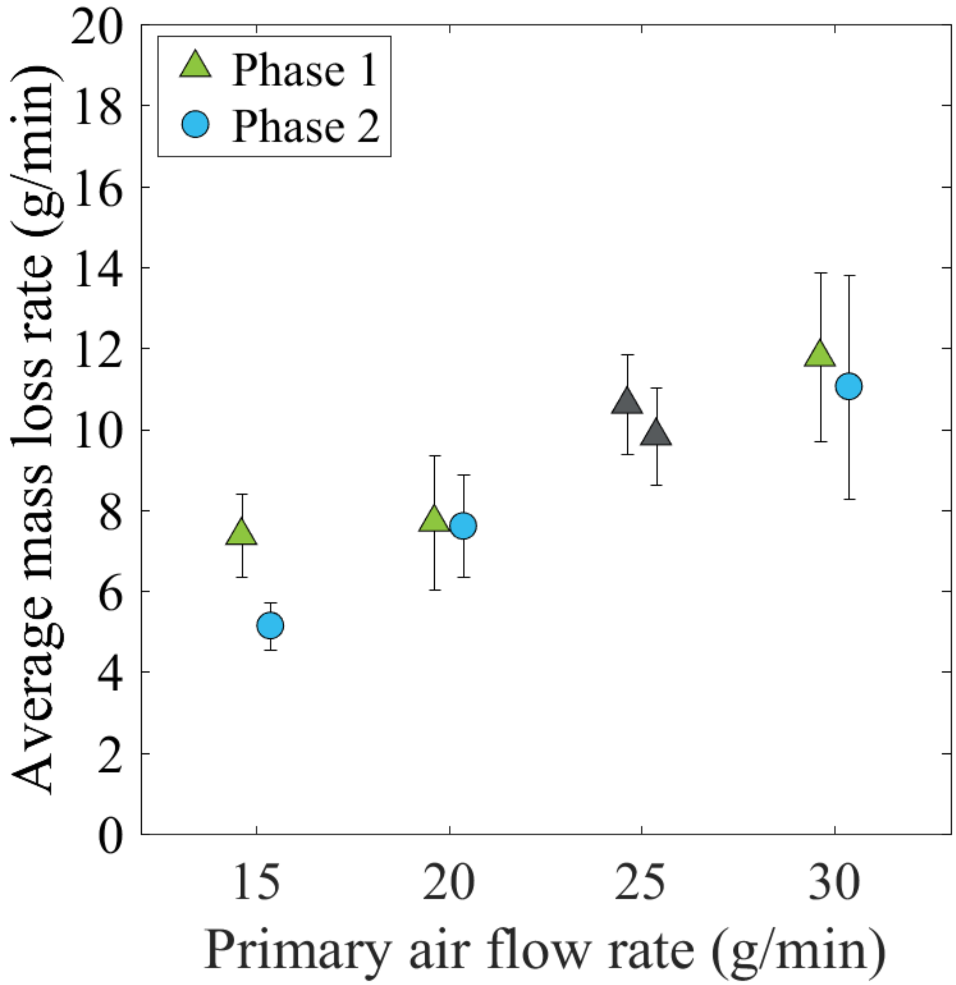

Figure 126 – Average fuel mass loss rate (g/min) vs. primary airflow rate (g/min).

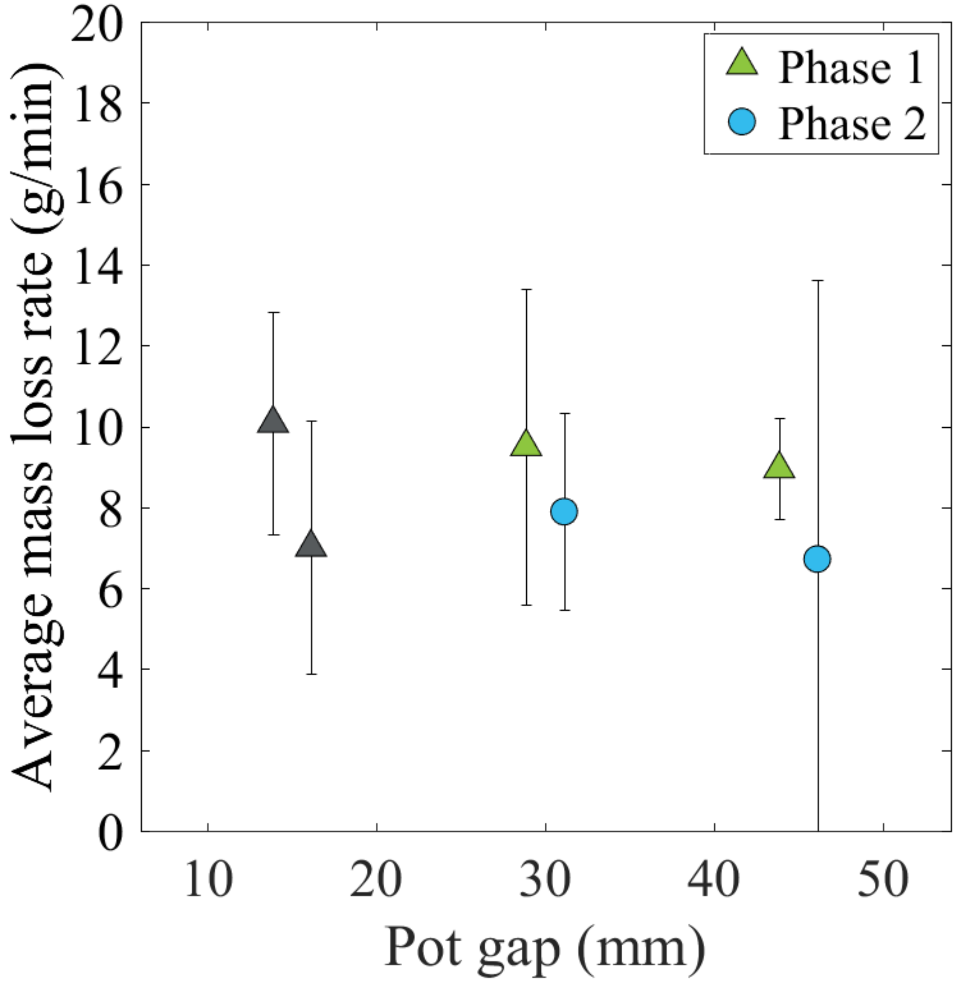

Figure 127 – Average fuel mass loss rate (g/min) vs. pot gap (mm)

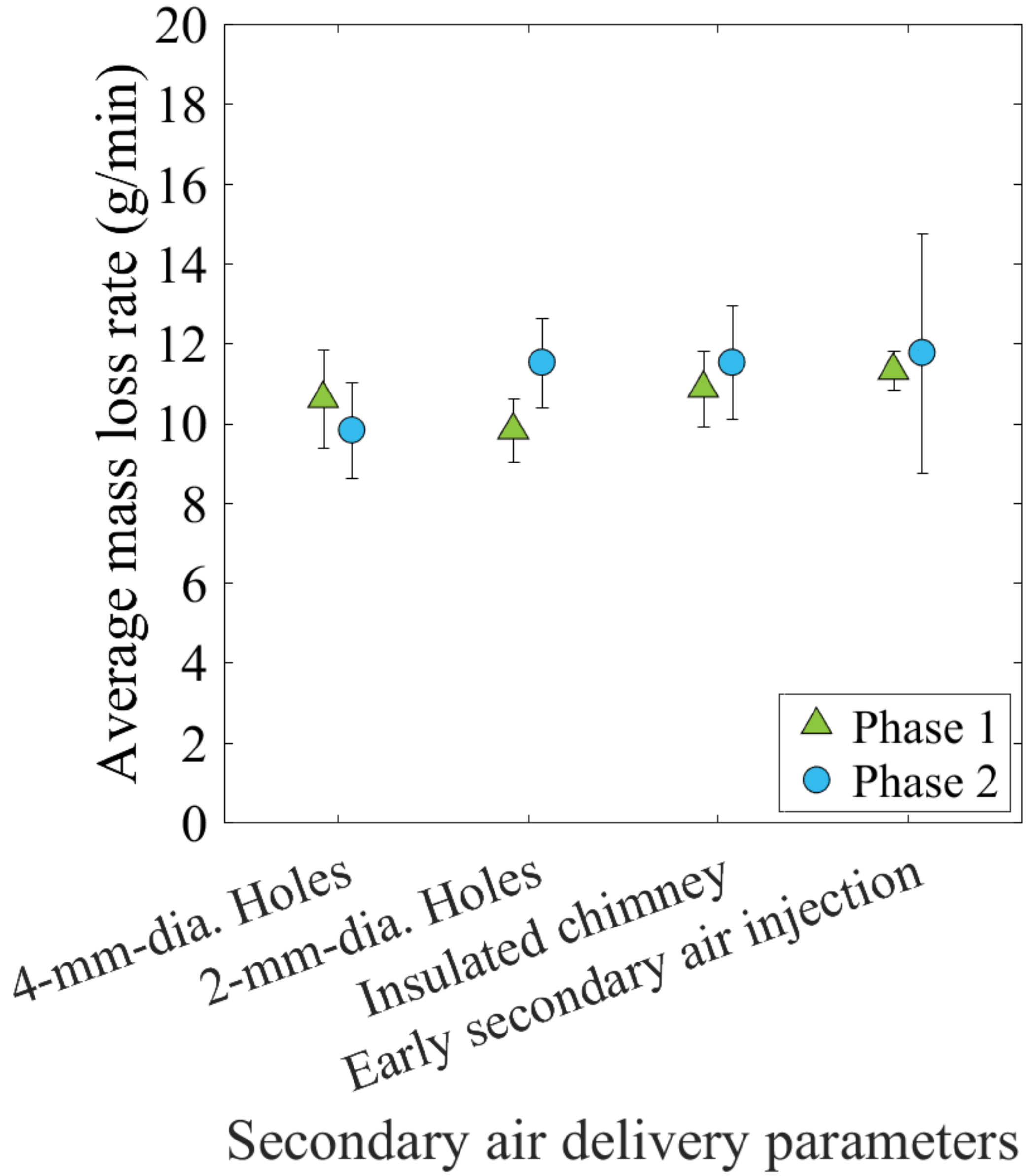

Figure 128 - Average fuel mass loss rate (g/min) vs. secondary air delivery parameters.

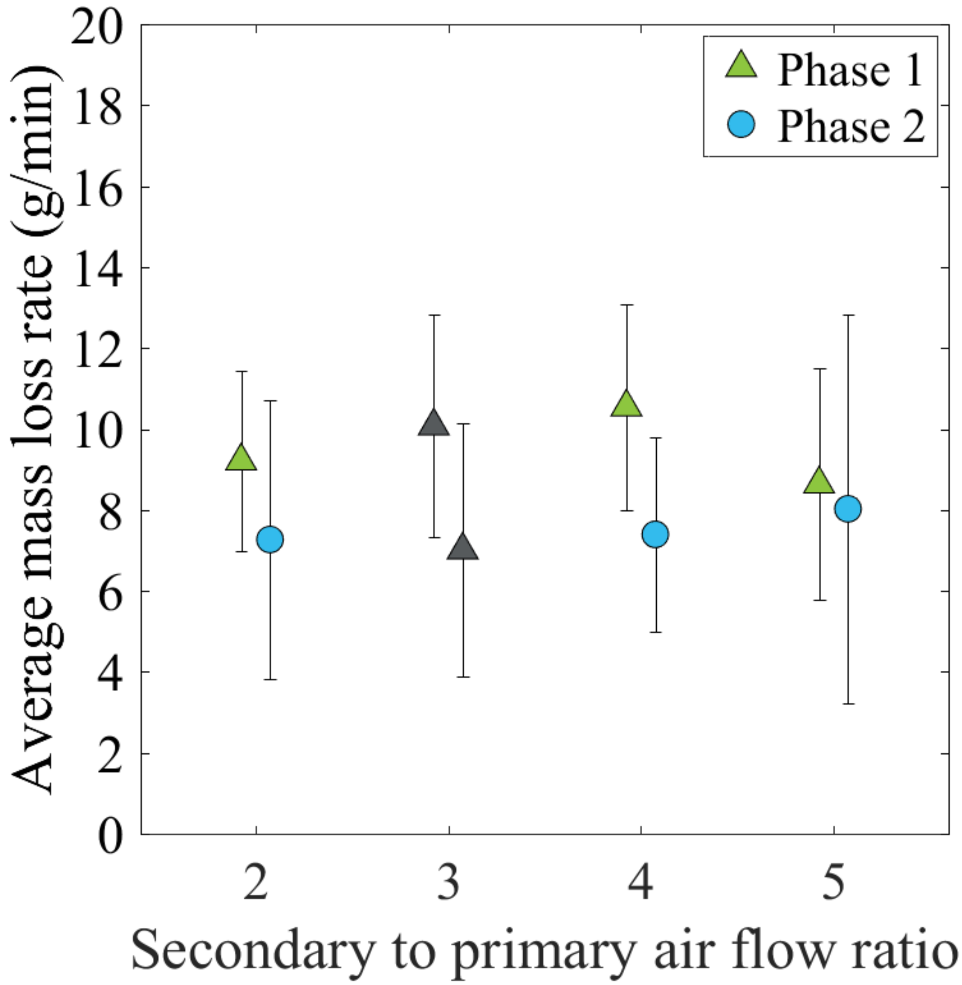

Figure 129 - Average fuel mass loss rate (g/min) vs. secondary to primary airflow ratios

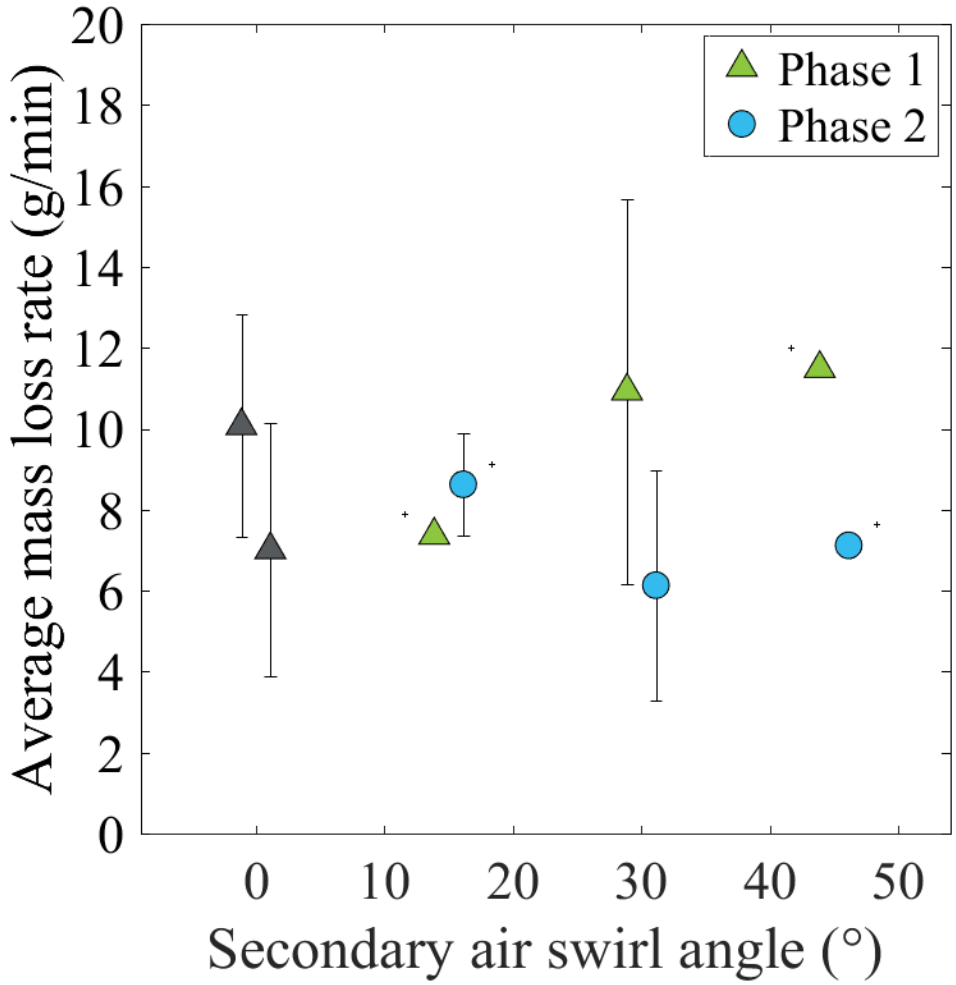

Figure 130 – Average fuel mass loss rate (g/min) vs. secondary air inlet swirl angle (° with respect to the radial axis)

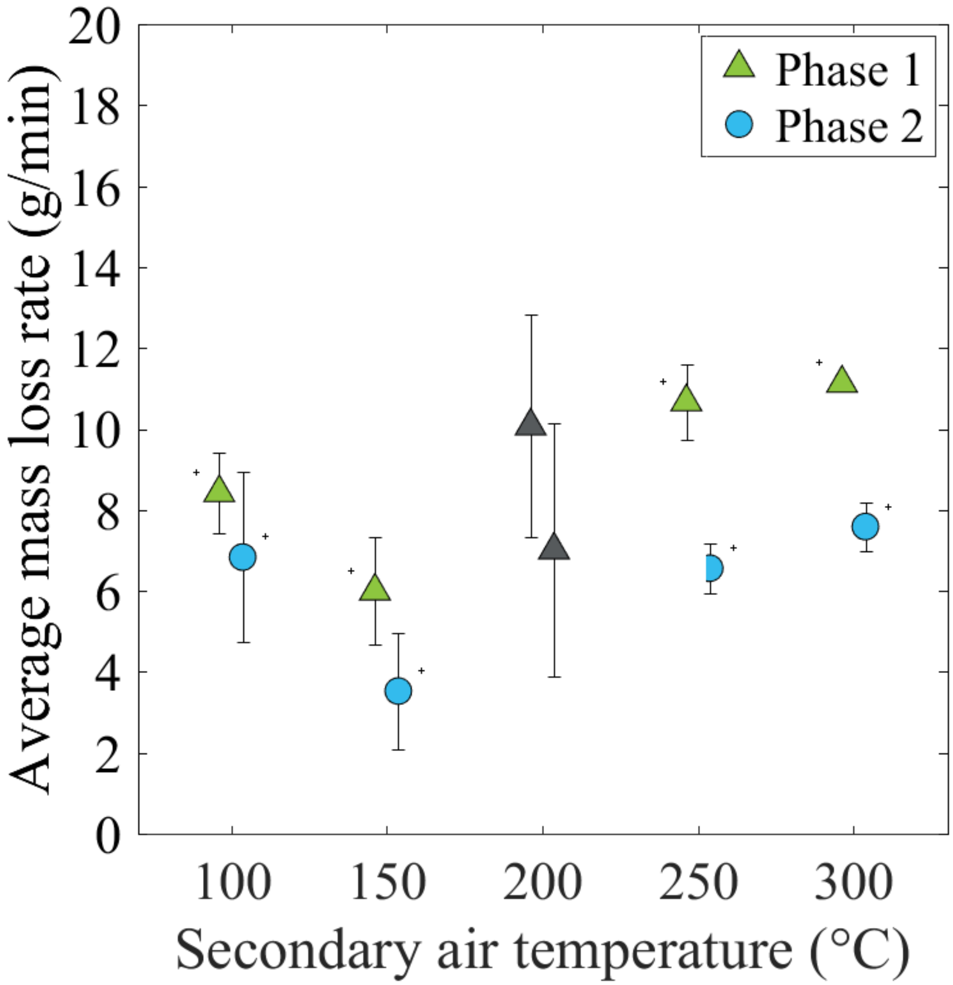

Figure 131 – Average fuel mass loss rate (g/min) vs. secondary air temperature (°C).

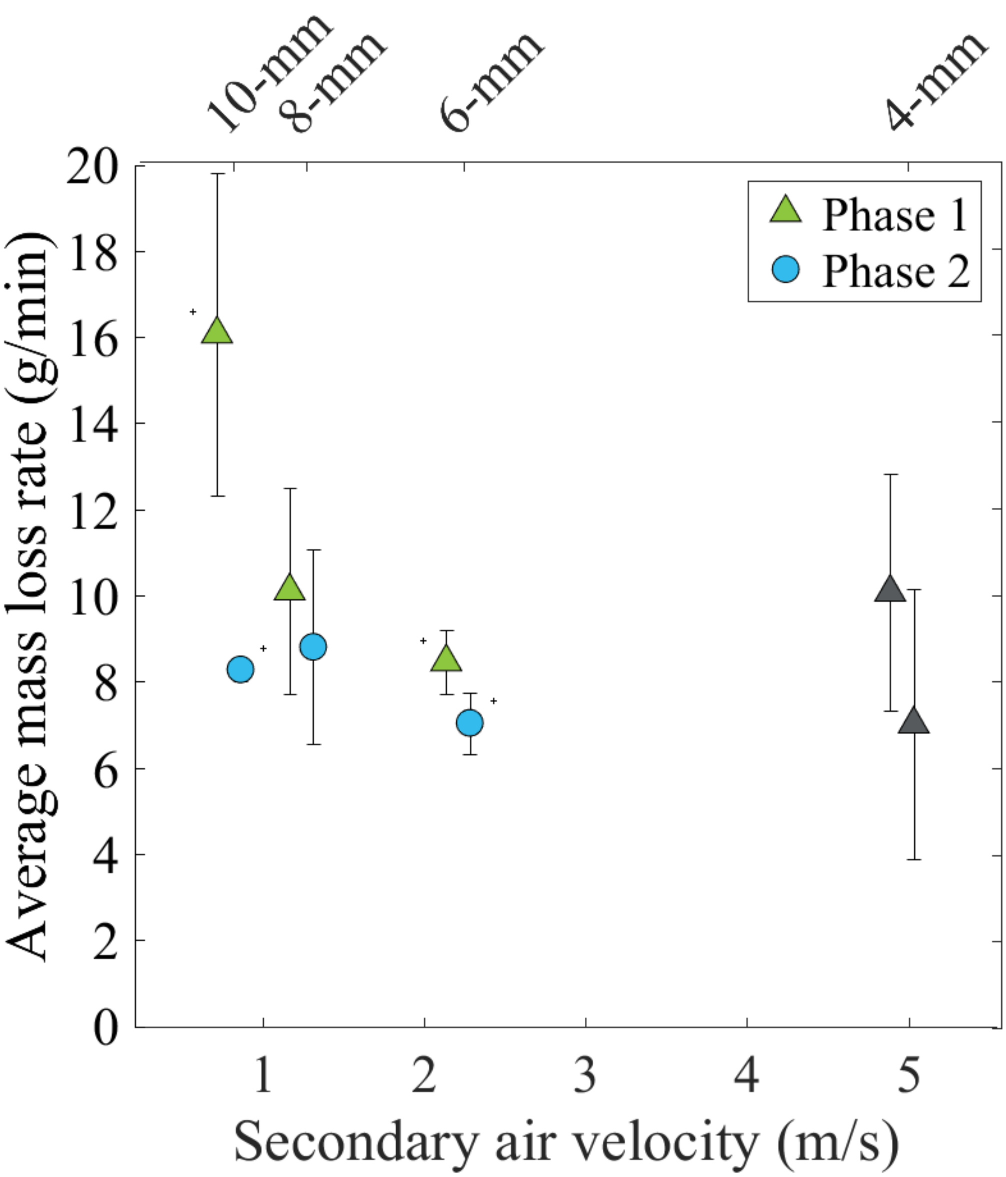

Figure 132 – Average fuel mass loss rate (g/min) vs. secondary air velocity (m/s)

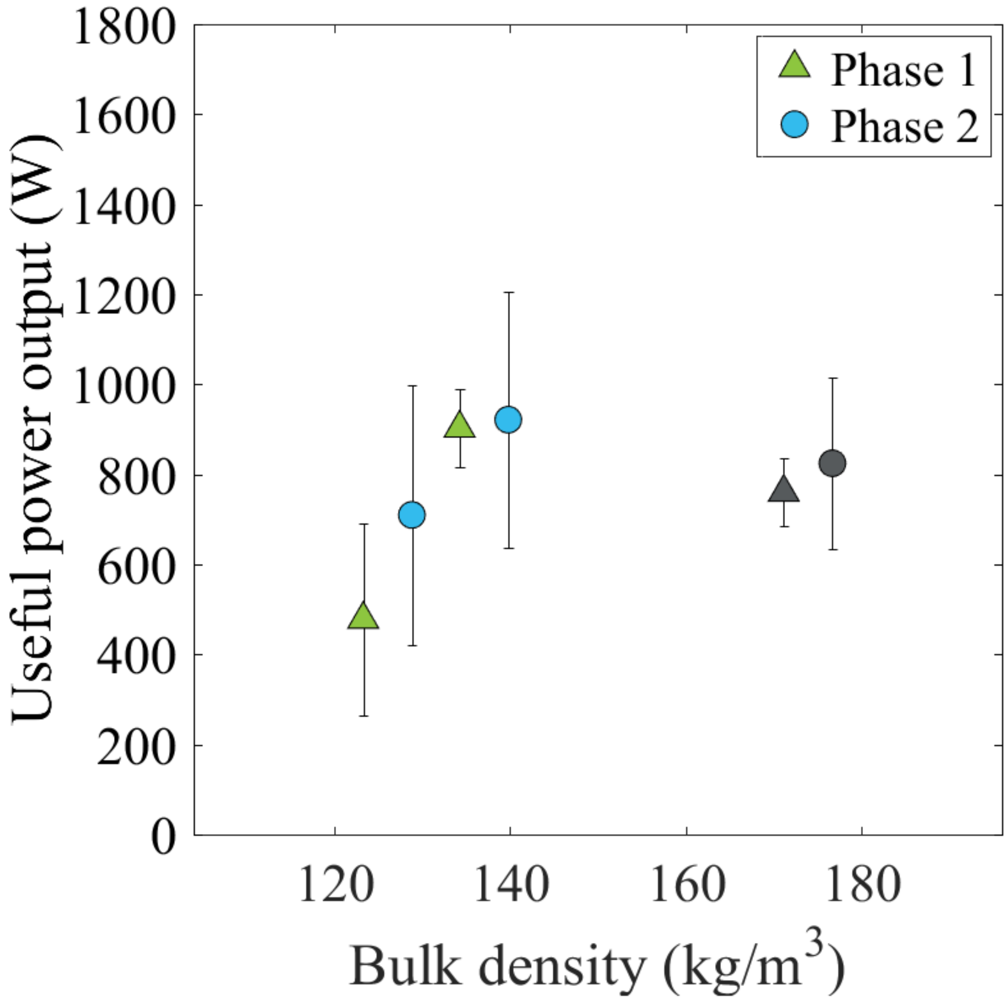

Figure 133 – Useful power output (W) vs. secondary air downward angle (° with respect to horizontal)

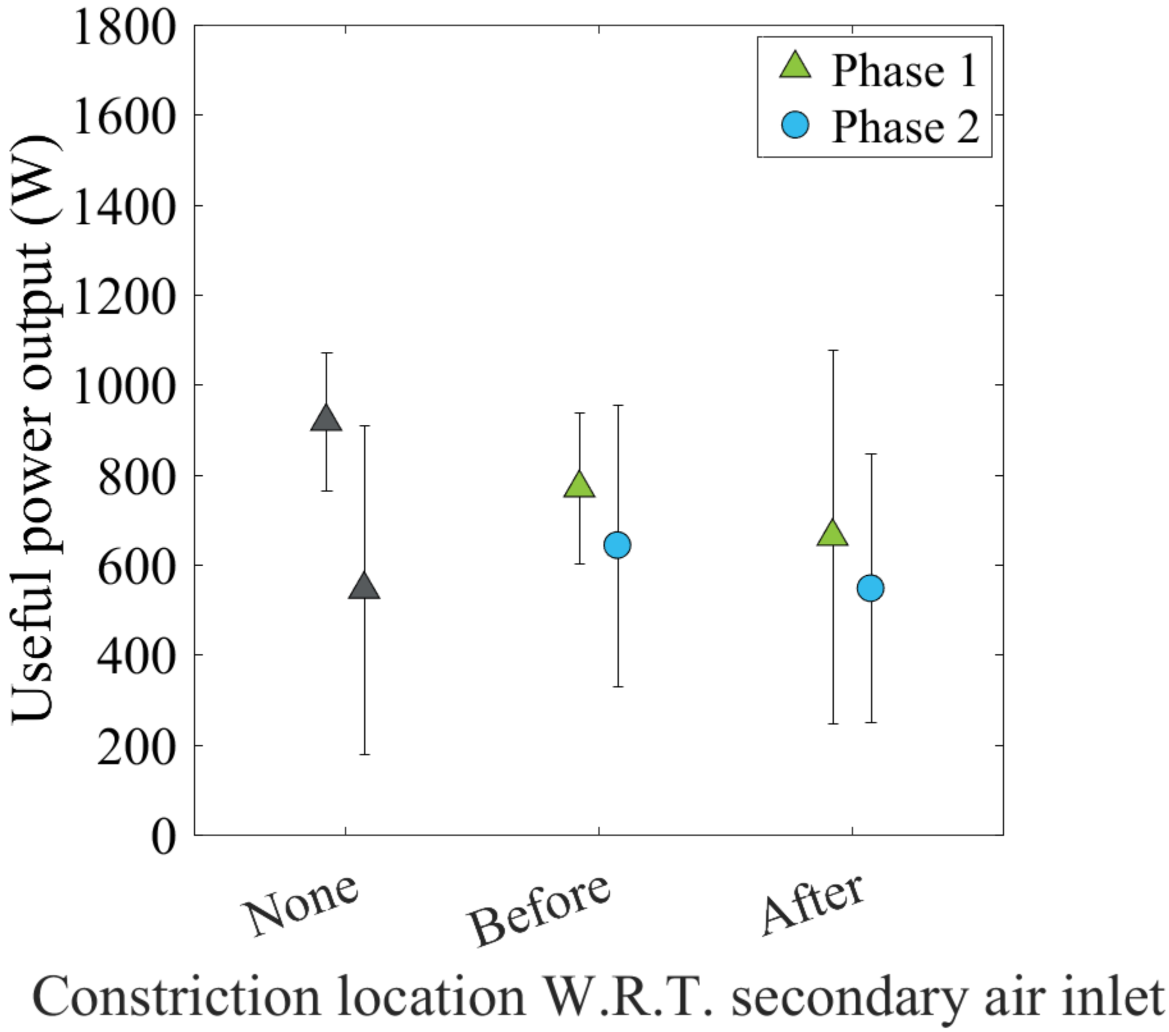

Figure 134 – Useful power output (W) vs. constriction location with respect to the secondary combustion stage air inlet.

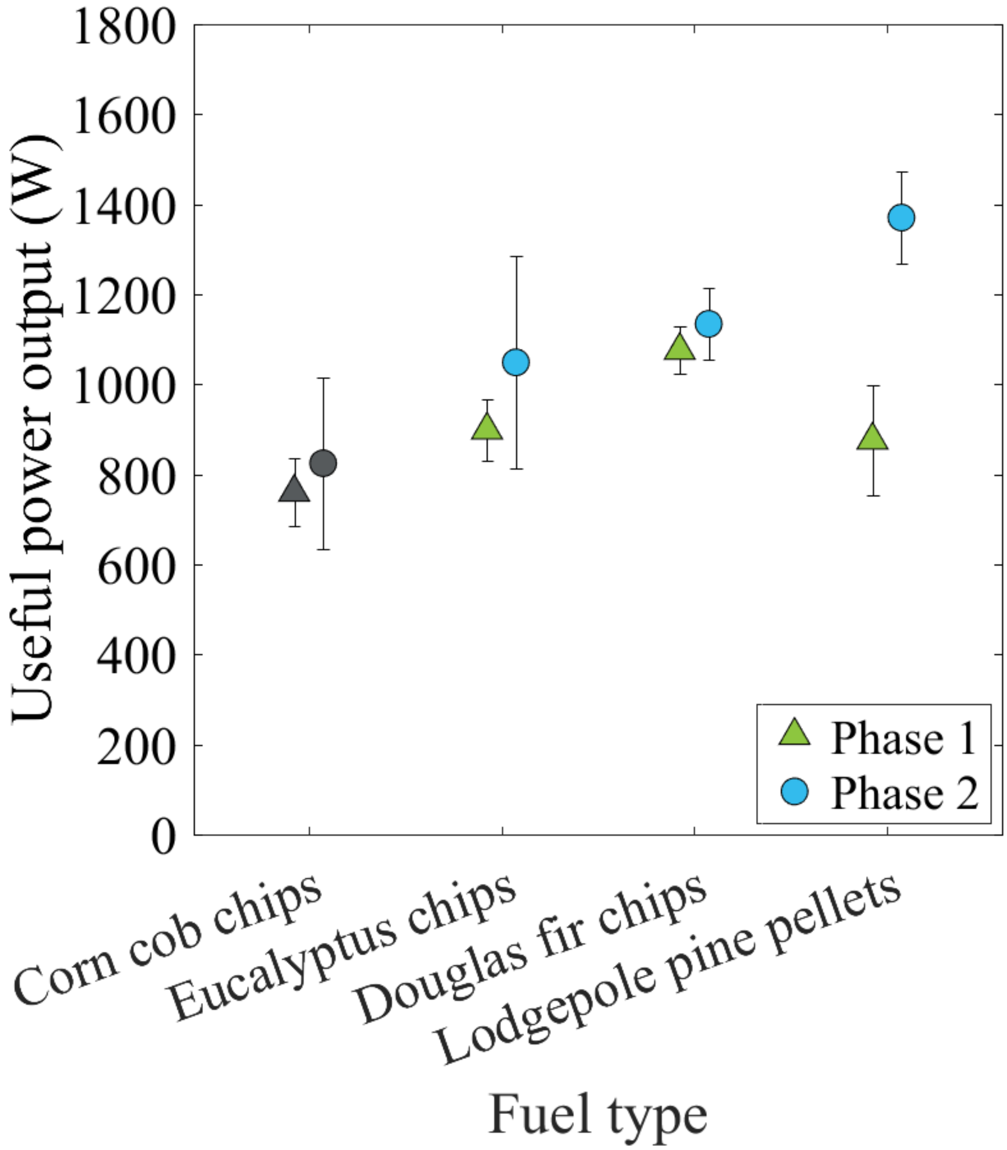

Figure 135 – Useful power output (W) vs. fuel type.

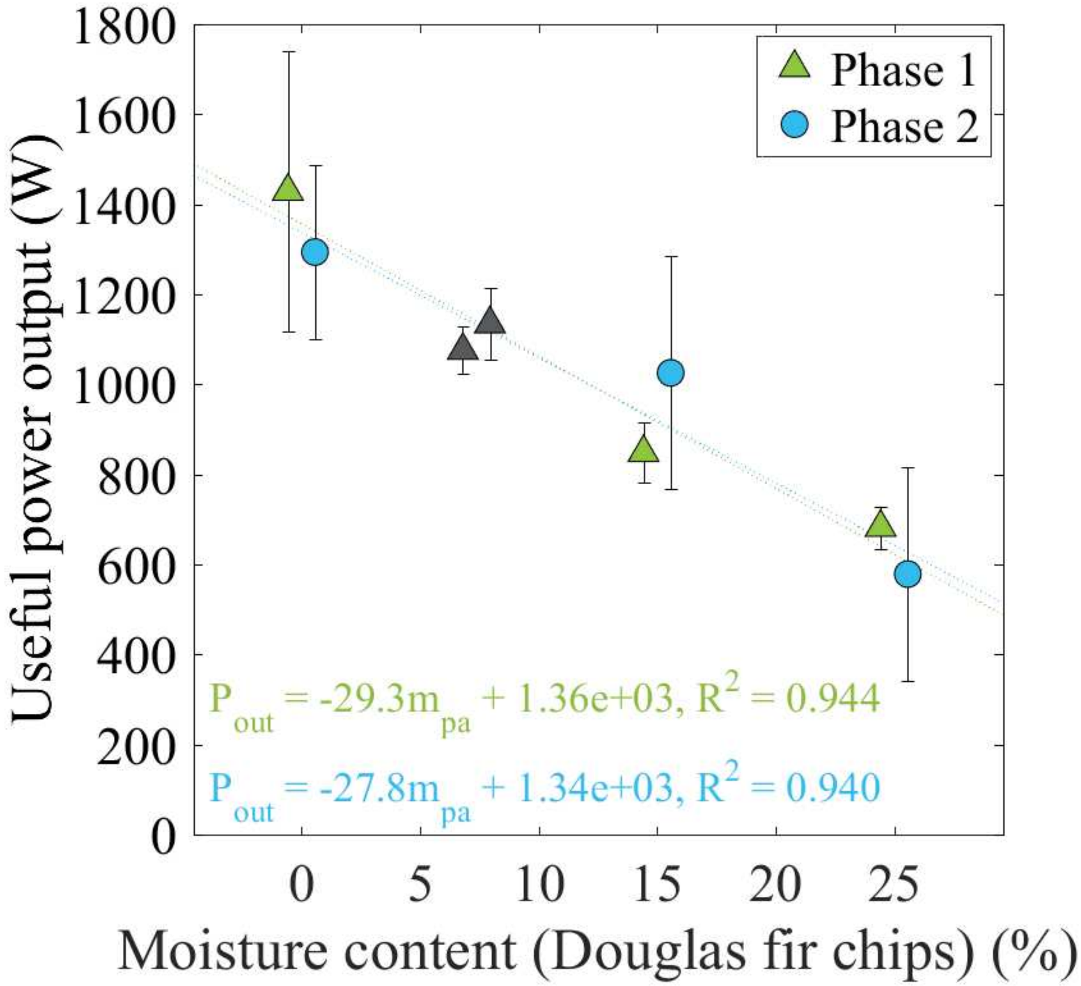

Figure 136 – Useful power output (W) vs. moisture content (%)

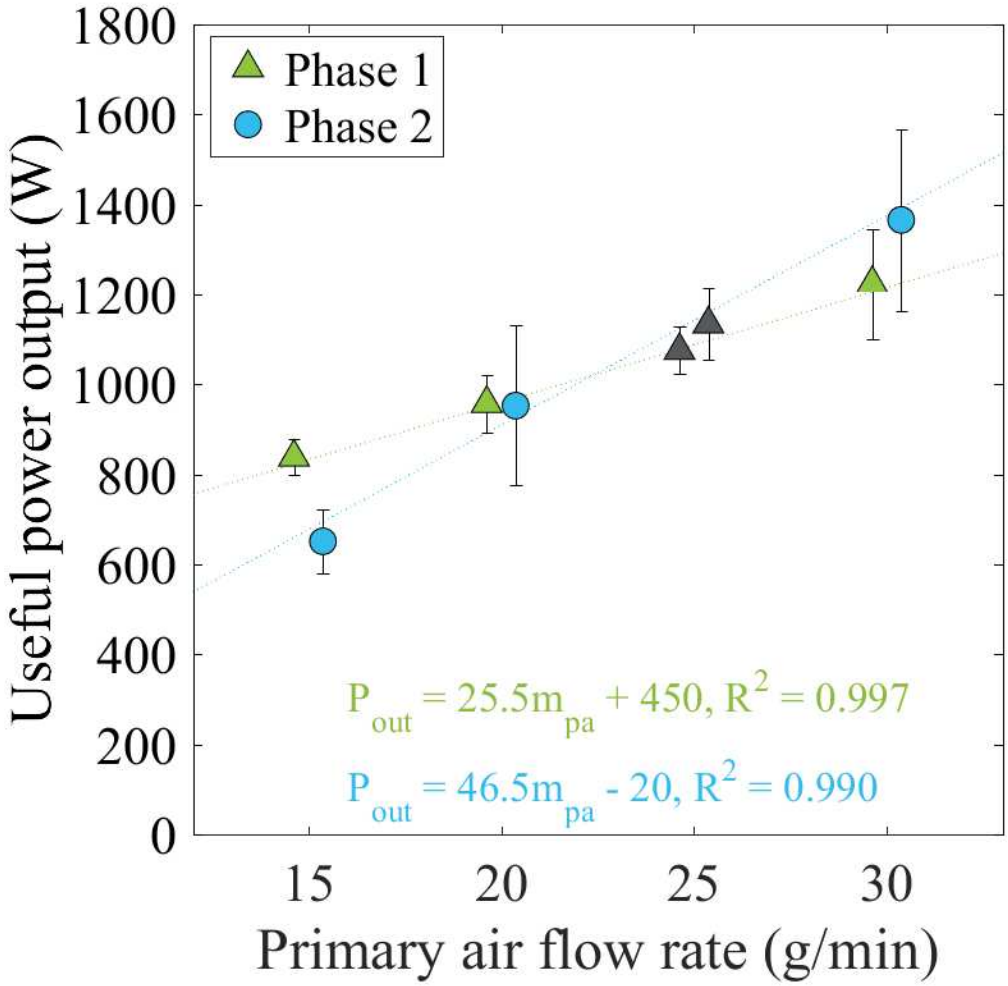

Figure 137 – Useful power output (W) vs. primary air flow rate(g/min).

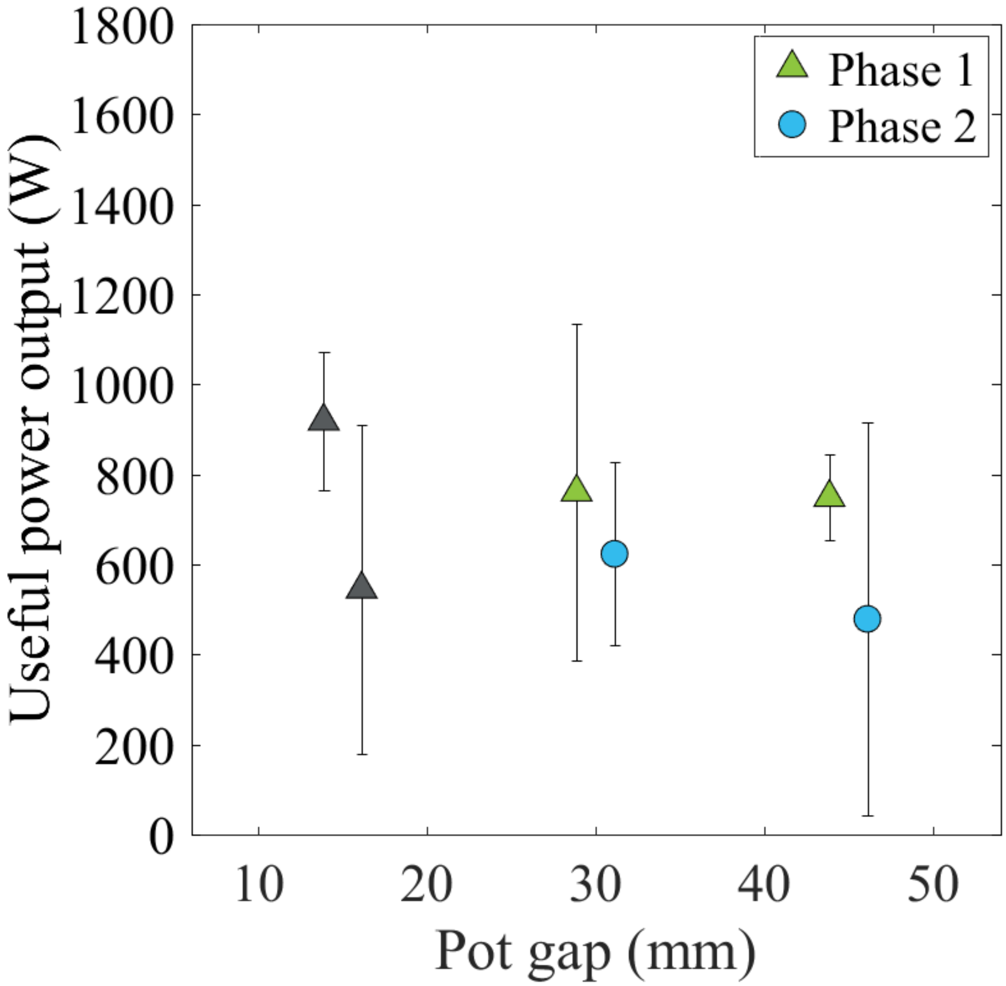

Figure 138 – Useful power output (W) vs. pot gap (mm)

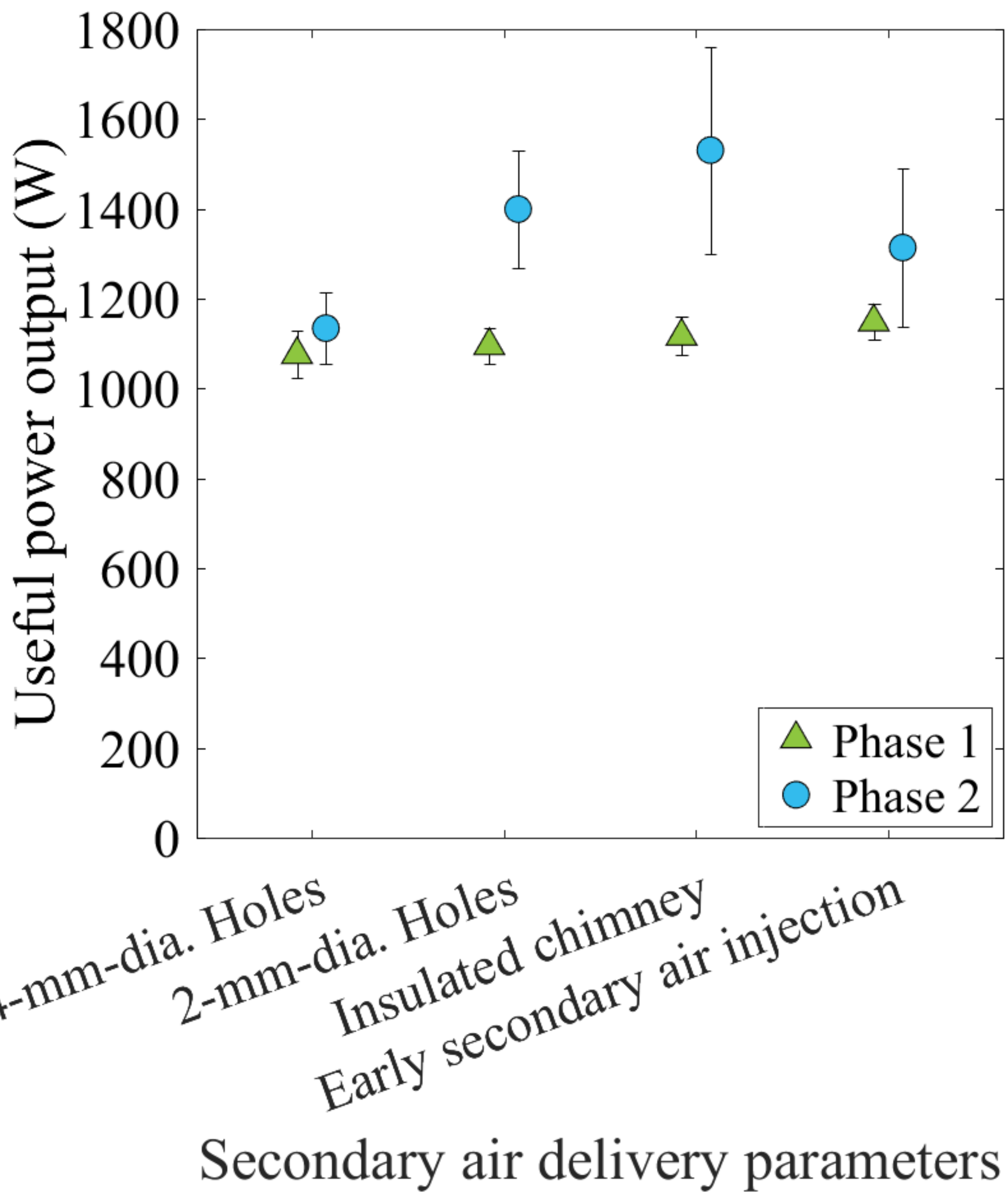

Figure 139 – Useful power output (W) vs. secondary air delivery parameters.

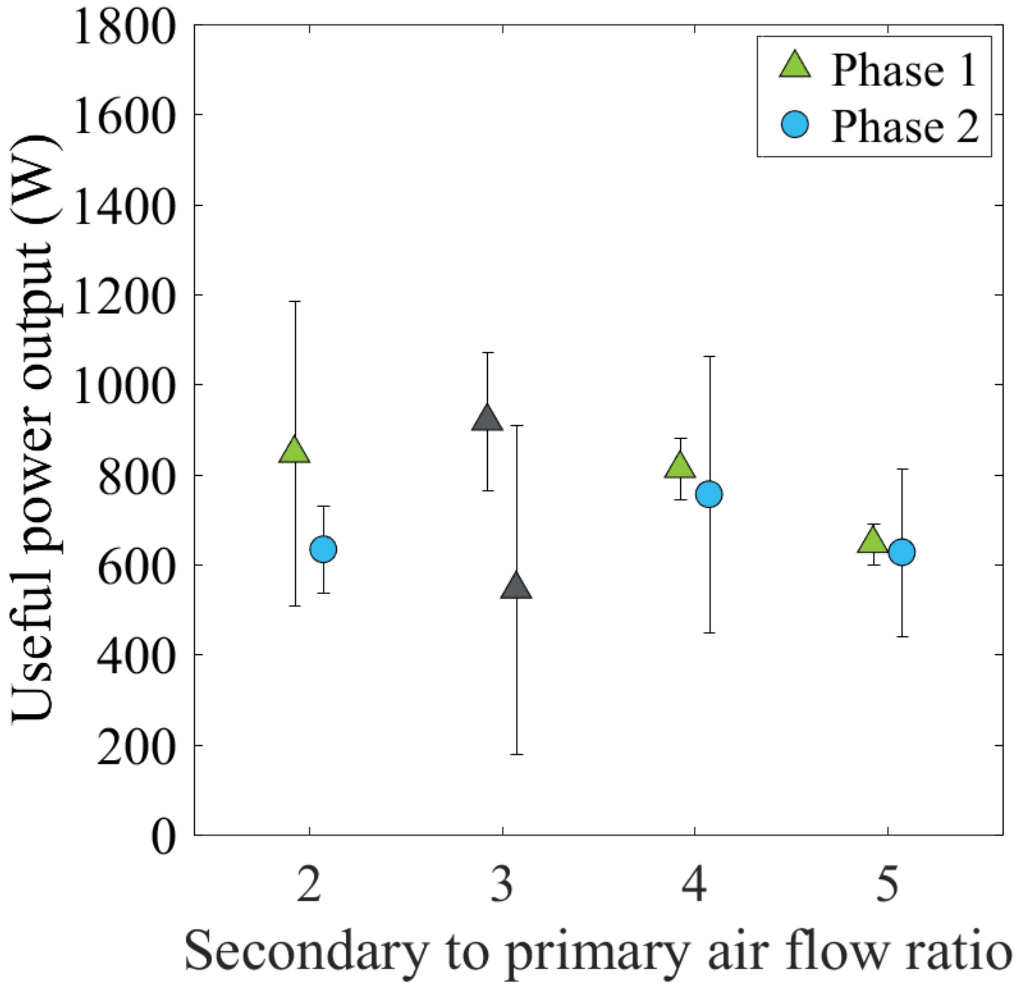

Figure 140 – Useful power output (W) vs. secondary to primary air flow ratio.

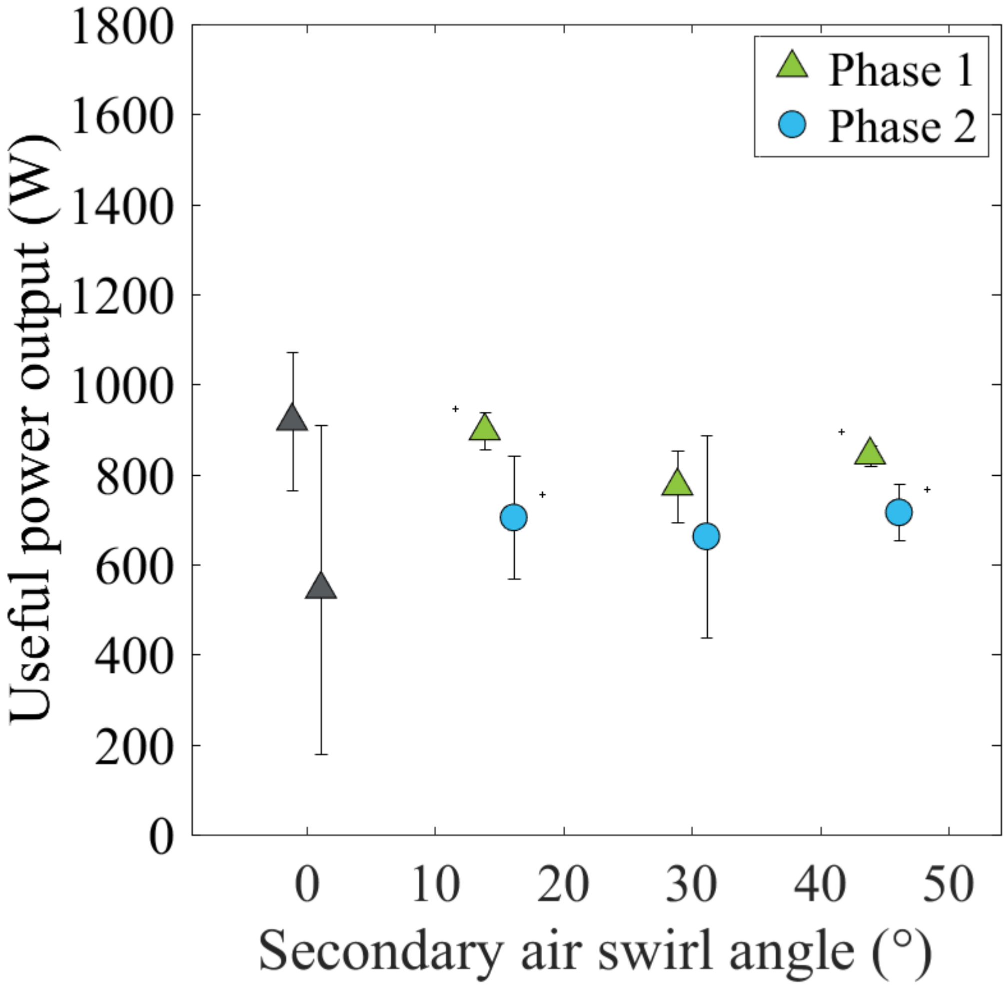

Figure 141 – Useful power output (W) vs. secondary air swirl angle (° with respect to the radial axis).

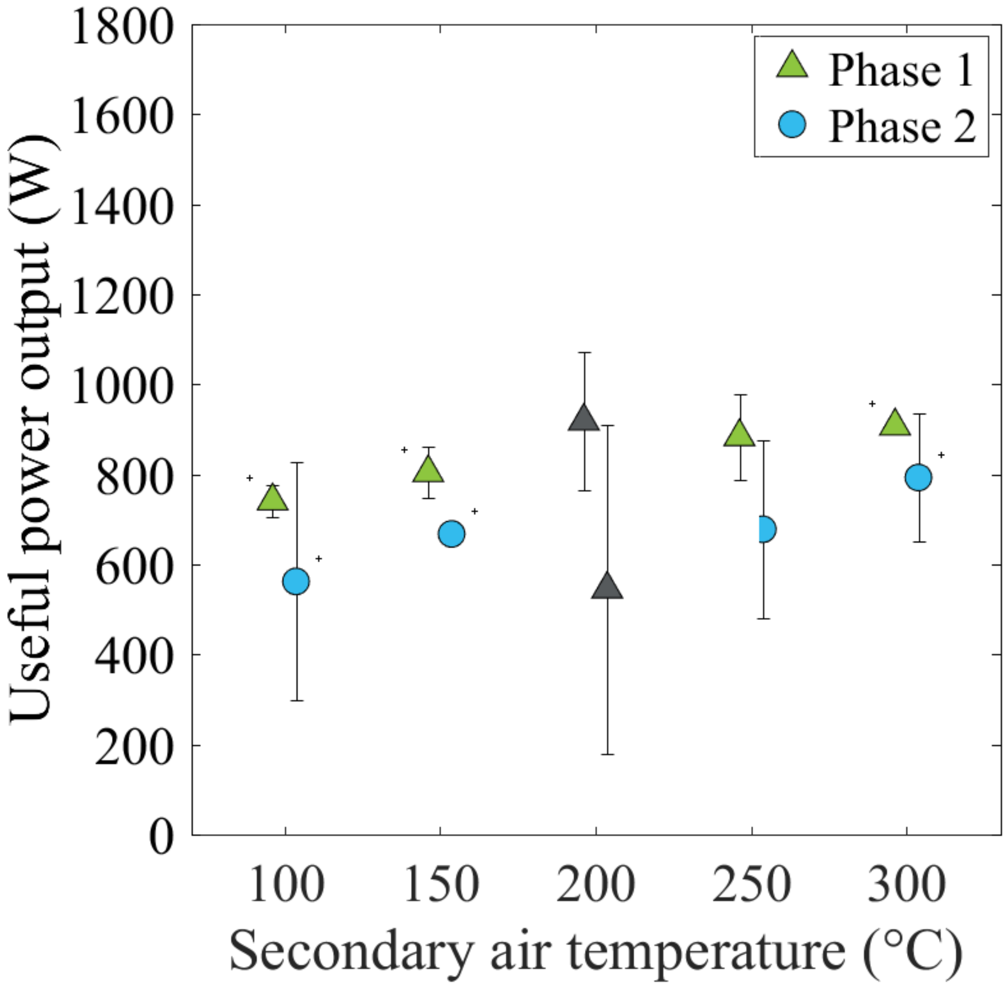

Figure 142 – Useful power output (W) vs. secondary air temperature (°C).

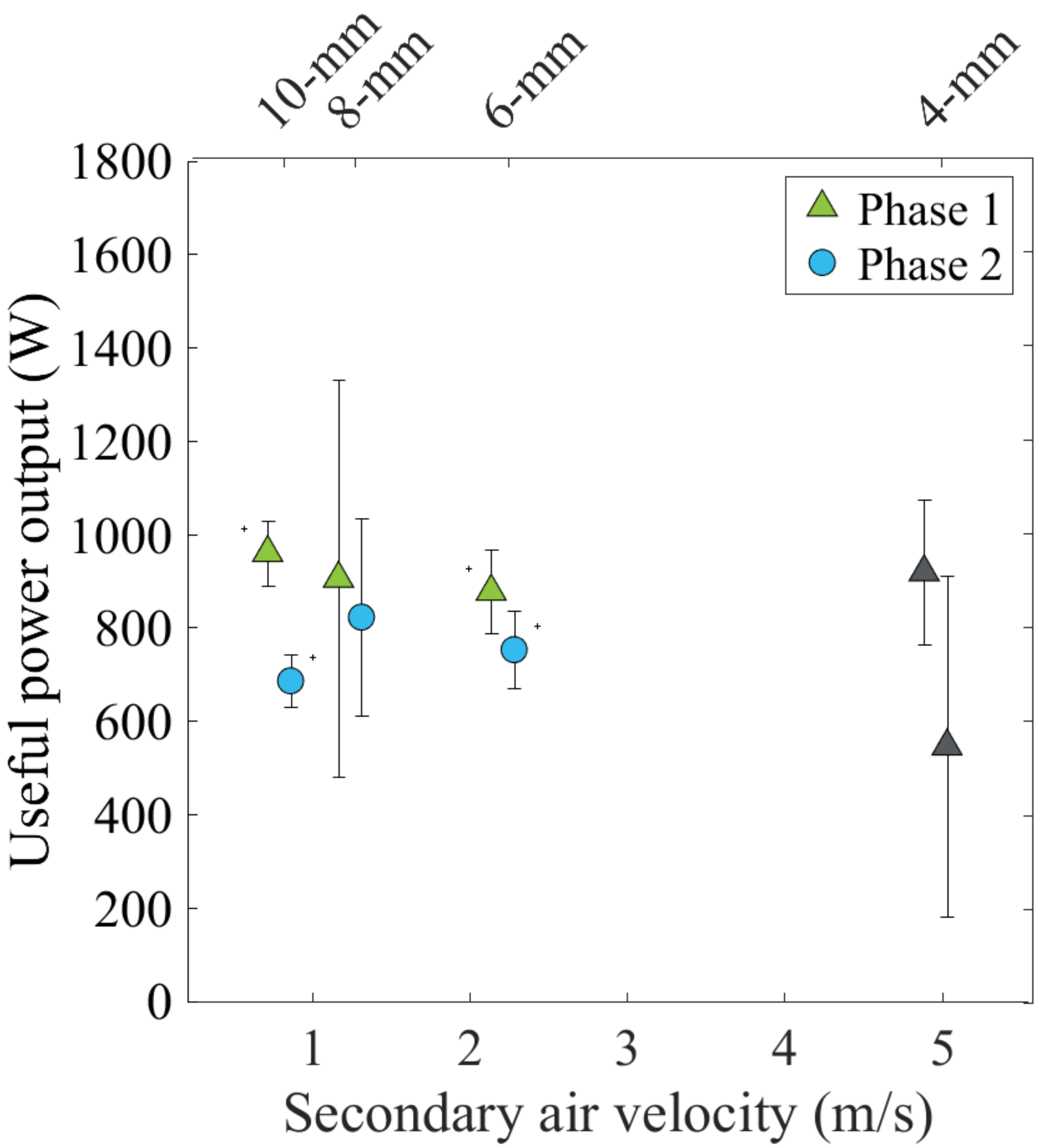

Figure 143 – Useful power output (W) vs. secondary air velocity (m/s).

Secondary Combustion Equivalence Ratio

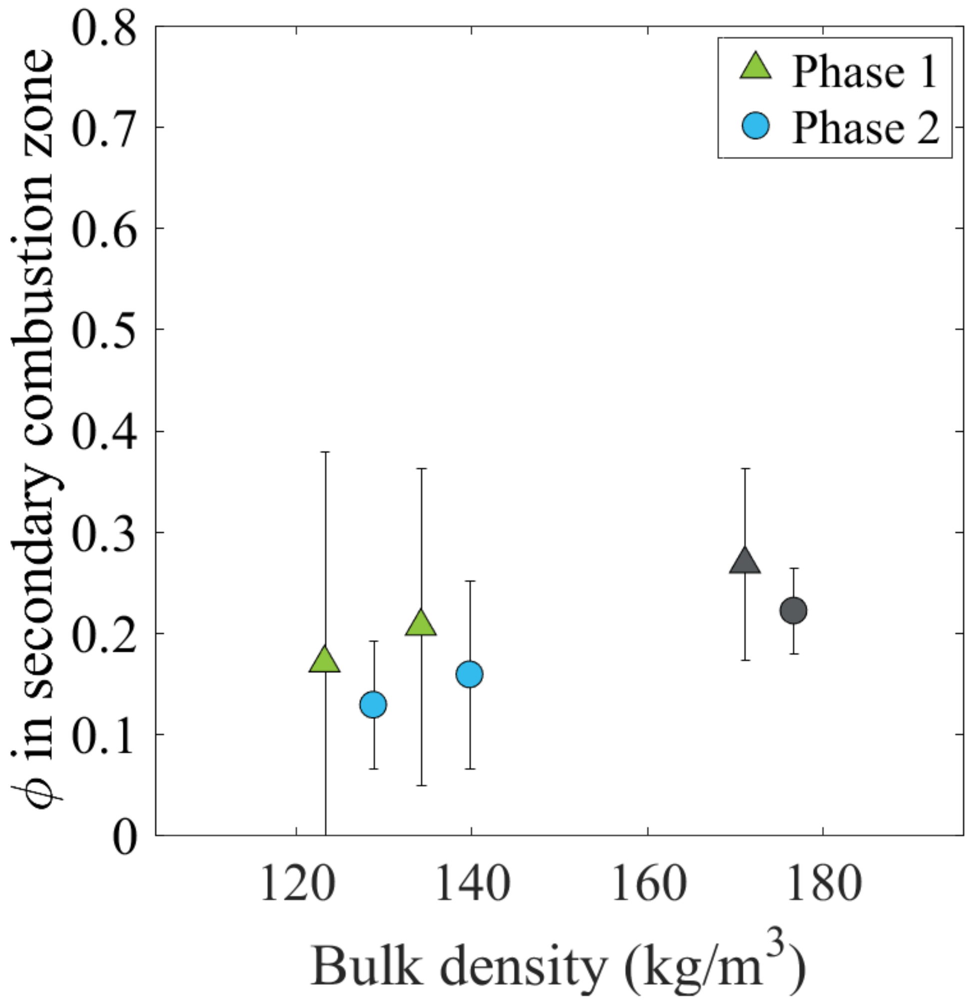

Figure 144 – secondary stage combustion Φ vs. fuel bulk density (kg/m^3).

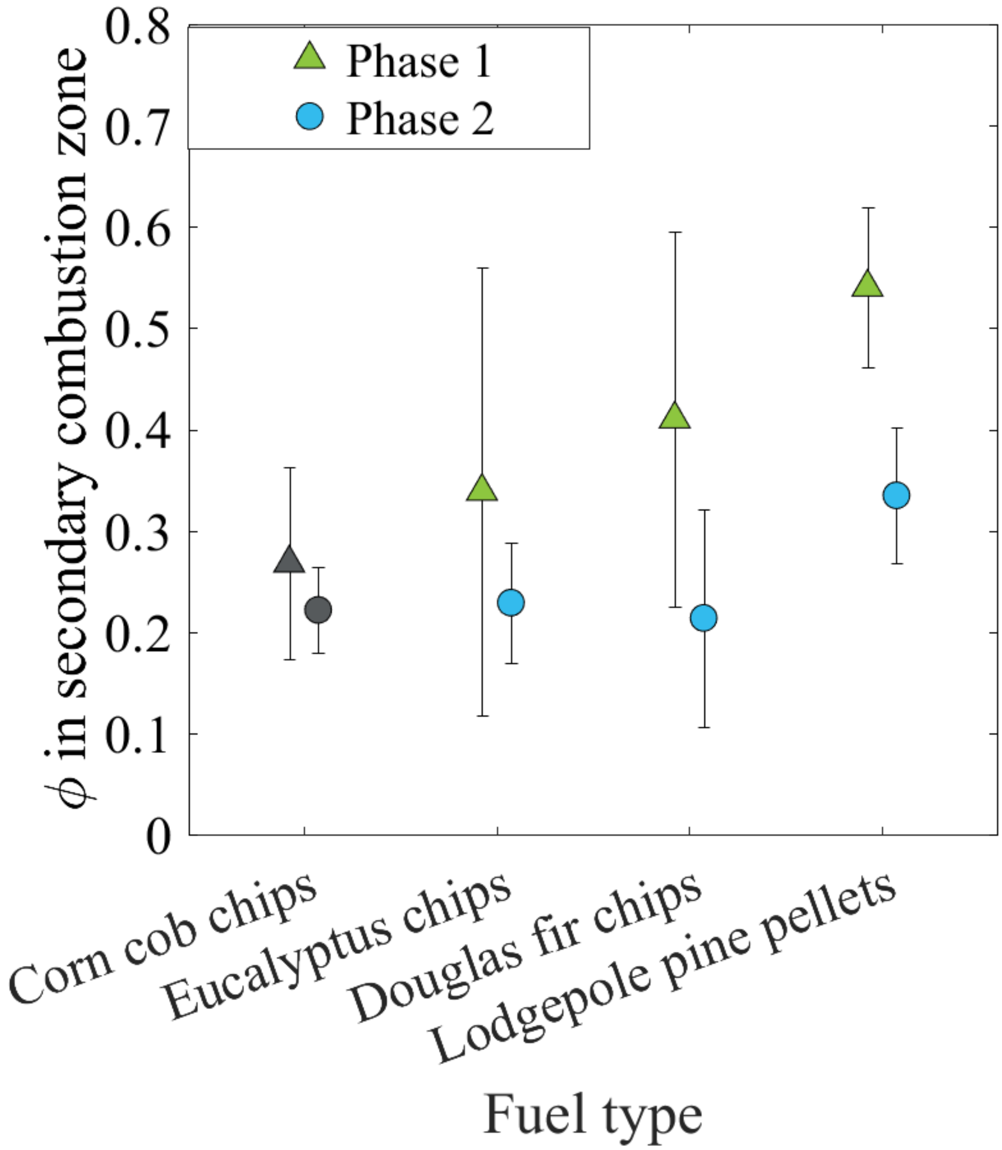

Figure 145 – secondary stage combustion Φ vs. Fuel type.

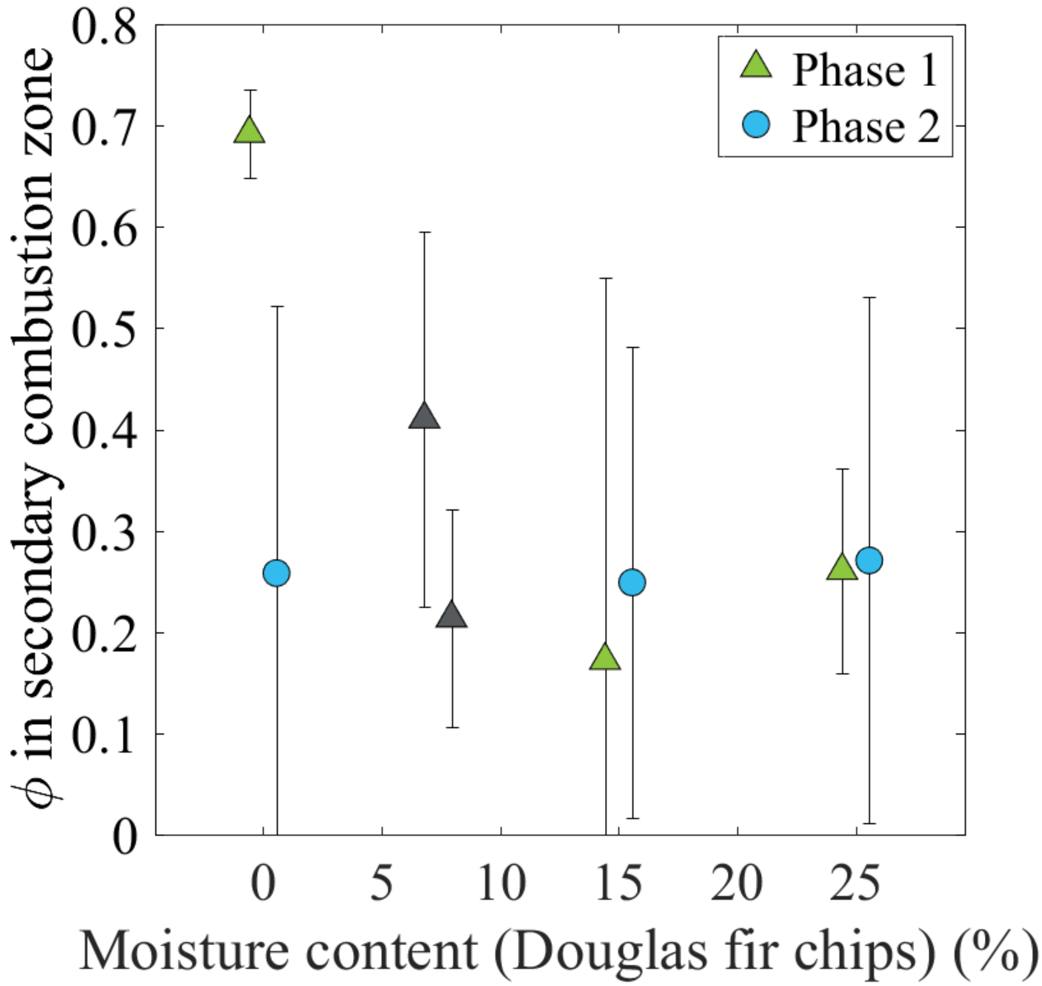

Figure 146 – secondary stage combustion Φ vs. moisture content.

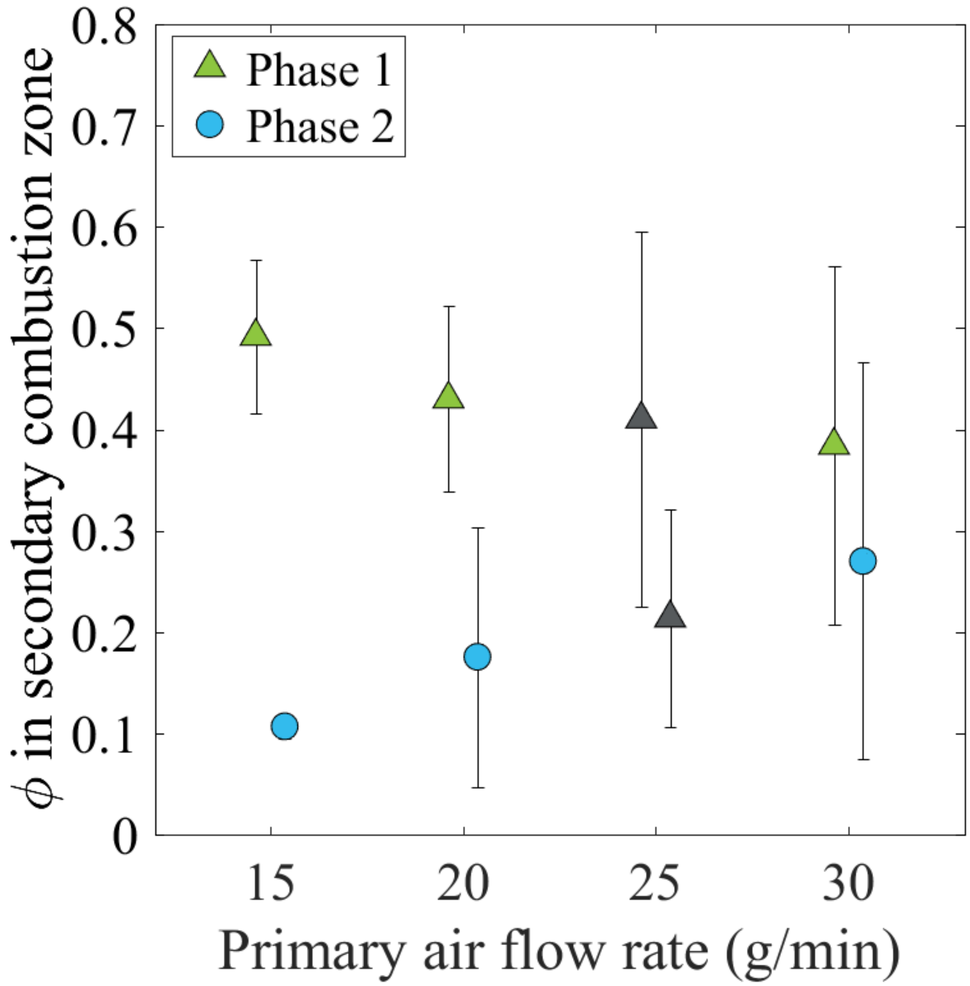

Figure 147 – secondary stage combustion Φ vs. primary air flow rate (g/min)

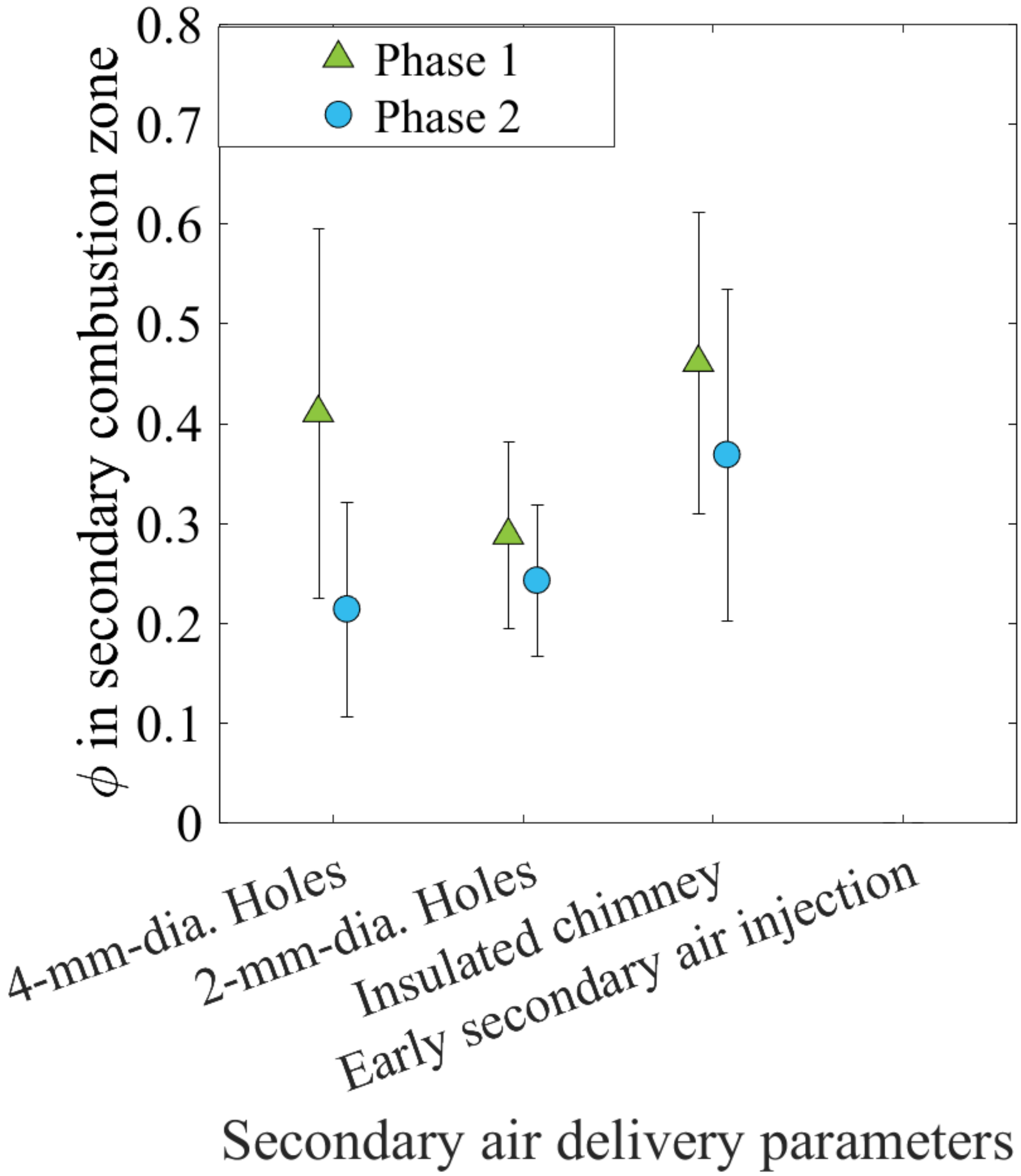

Figure 148 – secondary stage combustion Φ vs. secondary air delivery parameters.

APPENDIX 6: P2 FIELD READY PROTOTYPE DATA

Table 8 – P2 Prototype test case descriptions. Including replicate number, stove description, test description, and fuel used.

Test Name	Replicates	Stove Description	Test Description	Fuel Used
CSU 600g	4	P2 prototype with variable geometry chamber	EPTP - Cold Start, Hot Start, Simmer	Rocky Mtn. Pellet
CSU 550g	2	P2 prototype with variable geometry chamber	EPTP - Cold Start, Hot Start, Simmer	Rocky Mtn. Pellet
LBNL 600g	12	P2 prototype with variable geometry chamber	Cold start and 15 min simmer	Rocky Mtn. Pellet
LBNL 550g	6	P2 prototype with variable geometry chamber	Cold start	Rocky Mtn. Pellet
Extended Pot Deck	1	P2 Prototype with Extended Pot Deck	EPTP - Cold Start, Hot Start, Simmer	Rocky Mtn. Pellet
4 -mm Secondary Holes	1	P2 Prototype, 4 -mm secondary holes	EPTP - Cold Start, Hot Start, Simmer	Rocky Mtn. Pellet
No Insulation	1	P2 Prototype No Insulation	EPTP - Cold Start, Hot Start, Simmer	Rocky Mtn. Pellet
7 -mm Pot Gap	1	P2 VGC Prototype 7mm-pot gap	EPTP - Cold Start, Hot Start, Simmer	Rocky Mtn. Pellet
Standard Pot	1	P2 Prototype VGC Standard Pot	EPTP - Cold Start, Hot Start, Simmer	Rocky Mtn. Pellet
Corncob pellets	1	P2 Prototype with Corn Cob Pellets	EPTP - Cold Start, Hot Start, Simmer	Corncob Pellets

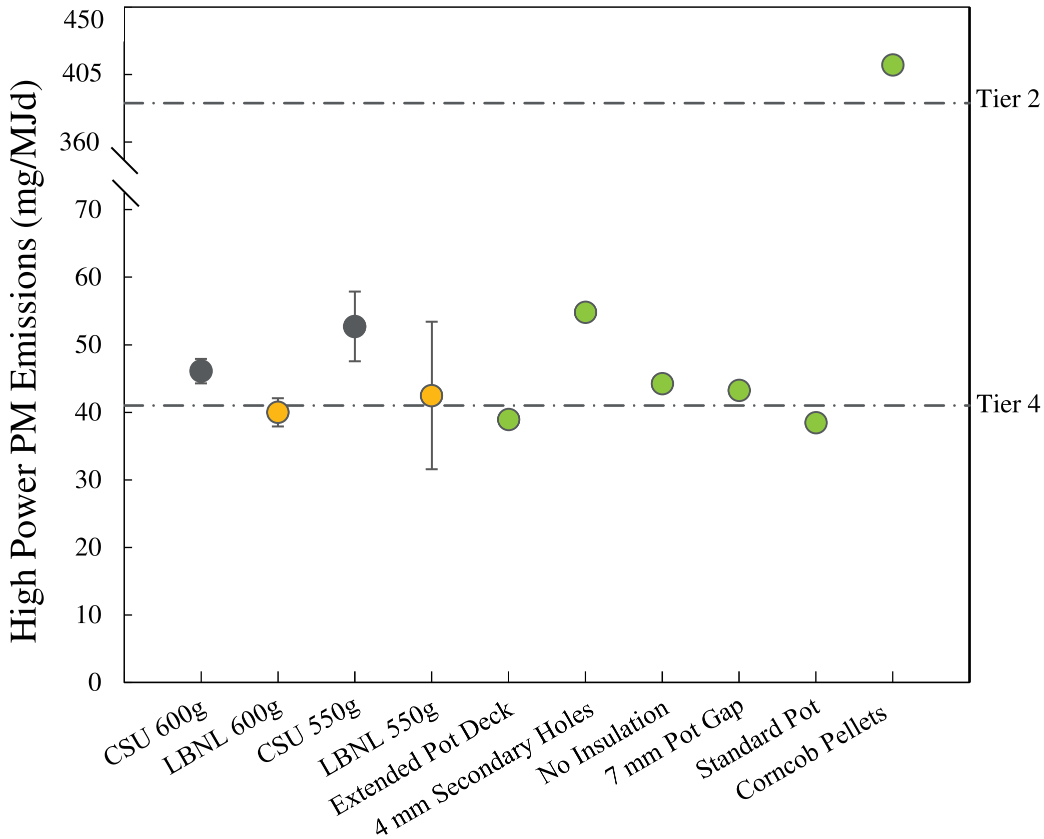

Figure 149 – P2 prototype high power PM results. The majority of the results were between tier 3 and tier 4 with a few ideal cases meeting the tier 4 guideline. A notable exception is the test case with corncob pellets, which resulted in low stove tier 1 PM emissions. Error bars indicate a 90% CI. All green points have a single replicate

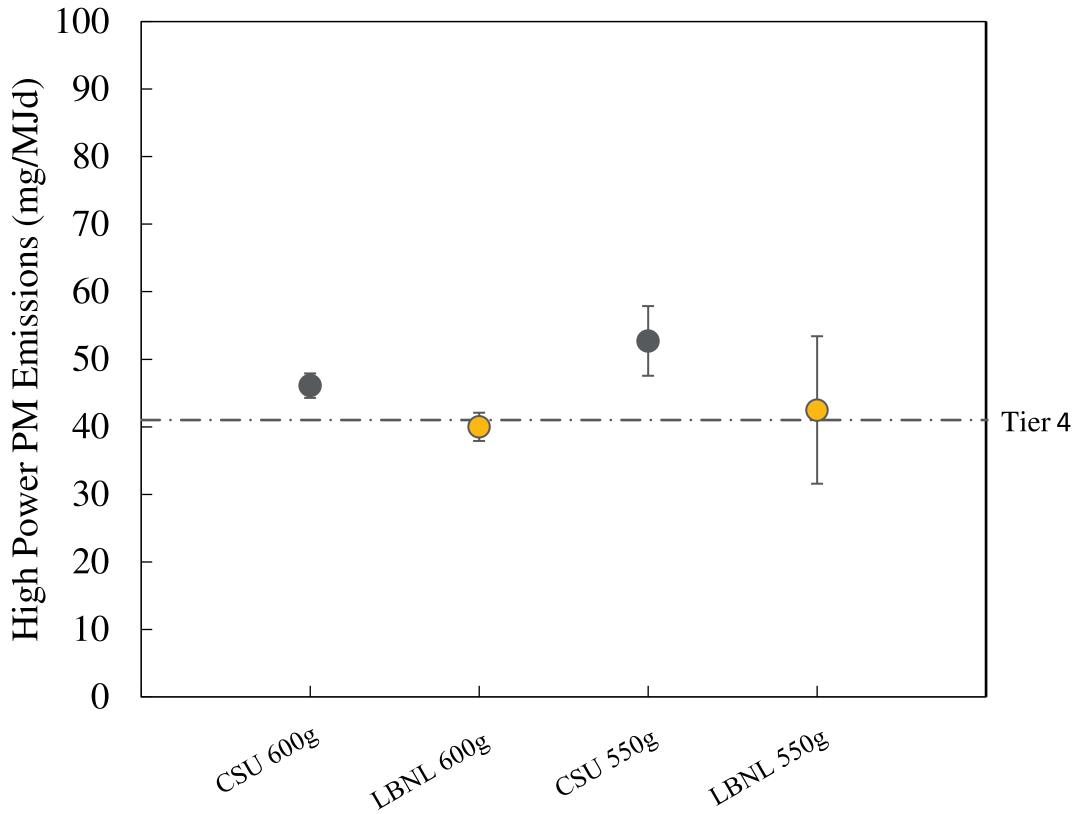

Figure 150 – P2 prototype high power PM results from test cases where the starting mass of fuel was varied. Test cases labeled CSU were run in July, prior to testing at LBNL, test cases labeled LBNL were run immediately the following testing at LBNL using the same hardware deployed to LBNL for testing to validate the design and testing done at LBNL. Both stove chambers and fan control software version were the same. Error bars indicate a 90% CI. See Table 8 for information regarding test cases and replicate numbers.

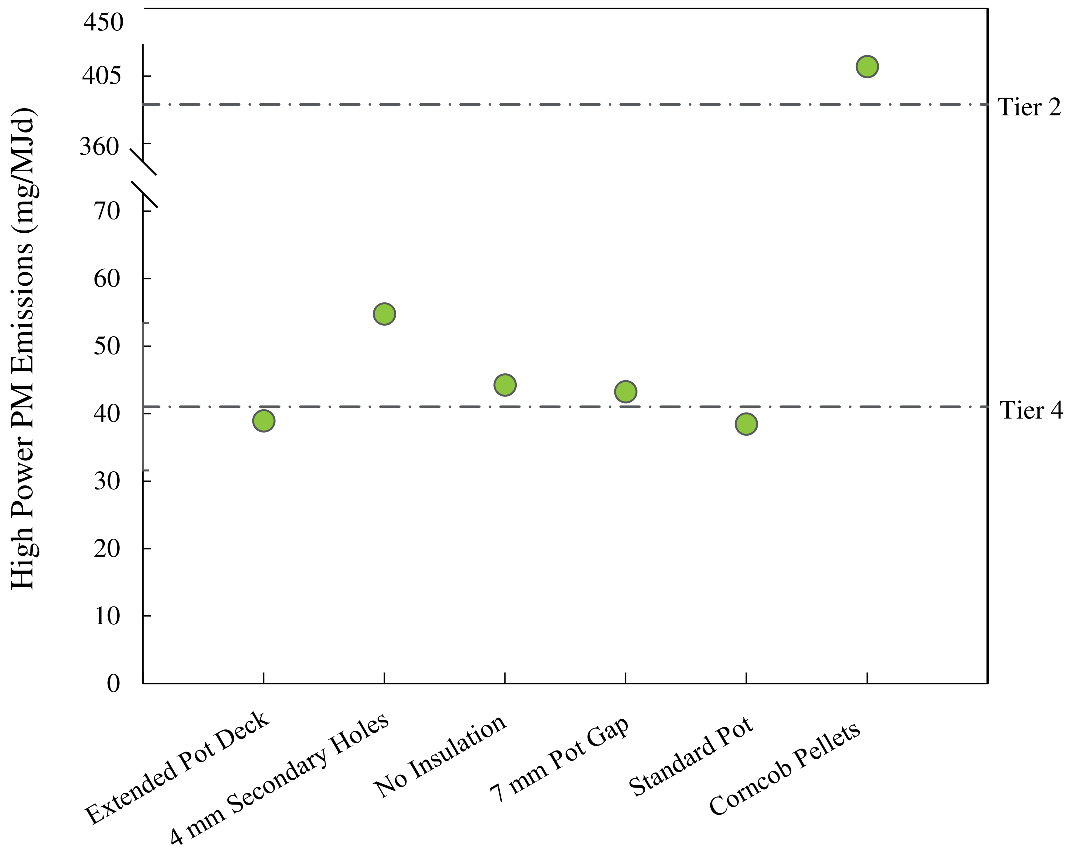

Figure 151 – P2 high power PM emissions results for test cases with different stove configurations, except the test cases using corncob pellets which was completed using the same stove configurations as the CSU and LBNL test cases. All test cases are shown here have one replicate.

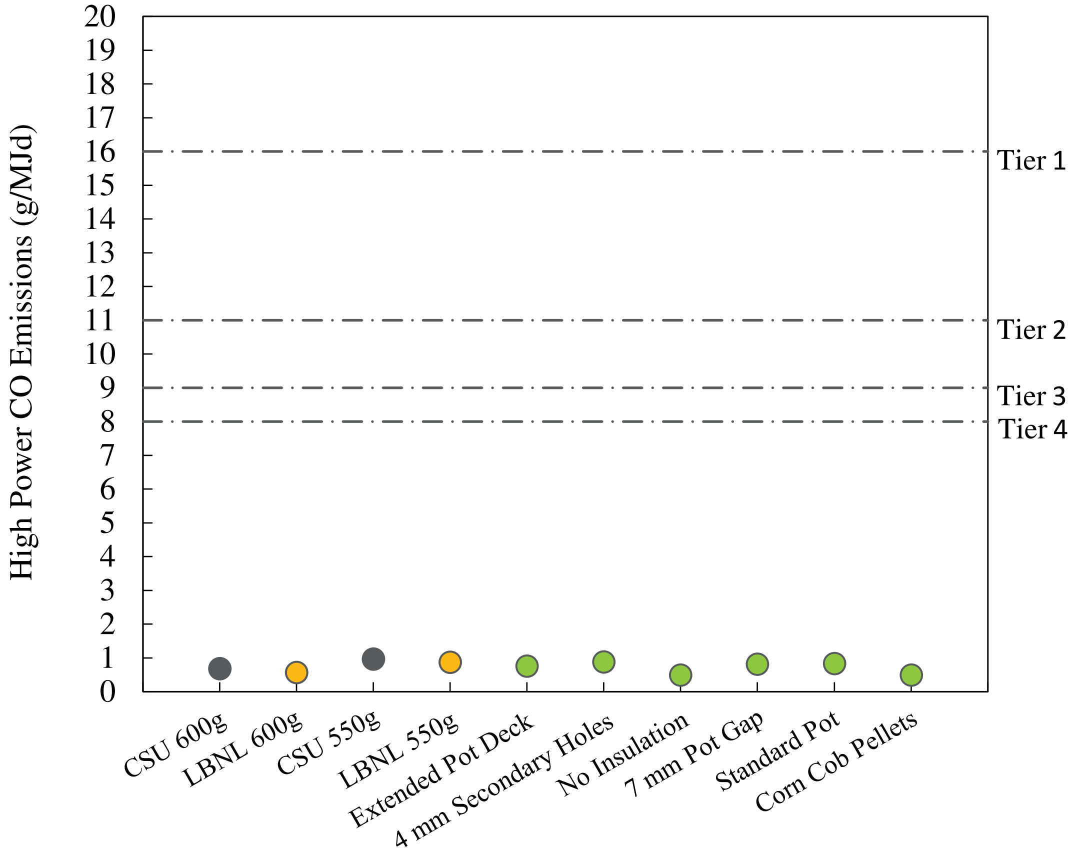

Figure 152 – P2 Prototype high power CO emissions results. All test cases easily exceeded the tier 4 guideline for high power CO emissions in this testing. All green points have one replicate.

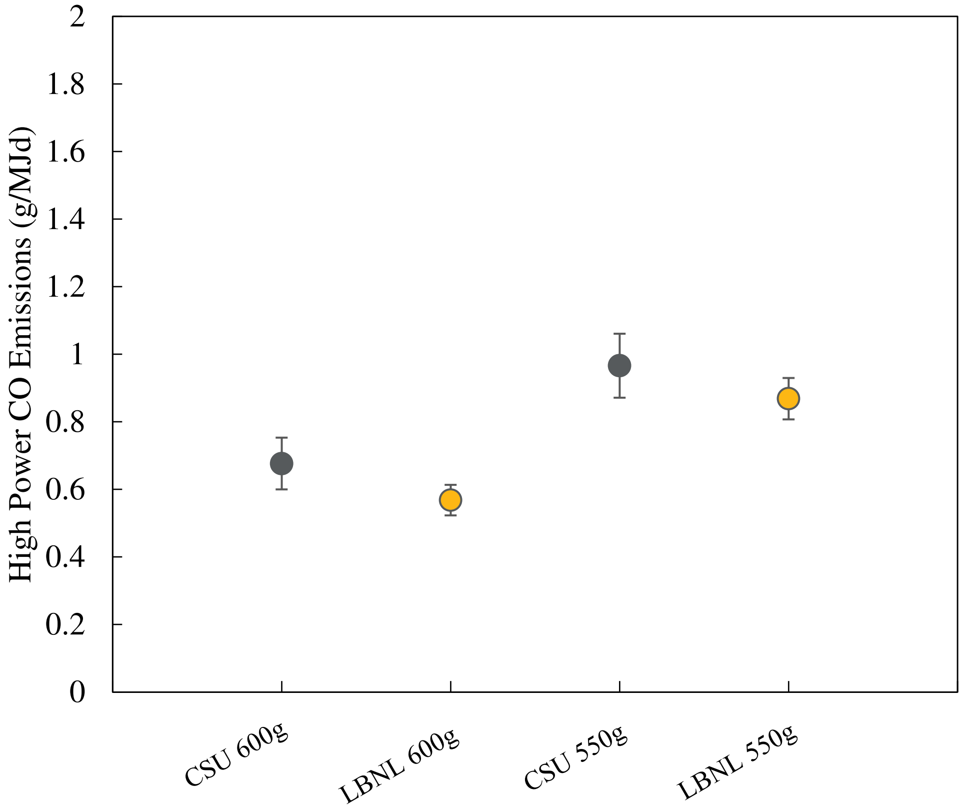

Figure 153 – P2 prototype high power CO results from test cases where the starting mass of fuel was varied. Test cases labeled CSU were run in July, prior to testing at LBNL, test cases labeled LBNL were run immediately the following testing at LBNL using the same hardware deployed to LBNL for testing to validate the design and testing done at LBNL. Both stove chambers and fan control software version were the same. Error bars indicate a 90% CI. See Table 8 for information regarding test cases and replicate numbers.

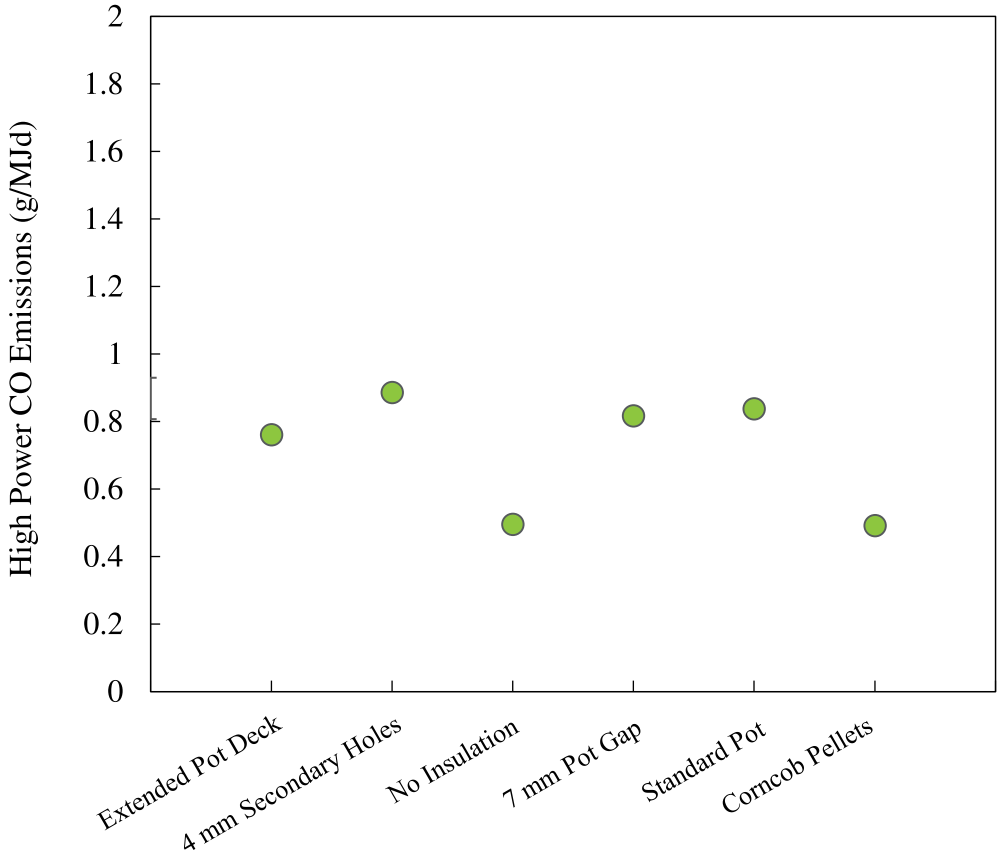

Figure 154 - P2 high power CO emissions results for test cases with different stove configurations, except the test cases using corncob pellets, which was completed using

the same stove configurations as the CSU and LBNL test cases. All test cases easily exceed the tier 4 emissions guidelines. All test cases are shown here have one replicate.

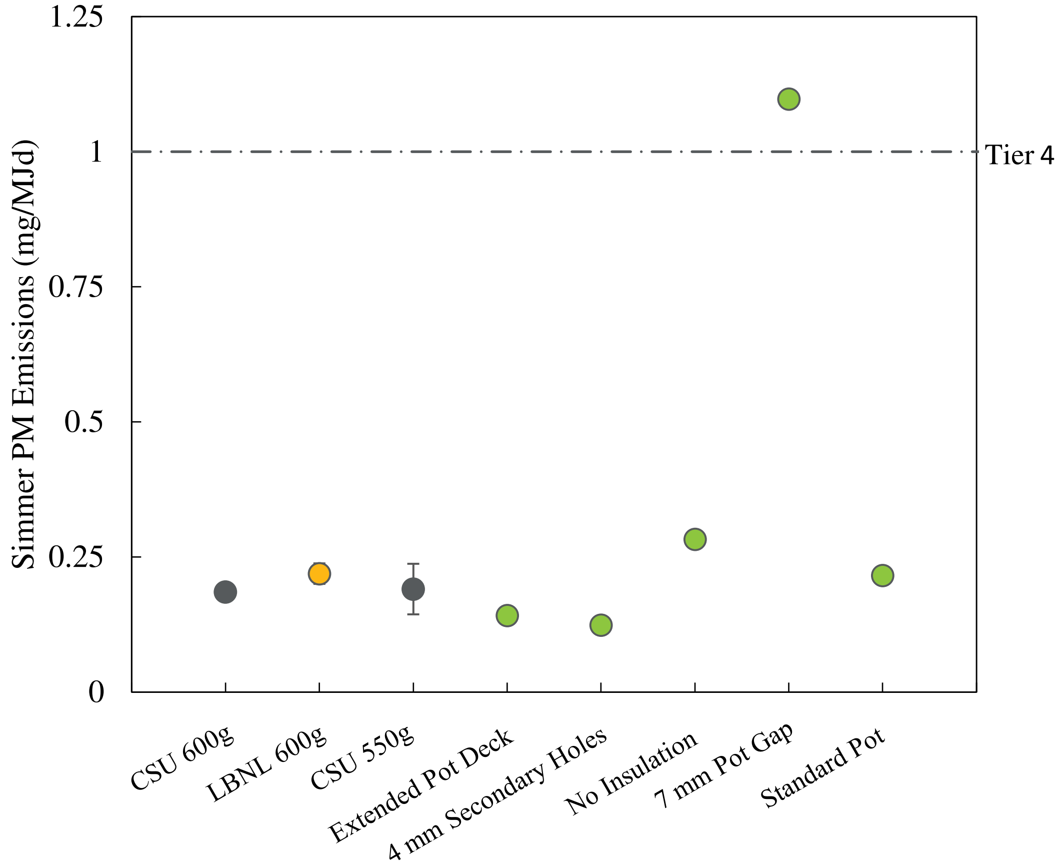

Figure 155 - P2 prototype low power PM emissions results. Most test cases easily exceeded the tier 4 guideline for low power CO emissions in this testing. The test case where the pot gap was reduced from 15-mm to 7-mm resulted in a significant increase in PM emissions during the low power simmer phase of the test. Error bars represent a 90% CI. All green points have one replicate.

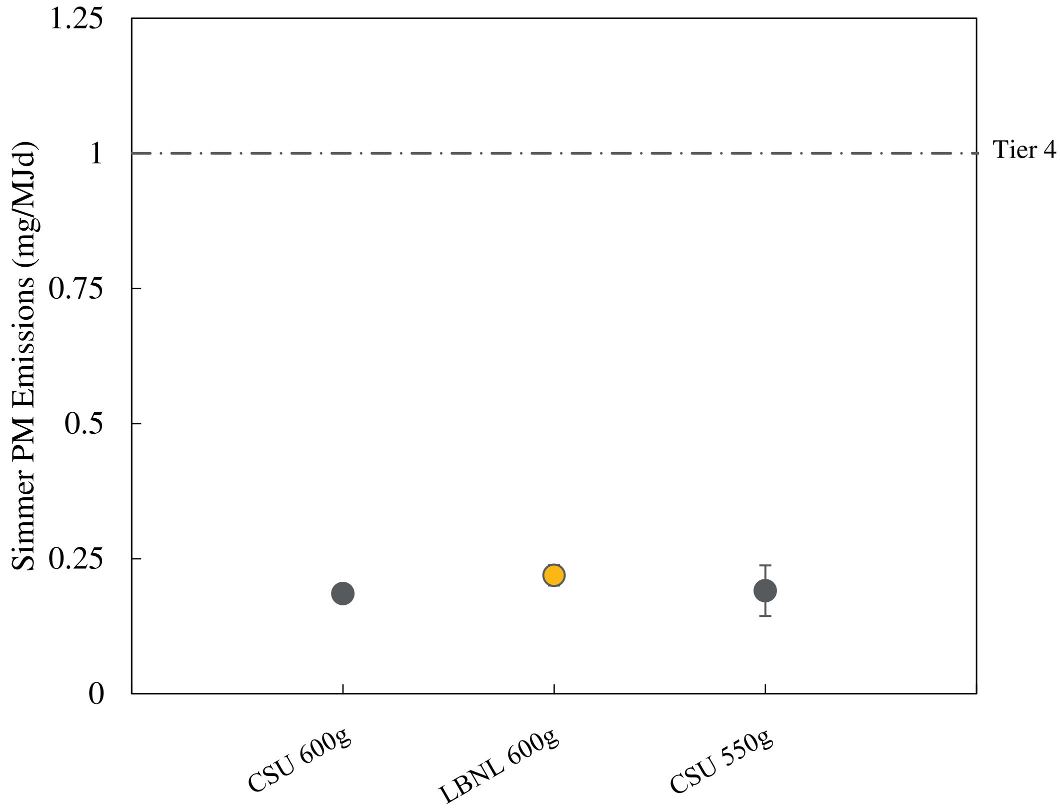

Figure 156 - - P2 prototype low power CO emissions results for test cases where starting fuel mass was varied. All test cases easily exceeded the tier 4 guideline for low power CO emissions in this testing. Error bars represent a 90% CI.

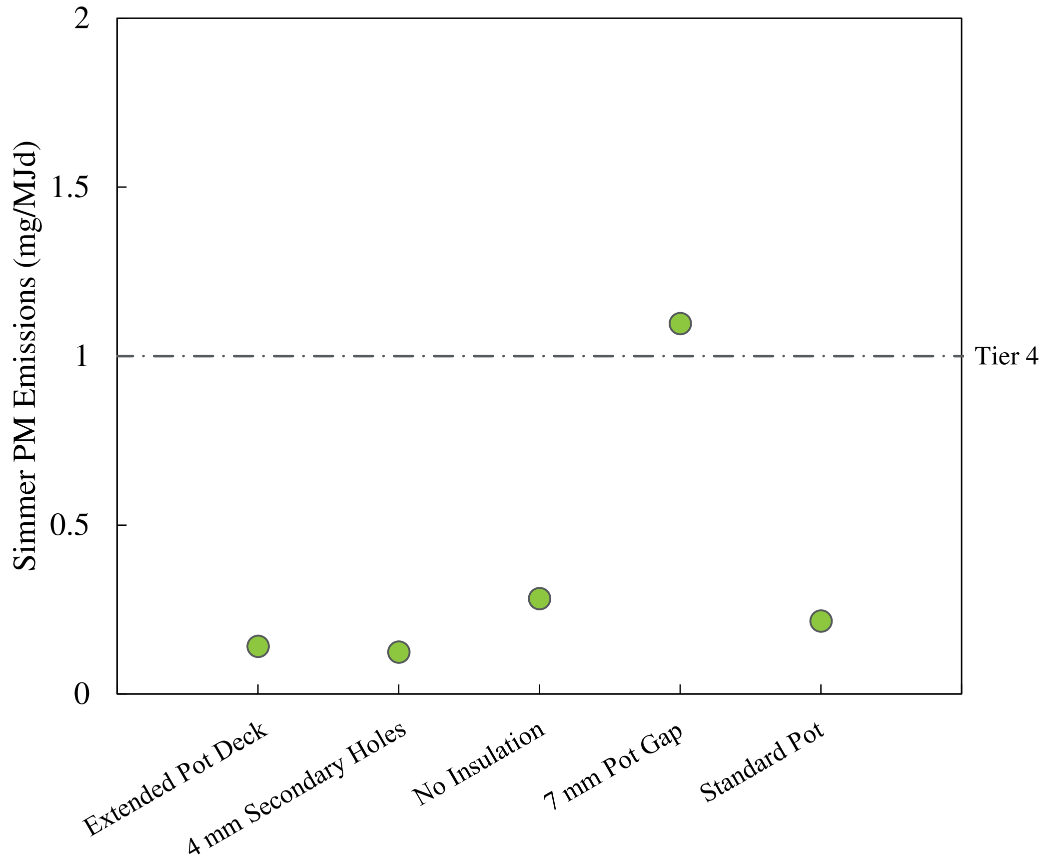

Figure 157 - P2 prototype low power CO emissions results with different stove configurations. Most test cases easily exceeded the tier 4 guideline for low power CO emissions in this testing. The test case where the pot gap was reduced from 15 -mm to 7 -mm resulted in a significant increase in PM emissions during the low power simmer phase of the test. All test cases are shown here have one replicate.

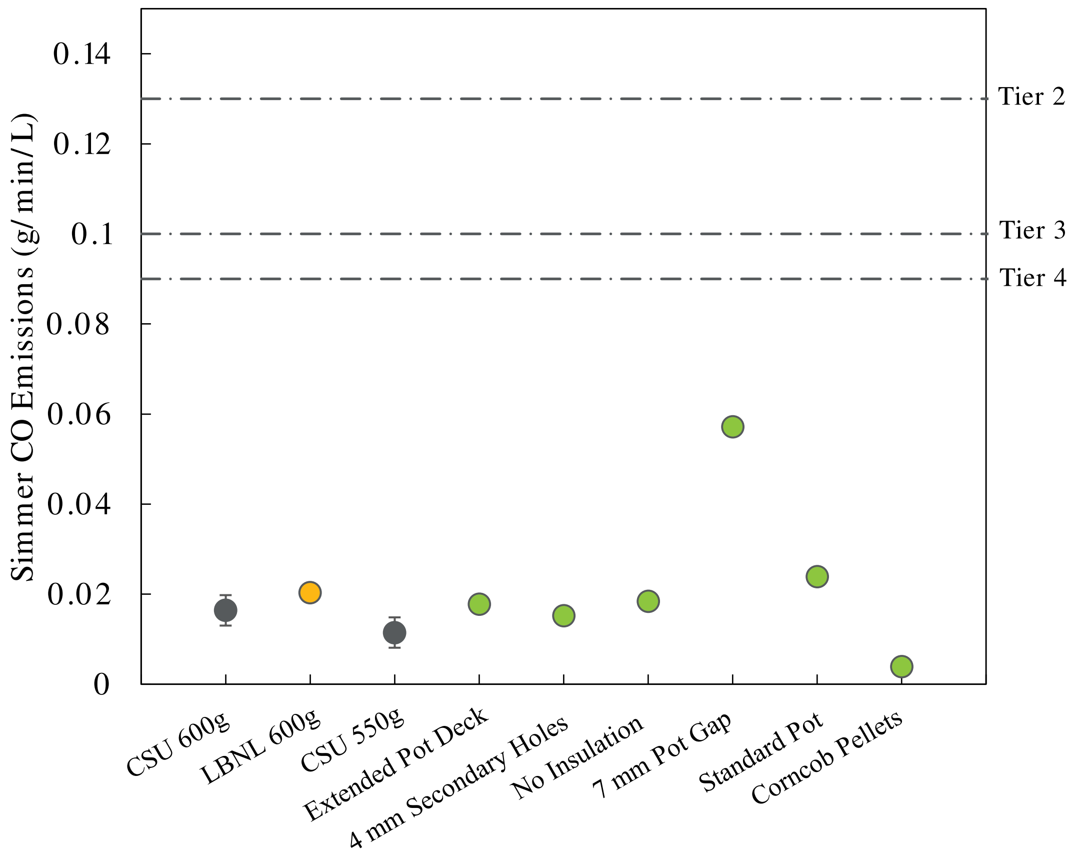

Figure 158 – P2 prototype low power (simmer) CO emissions results. All test cases easily exceed the tier 4 guideline. Error bars represent a 90% CI. All green points have one replicate.

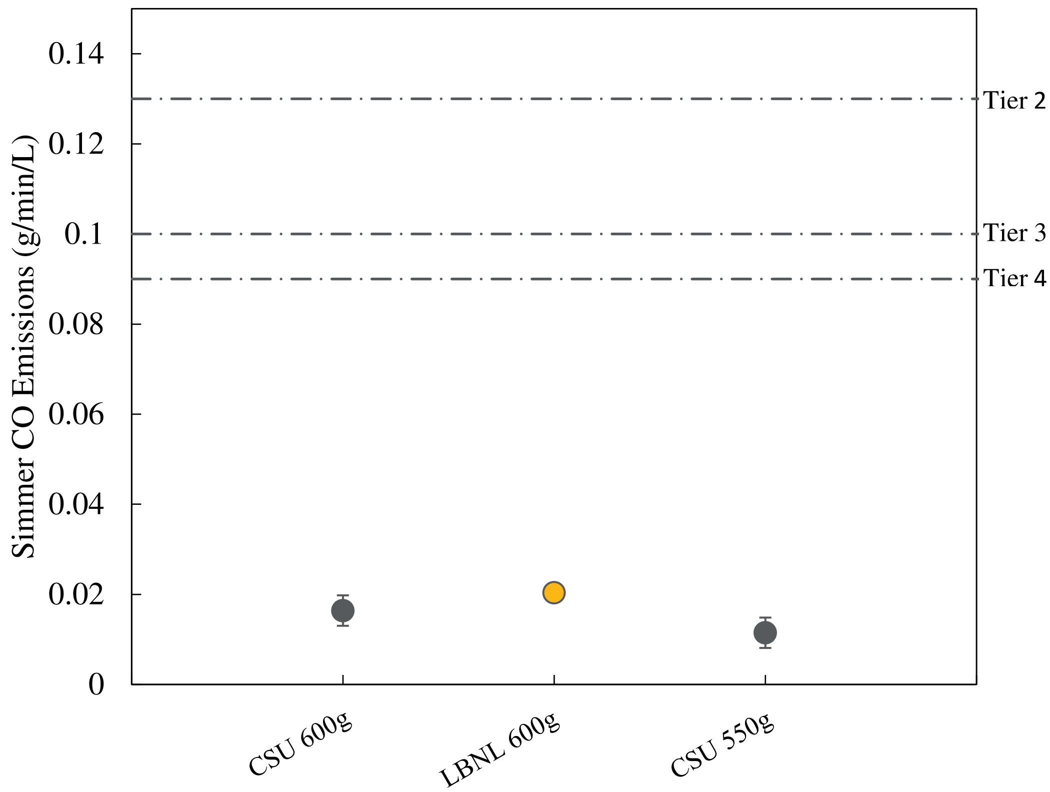

Figure 159 – P2 prototype low power (simmer) CO emissions results for test cases where starting fuel mass was varied. All test cases easily exceeded the tier 4 guideline for low power CO emissions in this testing. Error bars represent a 90% CI.

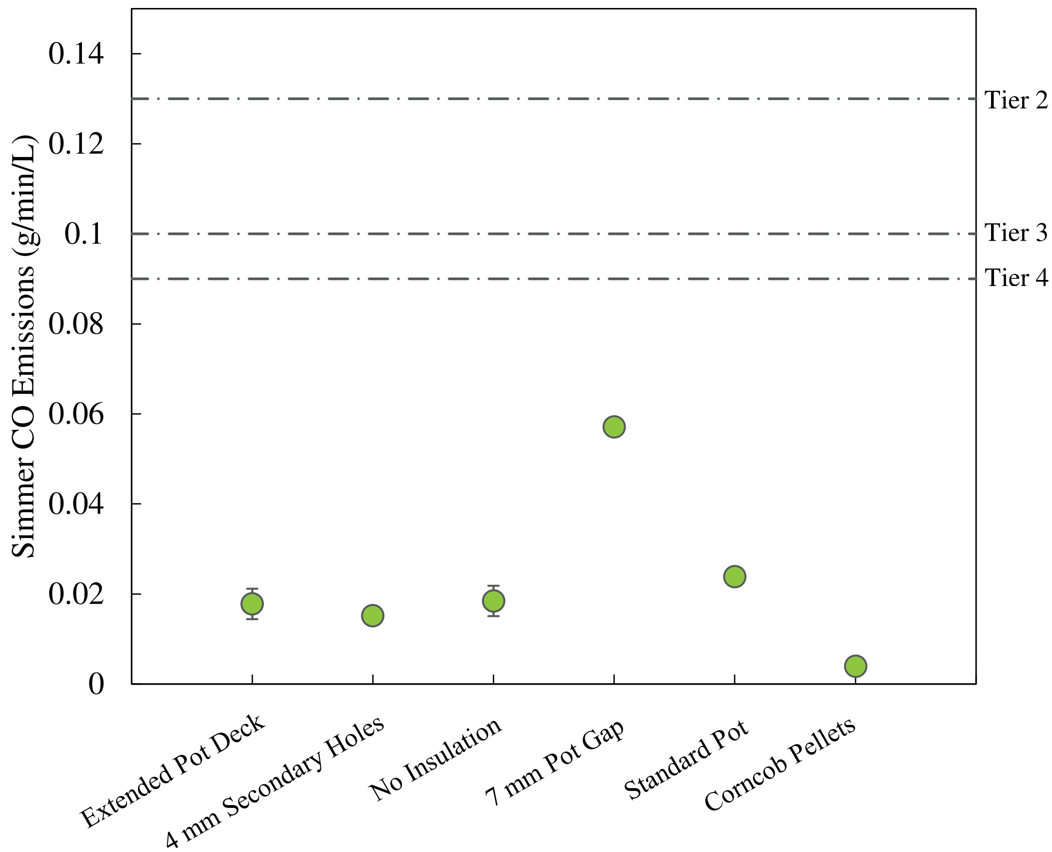

Figure 160 - P2 prototype low power CO emissions results with different stove configurations. Most test cases easily exceeded the tier 4 guideline for low power CO emissions in this testing. The test case where the pot gap was reduced from 15 -mm to 7 -mm resulted in a moderate increase in CO emissions during the low power simmer phase of the test. All test cases are shown here have one replicate.

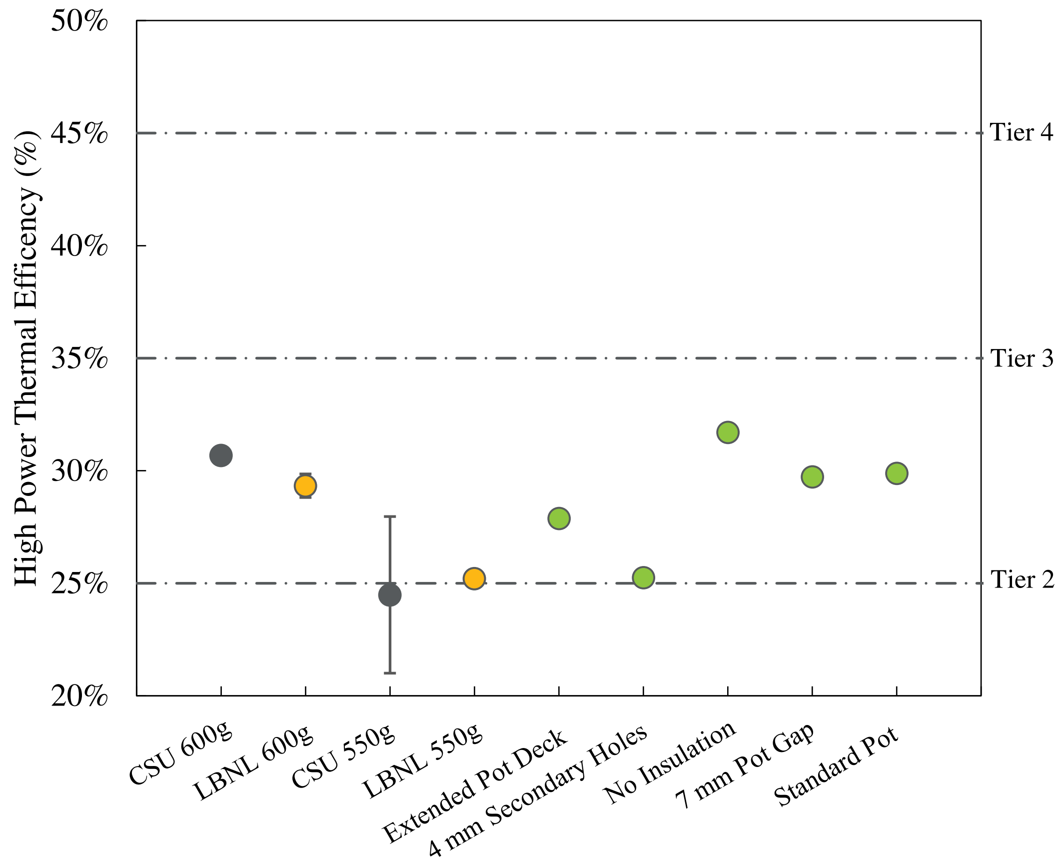

Figure 161 - P2 prototype high power thermal efficiency results. No test cases met the tier 4 guideline. Most test cases were tier 2 with CSU 550g falling into the tier 1 category. Error bars represent a 90% CI. All green points have one replicate.

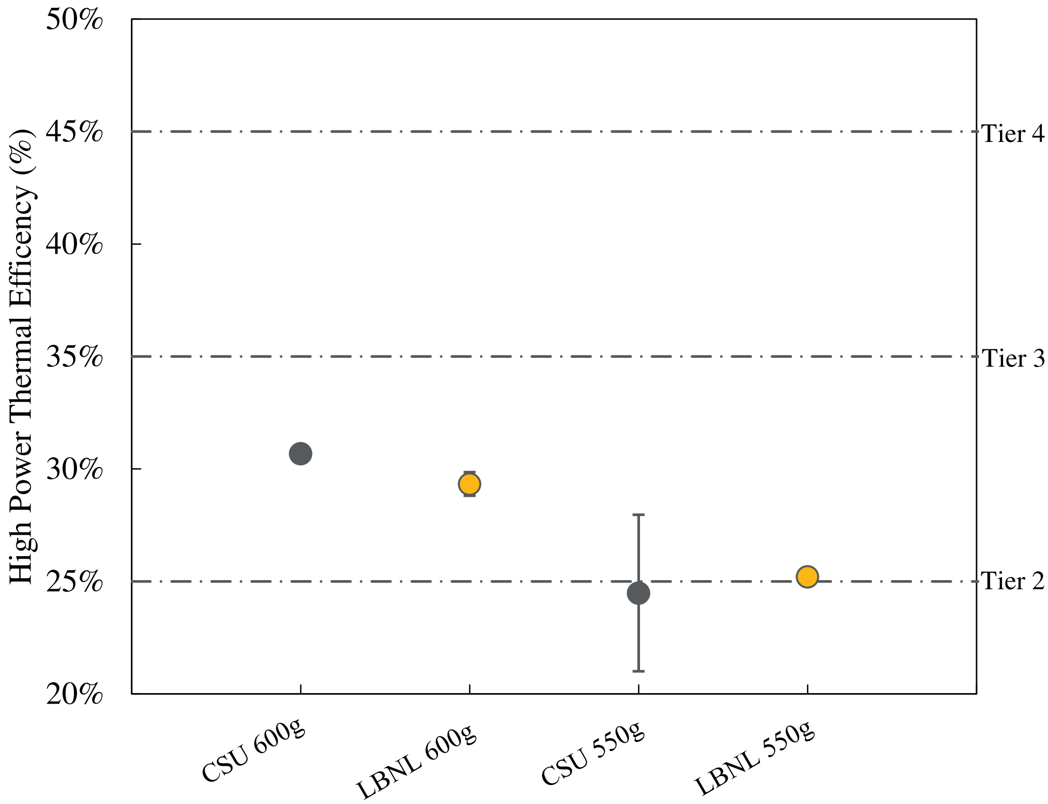

Figure 162 - P2 prototype high power thermal efficiency results for test cases where starting fuel mass was varied. Most test cases were tier 2 with CSU 550g falling into the tier 1 category. Error bars represent a 90% CI.

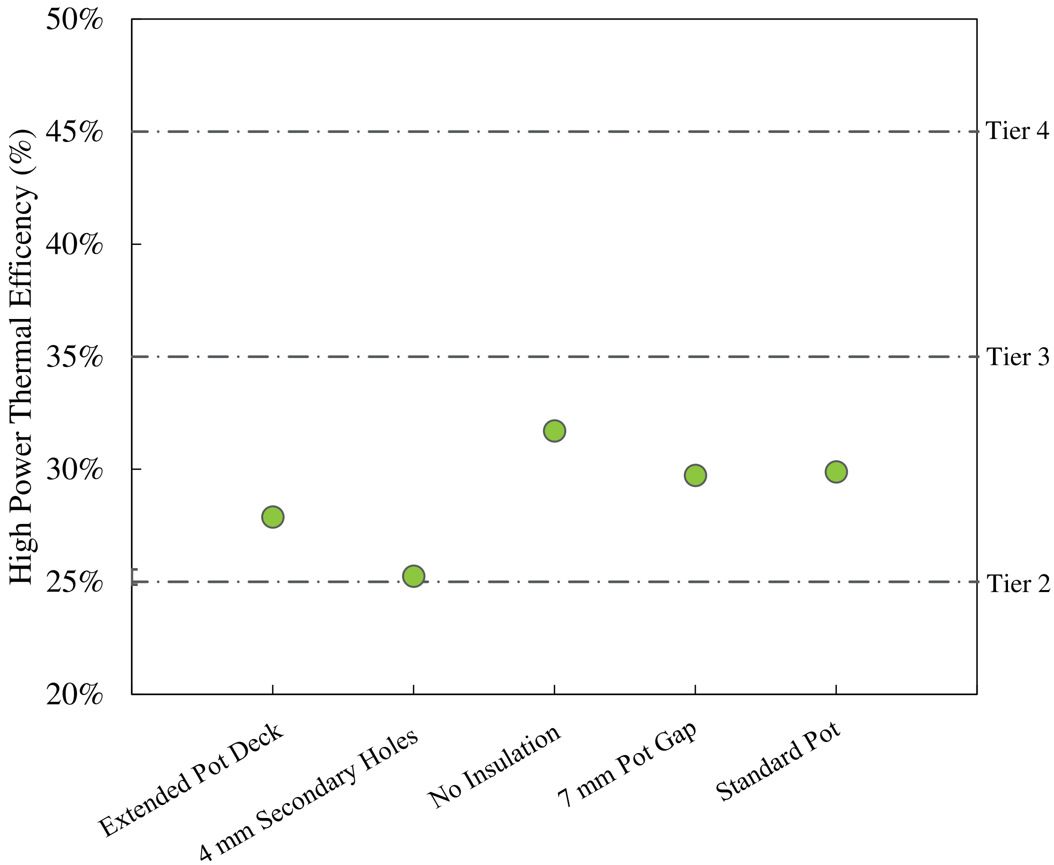

Figure 163 - P2 prototype high power thermal efficiency results with different stove configurations. All test cases were tier 2. All test cases are shown here have one replicate.

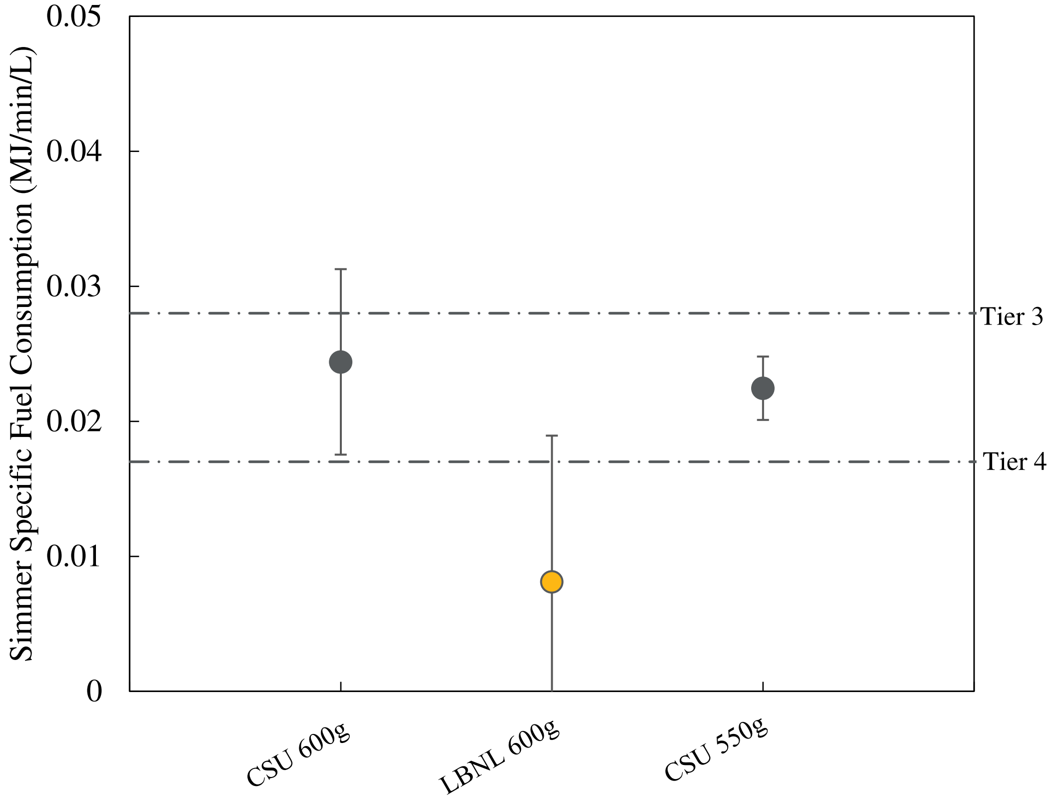

Figure 164 - P2 prototype low power (simmer) specific fuel consumption results for test cases where starting fuel mass was varied. Results fell between tier 3 and tier 4 with LBNL 600g mean falling exceeding the tier 4 guideline. Error bars represent a 90% CI.

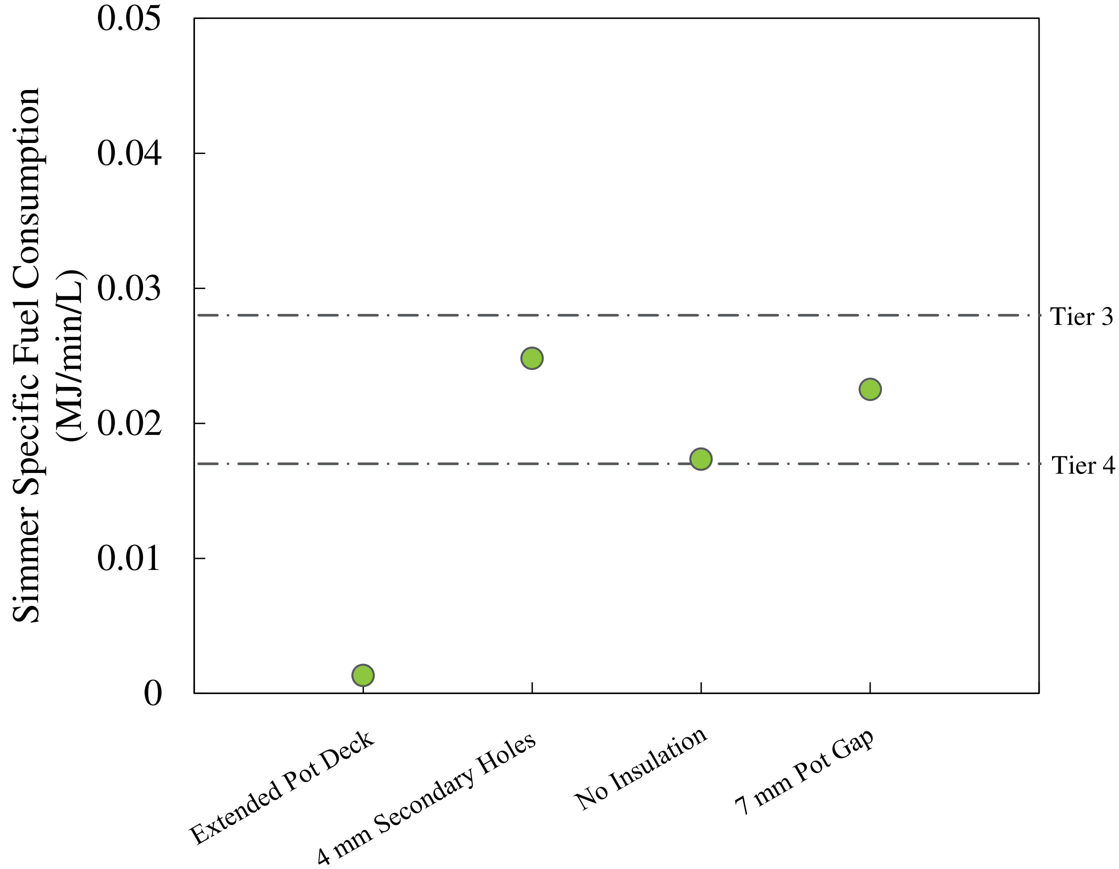

Figure 165 - P2 prototype low power (simmer) specific fuel consumption results for test cases where starting fuel mass was varied. Results fell between tier 3 and tier 4 with LBNL 600g mean falling exceeding the tier 4 guideline. Error bars represent a 90% CI.

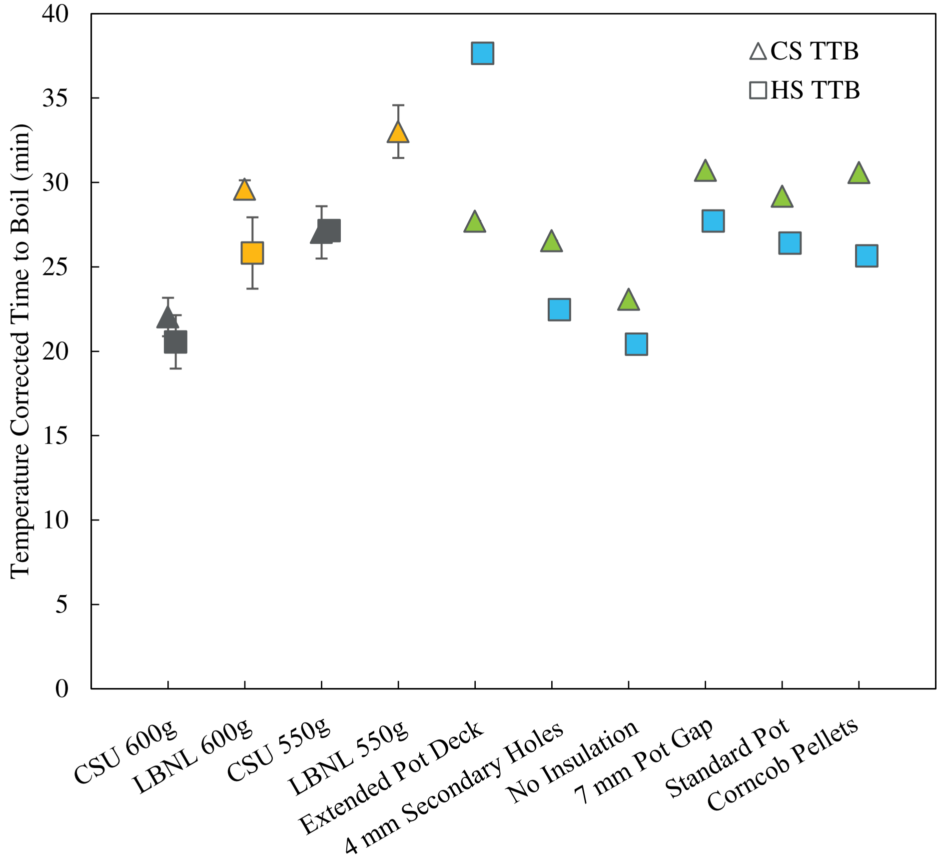

Figure 166 – P2 prototype temperature corrected time to boil results. Cold start time to boil was generally longer than hot start time to boil. Error bars represent a 90% CI. Green and blue data points have only one replicate.

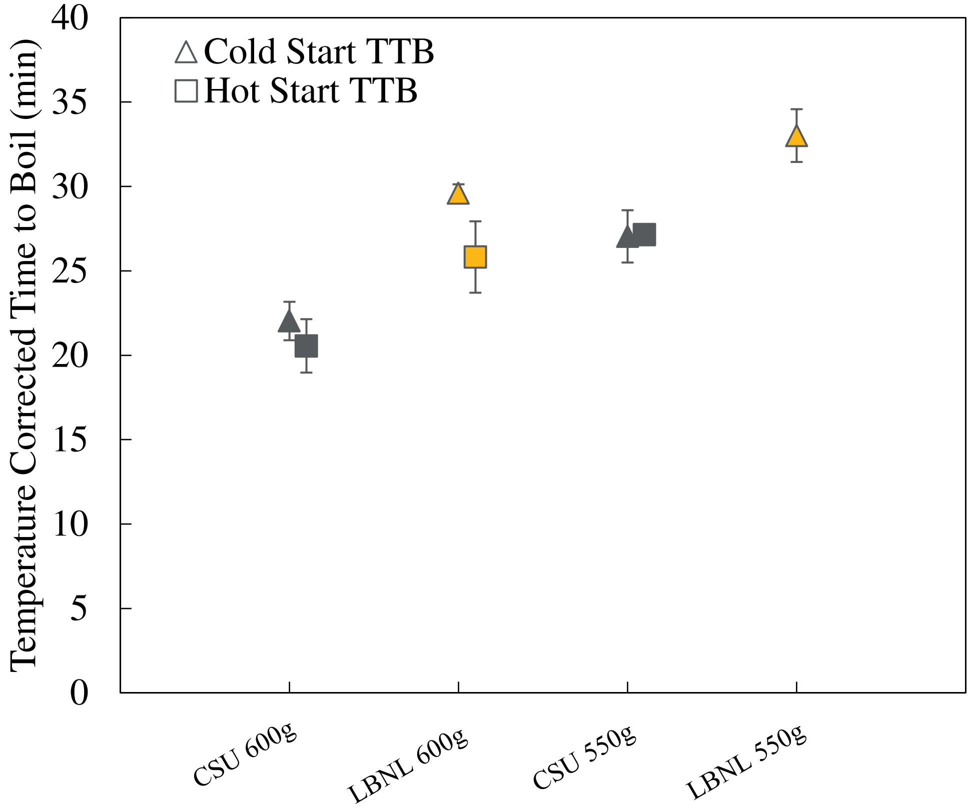

Figure 167 - P2 prototype cold start and hot start high power temperature corrected time to boil results for test cases where starting fuel mass were varied. Mean results fell between 20.56 minutes and 33.02 minutes. Mean hot starts were generaly slightly faster than cold starts. Times for test cases fueled with 600g were faster than test cases fueled with 550g. Error bars represent 95% CI.

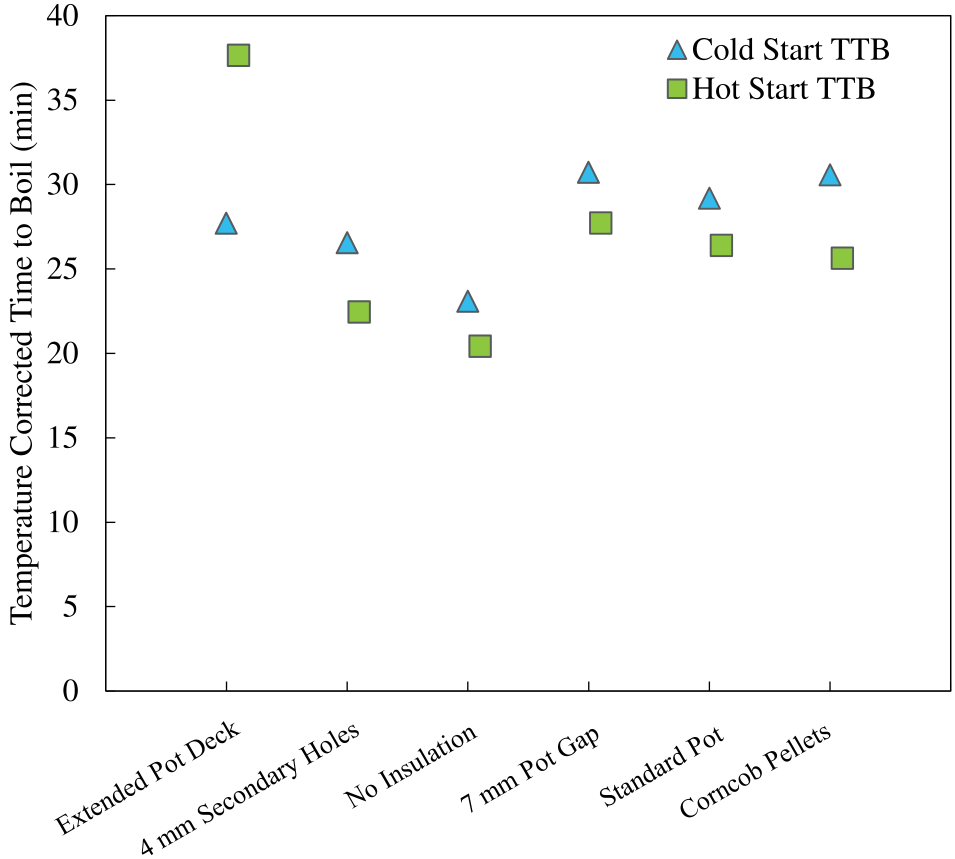

Figure 168 - P2 prototype cold start and hot start high power temperature corrected time to boil results for test cases where stove configuration and fuel type is varied. With the exception of the test case with the extended pot deck, hot start tests had a faster temperature corrected time to boil than cold start tests. All test cases shown have one replicate.

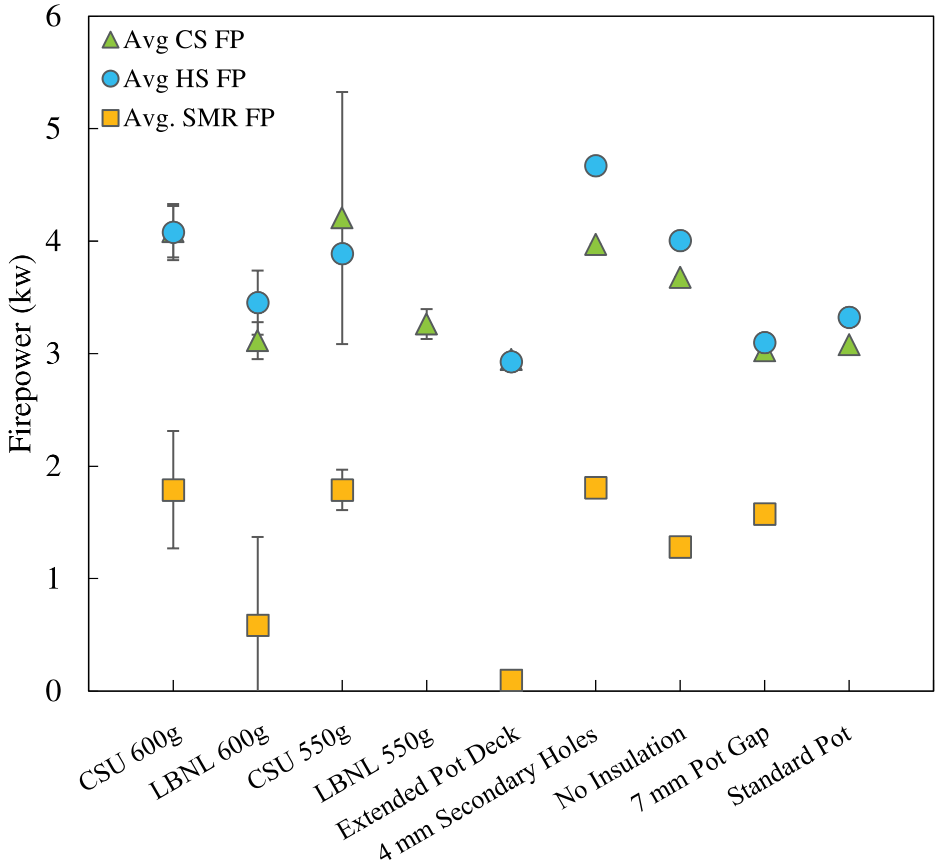

Figure 169 – P2 prototype average thermal power output for high power cold start, hot start, and low power simmer tests. Mean high power results fall between 2.9 kw and 4.7 kw. Mean low power results fall between 0.1 kw and 1.8 kw.

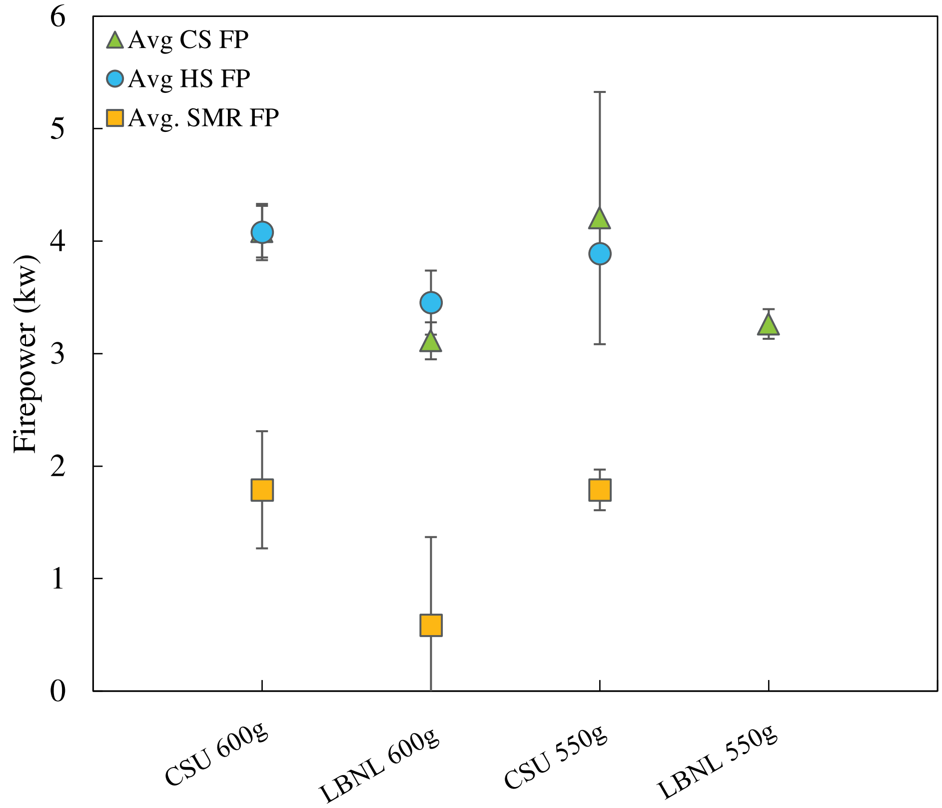

Figure 170 - P2 prototype average thermal power output for high power cold start, hot start, and low power simmer tests where initial fuel mass was varied. Mean high power results fall between 3.1 kw and 4.2 kw. Mean low power results fall between 0.58 kw and 1.8 kw.

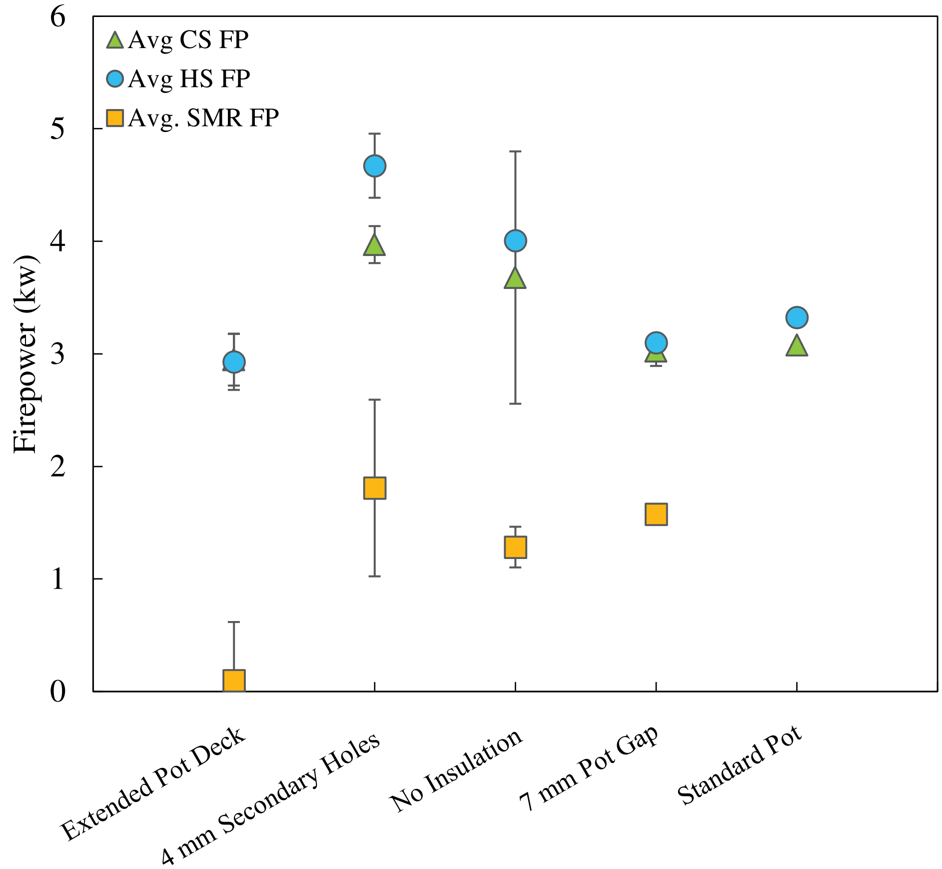

Figure 171 - P2 prototype average thermal power output for high power cold start, hot start, and low power simmer tests where stove configuration is varied. Mean high power results fall between 2.9 kw and 4.7 kw. Mean low power results fall between 0.1 kw and 1.8 kw.

APPENDIX 7: CHILDREN'S BOOK ADAPTATION

The following book adapts the primary philosophical conclusions as well as some technical results from my thesis work to a children's story which my two beautiful daughters can read and (hopefully) understand. As much as this work has cost me in time and effort, it has cost them more bereft of a time with their father, and I hope that this story can be a personal and accessible summary of what I have been working on these long years they will have a chance to participate in this monumental effort.

Abby and Hailey thank you for being patient with me through this long process which I am sure, to your young eyes, seemed never-ending. Your contributions of encouragement, reminders to work on my "tee-sis" and drooling on my rough drafts have driven me to complete this work so I can spend more time with you!

All My Love,

Daddy

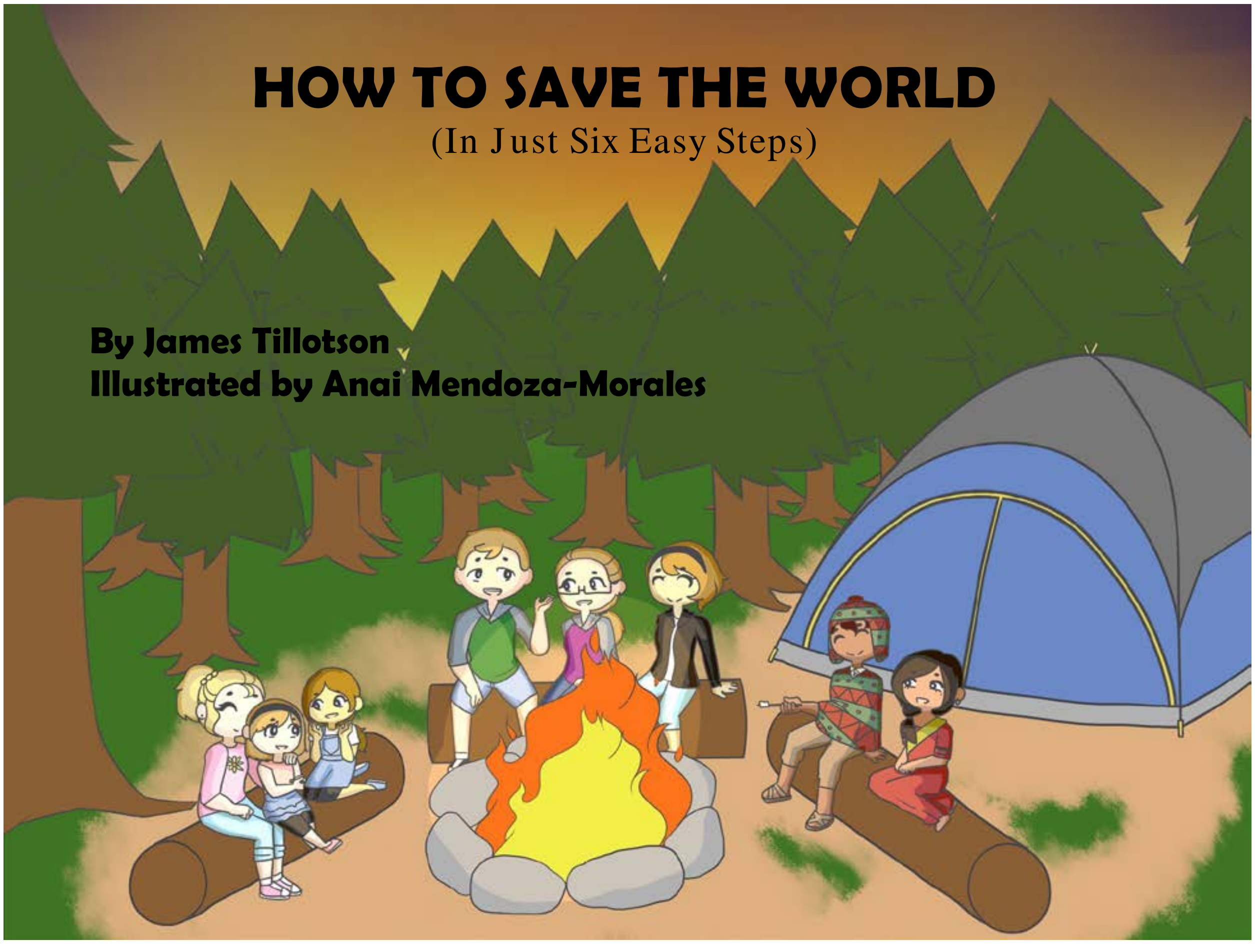
HOW TO SAVE THE WORLD
(In Just Six Easy Steps)
By James Tillotson
Illustrated by Anai Mendoza-Morales

One summer evening while Abby and Hailey were camping in the mountains of Colorado with Mom and Dad, Abby noticed that the campfire made her cough.

She asked Hailey, "Does the smoke make you cough, too?"

Hailey replied, "Yes, the smoke from our cooking with a campfire makes my throat itch and my eyes water too!"

Abby wondered, "Is the smoke bad for us to breathe or is it just annoying?"

Dad told Abby and Hailey that they were asking an excellent question and they should use the scientific method to find the answer.

Abby and Hailey both asked, “What is the scientific method?”

“It is a way of thinking about a question so that you can find the right answer quickly. Let me show you how it works.”

“There are six steps to the scientific method,” Dad said.

“The first one is to make an observation.”

“What is an observation?” Hailey asked.

“An observation is when you find something interesting that you don’t understand,” said Mom.

Dad added, “When you coughed because of the smoke, you made an observation about smoke. You noticed that it makes your eyes water and throat itch.”


MAKE AN OBSERVATION

Mom said, “The next step is to ask a question about your observation.”

“Just like I did when I wondered if the fire was bad for us or if it was just annoying,” Abby exclaimed.

“That’s right, Abby,” said Dad.

Hailey added, “I have a question, too. Can we make the fire have less smoke?”

“Excellent question,” Dad replied.


MAKE AN OBSERVATION
ASK THE QUESTION

“Next,” Dad said, “You need to do some research. This means reading books and talking to people about your question. It is the start of an adventure that will lead you to the answer!”

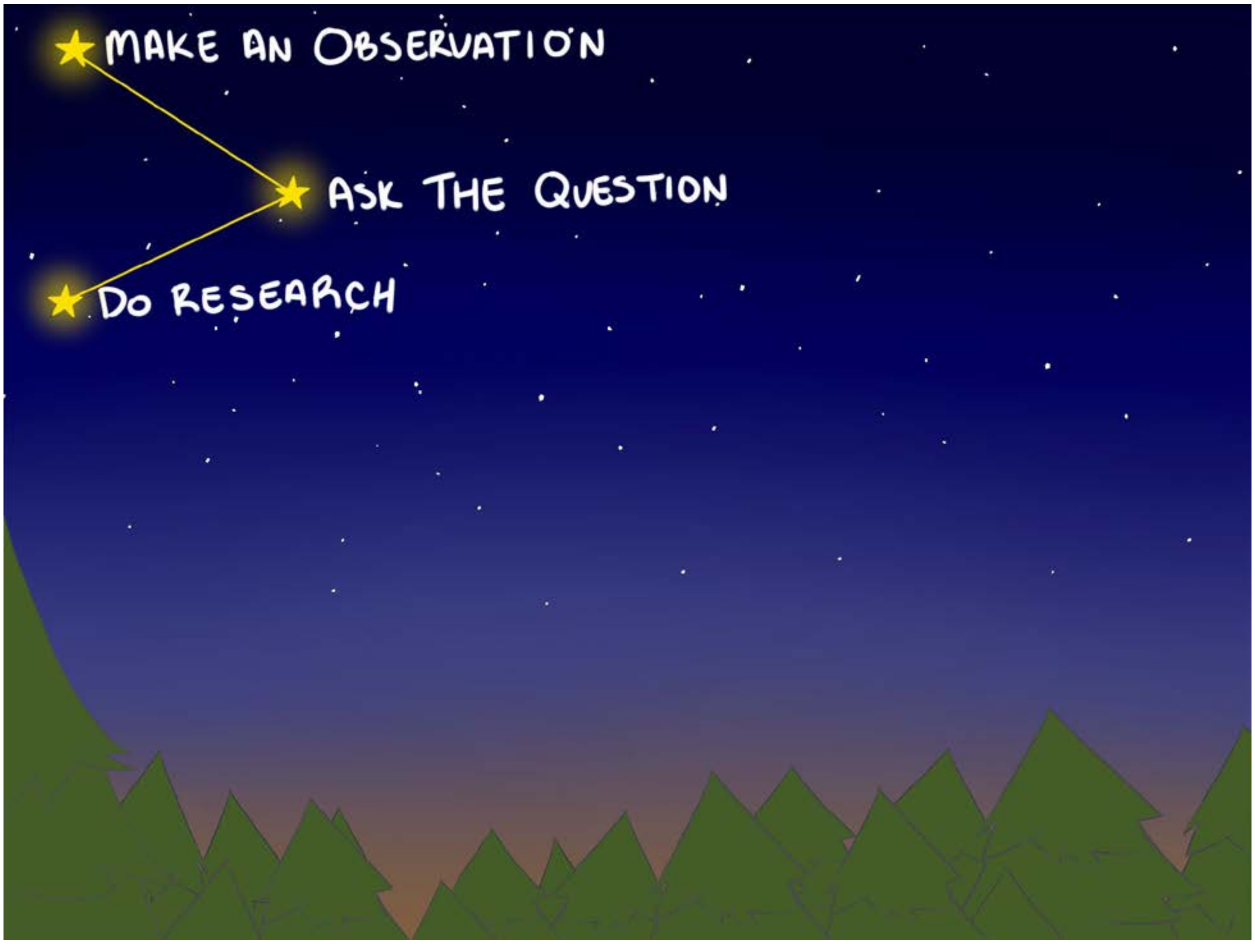
MAKE AN OBSERVATION
ASK THE QUESTION
DO RESEARCH

Mom said, “The fourth step is to make a hypothesis.”

“What is a hypothesis?” said Abby and Hailey together.

Dad explained,

“Hypothesis is a big word. It means a guess to the answer to your question. Your guess should come from your research.”

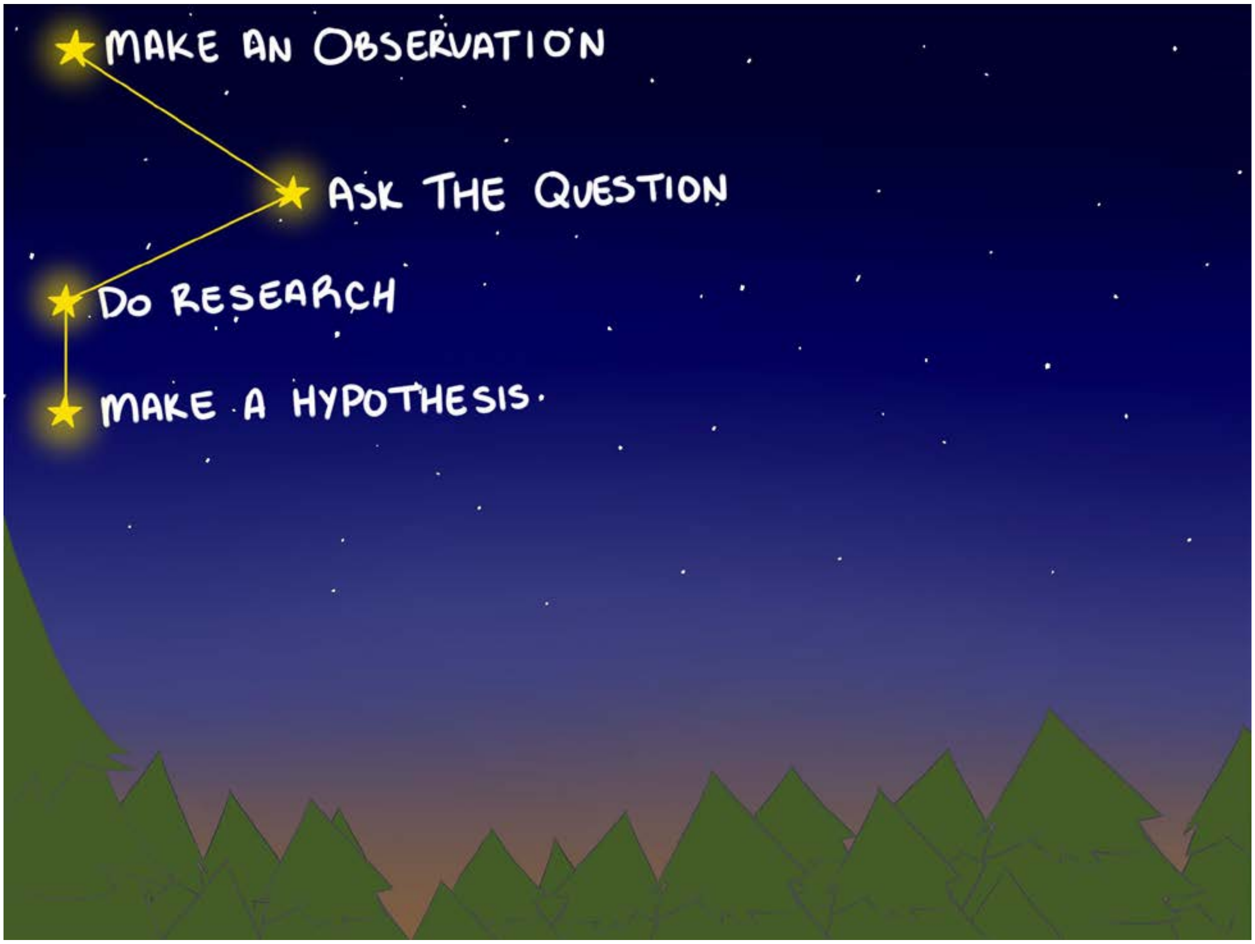
MAKE AN OBSERVATION
ASK THE QUESTION
DO RESEARCH
MAKE A HYPOTHESIS.

“The next step after that is to do an experiment,” said Mom.

Dad added, “An experiment is a project that lets you try out your hypothesis to see if it is right or wrong. The most important part is to write down everything that happens when you do your experiment.”

Hailey said, “Oh dear! I don’t know how to write yet; I can’t do the scientific method.”

“That is okay,” Abby said, “I can write for both of us.”

Mom said, “Hailey, you can draw and paint nice pictures, and that is an important part of writing things down too.”

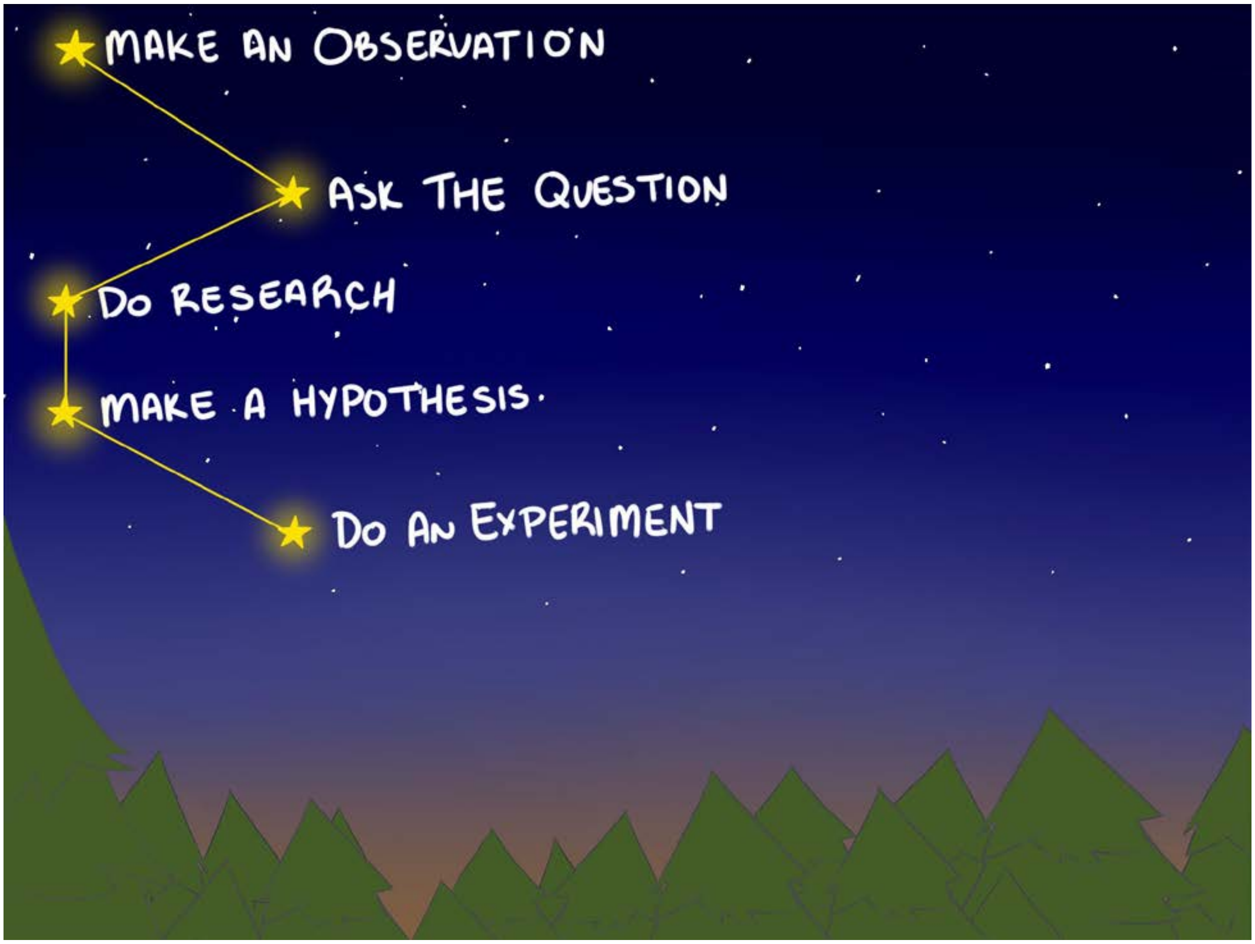
MAKE AN OBSERVATION
ASK THE QUESTION
DO RESEARCH
MAKE A HYPOTHESIS
DO AN EXPERIMENT

The last step in the scientific method is to look at your notes and decide if your hypothesis was right or wrong," Dad said.

"What happens if the hypothesis is wrong?" Abby asked.

Dad said, "It is okay to find out that your hypothesis is wrong. Then you make a new hypothesis and do another experiment to see if your new hypothesis is right or wrong."

Mom added, "Sometimes the wrong hypothesis is the most fun of all because when you have a wrong hypothesis, you are about to learn something you have never thought of before!"

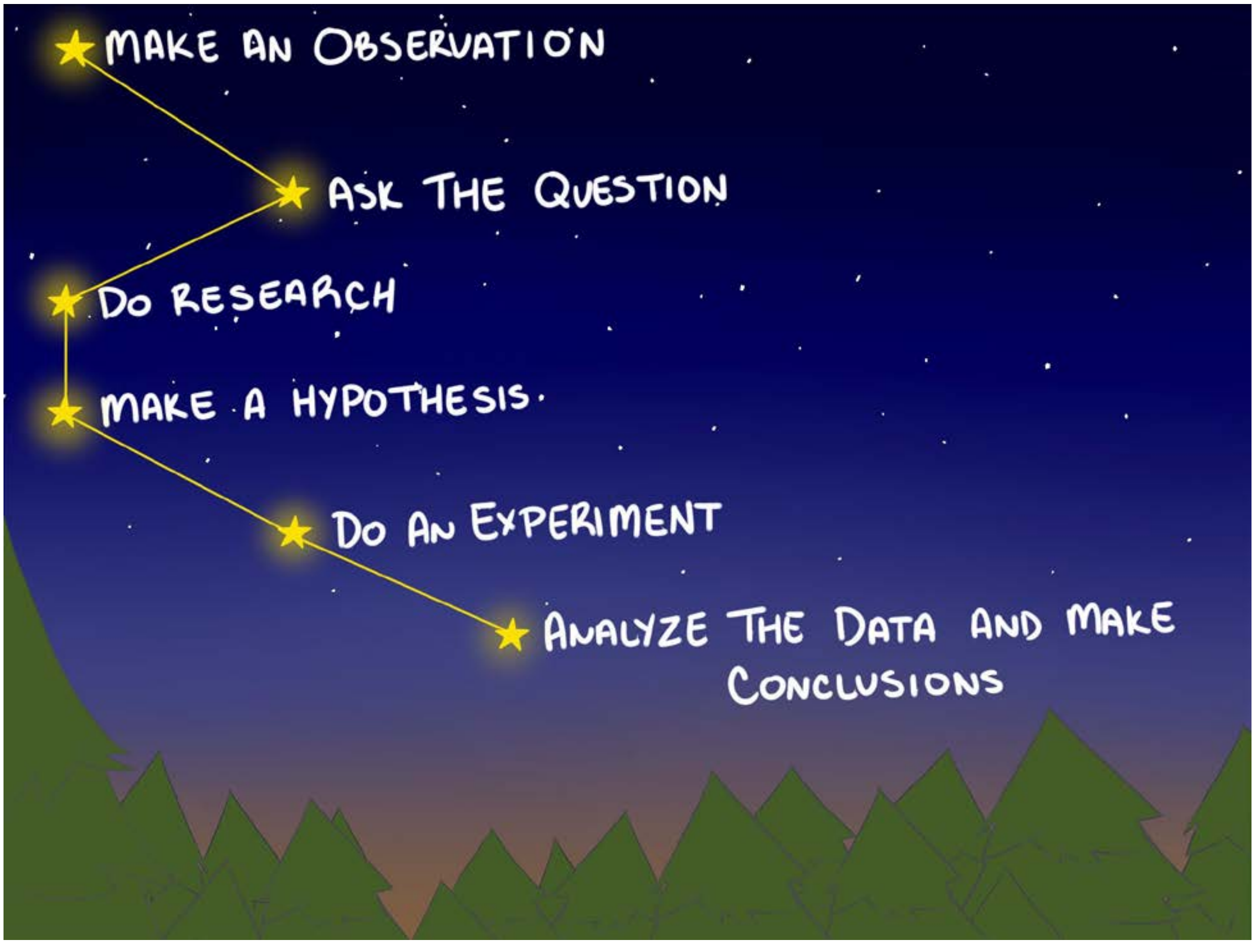
MAKE AN OBSERVATION
ASK THE QUESTION
DO RESEARCH
MAKE A HYPOTHESIS
DO AN EXPERIMENT
ANALYZE THE DATA AND MAKE CONCLUSIONS

Mom said, "Now that you know about the scientific method< you should go on an adventure to find the answer to your question about smoke from our cooking fire."

"That is a great idea," Dad said.

"Hooray," Abby and Hailey exclaimed together. "An adventure to answer a question! What fun!"

"Most importantly," Dad reminded the girls. "Make sure you ask for help from people all around you; you can't find the answer by yourselves."

Abby and Hailey set off on a big adventure to find the answer to their question.

First stop was the National Library of India in Kolkata to start their Scientific Method journey.

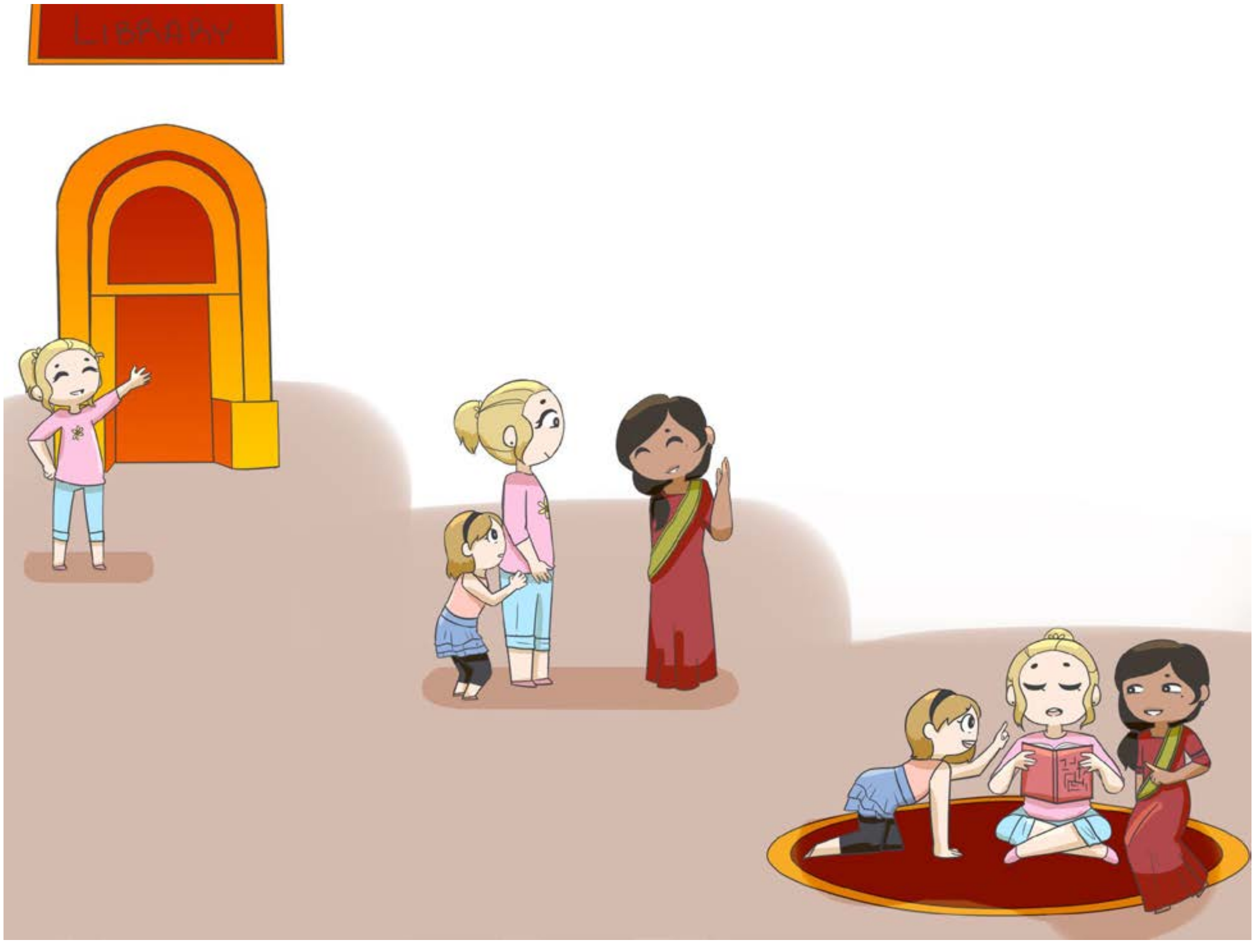

“To find the answer to our question we need to read some books,” Abby said to Hailey.

“Yes, and we should talk to people here too.” Hailey replied.

They met a little girl at the library in India named Aanya who offered to help them find the answer to their question about cooking fire smoke.

Together the three girls read books and talked to people who cook over a fire so they could learn more about fires, smoke, and cooking.

“Now that we have done our research, we need to make our hypothesis,” Abby said to the others.

"Yes," Hailey said, "Let's go to Peru next. The books we read showed us that many people in Peru cook on stoves. Maybe we will meet someone there to help us."

So, the three girls set off for Lima, Peru to find more help with their hypothesis.

When the girls arrived in Lima, Peru, they met a boy named Alejandro who wanted to help.

Hailey said, “Remember, our hypothesis question is this: is breathing the smoke from a cooking fire bad for you, and can you make a fire smoke less?”

Abby said, “I think that smoke is bad for people. If it hurts to breathe and makes your eyes and throat itch, that must not be very good.”

“I agree,” said Aanya, “The books we read for our research at the library said that breathing smoke was terrible for your lungs.

“I think it might be possible to make cooking fires smoke less, too,” said Alejandro, “And that will be good for everybody who cooks with fire.”

"Where can we go to do an experiment to test our hypothesis?" Aanya asked.

Abby replied, "Dad told me about some scientists there who might be able to help us, let's go there."

They all agreed that this would be a good idea, so the two sisters and their new friends boarded a plane to fly to Paris, France to do an experiment that tested their hypothesis.

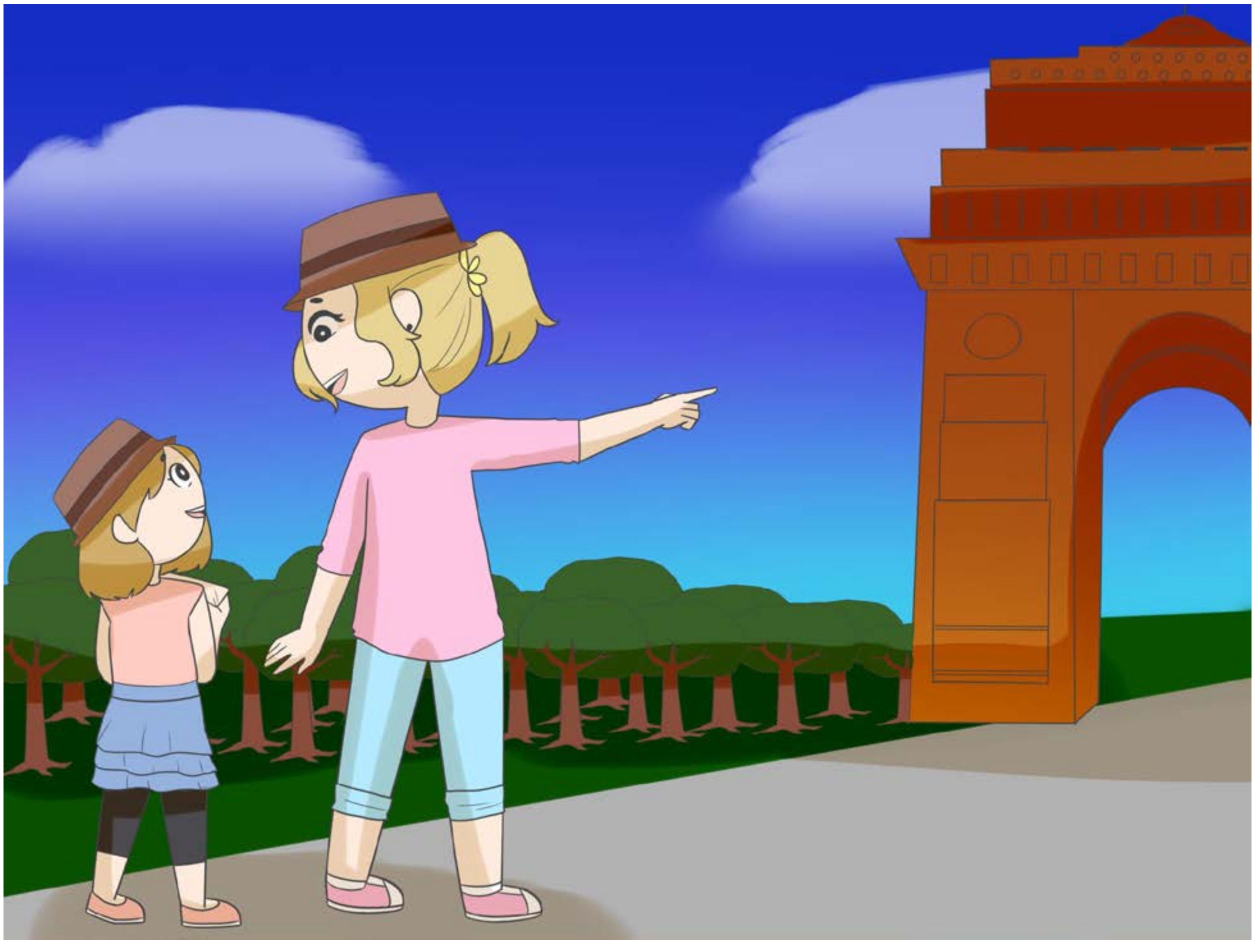

In Paris, the four friends met Louise on the Champs-Élysées near the Arc de Triomphe.

Louise was excited to hear what the friends were doing and agreed to help them test their hypothesis at her laboratory in her hometown of Nancy, France.

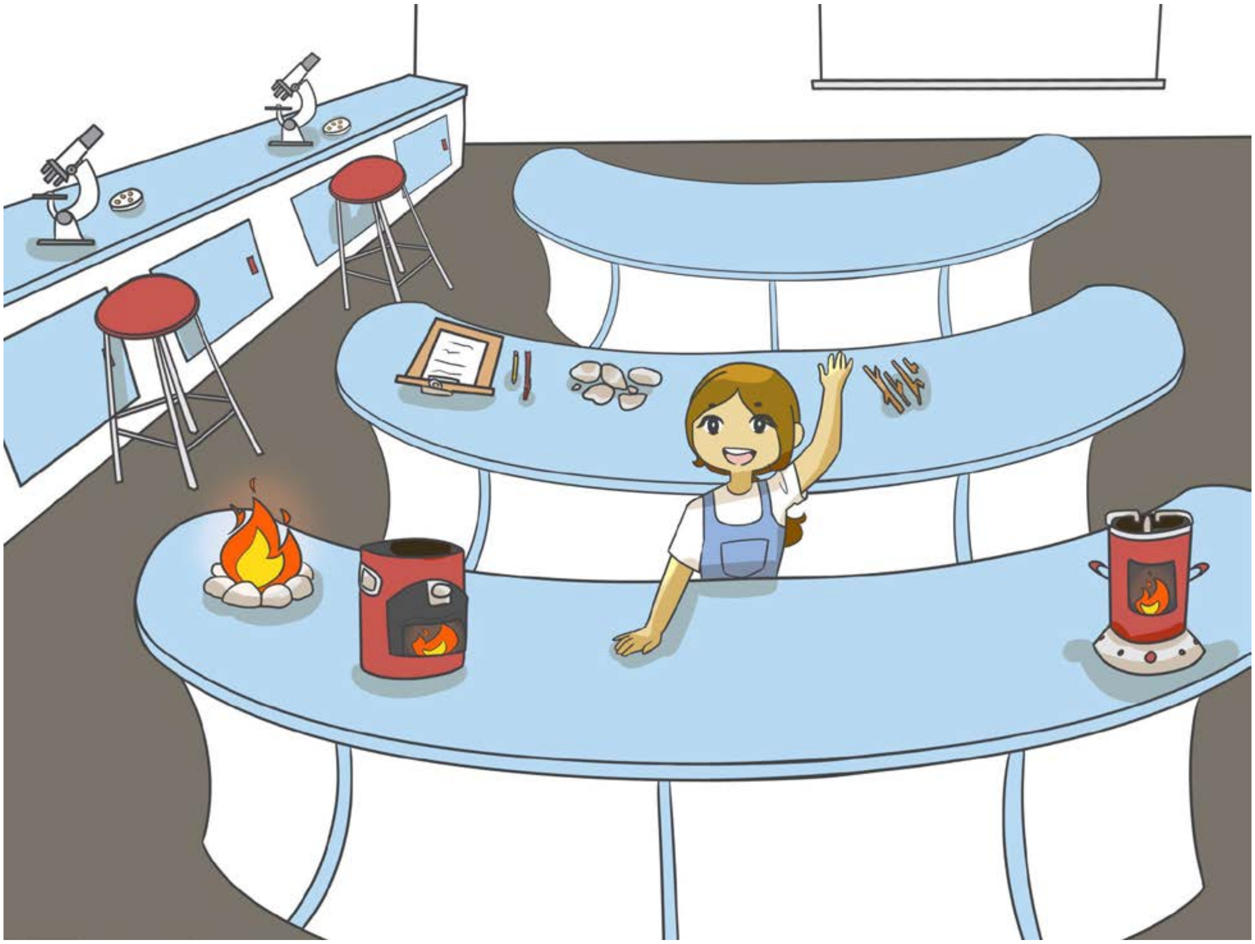

When they arrived in Nancy, the new friends were so excited they went right to the laboratory to test their hypothesis.

“First we should try a smoky fire like the fire we were using on our camping trip,” Abby said.

“Next we should test a simple cooking stove that used sticks to heat a pot but gave the sticks a chimney and lifted them off the ground,” said Hailey

The last stove the 5 friends decided to try was a complicated stove that used a fan to blow air on the sticks to make them burn bright

They wrote down what they saw with each of the three fires they tested.

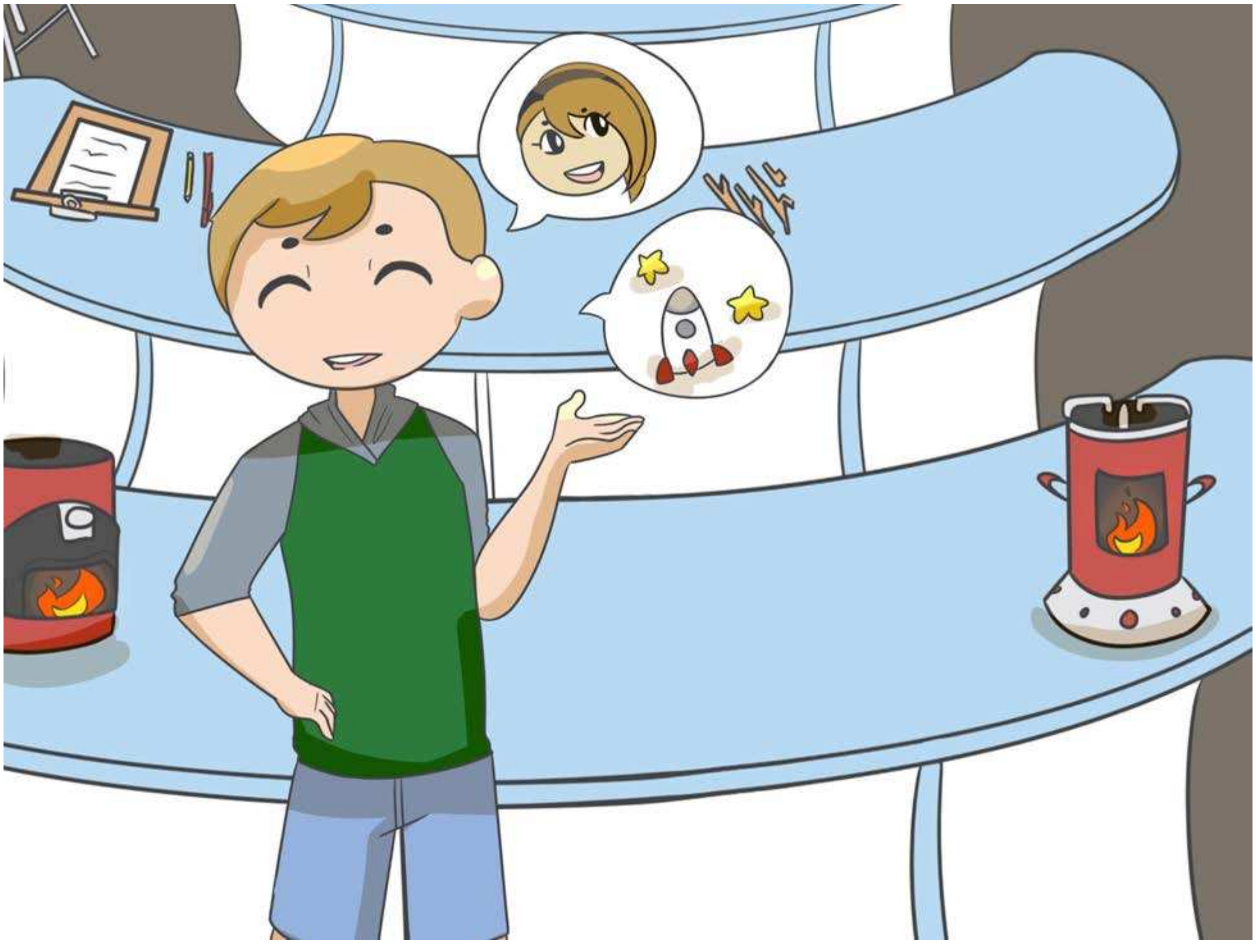

“Now we have to analyze the data,” said Abby.

“Yes, but who can help us?” cried the others.

“Perhaps there is a scientist who can help us understand our experiments,” said Hailey.

“I know a scientist named Dr. Jessica who can help you,” Dad said. “She is in space so you will have to fly there to ask her.”

“That sounds fun!” Everyone shouted at once. So, off the five friends went to ask Dr, Jessica about their experiments.

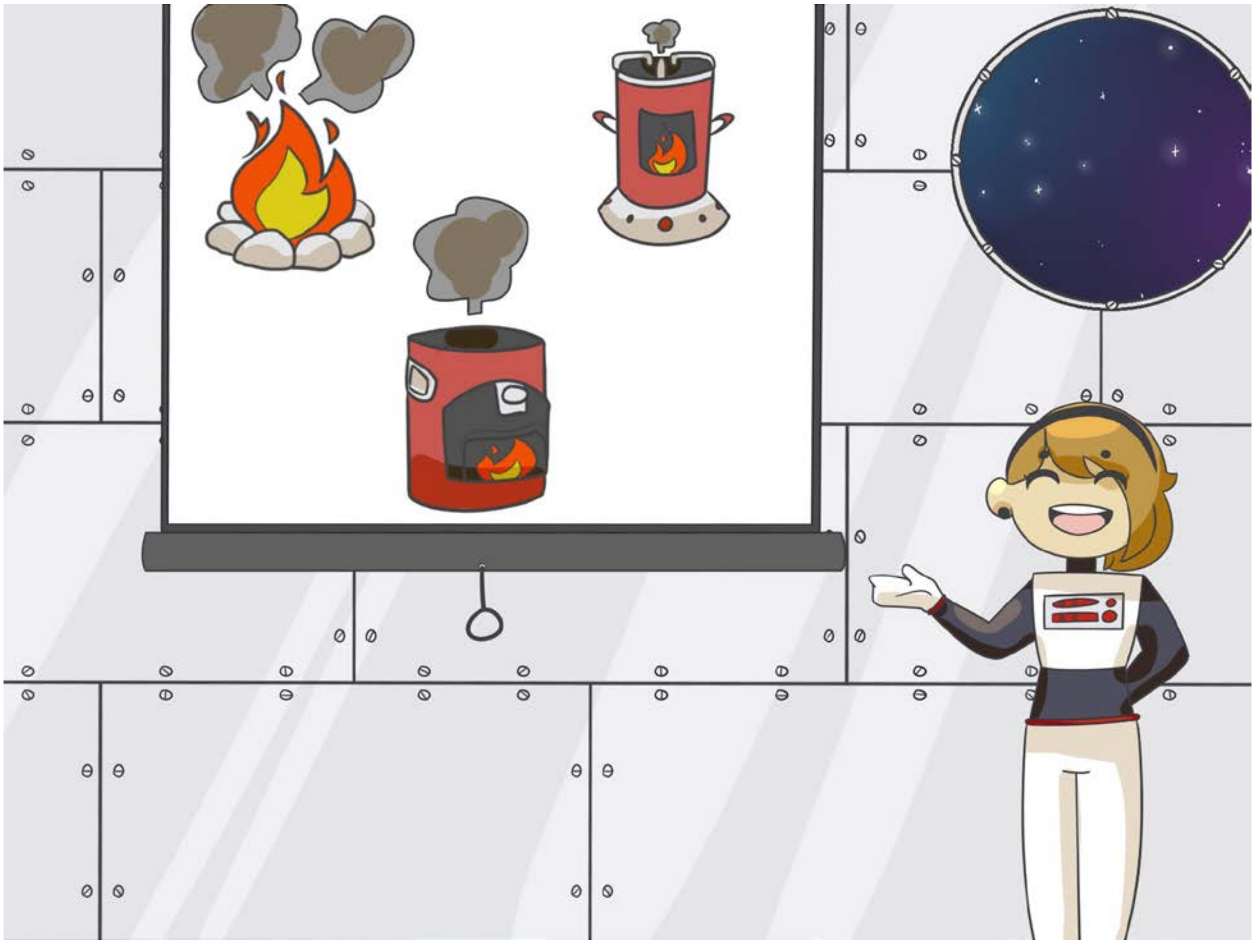

The five friends arrived at the space station to ask Dr. Jessica about the notes from their experiments.

Dr. Jessica told them, “You need to make a graph which is a way to draw a picture using your observations.”

“Yay! I know how to draw a picture,” Hailey said.

So the friends drew a picture showing that the campfire made a lot of smoke, the simple stove made less smoke, and the complicated stove made the littlest smoke of all.

“This picture makes me think that the complicated stove would be better for cooking.” said Abby

Dr. Jessica said she thought that was good too.

And the five friends thanked her and returned to earth to talk about what they learned.

When the five new friends landed at Abby and Hailey's house, they discussed how they learned to use the scientific method to answer their question.

Abby said, "I learned to ask questions about what I see."

Hailey said, "I learned to read lots of books and talk to lots of people to research a question I have."

Aanya said, "I learned that making a hypothesis is important if you want to learn the right answer to a question."

Alejandro said, "I learned that writing down good notes when doing experiments can help you answer your question too!"

Louise said, "I learned that if you can make a good picture of your notes, you can decide if your hypothesis is right or wrong."

"And most importantly," Abby finished, "Was that we learned we need each other to answer hard questions. We need to ask good questions, make a good hypothesis, invent good experiments, and finally, look at the research we find so that we can come to the right answer to our questions."

"This is so much fun! Now that we know how to use the scientific method let's have another adventure and find the answer to another question!" Abby exclaimed.

"Yes, lets!" Hailey said, "Maybe we will make some more friends, too!"

And the five friends set off together, ready for another new adventure.

The End